Connecting the Rheological Behavior to the Processing of Thermotropic Liquid Crystalline Polymers in the Super-cooled State

Chen Qian

Dissertation submitted to the Faculty of

Virginia Polytechnic Institute and State University

in partial fulfillment of the requirements for the degree of

DOCTOR OF PHILOSOPHY

in

Chemical Engineering

Donald G. Baird, Chairman

Timothy E. Long

Stephen M. Martin

Garth L. Wilkes

April 15th, 2016

Blacksburg, VA

Keywords: thermotropic liquid crystalline polymer, rheology, super-cooled state

Connecting the Rheological Behavior to the Processing of Thermotropic Liquid Crystalline Polymers in the Super-cooled State

Chen Qian

Abstract

Thermotropic liquid crystalline polymers (TLCPs) have attracted great interest because of the combination of their promising properties, which includes high stiffness and strength, excellent processability, and outstanding chemical resistance. TLCPs exhibit inherently low viscosity relative to many other conventional thermoplastics. The low melt viscosity is detrimental to processes requiring high melt strength, such as extrusion blow molding, film blowing, thermoforming and multilayer coextrusion. Our laboratory has developed a unique method to increase the viscosity of TLCPs by first raising the temperature above the melting point (T_m) to exclude all solid crystalline structure, and then lowering the temperature below T_m to super cool the materials. Additionally, the super-cooling behavior of TLCPs allows them to be blended with other thermoplastics possessing lower processing temperatures.

The initial focus of this dissertation is to investigate the processing temperature of a representative TLCP in the super-cooled state, using the methods of small amplitude oscillatory shear (SAOS), the startup of shear flow and differential scanning calorimetry (DSC). The TLCP used in this work is synthesized from 4-hydroxybenzoic acid (HBA), terephthalic acid (TA), hydroquinone (HQ) and hydroquinone derivatives (HQ-derivatives). The TLCP of HBA/TA/HQ/HQ-derivatives has a melting point, T_m, of around 280 ^oC. Once melted, the TLCP can be cooled 30 ^oC below the T_m while still maintaining its processability. As the TLCP was cooled to 250 ^oC, a one order magnitude increase in viscosity was obtained at a shear rate of 0.1 s^-

[1]. Additionally, super cooling the TLCP did not significantly affect the relaxation of shear stress after preshearing. However, the recovery of the transient shear stress in the interrupted shear measurements was suppressed to a great extent in the super-cooled state.

The second part of this work is concerned with the extrusion blow molding of polymeric blends containing the TLCP of HBA/TA/HQ/HQ-derivatives and high density polyethylene (HDPE), using a single screw extruder. The blends were processed at a temperature of 260 ^{o}C which is 20 ^{o}C below T_m of the TLCP such that the thermal degradation of HDPE was minimized. Bottles were successfully produced from the blends containing 10, 20 and 50 wt% TLCP. The TLCP/HDPE blend bottles exhibited an enhanced modulus relative to pure HDPE. However, the improvement in tensile strength was marginal. At 10 and 20 wt% TLCP contents, the TLCP phase existed as platelets, which aligned along the machine direction. A co-continuous morphology was observed for the blend containing 50 wt% TLCP. The preliminary effectiveness of maleic anhydride grafted HDPE (MA-g-HDPE) as a compatibilizer for the TLCP/HDPE system was also studied. The injection molded ternary TLCP/HDPE/MA-g-HDPE blends demonstrated superior mechanical properties over the binary TLCP/HDPE blends, especially in tensile strength. Consequently, it is promising to apply the ternary blends of TLCP/HDPE/MA-g-HDPE in the blow molding process for improved mechanical properties.

Finally, this work tends to determine how the isothermal crystallization behavior of a TLCP can be adjusted by blending it with another TLCP of lower melting point. One TLCP (T_m~350 ^{o}C) used is a copolyester of HBA/TA/HQ/HQ-derivatives with high HBA content. The other TLCP (T_m~280 ^{o}C) is a copolyesteramide of 60 mol% hydroxynaphthoic acid, 20 mol% terephthalic acid and 20 mol% 4-aminophenol. The TLCP/TLCP blends and neat TLCPs were first melted well above their melting points, then cooled to the predetermined temperatures below the melting

temperatures at 10 ^{o}C/min to monitor the isothermal crystallization. As the content of the low melting TLCP increased in the blends, the temperature at which isothermal crystallization occurred decreased. Comparing with neat TLCPs, the blend of 75% low melting TLCP crystallized at a lower temperature than the pure matrices, and the blend remained as a stable super-cooled fluid in the temperature range from 220 to 280 ^{o}C. Under isothermal conditions, differential scanning calorimetry (DSC) was not capable of reliably detecting the the low energy released in the initial stage of crystallization. In contrast, small amplitude oscillatory shear (SAOS) was more sensitive to detecting isothermal crystallization than DSC.

Original Contributions

- The processing temperature of a representative TLCP in the super-cooled state was studied using the combined techniques of small amplitude oscillatory shear (SAOS), differential scanning calorimetry (DSC), and the startup of shear flow measurements. This work is the first to employ the transient melt shear measurements to guide the processing of TLCP in the super-cooled state. Additionally, although the transient rheology of TLCPs has been well documented above the melting point, this is the first time the transient rheological behavior of the TLCP is reported in the super-cooled state.
- The bottles of TLCP/HDPE blends were successfully developed using extrusion blow molding. Comparing with HDPE, the blend bottles exhibited improved mechanical properties. To the author's knowledge, this is the first time the blends of TLCP/HDPE are processed by extrusion blow molding.

The isothermal crystallization of the TLCP/TLCP blends was investigated using both SAOS and DSC in the time sweep mode. The processing temperature range of the TLCP/TLCP blends in the super-cooled state is reported for the first time. Moreover, this is the first time the sensitivities of SAOS and DSC on detecting the isothermal crystallization were compared. SAOS is more sensitive to characterizing isothermal crystallization, and it should be used in determining the processing temperatures in the super-cooled state for neat TLCP resins and TLCP/TLCP blends.

Format of Dissertation

Chapter 1 provides the motivation as well as the objectives of this dissertation. Chapter 2 summarizes the detailed progress and background information relating to the objectives. Chapters 3 to 5 are self-contained papers, which will be submitted for journal publication. Each chapter contains a separate introduction, motivation, experimental results and conclusions. The detailed experimental results, including figures and tables, are presented after the reference section in each chapter. Finally, the overall conclusions and proposed future work are presented in Chapter 6.

Acknowledgments

First of all, the author owes his deepest gratitude to his PhD advisor, Dr. Donald G. Baird. This dissertation would not have been possible without Dr. Baird's support and guidance. The author greatly appreciates the tremendous time and effort Dr. Baird invested for improving the author's research skills and motivating the author to understand his subjects in a much deeper level. Beyond supervising the author on his laboratory research, Dr. Baird also kindly and patiently improved the author's language and communication skills, especially writing, which is critical for an international student.

The author is also very grateful to his committee members as follows:

Prof. Garth Wilkes is always open for discussions even though he is quite busy and has limited free time. The discussions with Dr. Wilkes are always productive, which intrigues the author to analyze the existing experiment results more thoroughly, as well as develops new ideas in his research.

Prof. Steve Martin kindly provides the access to the equipment in his laboratory. The author would also like to thank Dr. Martin for attending his departmental seminar and providing valuable suggestions and comments.

Prof. Tim Long assisted the author with his questions regarding the chemistry of the materials. The author would also like to thank Dr. Long for asking intriguing questions in his prelim examination.

Besides the faculty members in his committee, the author would like to thank Prof. Charles Frazier in the Department of Sustainable Materials for granting access to the differential scanning calirometry instrument in his laboratory.

The author thanks his many colleagues in the polymer processing lab for the experimental assistance as well as various discussions (in no particular order): Jianhua Huang, Chen Chen,

Kevin Meyer, John Hofmann, Syed Mazahir, John Quigley, Kevin Harrington, Mark Cieslinski, Craig Mansfield, Rebecca Minnick, Hongyu Chen, Greg Lambert, Jianger Yu and Juan Caceres.

The author would like to thank the staff in the Chemical Engineering Department at Virginia Tech: Diane Cannaday, Tina Russell, Nora Bentley, Jane Price, Malenie Darden, Kevin Holshouser and Michael Vaught.

This dissertation is dedicated to the author's wife and his parents Nan Hu, Junhua Qian and Jianhua Wang. The author also appreciates the support from his parents in law Linshan Hu and Yunpeng Li. Without their unconditional love and support, the completion of this dissertation would be impossible.

Table of Contents

List of Figures

List of Tables

1 Introduction

Thermotropic liquid crystalline polymers (TLCPs) have attracted great interest because of the combination of their promising properties, which includes high stiffness and strength, excellent processability, low permeability to gas molecules, low linear thermal expansion coefficient, reduced dielectric constants and outstanding chemical resistance [1-5]. Because of these properties, TLCPs have been used in various applications, such as the reinforcing components in TLCP/thermoplastic blends, barrier material for packaging, as well as electrical parts [4, 6-9]. TLCPs also show promise in emerging fields, such as high pressure hydrogen fuel storage and fused filament fabrication [10-12].

The overall goal of this dissertation is to understand the rheological behavior of the neat TLCPs and the TLCP/TLCP blends in the super-cooled state, and apply that knowledge to practical processing, such as extrusion blow molding. This chapter provides some brief background information on the TLCP materials as well as summarizes the previous work relating to this dissertation and specifies our objectives.

1.1 An introduction to the properties of TLCPs

TLCPs are high performance engineering thermoplastics, which offer a balance of properties unmatched by most other resins. TLCP materials are known for their outstanding strength and high stiffness. For example, the strength and modulus of TLCP fibers approach 1500 MPa and 100 GPa, respectively [13], which are values approaching to the mechanical properties of carbon fibers (strength 3500~4500 MPa, modulus 150~200 GPa [14]). The mechanical properties of the injection molded TLCP parts are in the range of 100 to 200 MPa for strength and 8 to 20 GPa for modulus, depending on the processing conditions. Moreover, TLCPs are one of the least permeable polymeric materials. Although the liquid crystalline order does not

dramatically impede the transportation of gas molecules, it effectively lowers the solubility of gases in TLCPs, offering TLCPs exceptional barrier properties [15-16].

1.2 Shear rheology of TLCPs

Commercial TLCPs exhibit inherently low viscosity relative to many other conventional thermoplastics. The low melt viscosity gives rise to enhanced processability of TLCPs using techniques such as injection molding. However, it is detrimental to processes requiring high melt strength, such as extrusion blow molding, film blowing, thermoforming and multilayer coextrusion [17]. Several methods have been developed to modify the rheological characteristics of TLCPs, such that their viscosity can be enhanced. These methods include adding fillers to the TLCP matrices, and chemically modifying the structure of TLCP molecules.

Done and Baird [18-19] developed a unique method to increase the viscosity of TLCPs by first raising the temperature above the melting point (T_m) to exclude all solid crystalline structure and then lowering the temperature below T_m to super cool the materials [20]. The processing temperature window in the super-cooled state was determined by small amplitude oscillatory shear (SAOS) measurements in the temperature ramp mode. When being processed in the super-cooled state, the viscosity and melt strength of TLCPs were effectively improved. Such a method resulted in the successful extrusion blow molding and film blowing of TLCPs. However, the viscosity increment in the super-cooled state was not quantified. In this work, we used the combined methods of SAOS, DSC and the startup of shear flow to determine the processing temperature of a representative TLCP in the super-cooled state. The viscosity increment in the super-cooled state was also obtained from the startup of shear flow.

TLCPs demonstrate much more complicated transient rheological behavior than conventional flexible polymers. In the startup of shear flow, multiple stress overshoots were observed [21-25], the stress relaxation contained a rapid initial part and a subsequent long tail upon flow cessation [24]. The interrupted shear measurements showed a sufficient period of relaxation was required to regain the stress overshoots [22, 25], and the flow reversal seemed to not have significant influence on the stress response [25]. The unusual rheological behavior originated from the two structure entities in the nematic melt. On the molecular level, the orientation of the rigid, rod-like TLCP molecules is coupled with the flow in a complex way that the rheological response actually reflects the orientation dynamics of the molecules. On the mesocopic level, the orientation of the molecules varies spatially. The molecules with the relative uniform orientation are clustered to form the polydomain structure, as shown in Fig 1.1. The transient rheological response is also related to the deformation/rearrangement of the microstructure.

Although the transient rheology of TLCPs above T_m has been well documented, the transient rheology of TLCPs in the super-cooled state has yet to be investigated. In this work we try to determine how cooling the TLCP to the super-cooled state will affect the transient rheological behavior, such as the transient stress response in the flow cessation and interrupted shear measurements.

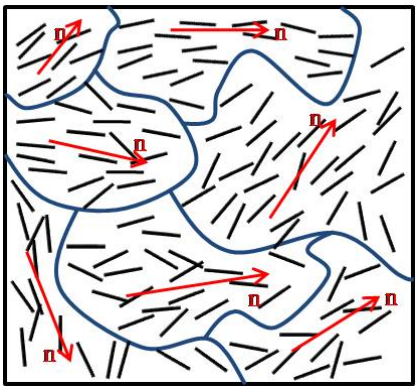

Figure 1.1: Polydomain structure of liquid crystalline polymer. Each domain is composed of rod like molecules and has irregular shape. The average orientation of each domain is represented by a director **n**.

1.3 Processing of TLCP/polyolefin blends

To exploit the outstanding mechanical properties of TLCPs, TLCPs have been blended with various thermoplastics. For most polymeric blends reported so far, TLCPs are the minor components and form a microfibrillar phase to provide mechanical reinforcement. The blends with superior mechanical properties relative to the pure matrices are usually referred to as in situ composites.

The in situ composites based on TLCP and polyolefins have been developed using techniques such as injection molding [26] and film blowing [27-28]. The in situ composites usually demonstrates improved moduli relative to the polyolefin matrices, but the increment in strength is marginal due to the lack of interaction between the two phases. Although the TLCP/polyolefins blends have been processed by means of injection molding, film extrusion, filament extrusion and film blown. Nevertheless, it remains unknown whether bottles based on TLCP and HDPE can be produced by extrusion blow molding. In this work we try to determine the processing conditions for the extrusion blow molding of TLCP/HDPE.

1.4 Properties of blends containing two TLCPs

Because of the limited types of commercial TLCPs available, researchers have blended two TLCPs to expand the potential applications of TLCPs. The TLCP/TLCP blends have demonstrated distinctive properties relative to the neat components. One important characteristic possessed by the blends is the improved mechanical properties [29-33]. Both the modulus and strength of the TLCP/TLCP blends could be greater than those of the neat components. Some of the TLCP/TLCP blends also exhibit lower viscosity relative to the neat resins, which could be beneficial for processing [30, 34-35].

The thermal properties of the TLCP/TLCP blends may also vary from those of the neat materials. McLeod and Baird [36] reported the melting and crystallization temperatures of a TLCP can be tailored by blending it with a second TLCP of lower melting point. Both TLCPs used in this work were synthesized from HBA, terephthalic acid, hydroquinone and hydroquinone derivatives, but the monomer ratios were different for the two TLCPs. The TLCP containing a greater amount of HBA exhibited a higher melting point of around 330 ^{o}C, while the other TLCP melted at about 272 ^{o}C. One intriguing observation was that the crystallization temperature of the blends was a linear function of the ratio of two TLCPs. The lower melting and crystallization temperatures of the TLCP/TLCP blends allowed them to be combined with thermoplastics possessing lower processing temperatures.

McLeod and Baird's work focused on the effect of the cooling rate on the crystallization temperatures of the TLCP/TLCP melts. However, to process TLCP/TLCP blends in the super-cooled state, knowing the melting and crystallization temperatures from the temperature ramp experiments is not enough. So far no work has been done on melting the TLCP/TLCP blends first, and then cooling them down to the predetermined temperatures below the melting point and

tracking isothermal crystallization. The isothermal crystallization behavior at different temperatures below the melting point is of critical importance on guiding processing. If at certain temperatures the TLCP/TLCP blends crystallize too fast, then these temperatures can not be applied in processing. The last objective of this work is to determine how the isothermal crystallization behavior of a TLCP can be adjusted by blending it with another TLCP of lower melting temperature. In this work the TLCP/TLCP blends and neat resins were fully melted first, and then cooled down to constant temperatures below the melting point. The isothermal crystallization was monitored using both dynamic mechanical and DSC techniques.

1.5 Research objectives

The three research objectives of this dissertation are summarized as follows:

1. Determine the temperatures in the super-cooled state that could be used for TLCP processing, using the combined techniques of SAOS, DSC and the startup of shear flow. Another focus is to determine how cooling the TLCP to the super-cooled state could affect the transient rheological behavior.

2. Determine the processing conditions for the extrusion blow molding of TLCP/HDPE blends, and assess the mechanical properties as well as the morphology of the blow molded bottles.

3. Determine how the isothermal crystallization behavior of a TLCP can be adjusted by blending it with another TLCP of lower melting temperature, using SAOS and DSC in the isothermal time sweep mode. Additionally, evaluate the sensitivities of the two approaches for detecting isothermal crystallization.

References

[1] H. G. Chae and S. Kumar, "Rigid-rod polymeric fibers", *Journal of Applied Polymer Science*, vol.100, pp 791-802, 2006.

[2] J. S. Chiou and D. R. Paul, "Gas transport in a thermotropic liquid-crystalline polyester", *Journal of Polymer Science Part B: Polymer Physics*, vol.25, pp 1699-1707, 1987.

[3] N. R. Miranda, J. T. Willits, B. D. Freeman and H. B. Hopfenberg, "Organic vapor sorption and transport in a thermotropic liquid crystalline polyester", *Journal of Membrane Science*, vol.94, pp 67-83, 1994.

[4] T.-s. Chung, *Thermotropic liquid crystal polymers : thin-film polymerization, characterization, blends, and applications*, Technomic Pub. Co., Lancaster, 2001.

[5] A. Donald, A. Windle and S. Hanna, *Liquid Crystalline Polymers*, Cambridge University, 2006.

[6] X. Zhao, K. Nair, P. Yung, G. Barber, S. Gray, Y. S. Kim and A. Maliqi, U.S. Patent, US9206300 B2,2015.

[7] A. A. Handlos and D. G. Baird, "Processing and Associated Properties of In Situ Composites Based on Thermotropic Liquid Crystalline Polymers and Thermoplastics", *Journal of Macromolecular Science, Part C*, vol.35, pp 183-238, 1995.

[8] J. Lange and Y. Wyser, "Recent innovations in barrier technologies for plastic packaging - a review", *Packaging Technology and Science*, vol.16, pp 149-158, 2003.

[9] R. Lusignea, "High-barrier packaging with liquid crystal polymers", *Tappi Journal*, vol.80, pp 205-212, 1997.

[10] C. Qian, C. Mansfield and D. G. Baird, "Thermotropic liquid crystalline polymers and their fiber reinforced composites for hydrogen storage applications", *Annual Technical Conference*, edited by (Society of Plastics Engineers, 2014), vol.

[11] R. W. Gray, D. G. Baird and J. H. Bøhn, "Effects of Processing Conditions on Short TLCP Fiber Reinforced FDM Parts", *Rapid Prototyping Journal*, vol.4, pp 14-25, 1998.

[12] D. G. Baird, M. Ansari, C. D. Mansfield and C. Qian, "Generation of thermotropic liquid crystalline polymer thermoplastic composite filaments and their processing in fused filament fabrication", *251st ACS National Meeting*, edited by (American Chemical Society, 2016), vol.

[13] E. Kalfon-Cohen, G. Marom, E. Wachtel and A. Pegoretti, "Characterization of drawn monofilaments of liquid crystalline polymer/carbon nanoparticle composites correlated to nematic order", *Polymer*, vol.50, pp 1797-1804, 2009.

[14] M. W. Hyer and W. S. R., *Stress analysis of fiber-reinforced composite materials*, DEStech Publications Inc, Lancaster, PA., 2009.

[15] A. A. Collyer, *Liquid crystal polymers : from structures to applications*, Elsevier Applied Science, London, 1992.

[16] D. H. Weinkauf and D. R. Paul, "Gas transport properties of thermotropic liquid-crystalline copolyesters. I. The effects of orientation and annealing", *Journal of Polymer Science Part B: Polymer Physics*, vol.30, pp 817-835, 1992.

[17] Z. Li, Z. Zhou, S. R. Armstrong, E. Baer, D. R. Paul and C. J. Ellison, "Multilayer coextrusion of rheologically modified main chain liquid crystalline polymers and resulting orientational order", *Polymer*, vol.55, pp 4966-4975, 2014.

[18] K. G. Blizard and D. G. Baird, "Blow molding of thermotropic liquid crystalline polyemrs", *International Polymer Processing*, vol.3, pp 172, 1989.

[19] K. G. Blizard, T. S. Wilson and D. G. Baird, "Film blowing of thermotropic liquid-crystalline polymers", *International Polymer Processing*, vol.5, pp 53-61, 1990.

[20] D. Done and D. G. Baird, "Solidification behavior and recovery kinetics of liquid crystlline polymers", *Polymer Engineering and Science*, vol.30, pp 989, 1990.

[21] F. Beekmans, A. D. Gotsis and B. Norder, "Transient and steady-state rheological behavior of the thermotropic liquid crystalline polymer Vectra B950", *Journal of Rheology*, vol.40, pp 947-966, 1996.

[22] T. Guo, G. M. Harrison and A. A. Ogale, "Transient shear rheology and rheo-optical microstructural characterization of a thermotropic liquid crystalline polymer", *Polymer Engineering and Science*, vol.45, pp 187-197, 2005.

[23] S. M. Guskey and H. H. Winter, "Transient shear behavior of a thermotropic liquid-crystalline polymer in the nematic state", *Journal of Rheology*, vol.35, pp 1191-1207, 1991.

[24] H. C. Langelaan and A. D. Gotsis, "The relaxation of shear and normal stresses of nematic liquid crystalline polymers in squeezing and shear flows", *Journal of Rheology*, vol.40, pp 107-129, 1996.

[25] G. G. Viola and D. G. Baird, "Studies on the transient shear flow behavior of liquid crystalline polymers", *Journal of Rheology*, vol.30, pp 601-628, 1986.

[26] A. Datta and D. G. Baird, "Compatibilization of thermoplastic composites based on blends of polypropylene with two liquid crystalline polymers", *Polymer*, vol.36, pp 505-514, 1995.

[27] S. Saengsuwan, S. Bualek-Limcharoen, G. R. Mitchell and R. H. Olley, "Thermotropic liquid crystalline polymer (Rodrun LC5000)/polypropylene in situ composite films: rheology, morphology, molecular orientation and tensile properties", *Polymer*, vol.44, pp 3407-3415, 2003.

[28] W. Chinsirikul, T. C. Hsu and I. R. Harrison, "Liquid crystalline polymer (LCP) reinforced polyethylene blend blown film: Effects of counter-rotating die on fiber orientation and film properties", *Polymer Engineering and Science*, vol.36, pp 2708-2717, 1996.

[29] F. J. Vallejo, I. Iribarren, J. I. Eguiazabal and J. Nazabal, "Structure and mechanical properties of blends of two thermotropic copolyesters", *Polymer Engineering and Science*, vol.42, pp 1686-1693, 2002.

[30] S. Kenig, M. T. DeMeuse and M. Jaffe, "Properties of blends containing two liquid crystalline polymers", *Polymers for Advanced Technologies*, vol.2, pp 25-30, 1991.

[31] F. J. Vallejo, J. I. Eguiazábal and J. Nazábal, "Blends of a thermotropic copolyester and a thermotropic copoly(ester–amide): structure and mechanical properties", *Polymer*, vol.42, pp 9593-9599, 2001.

[32] F. J. Vallejo, J. I. Eguiazabal and J. Nazabal, "Blends of two thermotropic liquid crystalline polymers: the influence of reactions during injection molding on the phase structure and the mechanical behavior", *Polymer Engineering and Science*, vol.41, pp 1115-1123, 2001.

[33] M. Garcia, J. I. Eguiazabal and J. Nazabal, "Miscibility level and mechanical characterization of blends of two liquid-crystalline polymers based on p-hydroxybenzoic acid", *Journal of Polymer Science Part B: Polymer Physics*, vol.41, pp 1022-1032, 2003.

[34] Y. G. Lin and H. H. Winter, "Rheology of phase-separated blends of two thermotropic liquid-crystalline copolyesters", *Polymer Engineering and Science*, vol.32, pp 773-776, 1992.

[35] T.-T. Hsieh, C. Tiu, G. P. Simon and R. Yu Wu, "Rheology and miscibility of thermotropic liquid crystalline polymer blends", *Journal of Non-Newtonian Fluid Mechanics*, vol.86, pp 15-35, 1999.

[36] M. A. McLeod and D. G. Baird, "The crystallization behavior of blends of thermotropic liquid crystalline polymers", *Polymer*, vol.40, pp 3743-3752, 1999.

2 Literature Review

2.1 Liquid Crystalline Polymer Fundamentals

2.1.1 Orientation of Rod Like Molecules in Liquid Crystalline Phases

The term mesophase refers to the stable intermediate ordered phase between the isotropic liquid and ordered solid states, and it is usually used synonymously with the liquid crystalline phase nowadays. Interestingly, the original name of 'liquid crystals' lead to the misunderstanding of the structure being either crystalline or liquid. The term 'mesophase' was first introduced to clarify the conceptual error and emphasize the uniqueness of the distinct intermediate phase [1]. The three most common mesophases are the nematic, the semectic and the cholesteric. A schematic representation of these mesophases is shown in Figure 2.1. The ellipsoids in this figure are the molecular species which are capable of forming the liquid crystalline phases. In the nematic phase, molecules possess long range orientational order, as specified by the director **n**, but they lack any short range positional order. Smectic phases are so named because they have layered structures. Molecules packed in each layer exhibit the same orientation, and the orientation directors of all layers are parallel with one another. In any layer, there is no long range positional order among molecules. Likewise, there is no correlation between the lateral positions of the molecules in successive layers. Smectic A and smectic C are the two common variants of the smectic phase. In the smectic A phase, the layer director **n** lies along the layer normal, while there is a tilt angle between the layer director and layer normal in the smectic C phase. The cholesteric mesophase is composed of a pile of nematic layers along an axis perpendicular to layer directors. Each nematic layer is twisted from its neighboring layer with a constant angle.

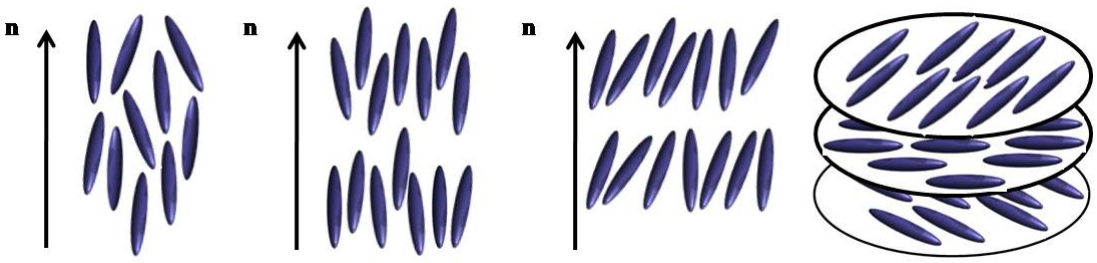

Figure 2.1: From left to right: the nematic phase, the smectic A phase, the smectic C phase and the cholesteric phase.

2.1.2 Polydomain Structure and Defects

For low molecular weight liquid crystal molecules, the monodomain is the common structure, in which all molecules orient in roughly same direction. On the other hand, for main-chain liquid crystalline polymers, the monodomain micro-structure is difficult to obtain. Typically, the orientation directors of the molecules varying spatially, rendering the polydomain texture [2]. The size of each domain is on the scale of a few microns [3]. Within each domain, the orientations of the molecules are relative uniform and can be represented by a domain orientation director **n**. However, the domain orientations are distributed heterogeneously in space. A two dimension polydomain structure scheme is demonstrated in Figure 2.2. The polydomain structures usually contain defects where the molecular orientation changes discontinuously with the most prevalent defects being disclination lines [2].

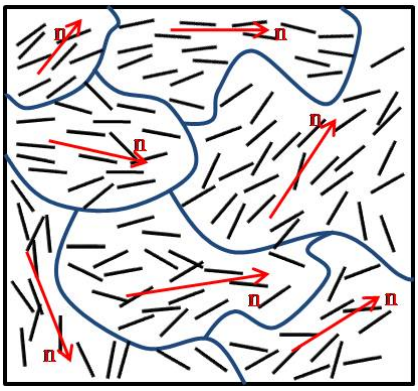

Figure 2.2: Polydomain structure of liquid crystalline polymer. Each domain is composed of rod like molecules and has irregular shape. The average orientation of each domain is represented by a director **n**.

2.1.3 Molecular Architecture of The Main Chain Thermotropic Liquid Crystalline Polymers

Based on the conditions required to exhibit mesophases, liquid crystalline polymers can be divided into two categories: lyotropic liquid crystalline polymers (LLCPs) and thermotropic liquid crystalline polymers (TLCPs). For LLCPs, the appearance of the mesophases depends on the concentrations of the polymer solutions. On the other hand, the liquid crystalline phase transitions are determined by temperature for TLCPs. Main chain TLCPs are the focus of this dissertation, along with their molecular architectures and the chemical compositions.

Rigid aromatic units (also known as mesogens) largely contribute to the formation of the liquid crystalline phases in the main chain TLCPs. Nevertheless, the melting points of polyesters, such as poly(4-oxybenzoyl) and poly(p-phenylene terephthalate, are so high that these polymers degrade before they melt. Therefore, main chain TLCPs are designed to contain other chemical units to lower the melting point while maintaining the linear confirmation and the capability of forming liquid crystalline phases. Main chain TLCPs with lower melting points are prepared by

three copolymerization techniques [4], which are disruptive chain packing, flexible spacers and non-linear links, respectively. A schematic illustration of these techniques is shown in Figure 2.3.

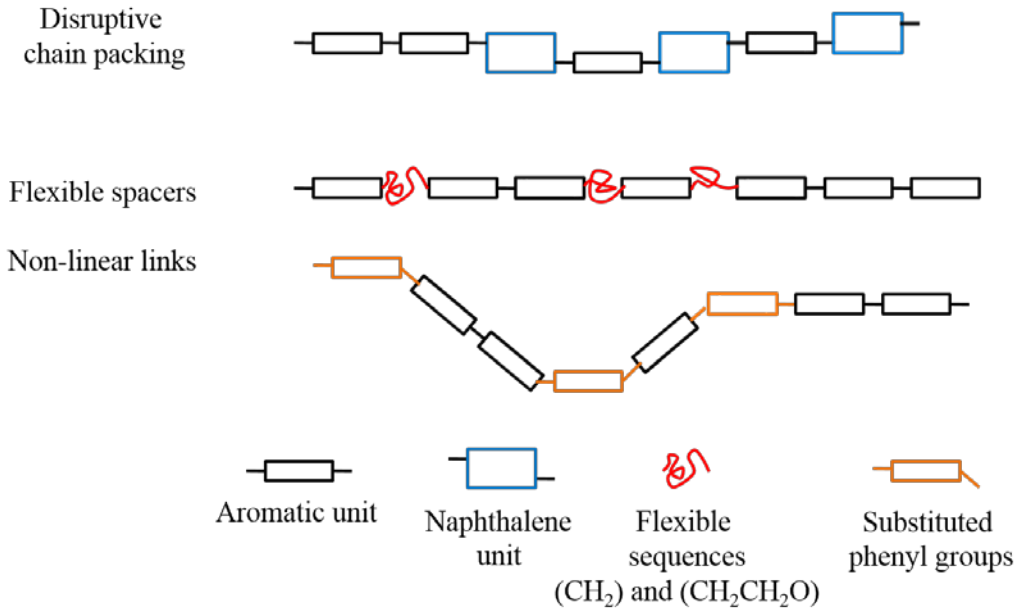

Figure 2.3: Lowering the melting points (T_m) of the main chain TLCPs by controlling the molecular architecture.

Disruptive chain packing utilizes the mechanism of increasing the inter-chain distances by steric effects and makes crystallization difficult. The naphthalene unit, biphenyl and substituted phenyl groups have been explored for this application [5-9]. Addition of the naphthalene units reduces the T_m very effectively. One of the most widely marketed commercial TLCPs, the Vectra A series by Ticona-Celanese, was synthesized by the copolymerization of the aromatic and the naphthalene units. In contrast, biphenyl and substituted phenyl groups were not as successful as the naphthalene unit in either lowering the T_m or maintaining the thermal stability of the molecules. Flexible spacers refers to the short flexible sequence such as (CH_2) and (CH_2 CH_2O) [10]. The incorporation of (CH_2CH_2O) led to production of the first commercial TLCP, X7G by Eastman

Kodak, which is a copolyester of p-hydroxybenzoic acid (HBA) and polyethylene terephthalate (PET). The third strategy for lowering the T_m is incorporating non-linear links, which can take the form of meta- or ortho-substituted phenyls and 1,6- or 2,5-linked naphthalenes [10-12].

2.1.4 Chemical Composition of Commercial TLCPs

Due to the changes in the product names and material manufacturers, tracking the chemical composition and properties of one particular commercial grade TLCP could be very challenging for newcomers in TLCP research field. Table 2.1 summarized the chemical formulations of certain commercial TLCPs. The manufacturers and monomer content (if available) is provided in Table 2.1 as well.

Table 2.1: Commercial thermotropic liquid crystalline polymers.

Material	Chemical Composition	Comments
Rodrun	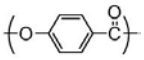 (HBA) 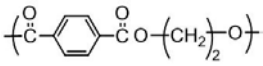 (PET)	Rodrun was developed under the codename of X7G by Eastman Kodak, it is now manufactured by Unitika, Japan. It is the first commercial TLCP available, containing either 60 mol% 4-hydroxy benzoic acid (HBA) -40 mol% polyethylene terephthalate (PET) or 80 mol% HBA-20 mol% PET. X7G was withdrew from the US market soon after its commercialization due to its poor performance at high temperatures.

(*cont.*)

Table 2.1 (*cont.*)

Material	Chemical Composition	Comments
Vectra	Vectra A 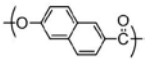 (HNA) 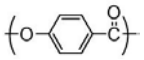 (HBA) Vectra B 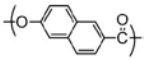 (HNA) 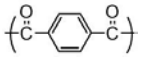 (TA) 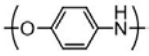 (AP)	Vectra series is a broad range of TLCPs developed by Hoechst, which is now marketed by Ticona-Celanese. The well studied Vectra A 950 is a copolyester containing 27 mol% 2-hydroxy-6-naphthoic acid (HNA) and 73 mol% HBA. Vectra B 950 is a polyesteramide of 60 mol% HNA, 20mol% terephthalic acid (TA) and 20 mol% 4-aminophenol (AP). The Vectra series has been extensively discussed in the literature.
Zenite	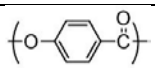 (HBA) 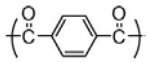 (TA) 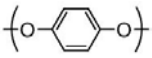 (HQ)	Zenite is a class of TLCPs originally developed by Dupont, then it was brought by Ticona-Celanese. Zenite molecules contain various amount of HBA, TA and hydroquinone (HQ), but the detailed monomer contents belong to the proprietor. Some grades of Zenite show good high temperature properties, such as HX-3000 and HX-6000 (melting point above 330 ^{o}C).

2.2 Crystallization and solidification behaviors of TLCPs

2.2.1 Crystalline Structure of TLCPs

The crystallization behavior of the TLCPs is distinctive from those of the conventional flexible polymers. Blundell [13] examined the quenched and slow-cooled 40 mol% HBA-60 mol% HNA nematic melts by monitoring their heat flow and structure change, using X-ray diffraction (XRD) and thermal analysis, respectively. Although the differential scanning calorimetry (DSC) traces of the two samples were very similar, which gave almost identical melting peaks for two thermal treatments, the XRD results only revealed well defined crystals in the slow-cooled sample, with no crystal scattering signal captured for the fast quenched sample. The author made the interpretation that the XRD technique used in this work was not able to detect the crystals less than 30 Å.

Blundell attributed such differences to the reduced surface energy of the nematic liquid crystal state. For flexible polymers, polymer chains can easily adjust their confirmations and incorporate their segments into the three dimensional crystal lattices, and thus the lamellar crystal morphology is commonly observed [14]. Their surface energy is mainly contributed by three parts:

(i) The interfacial energy associated with the boundary between the amorphous and the crystalline phases;

(ii) The strain energy due to the sharp folding of the molecules and the density adjustment across the fold surfaces;

(iii) The restriction in entropy of the molecule segments attached to the crystal lattices.

In contrast to flexible polymers, the movements of the stiff TLCP chains are spatially confined, making chain folding almost impossible. The above contributions (ii) and (iii) are

relative small compared with the interfacial contribution (i). Based on the discussion above, Blundell then pictured the morphology above and below the melting point for both flexible polymers and TLCPs, which is reproduced in Figure 3.4. For the nematic phase formed above the melting temperature, rod-like TLCP chains adopt extended confirmation rather than random coils, the molecules can only either slide pass each other along the chain direction (longitudinal translation), or rotate along their axes. Upon fast quenching, stable nuclei were formed in the regions where the chain segments possessed long range positional order. However, due to the restriction of the molecular motions, the perfection of crystals was prevented, resulting in small crystal sizes. The whole process was associated with low enthalpy and entropy of fusion, which were due to chain stiffness and retarded crystal growth, respectively.

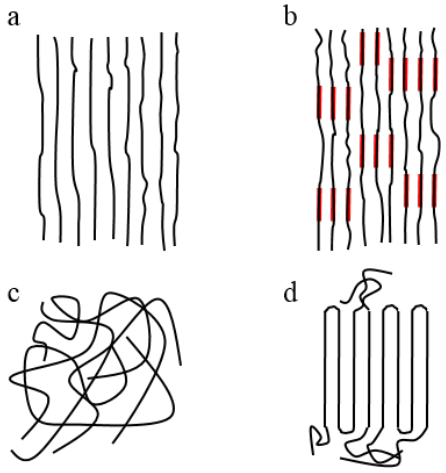

Figure 2.4: Schematic description of the morphologies above and below the melting points for both conventional flexible polymers and TLCPs: (a) nematic phase of a TLCP above the melting point, (b) crystalline structures of a TLCP below its melting point, the thicker regions highlight the crystal lattices, (c) entangled flexible polymer chains above melting point, and (d) the lamellar crystalline structure of flexible polymers. (Reprinted from ref [13])

2.2.2 The Crystallinity of TLCPs

Depending on monomer ratio, molecular weight, thermal and mechanical histories of the samples, measurement techniques, as well as interpretation methods, the reported crystallinities of TLCPs are scattered over a broad range. Blundell [13] reported a 21% crystallinity for the 40 mol% HBA-60 mol% HNA with molecular weight in the range of 10000 to 30000 g/mol. Butzbach *et al.* [15-16] clamed a much higher crystallinity of ~30% for the directly quenched 58 mol% HBA-42 mol% HNA, and with post crystallization upon thermal annealing a degree of crystallinity exceeding 60% was obtained. Unfortunately, neither the molecular weight nor the characterization technique was specified in Butzbach's work. Hanna *et al.* [17] analyzed a low molecular weight (~5000 g/mol) 75 mol% HBA-25 mol% HNA material, and a crystallinity of 19% was obtained for the sample annealed at 200 ^{o}C. Later the same group analyzed the same material using electron microscopy [18], a lower crystallinity (13%) was obtained for the sample being prepared under the same conditions. The contradictory results were attributed to the amount of the crystals destroyed by the electron radiation, leading to the conclusion that 13% crystallinity was likely an underestimation [18].

Wilson *et al.* [19] systematically investigated the crystallization kinetics and the crystallinity of the HBA-HNA TLCPs with wide ranges of monomer ratios (from 80 mol% HBA-20 mol% HNA to 25 mol% HBA-75 mol% HBA) and molecular weights (4600~14400). Precise XRD measurements offered the crystallinity values between 17.5% and 25.5%. Equal HBA/HNA ratio and thermal annealing induced lower crystallinity. It is interesting to note the crystallinities of the poly(HBA) and poly(HNA) were estimated to be 75% and 50% [20], respectively. The random copolymerization of HBA and HNA reduced not only the melting points of the two homopolymers, but their crystallinities.

2.2.3 Kinetics of Mesophase Transitions in TLCPs

Cheng [21] provided insights into the kinetics of mesophase transitions under both nonisothermal and isothermal conditions. The materials used were HBA/HNA copolymers with three monomer ratios: 75/25, 58/42 and 30/70, the molecular weights of all three grades were comparable (~30000). In nonisothermal experiments, all three copolymers behaved differently. For the 58/42 copolymer, the width of the exothermic peaks was almost unchanged under all cooling rates tested, indicating the transition rate was faster than the cooling rate. Such a process was defined as solidification rather than true supercooling [22-24]. In contrast to the 58/42 copolymer, peak width broadening was observed for the 75/25 copolymer as the cooling rate decreased. The crystallization mechanisms for the two copolymers were essentially different. The 75/25 copolymer was rich in the HBA unit, so the polymers were likely to migrate cross the phase boundary to aggregate and form crystals by matching the HBA counits while rejecting the minor HNA units. Because both the chain diffusion and the counits matching processes needed time, the crystallization of the 75/25 copolymer was highly cooling rate dependent. On the other hand, the monomer ratio in the 58/42 copolymer was close to equal and the two monomers altered randomly along the chain, such molecular composition rendered counit matching difficult, if not impossible. The nonisothermal transition of the 30/70 copolymer was expected to be closer to the 75/25 copolymer due to its richness in the HNA monomer. Remarkably, the 30/70 copolymer behaved more like the 58/42 copolymer rather than the copolymer with 75/25 monomer ratio because of the difficulties in matching the HNA counits. The formation of HNA crystals required the rotation of the HNA groups and the translational motion of the entire molecule. The former caused a twist of the molecular chain, which increased the rotational energy barrier, the later enhanced the

translational energy barrier due to the friction of the bulky HNA units, neither of which was easy to be achieved.

In isothermal experiments, two transition processes were distinguished for the copolymers with 75/25 and 30/70 compositions: a fast solidification (quenching) transition and a slow annealing transition. The crystals formed from quenching the nematic melts (fast process) were hexagonal packed, while the annealing generated more densely packed orthorhombic crystals. Two important conclusions were drawn from this study. Firstly, the growth of two crystal forms was completely independent of each other. The lower ordered hexagonal TLCP crystals were formed first, and they were not able to act as nucleation sites to stimulate the growth of the more closely packed orthorhombic crystals. Secondly, the unusual higher transition temperature of the less ordered hexagonal crystals was governed by entropy. The hexagonal crystals were expected to have lower transition temperatures compared with the more ordered orthorhombic form. However, this was not true in the experiments. Thermodynamically, the transition temperature was determined by the relative amplitude of ΔH and ΔS ($\Delta H/\Delta S$). For both the hexagonal and orthorhombic forms, the changes of enthalpy were relative small. The entropy change from the nematic melt to the orthorhombic crystal was lager due to its more ordered chain structure. Similar entropy determined transition temperatures can be found in polytetrafluoroethylene (PTFE) [25]. The work of Katio *et al.* [26] on the 73/27 HBA/HNA copolymer suggested the orthorhombic lattice might be composed of both HBA and HNA units. Chung *et al.*[27] revisited the isothermal crystallization mechanism of the 73/27 HBA/HNA copolyester. In the low-temperature region (<495 K), a fast transition was found with the heat of fusion relatively unchanged with annealing time, slow transition was also shown, which was characterized by the increases in the transition temperature as well as the heat of transition with increasing annealing time. The observations

above matched the results observed in the 75/25 HBA/HNA copolymer [21]. However, apparent differences were also shown for these two copolymers regardless of their extremely close monomer ratios. Two transition peaks were observed for the 75/25 HBA/HNA annealed at 505 K, in the study of the 73/27 HBA/HNA only one transition peak was obtained. Based on the comparison above, Chung *et al.* claimed the slow transition in the 73/27 HBA/HNA was faster than the 75/25 HBA/HNA. The crystal lattice of the 73/27 HBA/HNA was also perfected to a higher order relative to 75/25 HBA/HNA. A conclusion was made that the 73/27 HBA/HNA had better chain sequence or crystallization capability.

2.2.4 Solidification Behavior

Done and Baird [28] investigated the solidification behavior of TLCPs from a processing standpoint. Three TLCPs were used: 60/40 HBA/PET, 80/20 HBA/PET and 73/27 HBA/HNA. All samples were preheated to 330 ^{o}C to exclude all crystalline structures. Materials were then cooled at a rate of 5 ^{o}C/min. The growth of G', G" and η* were monitored using a rheometer. It is worth noticing G" was greater than G' even when the temperature was decreased below the melting point, indicating the material was still deformable and exhibited fluid character. Such behavior is referred to as supercooling [28]. At a certain temperature below the melting point, all three parameters started to increase rapidly and G' began to dominate G", which was a sign of solidification. The degree of supercooling for the 60/40 HBA/PET and 73/27 HBA/HNA was around 50 ^{o}C. On the other hand, there was only a 20 ^{o}C supercooling for the 80/20 HBA/PET, the lower degree of supercooling might be due to the highest content of HBA in the material. Comparing with the 80/20 HBA/PET, G' and G" increased more gradually for the 60/40 HBA/PET and 73/27 HBA/HNA. Thus 60/40 HBA/PET and 73/27 HBA/HNA were more suitable to be used in the processes such as film blowing and blow molding. Following this word, McLeod and Baird

[29] demonstrated the solidification temperature of one TLCP could be lowered by blending it with a second TLCP whose melting temperature was lower: the solidification temperatures of the blends of Zenite HX-8000 and HX-6000 decreased linearly with the increasing HX-8000 concentrations, in which Zenite HX-6000 and HX-8000 contained different ratios of HBA, TA and HQ, but HX-6000 showed a solidification temperature 60 ^{o}C higher than HX-8000. Lin and Winter [30] reported the similar supercooling behavior for the 73/27 HBA/HNA, but they emphasized the molecular orientation relaxation in supercooling state. The material was first annealed above 320 ^{o}C, then thermally quenched to the desired temperatures T below its T_m. The solidification rate became faster as the temperature interval T_m-T was enlarged. Molecular orientations were imparted on the supercooled melts at T by applying a constant torque. Nevertheless, up to 4% of the strain was recoverable once the shear motion stopped. If T was slightly below the T_m, a large portion of strain immediately recovered and the strain induced molecular orientation relaxed more quickly. Larger T_m-T actually helped to "lock down" the strain and orientation, unless the sample was reheated above the melting point. The authors attributed the elastic response of the supercooled melt to the elastic nature of macroscopic structure formed during shearing.

2.3 TLCP Melt Rheology

Understanding the unusual flow behavior of the TLCPs is of critical importance for optimizing the processing conditions and achieving the targeted material performance. A comprehensive review of all the existing rheological studies of the liquid crystalline polymers (lyotropic and thermotropic) is beyond the scope of this section. Instead, this section offers a brief summary of the unique rheological characteristics of the TLCPs which are closely related to

material processing and may provide guidance into the control of physical properties during processing.

2.3.1 Linear Viscoelasticity

Guskey and Winter [31] identified the linear viscoelastic region in the dynamic measurements for the Vectra A900. Vectra A900 is a random copolyester of 73/27 HBA/HNA. From the strain sweep measurements, the complex modulus, G*, was plotted against the strain amplitude in the frequency range of 1.0~15 rad/s. The onset of the nonlinear range was shown to be dependent on shear frequency. As the shear frequency increased, the nonlinear viscoelastic range shifted to lower strain. This phenomena distinguished Vectra A900 from the conventional flexible polymers, whose nonlinear viscoelastic region was limited by a characteristic strain and independent of frequency. Additionally, G* was normalized with respect to the values in the linear viscoelastic region, and normalized G* at different frequencies collapsed into one master curve when it was plotted against the shear stress amplitude, indicating a characteristic stress about $2X10^4$ Pa.

Romo-Uribe *et al.* [32] revealed the dependence of linear viscoelasticity on molecular weight (4600 to 30000 g/mol) for the Vectra A900. In small strain oscillatory measurements, the onset of nonlinear viscoelastic behavior occurred at a critical strain γ_c, which was independent of neither frequency nor molecular weights tested. This finding was actually in disagreement with the observations of Guskey and Winter [31]. The investigation on the existence of a characteristic stress for linear viscoelasticity was absent. Furthermore, in the linear viscoelastic region, storage modulus G' dominated loss modulus G'' over a broad range of dynamic frequency (10^{-2}~10^3 rad/s), providing molecular weight was higher than 5000 g/mol. For the lowest molecular weight, 4600

g/mol, G' was above G" at low frequency and G" started to surpass G' at high frequency. The change of mechanical loss angle δ (δ=tan^{-1}(G"/G')) with frequency (10^{-2}~500 rad/s) was also presented in this work. Almost all molecular weights showed concave shape curves with the minimum δ values around 1 rad/s, which corresponded to the rubbery-like behavior at intermediate frequency. On the other hand, the rheological behavior was predominately viscous at both ends of the frequency range. Somma and Nobile [33] extended the same topic to the higher molecular weight (3000 to 51000 g/mol) Vectra A900. The onset of nonlinearity (γ_c) was independent of molecular weights, but decreased with increasing frequency, as detected in strain sweep measurements. This finding supported the work of Guskey and Winter [31] in a qualitative manner. Meanwhile, the effects of molecular weights on the nonlinearity onset stress were more complicated. When the normalized G* was plotted as a function of stress, the characteristic stress shifted to a higher amplitude for several molecular weights, which was opposite to the trend shown by the critical strain. When G* was plotted as a function of stress, the data obtained with various molecular weights did not collapse onto one master curve. Somma and Nobile [33] also monitored the change of the dynamic moduli, G' and G", as shear frequency was increased from 0.1 to 500 rad/s. For molecular weight less than 3000, the crossover of G' and G" was found at intermediate frequencies. As molecular weights increased from 41000 to 51000, the crossover frequency occurred at lower frequencies. Most strikingly, although the shapes of the G' and G" curves were not exactly the same, the viscoelastic behavior of TLCP with the highest molecular weight (>50000) resembled that of conventional flexible polymers with the viscous region (G">G') at low frequency and the rubbery like region (G'>G") at high frequency. If such distinctive phenomena were not associated with the mechanical history of the samples, they can be interpreted as the molecular

entanglements of the TLCPs. Therefore, the higher molecular weight TLCPs demonstrated the combined features of both the nematic phase and the isotropic flexible polymers.

2.3.2 Steady State Shear Flow

Guskey and Winter [31] performed a thorough rheological characterization on Vectra A900 in the shear flow fields. Polymer pellets were molded into disks for the steady state measurement. Sample disks were equilibrated at 320 ^{o}C in the rheometer under nitrogen environment to completely melt the TLCP [34]. The temperature was then lowered to 290 ^{o}C for all the experiments. The viscosity of the Vectra A900 followed the power law function over the entire shear rate range (10^{-2}~10 s^{-1}) and no zero shear viscosity was observed. The first normal stress difference, N_1, was negative for shear rates below 0.5 s^{-1} and changed its sign for shear rates higher than 0.5 s^{-1}.

Cocchini *et al.* [35] pointed out the importance of sample preparation in obtaining reliable rheological data by showing the extreme long decay (>4000 s) of the normal stress after the Vectra A900 sample disk was loaded. The authors then adopted a strict sample preparation protocol to keep the consistency of the sample quality. The sample preparation procedures included extensive thermal relaxation and preshearing, by which the authors believed the complete normal force relaxation was guaranteed. A three region steady shear viscosity scheme was observed and shown in Figure 3.5, which was obtained by combining the data from both the rotational and capillary rheometers. As shown in Figure 3.5, the three zone viscosity scheme is considered one of the characteristic rheological behaviors of the liquid crystalline polymers [36]: a shear thinning region (region I) was first observed at low shear rates, followed by a viscosity plateau at intermediate shear rates (region II) and another shear thinning region at high shear rates (region III).

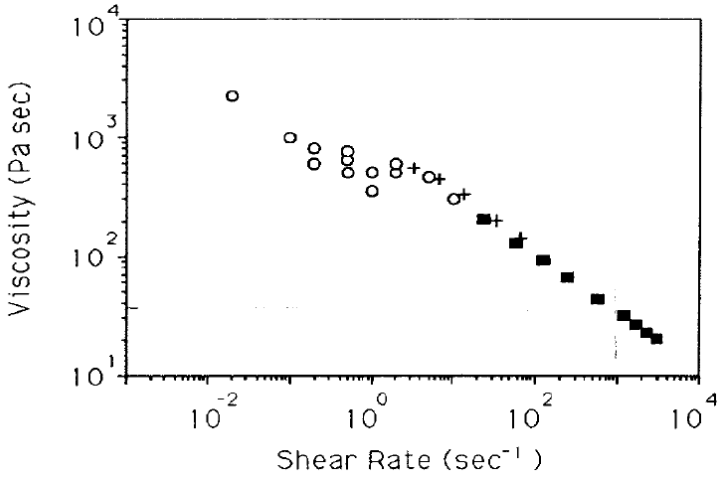

Figure 2.5: Steady viscosity versus shear rate for the Vectra A900. ○ represented data from rotational rheometer, ■ and + were obtained from capillary rheometer. At low and high shear rates (region I and III), material exhibited shear thinning. While at intermediate shear rate region (region II), the viscosity showed a Newtonian plateau. (Reprinted from ref [35])

Following the publications of Cocchini *et al.* [35], special efforts were made to control the TLCP sample quality for rheological measurements. Giles and Denn [37] developed a pressurized capillary rheometer, in which the flow of polymer melts were driven by the differential pressure instead of piston movement. This custom designed rheometer allowed for highly sensitive measurements in the relative low shear rate region. More importantly, sample bubble entrapments, which were caused by the evaporation of the volatile chemicals and degradation of the samples, were successfully eliminated when the sample was exposed to the hydrostatic pressure. Thus the shear measurements were no longer influenced by the foam texture. With offgassed samples, the viscosity flow curves were in qualitative agreement with the results obtained from the conventional rotational rheometer. In contrast, the viscosities of the samples without offgassing appeared to be higher.

In the majority of the studies the commercial TLCPs Vectra A900/950 were used. Both Vectra A900 and A950 are copolymers of HBA and HNA and they have the very similar monomer ratios (73/27 HBA/HNA for Vectra A900 and 75/25 HBA/HNA for Vectra A950), which presented the danger of considering the particular behavior of one material as the generalized properties of the whole class of materials. Thus, the rheological investigations on other commercial TLCPs were quite necessary. De'Neve *et al.* [38] presented an investigation on the rheological behavior of Vectra B950, which was another copolyesteramide produced by Ticona-Celanese. Comparing to the opaque Vectra A900/950, Vectra B950 was transparent at rest, which provided a better accessibility for the rheo-optical properties. The steady state viscosity as a function of shear rate was tested using both the cone-and-plate and capillary rheometers, covering shear rates from 0.1 to 10000 s^{-1}. A sliding plate apparatus was specially built for the rheo-optical measurements, which contained two glass plates: one stationary and the other movable. The adjustment of the velocity of the moving plate allowed controlling the shear rate from 0.1 to 10 s^{-1}. The apparatus was placed on the stage of a microscope, so that the texture change of the TLCP material under shear can be visually observed in a real time manner. At the same time the transmitted light flux, ϕ_t, was also recorded, serving as an independent method to investigate the shear-induced texture change. Unlike most publications, the authors did not give a detailed description on the sample loading/preshearing protocol, but they did mention the normal stress relaxed to zero within one minute, which was remarkable considering the extremely long normal force relaxation time of the Vectra A900/950 [35]. Both the steady state viscosity and N_1 curves showed two regions separated by a critical shear rate. At low shear rate, viscosity exhibited very weak shear thinning (almost a Newtonian plateau) and N_1 increased almost linearly with the shear rate. In the high shear rate region, there was a strong shear thinning for the viscosity and N_1 became

saturated. The texture of the Vectra B950 was governed by a well-defined critical shear strain, γ_{TW}, where the thread texture appeared at rest and transformed into a "worm texture" with a much higher defect density as the strain increased above γ_{TW} [38]. At the same time ϕ_t experienced a sharp drop above γ_{TW} due to the scattering of the light from the increasing defects. The critical shear strain, γ_{TW}, was independent of the sample thickness or the initial orientation of the sample, but γ_{TW} shifted to higher values as the shear rate increased.

Beekmans *et al.* [39] performed a more throughout rheological investigation on the Vectra B950. The initial state of the samples was defined by preshearing and relaxation. The shape of the viscosity curve resembled the classical one with three regions, as suggested by Onogi and Asada [36]. Comparing to the work of De'Neve *et al.* [38], the viscosities of the Newtonian plateau in both publications were on the same order. However, De'Neve and co-workers presented the absence of region I and a much lower viscosity in region III. Beekmans found the N_1 was everywhere positive and increased linearly with the shear rate. No saturation of N_1 was observed, as reported by De'Neve and co-workers.

2.3.3 Transient behavior

Viola and Baird [40] conducted one of the very first transient rheological studies on the TLCPs. The experimental results were compared with theoretical predictions to elucidate the nature of the transient shear behavior. In this work the Lesile-Ericksen theory [41] was employed, which predicted three phenomena in general:

(i) A shear stress overshoot and a normal stress undershoot should appear at a constant small shear strain (less than 1) before they relaxed to the steady state. The positions of extremes were independent of the shear rates.

(ii) The shear stress relaxed to zero instantaneously upon the shear cessation.

(iii) The stress overshot would occur due to the reorientation of the molecules, once the TLCP molecules were aligned, the orientation was maintained after the flow stopped. Stress overshoot could no longer be observed once the shear motion was recovered.

Different transient shear flow protocols (shear inception, interrupted shear and flow reversal) were used to monitoring the shear stress growth of the 60/40 HBA/PET copolymer. In the shear inception experiments, sharp overshoots appeared to be occurring at a constant shear strain value of less than one, independent of the shear rates adopted (5 s^{-1} to 40 s^{-1}). The amplitude of these overshoots was elevated as the shear rates increased. If the shear rates were higher than 10 s^{-1}, the second overshoots were observed at higher shear strains. The stress then relaxed to a steady state. Once the flow stopped, the shear stress decayed to zero almost instantaneously, indicating the lack of yield stress for the 60/40 HBA/PET material. Interrupted stress growth experiments were performed with a range of relaxation periods (1 to 180 s) between the flow cessation and the flow continuation. Even after 180 s relaxation, the stress growth in the continued flow failed to replicate that in the flow inception: the first overshoots observed at the low shear strains in the flow inception were noticeably absent when the flow was continued. Compellingly, the second stress overshoots and the stress relaxation were unaffected. The flow reversal was also applied after the initial shear was interrupted, the stress response was basically identical to that in the interrupted shear experiments.

The predictions of the Lesile-Ericksen theory were in qualitative agreement with the experimental observations in terms of the stress overshoots at low strains, the instantaneous stress relaxation upon flow cessation and the identical stress responses in the flow reversal and the interrupted flow. However, the XRD measurements on the quenched samples suggested an overall

random molecular orientation. Such a finding was contradictory to the shear aligned orientation predicted by the Lesile-Ericksen theory. Viola and Baird [40] concluded that the shear stress overshoot was due to destructing and rearranging the polydomain structure rather than orienting the molecules along the shear direction. The Lesile-Ericksen theory predicted the experimental results for the wrong reasons.

Done and Baird [42] studied the transient behavior of the 60/40 HBA/PET and HBA/HNA (monomer ratio unspecified) copolymers. The materials were exposed to step strain in the shear flow field and the relaxation of the modulus $G(t, \gamma)$ was recorded. The focus of this work was to investigate the existence of any unique transient behavior of the rigid TLCP molecules following step strains, which was compared with that of the flexible chain polymers, such as polystyrene (PS) and polyethylene terephthalate (PET). In the case of flexible chain polymers, the relaxation of the shear modulus $G(t, \gamma)$ was usually composed of two separate parts: a linear relaxation modulus $G^0(t)$ and a strain dependent function $h(\gamma)$ [43], in which $h(\gamma)$ was referred to as the damping function. For flexible polymers $G(t, \gamma)$ decayed continuously without any discontinuity in the slope. For both TLCPs reported, $G(t, \gamma)$ experienced a fast decay first, followed by a long relaxation tail. The length of the relaxation tail became more remarkable as the temperature was lowered. The slow modulus decay was believed to be caused by the unmelted crystals, which persisted in the melt. As the temperature was raised well above the melting temperature, the remaining solid structure was destroyed, and the long relaxation tail vanished. More interestingly, when the samples were quenched from temperatures well above their melting points, the modulus behaved as if the materials were still at high temperatures as a result of supercooling.

The transient rheology study on Vectra A900 was conducted by Guskey and Winter [31]. The transient viscosity showed an overshoot at low strain ($\gamma < 10$). At the highest shear rate (1.0 s^-

^{1}), an undershoot appeared and the viscosity reached the steady state at about 75 strain units. In the case of the first normal stress difference, N_1, an initial overshoot was observed, followed by an undershoot for all three shear rates measured. At low shear rates (<0.5 s^{-1}), N_1 stayed negative as long as the strain was higher than 5. The stress relaxation in the flow interruption experiment was quite different from the observations of Viola and Baird [40]. Instead of instantaneously decaying to zero, the shear stress was not fully relax in 500 s. Resumption of the flow at the rate of 0.1 s^{-1} resulted in the reappearance of the shear stress peaks, whose magnitude was proportional to the relaxation time, but it never fully recovered the height of the original peak. The N_1 completely relaxed to zero at 300 s after the flow cessation and the initial N_1 peak reappeared upon the continuation of the flow.

Cocchini *et al.* [35] attempted to keep the initial conditions of the Vectra A900 samples consistent by applying the thermal treatment and preshearing before the shear motion started. In the transient stress growth experiments performed at the shear rates from 0.2 to 1 s^{-1}, the normalized shear stresses at different shear rates were found to be scaled pretty well with strain and so were the normal stresses. Although the normal stress growth curves were not normalized, which made them unable to be compared with the results from Guskey and Winter [31], the normalized shear stress growth curves showed at least qualitative agreement: the overshoot peaks appeared at low strain (< 25) for the shear rates of 0.2 and 0.5 s^{-1}, while both the overshoot and the follow-up undershoot were observed at 1 s^{-1}.

One major discrepancy in the publications of Guskey and Winter [31] and Cocchini *et al.* [35] was the sign of the transient N_1. Although the 'mystery' of the negative N_1 values was believed to be well understood for the lyotropic liquid crystalline polymers [44]. The existence of the negative transient N_1 values was still under debate for the TLCPs. In contrast to Guskey and

Winter's [31] observations of the negative N_1 at low shear rates, Cocchini *et al.* [35] reported all positive N_1 values over the entire shear range (0.02~10 s^{-1}). To explain this disagreement, Cocchini *et al.* [45] published another paper, which demonstrated the long decay of the normal stress after sample loading/squeezing procedures and the significant residual normal stress in the startup shear flow. If the residual stress experienced by the transducer at the beginning of the startup shear flow was taken as the "zero level stress", during the transient experiments, then the continuous decay of the normal stress led to an erroneous interpretation of the negative N_1 values. Cocchini *et al.* also rationalized their sample preparation technique by showing the normal stress reached the true zero value after long preshearing.

Han and Chang [46] repeated Guskey and Winter' experiments and obtained similar results as those published by Cocchini *et al.* and thus confirmed the positive N_1 values for the Vectra A900. On the other hand, Han and Chang did point out the long preshearing may introduce other problems such as sample structure change, transesterification reaction and polymer degradation. They suggested using TLCP materials with low nematic-isotropic transition temperatures to clear out the thermal and mechanical history, such as the materials adopted by Kim and Han [47]. The work of Kim and Han will be discussed in more details later in this section.

Langelaan and Gotsis [48] confirmed the normal stress residue discussed by Cocchini *et al.* and also found the shear stress relaxed much faster and it decayed completely to zero. To understand this phenomenon, the structure of a squeezed sample was analyzed by means of scanning electron microscopy (SEM), and a layered structure was discovered. Langelaan and Gotsis attributed the difference between normal and shear stress relaxations to the presence of this structure. They proposed that the adjunct layers can easily slide over each other, disclinations

associated with the elastic forces may exist between layers in the normal direction resulting in energy storage during squeezing and a slow release afterward.

Most, if not all, commercial TLCPs have the clearing temperatures above their melting points such that the polymers degrade before the nematic-isotropic phase transition occurs. The high clearing temperatures post challenges to erase the thermal history of the samples, which causes the ill-defined initial conditions. One method to overcome such problems was to adopt TLCPs with lower clearing temperatures, in which the nematic-isotropic transition was achievable. In a series publications from Kim and Han [47, 49-50], an aromatic polymer, poly[(phenyl sulfonyl)-*p*-phenylene 1,10-decamethylene-bis(4-oxybenzoate)], or PSHQ10, was synthesized. DSC showed PSHQ10 had a glass transition temperature of 88 ^{o}C, a melting point of 115 ^{o}C and a clearing temperature of 175 ^{o}C. By preshearing the material in its isotropic region and then slowly cooling it to its nematic state, the thermal history of the sample was erased and a well defined morphology was obtained. Shear and normal stress growths were measured as a function of time for different shear rates (0.107 to 1.07 s^{-1}) and temperatures (130 to 160 ^{o}C). Although not identical, the shapes of the shear and normal stress growth curves resembled those of the 60/40 HBA/PET [40] and Vectra A900 [31] in the startup shear flow. The shear stresses reached the maximum values rapidly (less than 20 strain units) and a secondary peak was observed at the highest shear rate, the amplitudes of the shear stress peaks dropped as the shear rate decreased, and undershoots were observed in the growths of N_1.

In the intermittent shear flow studies of the PSHQ10 material, after the cessation of the initial shear flow, the subsequent transient stress responses were investigated as a function of the duration of the rest period [47]. The transient shear stress exhibited one peak while the transient normal stress showed multiple peaks. The longer the relaxation period, the larger the peak

amplitudes were. However, even with a 67 h rest period, the subsequential transient overshoots were not able to fully recovery the amplitude of the original stress responses. Similar to the interpretation of Viola and Baird [40], the stress overshoot was attributed to the texture change of the material. The polydomain structure was disrupted by the applied shear stress such that the domains were stretched along the shear direction and broke up. In the rest period after the flow cessation, the dispersed domains started to recoalesce. However, extreme long time (more than 67 h) was required to fully recover the original polymerdomain structure.

Kim and Han [49] also presented experimental results for the modulus, $G(t, \gamma)$, relaxation in the step strain experiments using PSHQ10. In the isotropic region, the relaxation of $G(t, \gamma)$ can be separated into the product of two functions ($G^0(t)$ and $h(\gamma)$), just like for flexible chain polymers. Nevertheless, in the nematic state the relaxation of $G(t, \gamma)$ became slower such that $G(t, \gamma)$ was no longer factorable. The relaxation rate of $G(t, \gamma)$ with time increased as the temperature approached the clearing temperature. Preshearing had a great impact on the relaxation rate of $G(t, \gamma)$ in the nematic state, which altered the microstructure of the samples. When the samples were subjected to steady shear prior to the step strain experiments, $G(t, \gamma)$ decayed faster. Unfortunately, there was no existing theory relating the modulus relaxation to the microstructure of the materials.

The Vectra B950 copolymer exhibited distinctive transient shear behaviors compared to the Vectra A900/950 and PSHQ10. In the work of Beekmans and co-workers [39], the test samples were presheared/relaxed before shear inception. The shear stress growth curves of different shear rates scaled well with the strain, and they showed reproducible shoulder peaks at 10 and 70 strain units, after which the peaks reached their maximum values at approximately 180 strain units and oscillated for another 110 strain units before the final steady state was reached. The growth of the first normal stress difference gave the same trend. First a clear shoulder peak at 10 strain units and

then two oscillations with their maximums at 90 and 176 strain units. The shape of the stress growth curves of both the shear stress and the normal stress was rather unusual from that of all the TLCPs discussed above. Usually after preshearing and relaxation, a single overshoot would be found at the low shear strain instead of a shoulder peak. The stress may also drop to create an undershoot rather than increasing gradually to its maximum. The stress growth curves also had several oscillations, which was a common feature of the lyotropic liquid crystalline polymers but was rarely observed in TLCPs. Optical microscopy confirmed the threaded-wormlike texture transition upon the startup of shear flow, but the transmitted light intensity measurements were unable to identify the existence of a critical texture transition strain, as reported by De'Neve *et al.* [38]. Other transient experiments included the flow reversal and the stepwise increase/decrease of the shear rate. In all three types of experiments, transients were stronger in the normal stress than in the shear stress. In contrast, for the Vectra A900 the transient responses were equally low for both the shear and normal stresses upon flow reversal and stress overshoots were regained only if enough relaxation time was allowed. The behavior of Vectra B950 seemed to be closer to that of the lyotropic LCPs, in which a clear response in the shear stress and an even more pronounced increase in the normal stress were observed in flow reversal [51-52].

Guo and co-workers [53] performed in situ rheo-optical measurements on Vectra V400P to characterize the microstructures of the material in transient shear flow. Vectra V400P was a special grade of TLCP designed for packaging applications [54]. The normalized shear stress showed two peaks in the startup of shear flow. The first peak occurred at 2 strain units with a maximum stress value of 1, while the second peak appeared at about 100 strain units and its maximum stress value was 1.5. At 300 strain units, the shear stress finally reached the steady state. Meanwhile the evolution of the microstructure was recorded with a shear cell and a polarized

transmission optical microscope. The hot shear cell with two parallel quartz plates was staged in between the two polarizers of the microscope, whose polarization directions were perpendicular to each other. Similar to the observations reported before, the material showed threaded texture at rest, at precisely 2 strain unit (first shear stress peak in the start-up flow), and the domains started to align along the flow direction [38-39]. As the strain increased, the domains were broke up into smaller sizes and new defects were generated rapidly, leading to more black lines on the optical images and a sharp decrease in the transmitted optical intensity. Finally, at 25 strain units, the "explosion" of defects gave rise to completely darkened images, which were accompanied by the damped optical intensity. The texture change of the material was actually reversible in the relaxation period after the flow cessation, and the domains coalesced and recovered the threaded texture after 400 strain units. Meanwhile the optical intensity also increased to the level before the shear started. The visualization of the microstructure deformation/recovery provided direct evidence to support the earlier interpretation of the stress overshoots in the interrupted flow experiments [40].

Transient shear flow experiments have been adopted to investigate the orientation dynamics of the director. A director is a unit vector representing the preferred molecular alignment of a domain, as described in § 2.1.2. The behavior of the director can be classified into two modes in the nematic state: flow alignment and/or tumbling. In the case of flow alignment, the hydrodynamic torques on the director were balanced such that the director was aligned by the shear motion and maintained a fixed angle ("Leslie" angle) with respect to the shear direction [55]. Conversely, director tumbling occurred if the director experienced unbalanced hydrodynamic torques, resulting in the continuous rotation of the director. Director tumbling has been shown in lyotropic systems [56-57] with its most direct rheological demonstrations including the

pronounced stress oscillation [58-59] and the degree of molecular orientation in response to step changes in the shear rates [2, 60-61]. Tumbling also contributes to the negative N_1 values observed in the lyotropic LCPs [62-63].

Rendon *et al.* [64] investigated the orientation dynamics of both Vectra A950 and B950 in transient shear flow, using the in situ X-ray scattering technique. The custom built X-ray scattering platform contained a synchrotron X-ray source in conjunction with a high temperature shear cell and a high speed detector, which provided sufficient time resolution to observe the real time change in the molecular orientation. The 'anisotropy factor' (AF) was subtracted from the two dimensional X-ray scattering pattern to quantitatively describe the local orientation. In the limit of AF=1, molecules were perfectly aligned, whereas AF=0 indicated a random orientation status. Rendon *et al.* adopted the same sample preconditioning procedures developed by Beekmans and co-workers [39], but instead of keeping track of the growth of stresses, the 'anisotropy factor' was monitored in different transient flow protocols (flow inception, interrupted shear, flow reversal, shear rate step changes and flow cessation). The transient responses of the two materials in the flow inception and flow reversal did not clearly indicate whether these materials were the tumbling class or flow aligning class. However, Vectra A950 exhibited a strong transient response to the step increase/decrease in shear rate, which was strongly contradictory to the signatures of the flow aligning materials. Vectra B950 showed increased orientation in the relaxation period after flow cessation, which was absolutely incompatible with the shear-aligning dynamics. These indirect evidence suggested both Vectra A950 and B950 are materials in the director tumbling class.

2.3.4 Extensional rheology

Wilson and Baird [65] reported the transient elongational viscosity of the Vectra A900, using a rotary clamp extensional rheometer. The specially constructed system was capable of

handling low viscosity material at high temperature. The transient elongational viscosity showed the linear viscoelastic behavior at low strain level, followed by a subsequential mild strain hardening. This behavior was quite similar to that of the isotropic polymer melts such as HDPE [66] and PS [67]. However, for HDPE and PS, strain-hardening resulted from the branched molecular architecture or high molecular weight components in the molecular weight distribution, which may not be the case for TLCPs. Instead, residual crystallinity or strain induced crystallization were suspected to cause the strain-hardening. Another event worth noticing was the transient elongational viscosities slightly increased with the increasing deformation rates. Gotsis and Odriozola [68] studied the extensional viscosity of Vectra A950 in a commercial constant strain rate rheometer. With a fixed amount of strain, rate-thinning curves were obtained when extensional viscosities were plotted as a function of deformation rates. Besides, the thermal and mechanical histories of the samples played important roles in extensional viscosity. For example, because of the higher degree of molecular orientation, injection molded samples showed higher extensional viscosity than compression molded samples. Kernick and Wagner [69] investigated the transient elongation viscosity of the Zenite HX-8000-210 by Dupont. HX-8000-210 was a special grade of with a melting temperature of 210 ^{o}C. Plotting as a function of time, the transient elongation viscosity curves of the HX-8000-210 were very different from those of the Vectra A900 [65]. First of all, the material initially demonstrated a weak strain hardening, followed by a significant strain hardening which never reached a steady state. Secondly, elongational viscosity decreased with increasing deformation rate. When the transient elongational viscosities were replotted versus the accumulated strain, the extreme strain hardening regions all collapsed on the same "master curve", indicating the TLCP molecules all achieved the same highly ordered state along the elongation axis despite of the elongation rates. This interpretation was later confirmed

by measuring the molecular order parameters using XRD. Kernick and Wagner [69] stated the extreme strain hardening may be the source of the low flash (flash refers to the excess material attached to the molded product) of TLCPs in injection molding and allow precise mold filling applications. Last but not least, similar to Vectra A950 [68], rate-thinning behavior of the transient elongation viscosity was again observed.

2.4 Processing of TLCPs

TLCPs are high performance engineering thermoplastics, which offer a balance of properties unmatched by most other thermoplastic resins. TLCP materials are known for their great thermal stability, outstanding strength, high stiffness, excellent dimensional stability, very low warpage and shrinkage of molded parts, along with exceptional barrier properties. The inherent low melt viscosity of TLCPs arises from the ordering of rigid, rod-like molecules, and it leads to the high degree of melt processability of the materials. The combination of these properties makes TLCPs attractive candidates for extensive applications, such as high precision molding parts, ultra-high strength fiber, packing materials, as well as storage vessels for cryogenic fluids and high pressure gases. However, the unique molecular structure and flow behavior of the TLCPs also posses challenges for polymer engineers. The properties of TLCPs are largely determined by the molecular orientation, and the orientation and anisotropic properties remain a tough challenge to be conquered. The low viscosity makes TLCPs easier for extrusion compared with other high performance engineering plastics, such as polyethersulfone (PESF), polyetherimide (PEI) and polyether ether ketone (PEEK), but the same character is disadvantageous for the processes requiring high melt strength, such as extrusion blow molding, film blowing and thermoforming.

Common TLCP processing techniques are introduced in this section, along with the morphology and performance of the resulting products.

2.4.1 Injection molding

As one of the major polymer processing techniques, around 40% of all polymeric products are manufactured by injection molding [70]. Short cycle time, high flow in thin sections and exceptional repeatability of dimensions make TLCPs ideal materials for injection molding. Injection molded TLCP articles exhibit high mechanical properties, extremely low shrinkage and warpage and good dimensional stability at high temperature. Meanwhile anisotropy in physical properties, measured in the flow direction and across the flow direction, is usually observed due to the heterogeneous orientation distribution of the rod like molecules. The TLCP molecules are overall aligned in the flow direction and favors the properties in that direction.

2.4.1.1 Structural Characterization of Injection Molded TLCPs

Before discussing the influence of the injection molding parameters on the material properties, it is necessary to describe the morphology (hierarchical structure). The complex flow field in the mold filling process leads to a skin-core morphology of the injection molded TLCP articles. Ophir and Ide [71-72] found in the combined shear-elongation flow field, the elongation flow field was more effective in aligning the molecules along the flow direction rather than the shear stress, which was the major cause for the skin-core morphology of the articles. Thapar and Bevis [73] also observed the sheet-like structures by viewing the etched surfaces in the SEM. Weng *et al.*[74] developed a model to quantitatively describe the skin-core structure, which served as a basis to understand the properties anisotropy of injection molded TLCPs. The model is illustrated in Figure 2.6. The injection molded plaques were found to consist of three main

macrolayers: an isotropic core layer sandwiched between two more oriented skin layers. Each macrolayer accounted for approximately one-third of the total thickness. Three subdivisions can be distinguished based on their degree of orientation in each of the skin macrolayers. The top subdivision of the skin macrolayer was 20 μm thick and had the highest degree of orientation. The second subdivision beneath it contained several sub layers. Each sub layer was 30 to 50 μm thick and possessed a "mica-like" texture. The remaining innermost subdivision was a 500~700 μm thick region, in which the molecular orientation decayed gradually. The authors described this region as the less orientated subdivision. In the core region, plug flow gave rise to the parabolic shape flow lines, which were visible to the naked eye. The preferred orientation of TLCP molecules were found to be parallel to the flow lines. Similar skin-core morphology was also observed by other research groups [75-76].

Pirnia and Sung [77] outlined the three dimensional orientation profile in an injection molded end-gated plaque, which was dictated by the complex flow field during mold filling. The mold filling process is depicted in Figure 2.7. In the x-y plane the melt front was initially circular and started to flatten out as the filling time increased (t_1 to t_7). The x-z plane showed the cross section of the flow front. Far away from the gate, a strong z-component prevailed at the advancing front (fountain flow). Such elongation flow, combined with the high shear stress near the mold wall region, orientated the molecules along the flow direction. The low mold wall temperature immediately froze the orientation, inducing the formation of the skin layers. On the other hand, the influence of the shear stress on the molecular orientation was negligible in the core region, because the core region was distant from the mold wall. Thus, the core region possessed an overall in-plane (x-y plane) random orientation. The orientation results of rod-like molecules were in qualitative agreement with those of the short glass fiber reinforced thermoplastic [78-79].

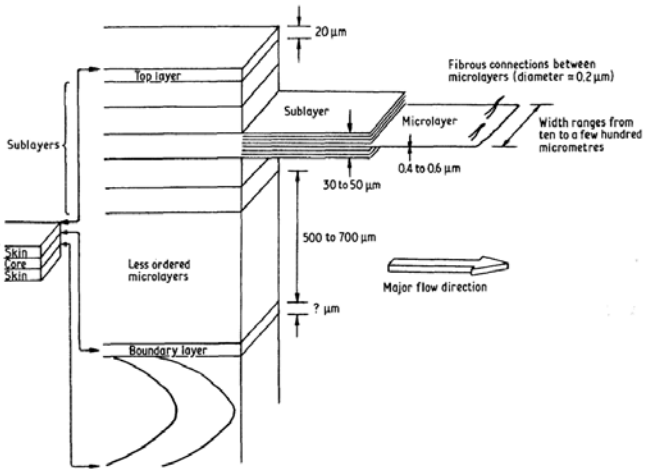

Figure 2.6: Proposed model of the hierarchical structure in injection molded TCLP plaques. (Reprinted from ref [74])

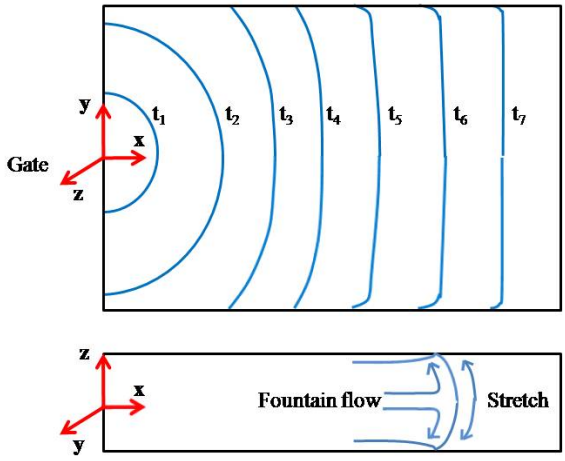

Figure 2.7: Top: flow front (blue lines) advance in the x-y plane as time increase (from t_1 to t_7). Bottom: cross section of the advancing front in the x-z plane.

2.4.1.2 The Influence of the Injection Molding Conditions on the Mechanical Properties

The injection molding parameters significantly impact the mechanical properties of the TLCP articles. Key parameters include, but are not limited to, barrel temperature, injection speed, mold temperature and mold thickness. The processing conditions and the resulting TLCP

mechanical properties are listed in Table 2.2. The purpose is to not only reveal the processing-properties relationship, but outline a typical range of the TLCP mechanical properties. Ophir and Ide [71] injection molded 60% HBA, 20% TA and 60% HNA into ASTM standard 8.5" tensile specimen and 5" flex bars with different combinations of the barrel temperatures, injection speeds and mold temperatures. The results are given in Table 2.2. Wang *et al.* [80] have carried out an investigation on the mechanical properties in both the machine (injection direction) and transverse directions, with an emphasize on the mold thickness effect. In the work of Wang *et al.* the 73/27 HBA/HNA was injection molded into end-gated plaques, from which the ASTM standard dumbbell-shaped specimen were cut along the machine and transverse directions for tensile measurements. The tensile properties are presented in Table 2.3.

From these two publications, the tensile properties in the machine direction showed a general trend to increase with lower injection speed, lower barrel (closer to the nominal melting point) and mold temperatures and smaller plaque thickness. Intuitively, higher injection speed leads to higher degree of orientation. On the other hand, it is worth noticing the higher the injection speed, longer time it took to cool the melt, which left the nematic melt more time for orientation relaxation. The relaxed orientation gave rise to the reduced mechanical properties at higher injection speeds. Similarly, the higher the barrel/mold temperatures, the more time the molecules have for orientation relaxation, and the less favorable the mechanical properties would be. Meanwhile, a thinner plaque reduced the thickness of the less oriented core region relative to that of the highly aligned skin region. In other words, a greater amount of molecules could "feel" the shear stress imposed by the mold wall and start to align in the machine direction. Additionally, a thin plaque cooled faster than a thick plaque, and fast cooling helps lock in the orientation. Rendon *et al.*[81] arrived at the similar conclusions on the influence of processing parameters by

incorporating the processing variables discussed above into one single anisotropy factor ($AF_{specimen}$), which simplified the processing-property relationship. The $AF_{specimen}$ was found to be critically dependent on the mold thickness and the barrel/mold temperatures, while its weak dependence of the mold filling speeds was also observed.

Table 2.2: Mechanical properties of injection molded tensile specimen and flex bars by Ophir and Ide [71]. The TLCP used in this study was a copolymer of 60 mol% 4-acetoxybenzoic acid, 20 mol% TA and 20 mol% naphthalene diacetate.

Mechanical properties	Barrel temperature / ^{o}C					
	320	340	340	340	340	340
Mold temperature /^{o}C	40	40	40	100	100	100
Injection speed	Fast	Fast	Slow	Slow	Fast	Fast
Tensile modulus /GPa	17.2	20.0	19.3	18.6	15.2	16.5
Tensile strength /MPa	192	173	189	208	176	153
Tensile elongation /%	1.8	1.3	1.5	1.6	2.5	1.5
Flex modulus /GPa	15.2	15.2	15.2	14.5	13.1	13.1
Flex strength /MPa	178	174	175	175	170	176
Impact strength /J•m^{-1}	395	427	230	283	283	347

Table 2.3: Tensile properties of the 73/27 HBA/HNA copolymer in both machine and transverse directions as a function of the plaque thickness, reported by Wang *et al.*[80].

Plaque thickness /mm	Direction	Tensile modulus /GPa	Tensile strength /MPa	Tensile elongation /%
1	Machine	9.8±0.8	231.8±13.8	5.6±0.8
	Transverse	2.0±0.2	40.6±2.0	4.9±1.0
2	Machine	4.4±0.6	151.8±15.8	7.5±0.7
	Transverse	1.9±0.1	47.8±6.6	8.3±2.9
3	Machine	4.3±0.9	130.6±14.2	7.1±0.8
	Transverse	2.0±0.1	52.0±4.1	9.6±2.6
4	Machine	3.6±0.6	122.0±11.9	7.0±1.3
	Transverse	1.8±0.1	55.0±2.1	9.6±1.5

2.4.1.3 Property Anisotropy of Injection Molded TLCPs

One major disadvantage of the injection molded TLCPs is their mechanical anisotropy along and across the injection direction, which is pretty obvious in Table 2.3. The addition of glass fiber is one common method to reduce the stiffness anisotropy. Plummer *et al.* [82] performed the injection molding of the 30 wt% glass fiber reinforced 73/27 HBA/HNA and tested the tensile properties at 0^o and 90^o to the flow direction. Although the addition of glass fiber did not improve the tensile modulus significantly in the 0^o direction, it doubled the tensile modulus in the 90^o

direction, which lowered the modulus anisotropy factor from 4 to about 2. Interestingly, glass fiber did not enhance the tensile strength in either direction. Boles *et al.* promoted the mechanical isotropy by using the microstream injection molding method [83]. A fine metal mesh was placed at the gate of the mold cavity, which split the TLCP melt into a great number of highly oriented microstreams before the mold filling process started. In the core region, these microstreams intertwined and produced streams which were capable of maintaining their local orientations under the extensional and shear deformations. At the same time the microstreams changed their flow direction frequently, leading to the global mechanical isotropy. The presence of the mesh had very limited effect on the skin layers, whose formation was dominated by the substantial shear stress. The authors suggested this technique to be applied for thicker articles, because the ratio of the skin layers will be suppressed. Notably, the most balanced property was the tensile stress. The gap was narrowed down from originally 52 MPa (machine direction)/36 MPa (transverse direction) to approximately 47 MPa in both directions. The tensile modulus was in the range of 1.0 to 1.2 GPa in all directions. Given that the mechanical isotropy was realized, it seems the tensile properties reported by Boles *et al.* were well below the typical values of the TLCPs in either direction, as shown in Table 2.3. Especially the tensile modulus was much lower than expected, as it was 1 GPa tensile modulus, which is only comparable with the values of the conventional flexible chain polymers, like polypropylene. It will be more encouraging to find out if the isotropy in properties can be achieved without substantially reducing the mechanical properties.

2.4.1.4 Common Problems in the Injection Molding of TLCPs

TLCPs have a very low degree of post-extrusion swell due to the lack of chain entanglements in the nematic melt. This is desirable to maintain the precise shape of the extrusion products, but may cause problem in injection molding if the mold is not well designed. Ideally, the

melt front should uniformly expand as it fills the mold. Due to the lack of die swell, the TLCP melt may jet into the mold, adhere to the mold wall, and starts solidify before the mold is filled normally, which leaves marks on the final article. Jetting can usually be solved by re-design of the mold and increase of the gate size.

Controlling weldlines is probably the most perplexing problem in the injection molding of TLCPs. The formation of weldlines can be visualized in Figure 2.8. Suppose the advancing melt is cut into two streams by an obstacle in the mold, when the two melts converge again after passing the obstacle, the re-entanglement of polymer chains at the two impinging fronts is likely to be incomplete. Re-entanglement requires diffusion and molecular conformation adjustment, which becomes difficult in the low temperature mold. The low mold temperature slows down diffusion and freezes the molecular conformations, resulting in few molecules bridging the weld interface [84]. Weld-line strength was 25~98% of the bulk strength for some common thermoplastics, depending on the material and processing conditions [85]. For TLCPs, the weld-line strength could be even worse due to their low diffusion coefficients and non-entanglement nature. The weld-line strength of unfilled TLCPs was only 5-10% of the bulk strength. With the addition of 30 wt% glass fiber, the weld-line strength was doubled, but still below 20% of the bulk strength [86]. Engberg *et al.* [87] carried out a thorough measurement on the strength of two types of weldlines. The cold weldline referred to the defects formed by the merging of two co-linear melt fronts. The molecules oriented perpendicular to the knit-line region. The warm weldline was formed by splitting and rejoining of the melt, as indicated in Figure 2.8. Molecules aligned along the weldline in this case. The cold weld-line strength was 10~15% of the bulk strength for the unfilled TLCP. With 30% glass fiber reinforcement, this value increased to ~20 %. The strength of the warm weldline was

much greater, which accounted for 10~55% and 20~40% of the full strength of the materials, for unfilled and glass fiber reinforced materials, respectively.

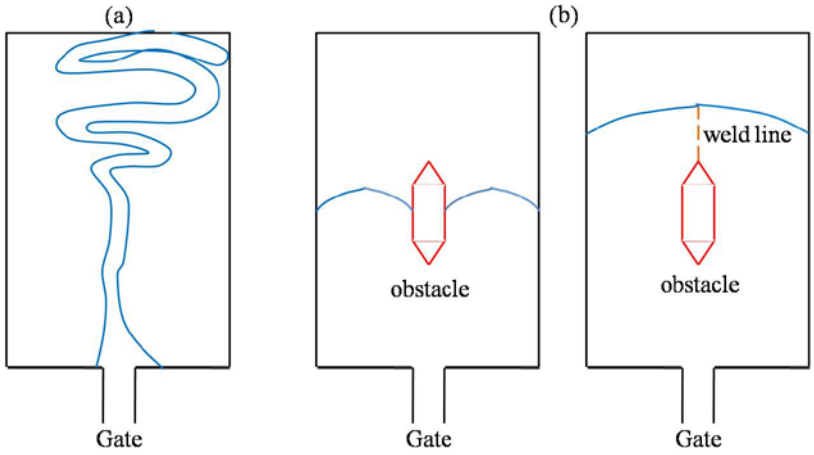

Figure 2.8: Common problems encountered in the injection molding of TLCPs: (a) jetting, and (b) the formation of a hot weld line.

2.4.2 Fiber spinning

Melt fiber-spinning is one important application for the TLCPs due to their inherent properties. TLCP fibers are produced by extrusion of the polymer melts through a die containing a number of symmetrically arranged small holes, and the so formed strands are subjected to post-die treatments including cooling and drawing. The rod-like molecules can be easily align along the fiber axis in the elongation flow field during fiber stretching, giving the fiber extraordinary stiffness and strength. Heat treatment is frequently applied to further improve the fiber strength.

2.4.2.1 Mechanical Properties of Melt-spun TLCPs

One of the first TLCP fiber work was done by Acierno *et al.* [88]. The 70/30 PET/HBA copolymer polymer yielded fibers with a maximum elastic modulus of 3 GPa and extensive PET crystallinity. A higher modulus of 32 GPa was achieved for the copolymer of 40/60 PET/HBA at

relative low spinning temperatures, and it was found that a low degree of crystallinity still persisted in the higher HBA content fiber. The authors speculated both the crystallinity and the frozen mesophase contributed to the enhanced stiffness. TLCP fiber composed of 58/42 HBA/HNA copolymer was produced at various melt temperatures and spin draw ratios [89]. The highest modulus achieved was around 45 GPa, which is approximately 40% higher than the value found in the PET/HBA copolymer fiber, which was probably due to the more rigid HBA/HNA molecules. With thermal treatment, the modulus could be further enhanced to 70 GPa. Heat treatment showed a greater effect on improving the tenacity: the strength of the HBA/HNA fiber was enhanced from 500 MPa to 1 GPa after thermal annealing. Thermal annealing at 10 to 20 ^{o}C below the melting point was found to be the optimum conditions in improving the tensile strength, although the associated enhancement in modulus was usually limited [90-91]. Most interestingly, tenacity could only be improved by the heat treatment when the degree of orientation was high enough. At moderate orientation, heat treatment was proved to have limited effect on the mechanical properties. Solid state polymerization between end-functional groups was speculated to occur during the thermal treatment. As a result of larger molecular weight and longer polymer chain, not only the strength, but the heat of fusion and the melting temperature were increased as well. Yoon *et al.* [92] explained the molecular origin of the improvement in the tensile strength by thermal annealing. The load transfer in TLCP fibers was through intermolecular interactions, and the fiber strength was determined by the intermolecular adhesion. Shear load concentration induced fracture usually originated at the chain ends, where less support was provided. Thermal annealing consumed the chain ends and introduced longer polymer chains and thus reduced the number of weak spots in the fibers.

2.4.2.2 The Influence of Fiber Spinning Conditions on Mechanical Properties

The dependence of fiber mechanical properties on temperature and spin-draw ratio was investigated in depth at constant mass flow rate [93]. The 75/25 HBA/HNA copolymer (melting temperature 280 ^{o}C) was nonisothermally melt spun at temperatures between 287 and 327 ^{o}C. At the lowest spin-draw ratio of 30, the tensile modulus was around 45 GPa, and the modulus was not affected by the spinning temperature (287 to 327 ^{o}C). As spin-draw ratio was raised above 50, the modulus slightly increased and then reached a plateau when the temperature was below 307 ^{o}C. Modulus data became scattered at the highest temperature (327 ^{o}C), albeit the highest 60 GPa modulus was obtained at 327 ^{o}C and the highest spin-draw ratio. Overall a high spin-draw ratio was not necessary to attain the highest modulus, because the molecular orientation development was a rather fast process in the extensional flow field. The tensile strength showed similar trends with respect to the spin-draw ratio, and higher strength was observed at 287 and 307 ^{o}C. Strength reached its highest value (1.2 GPa) at 287 ^{o}C with the highest spin-draw ratio. Conclusions were drawn that the best mechanical properties were obtained at a low spinning temperature (close to the melting temperature of the material), while the spin-draw ratio was not essential.

2.4.2.3 Hierarchical Structure of TLCP Fibers

Like injection molded articles, the hierarchy structure of TLCP fiber was widely studied and various fibrillar structural models have been posted [94-95]. Sawyer *et al.* presented a representative model which extended the finest structural unit to the molecular level, as illustrated in Figure 2.9. A minimum of two molecular chains organized into the smallest tape-like building block, known as the microfibril. The nano-sized microfibrils were the key elements to the macroscopic mechanical properties. TLCP molecules were usually considered to possess stick-like rigid-rod shape. However, high resolution imaging techniques indicated worm-like

confirmation of the microfibrils, such confirmation was somewhere in between a rigid-rod and a random coil. A main conclusion of this work was that the sizes of the microfibrils were relative consistent for fibers with different strength and modulus, but different arrangements of the microfibrils were responsible for the modulus variations. For example, as a result of the higher degree of local order, improvement in the tensile modulus can be obtained.

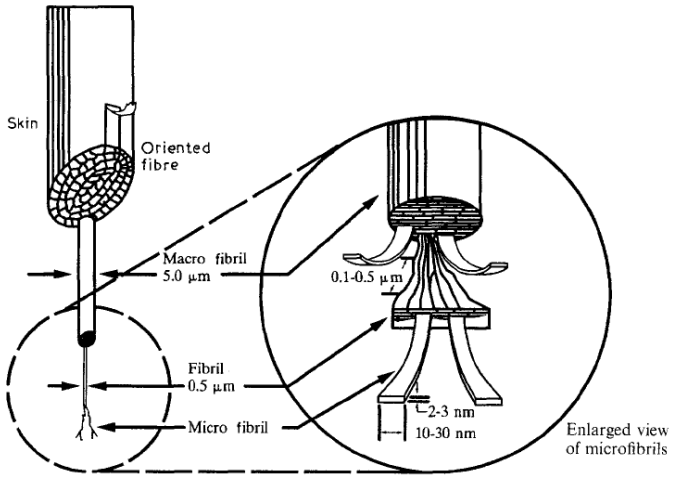

Figure 2.9: Extended hierarchical structural model for LCP fibers. (Reprinted from ref [96])

2.4.3 Blow molding

Blow molding is a process to manufacture hollow parts. The basic process has two fundamental steps. First, a parison or preform is formed at deformable temperatures. Second, pressured gas inflates the hot parison or preform against the cold mold wall until the finished article cools down. Blow molding can be classified into three categories: extrusion blow molding, injection blow molding, and stretch blow molding.

2.4.3.1 Extrusion Blow Molding

In extrusion blow molding, polymer pellets are melted in an extruder. The melt is then pumped through a specially designed annular die to form a tubular shape parison. A mold closes

around the parison, and the parison is then inflated by compressed gas. Extrusion blow molding operates on continuous and intermittent bases, as shown in Figures 2.10 and 2.11. In the continuous process, the extruder is kept running to produce parisons without pause. Under most circumstances, the parisons are transferred from the die head by moving the molds to the parisons. A cutoff knife is usually employed to trim the extra material hanging from the die. Short cycle time is allowed in the continuous extrusion blow molding to enhance productivity. Because the parisons experience gravimetric self loading in the downward-vertical extrusion, which is also known as the parison sag, high melt strength is required for the polymeric materials used in the continuous process to provide enough sag resistance. If the material melt strength is relatively low, or long mold cooling time is demanded, the intermittent process is preferred. In the intermittent extrusion blow molding, an accumulator head is connected to the extruder to collect polymer melt in its cavity, which gives rise to an intermittent process. Then the piston on the accumulator head pushes the melt through the flow channel at a relatively high speed, and thus the parison generation time is shortened and excessive sag is avoided.

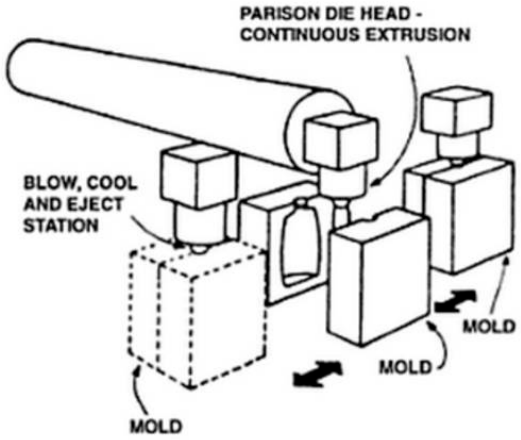

Figure 2.10: Schematic illustration of the continuous extrusion blow molding. (Reprinted from ref [97])

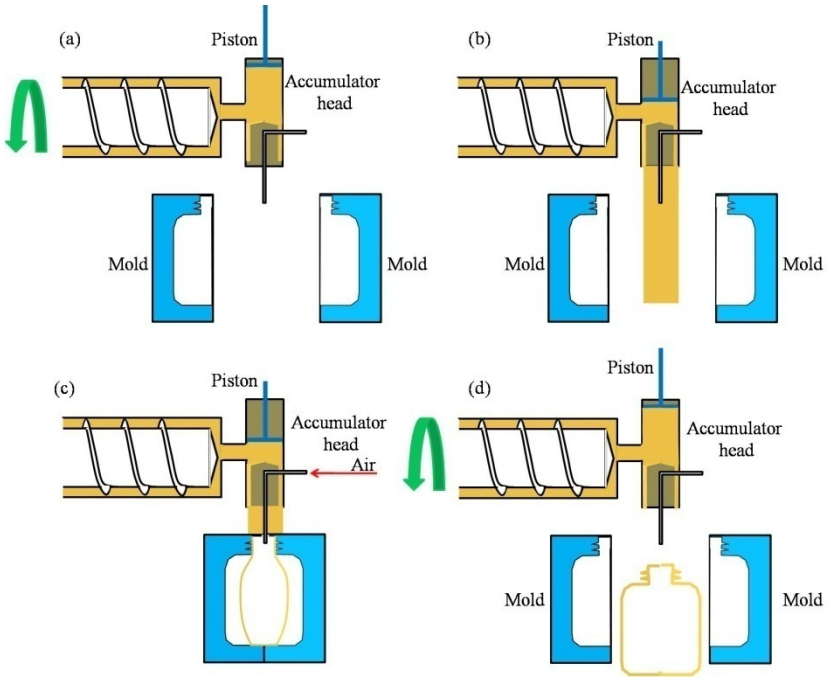

Figure 2.11: General operation steps in the intermittent extrusion blow molding: (a) a accumulator head gathers melt from a running extruder, (b) a hydraulic piston quickly push out melt to form a parison, (c) mold pinches the parison, pressurized gas inflates the parison against the mold wall, and (d) Mold opens to release the article, extruder restarts running for the next filling cycle.

2.4.3.2 Injection Blow Molding

As its name suggests, injection blow molding combines injection molding and blow molding. The injection molding phase produces a hollow, tube-shape article called the preform. The preform is supported by a core pin, and the preform and the supporting pin are later transferred to a blow mold for inflation. Despite the fact the injection blow molding equipment are more costly than those used in the extrusion blow molding, dimensions of the neck and final wall thickness can be more easily controlled. The screw thread is also formed with precision in the injection

molding phase. On the other hand, overcoming the nonuniform thickness induced by parison sag is always a challenge in extrusion blow molding.

2.4.3.3 Stretch Blow Molding

Stretch blow molding is typically used for producing soda bottles, as shown in Figure 2.12. As the most common material for making the soda bottle, PET is usually processed by stretch blow molding rather than extrusion blow molding, because its slow crystallization rate can not provide enough melt strength to support the parison. The preparation of preforms is quite similar to the process in injection blow molding. Biaxial stretching on a pre-heated preform is realized by the movement of a stretch rod in the machine direction and the expansion by pressurized gas in the hoop direction. Stretching imparts biaxial molecular orientation, and enhances not only the tensile strength, but drop impact and barrier properties [98].

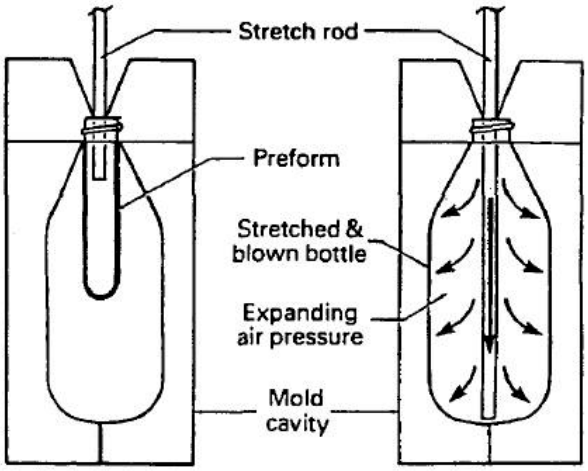

Figure 2.12: Stretch blow molding of a preform. (Reprinted from ref [99])

2.4.3.4 Extrusion Blow Molding of TLCPs

Extrusion blow molding of TLCPs is challenging due to their low melt strength [100]. Blizard and Baird [101] attempted to obtain biaxial orientation and properties in two copolyesters

(60/40 HBA/PET and 75/25 HBA/HNA) by varying the thermal history of the parisons. The die temperature was set below the melt temperatures of the TLCPs, so that the increased elasticity in the supercooled state was able to provide extra melt strength while maintaining the deformability of the parison. For the HBA/PET (melting point 250 ^{o}C), the die temperature was in the range of 190 to 200 ^{o}C. With the extruder barrel temperature set at 220 ^{o}C, the mechanical properties in the hoop direction were well above those in the machine direction (4.2 GPa vs 1.8 GPa in modulus and 85 MPa vs 38 MPa in strength). Barrel temperatures above the melting point gave rise to the machine direction properties being higher. The maximum modulus and strength of 6 GPa and 100 MPa were achieved in the machine direction in contrast to 1.8 GPa modulus and 44 MPa strength in the hoop direction. Thus, as the barrel temperature went up above the melting point, an orientation transition from the hoop direction to the machine direction can be anticipated. Regarding the blow molded HBA/HNA bottles, the tensile properties were more balanced in both directions. When processed at 300/290 ^{o}C barrel/die temperatures, a 5.7 GPa tensile modulus and 130 MPa strength were observed in the machine direction, while these values were 4.5 GPa and 97 MPa in the hoop direction. Tensile properties of the free blown bubbles (no geometric constriction from the mold) were also measured for both copolymers, and with a higher blow-up ratio (not quantified in the publication), the hoop properties were improved by 44% in modulus and 41% in strength. Due to the temperature gradient in the parison, the authors speculated the formation of a laminated structure, which consisted of layers of TLCPs with different orientations and textures. Corallo *et al.* [102] carried out sequential pre-heating treatment of the TLCP pellets to improve the parison sag resistance. According to their patent, thermal annealing near the melting point significantly increased the material viscosity, leading to containers which weighed 1.75 lbs. Due to the rough inner wall, the container wall thickness varied from 0.065" to 0.095". The

technique introduced in the patent appeared to be attractive. Nevertheless, neither mechanical properties nor orientation information was given. Lack of characterization results made the assessment of the pre-heating method rather difficult. A similar thermal annealing technique was applied to the glass fiber and mineral filled TLCPs [103], with 1.25 lbs container being successfully produced. Again, there were very few properties/performance discussed in the patent.

2.4.4 Film blowing

Film blowing is one of the most common methods of making films with biaxial orientation. Polymer pellets are extruded through an annular die, making a thin walled bubble. The top of the bubble is sealed by nip rollers, which rotate and stretch the bubble in the machine direction. Air is blown through the inner mandrel to solidify the molten film and inflate the bubble, providing stretching in the transverse direction. The film blowing process is shown in Figure 2.13. Biaxial orientation, realized by the simultaneous drawing and blowing of the film, is one of the most important advantages offered by film blowing. Another main benefit is some commercial articles are easier to be manufactured from a bubble rather than flat sheets. Take trash bags for example, after the bubble is conveyed past the nip rollers, it can be simply heat sealed for continuous production. For flat sheets produced from sheet extrusion, they have to be folded first before being welded on three sides.

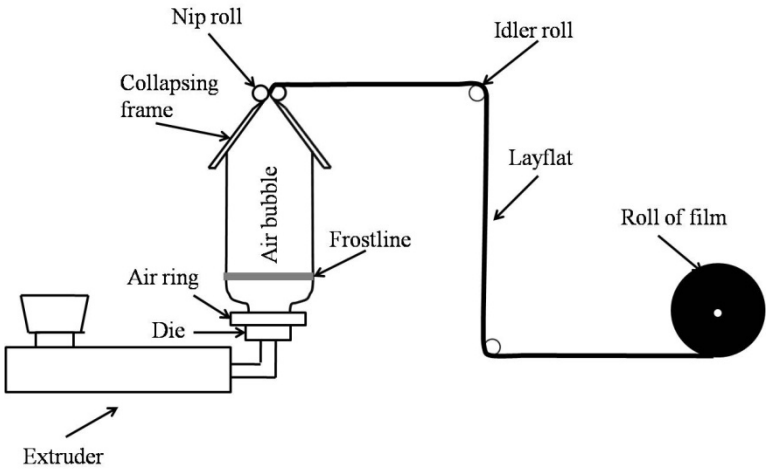

Figure 2.13: A scheme of the film blowing process. In the figure the frostline is the region where the melt starts solidifying.

Similar to blow molding, achieving biaxial/multiaxial orientation and isotropic mechanical properties are the main objectives in the film blowing of TLCPs. Blizard and Baird [104] attempted to impart biaxial orientation into two TLCPs (60/40 HBA/PET and 75/25 HBA/HNA) by controlling the blow-up ratio. As the blow-up ratio increased from 1.0 to 3.2, the tensile moduli in machine direction were not significantly altered from 10 GPa for the HBA/PET copolymer and 13 GPa for the HBA/HNA material. It was encouraging to find the tensile modulus in the hoop direction was doubled for the HBA/PET copolymer and tripled for the HBA/HNA TLCP, the values were raised from 1.45 to 3.1 GPa in the former case and from 1.0 to 2.6 GPa in the latter instance. Despite the promising increment, the modulus in the hoop direction was grossly inferior. Similarly to the modulus, the tensile strength was also significantly enhanced in both machine and hoop directions as the blow-up ratio was elevated. The strength in the machine direction was increased from 250 to 370 MPa, and the hoop strength was increased from 16 to 70 MPa. For the HBA/PET TLCP, both its machine and hoop strength experienced two fold increments: the

machine strength went up from150 MPa to 300 MPa and the hoop strength increased from 20 to 40 MPa. Again, the properties in the machine direction dominated those in the hoop direction.

Counter-rotating dies were developed to better control the orientation of the TLCP films [105-107]. A schematic representation of a counter-rotating die is shown in Figure 2.14. The idea is to promote biaxial or multiaxial orientation by counter rotating both of the concentric surfaces of the annular die. The motion of the concentric surfaces applies transverse shear stress through the melt, which orients the TLCP molecules toward the transverse direction. The combination of the drawing in the machine direction, the inflation in the transverse direction, as well as the transverse shear stress produces TLCP films with laminated structures. Assuming the orientation angle of the outer layer is $+\theta$ relative to the machine direction, then the orientation angle would be $-\theta$ for the inner layer. The orientation angles of each layer are governed by the rotation speed of the die. Such orientation distribution gives rise to the in-plane isotropy, and the tensile modulus and strength of the Vectra TLCP film prepared in this manner can achieve 10.3 GPa and 240 MPa, respectively [107]. TLCP films produced from the counter-rotating die tend to curl due to the residual thermal stress. This problem was solved by employing a tri-rotating die [108]. The so produced three-layer film exhibited symmetric orientation about the mid-plane that the two outer layers in contact with the die surfaces oriented $+\theta$ and the center layer oriented $-\theta$. Because the orientation was symmetric about the midplane, the residue stress was completely balanced. Additionally, because of the same chemical composition of each layer, the interlayer adhesion was outstanding.

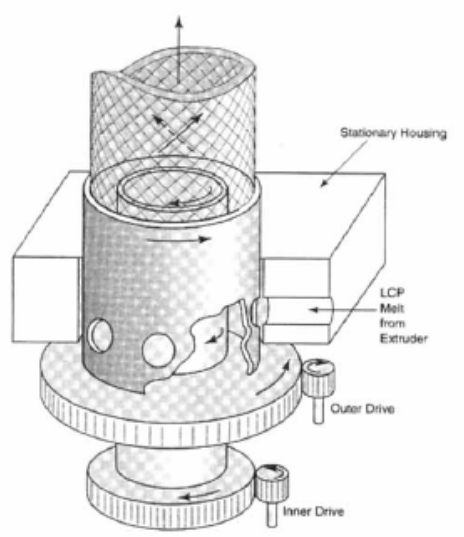

Figure 2.14: Schematic representation of a counter-rotating die. (Reprinted from ref [107])

2.5 TLCP/thermoplastic in situ composites

2.5.1 Mechanical properties

As a result of extremely high stiffness and strength, great processability, and recyclability, TLCPs have been blended with various thermoplastics to generate fibril reinforcement on an in situ basis. This section tends to cover the mechanical properties in the machine direction of the binary in situ composites over a wide range of thermoplastic matrices, where TLCP is the minor fraction. The author tends not to provide a comprehensive literature survey of the mechanical properties of all in situ composites developed so far. Instead, the properties of the representative in situ composites developed by different processing methods are summarized in Table 2.4.

Table 2.4: Mechanical properties of TLCP in situ composites in the machine direction as a function of processing methods.

Thermoplastic matrix	TLCP content	Tensile strength /MPa	Tensile modulus /GPa	Processing method	Ref
LLDPE/HDPE blend	0	16.0	0.4	Film blowing	[109]
	10% Vectra RD-501	25.0	1.2	Film blowing with a rotating die	[109]
	10% Vectra RD-501	22.0	1.0	Film blowing with a unrotating die	[109]
PP	0	31.2	1.4	Injection molding (tensile bars)	[110]
	30% Vectra A950	36.6	3.8		[110]
	20% 60/40 HBA/PET	28.7	2.1		[110]
	30% Vectra B950	23.1	3.7		[111]
	0	42.9	0.7	Film extrusion	[112]
	15% 80/20 HBA/PET	25.1	1.7		[112]
	0	0.7	N/A	Extrusion strand	[113]
	26% Vectra B950	13.5	N/A		[113]
	28% Vectra A950	4.7	N/A		[113]
	24% 60/40 HBA/PET	2.7	N/A		[113]

(*cont.*)

Table 4. (*cont.*)

Thermoplastic matrix	TLCP content	Tensile strength /MPa	Tensile modulus /GPa	Processing method	Ref
PVC	0	44.5	1.4	Injection molding (tensile bars)	[114]
	5% 60/40 HBA/PET	48.0	1.8		[114]
	10% 60/40 HBA/PET	46	1.6		[114]
	35% 60/40 HBA/PET	25.0	1.7		[114]
PS	0	32.0	3.1	Injection molding (tensile bars)	[115]
	25% Vectra A950	32.0	3.6		[115]
	25% Vectra B950	35.0	4.6		[115]
	0	28.0	1.5	Compression molded film	[116]
	10% 60/40 HBA/PET	22.5	1.7		[116]
	0	43.5	2.0	Fiber spinning	[116]
	10% 60/40 HBA/PET	37.5	2.6		[116]
PET	0	61.0	2.6	Injection molding (tensile bars)	[117]
	30% Vectra A950	74.0	4.1		[117]

(*cont.*)

Table 4. (*cont.*)

Thermoplastic matrix	TLCP content	Tensile strength /MPa	Tensile modulus /GPa	Processing method	Ref
PET	0	40.0	0.9	Compression molded film	[116]
	10% 60/40 HBA/PET	43.7	1.17		[116]
	0	60.5	1.9	Fiber spinning	[116]
	10% 60/40 HBA/PET	67.8	2.5		[116]
PBT	0	51.7	2.6	Injection molding (tensile bars)	[118]
	30% Vectra A950	37.9	3.5		[118]
PA66	0	62.0	1.1	Compression molded film	[119]
	20% Vectra A950	81.0	1.2		[119]
PA6	0	31.5	0.9	Injection molding (end-gated plaque)	[120]
	35 wt% HX-8000	42.5	2.9	Standard nozzle	[120]
	35 wt% HX-8000	54.0	3.5	Static mixer nozzle	[120]

(*cont.*)

Table 4. (*cont.*)

Thermoplastic matrix	TLCP content	Tensile strength /MPa	Tensile modulus /GPa	Processing method	Ref
PC	0	66.9	2.3	Injection molding (tensile bar)	[118]
	30% Vectra A950	121.0	5.7		[118]
	30% Vectra B950	154.0	6.6		[118]
PEN	0	83.0	N/A	Injection molding (tensile bar)	[121]
	30% Vectra A950	112.0	N/A		[121]
PEEK	0	84.1	3.5	Injection molding (tensile bar)	[118]
	30% Vectra A950	71.7	4.3		[118]
	0	116.0	5.0	Injection molding (tensile bar)	[122]
	25% Vectra A950	125.0	17.0		[122]
PES	0	64.3	2.5	Extrusion strands	[118]
	30% Vectra A950	115.8	4.1		[118]
	30% Vectra B950	164.1	5.7		[118]

(*cont.*)

Table 4. (*cont.*)

Thermoplastic matrix	TLCP content	Tensile strength /MPa	Tensile modulus /GPa	Processing method	Ref
PPS	0	82.0	3.7	Injection molding (tensile bar)	[123]
	25% Vectra A950	87.0	4.8		[123]
PEI	0	91.0	3.1	Injection molding (tensile bar)	[118]
	30 wt% Vectra A950	129.0	5.2		[118]
	30 wt% Vectra B950	95.8	7.5		[118]
	0	100.0	3.0	Injection molding (end-gated plaque)	[124]
	30 wt% HX-4000	135.0	5.8		[124]
	30 wt% Granlar	129.0	9.0		[124]

LLDPE = linear low density polyethylene; HDPE = high density polyethylene; PP = polypropylene; PVC = polyvinyl chloride; PS = polystyrene; PET = polyether terephthalate; PBT = polybutylene terephthalate; PA66 = polyamide 66, PA6 = polyamide 6; PC = polycarbonate; PEN = polyethylene naphthalate; PEEK = polyether ether ketone; PES = polyether sulfone; PPS = polyphenyol sufide; PEI = polyether imide.

2.5.2 TLCP fibrillation

Table 2.4 clearly suggests the superior mechanical properties of in situ composites, the increments in modulus were more impressive than strength. According to the composite theory, the TLCP/thermoplastic morphology plays a critical role in the resulting mechanical properties, the morphologies of in situ composites prepared via various processing techniques is extensively discussed in this section.

In order to reinforce thermoplastics effectively, the formation of TLCP fibrils with small diameter and large length to diameter (L/D) ratio is preferential. Several factors control the fibrillation of the TLCPs, including the viscosity ratio of the dispersed phase (TLCPs) to the continuous phase (thermoplastics), interfacial tension, blend compositions, and the combination of elongation/shear flow fields. An inspiring case that may illustrate the morphological formation of the in situ composites is the behavior of dispersed phase in a liquid medium. Many case studies have been carried out on the droplet/medium systems for both Newtonian and Non-Newtonian systems [125-132]. It has been shown the decisive factors for the deformation and breakup of the droplet are the ratio of viscosity ($\lambda = \mu_{dispersed}/\mu_{medium}$) and the Weber number. The Weber number quantifies the ratio of the viscous stress to the interfacial stress, in which the viscous stress tends to deform the droplet, while the interfacial stress resists the deformation and maintains the shape of the droplet. The effect of the TLCP content is closely related to the viscosity ratio. At low TLCP content, for example 10 wt%, the intrinsic small viscosity of the nematic melts prevents the droplets from deformation, thus the coalescence of the droplets into continuous fibrils becomes difficult [133]. According to Han [134], in a uniform shear flow field stable TLCP fibrils existed under the conditions where λ was either below $5X10^{-3}$ or above 5. However, Petrovic [135] reported fibrillation where λ was in between 0.01 and 0.001, so the value of λ may be material

dependent. On the other hand, if the TLCP contents are too high (> 50 wt%), phase inversion could occur, resulting in the formation of a continuous TLCP phase. Blizard and Baird [133] claimed the necessity of an elongation flow field in the formation of TLCP fibrils, which was supported by the work of others [136-138]. The development of a fibrillar morphology in the extensional flow field in capillary dies is a good example to illustrate the droplet coalescence and fibrillation process during processing [133, 136-138], as shown in Figure 2.15.

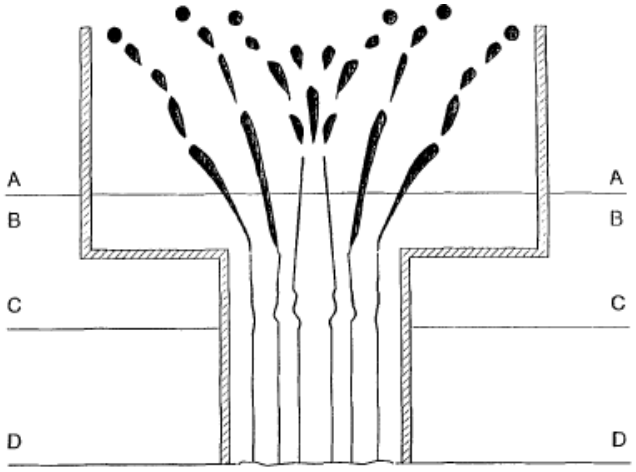

Figure 2.15: Fibrillation of TLCPs in the thermoplastic matrix. Four regions can be identified to describe this process: (A) tension and fiber forming; (B) flow narrowing; (C) relaxation zone; (D) shear field. (Reprinted from ref [132])

2.5.3 The morphology of in situ composites

Similar to the injection molded TLCP parts and melt spun TLCP fibers, the skin-core morphology is also found in the in situ composites. Although the boundary between each sublayer was hard to distinguish, the injection molded 25% Vectra A900/PET blend was found to contain three sublayers [139]. The morphology of each sublayer is shown in Figure 2.16. In sublayer (A), TLCP fibrils with 2~5 μm diameter were highly oriented along the injection direction. The

neighboring sublayer (B) was further away from the mold wall, and consisted of TLCP domains in the form of short cylinders. The overall orientation of TLCPs in sublayer (B) was relative lower than that in sublayer (A), but the general orientation was still along the flow direction. In sublayer (C), cylindrical LCP domains were perpendicular to the injection direction and arranged in a parabolic arc. The injection molding flow pattern is responsible for the formation of such hierarchical structure, as disscussed in § *2.4.1.1*.

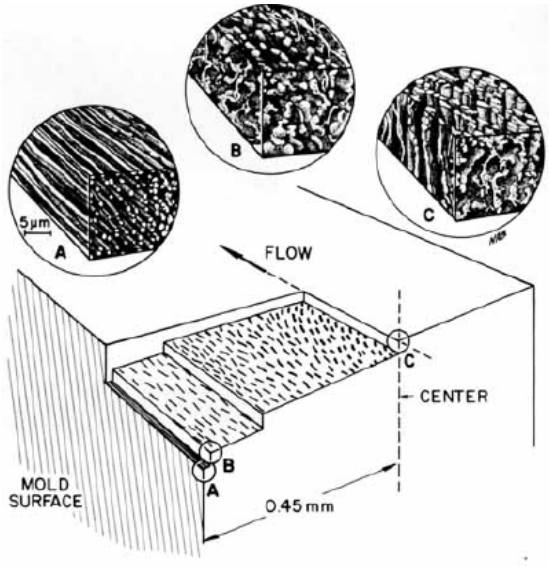

Figure 2.16: Morphology of 25% TLCP/PET blend. Inward from the mold wall: top sublayer (A), skin sublayer (B) and the central sublayer (C).

Baird and Sukhadia [140] patented a unique co-extrusion system as shown in Figure 2.17. Instead of dispersing TLCPs in thermoplastics in one single extruder, two extruders were used to deliver TLCP and thermoplastic melts separately. The melt streams met at a T-junction and were combined in a distinctive manner by a static mixer, where the TLCP stream was divided into layers to give the fibrillar morphology. Because the fibrillation was based on splitting the TLCP into fine substreams rather than elongating the TLCP droplets, the skin-core morphology as well as the

breakup of the TLCP fibrils was prevented. Additionally, the high melting temperature of TLCP may cause severe degradation of the thermoplastic matrix. For the same reason, injection molding was the predominant technique for preparing in situ composites, as shown in Table 2.4, due to its relative short resident time. Control of the thermal histories of the TLCP and thermoplastic in separate extruders allowed the processing of TLCP/thermoplastic pairs whose temperature ranges did not overlap. Last but not least, higher melt strength and easier drawing may be achieved by lowering the temperature of the thermoplastic matrix.

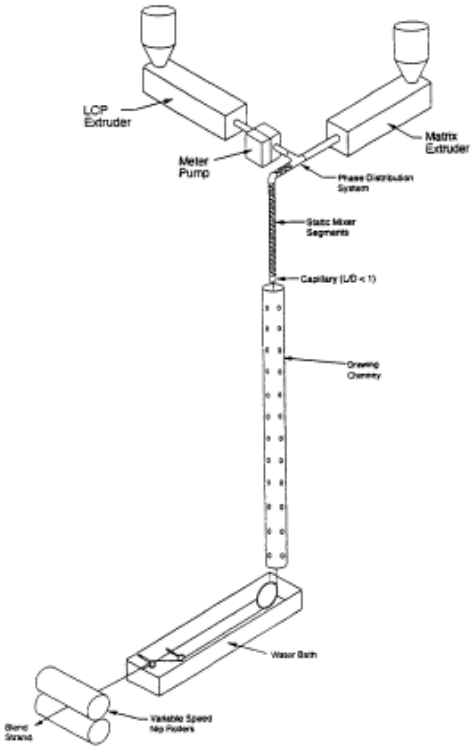

Figure 2.17: Schematic of the co-extrusion mixing system developed by Baird and Sukhadia, reprinted from ref [141].

2.5.4 Overcoming the anisotropy of in situ composites

As discussed above, the morphology of the injection-molded in situ composites is governed by the flow kinematics, where the skin-core hierarchy structure and the TLCP orientation distribution are similar to those of the injection molded pure TLCPs. Presumably, the anisotropy of injection molded in situ composites is one major drawback, which has been investigated by several authors [136, 142-145]. The degree of anisotropy (flow to transverse ratio) increased monotonically with TLCP concentration for the Vectra A950/PEEK in situ composite [142], with the values of 1.2 in modulus and 1.5 in strength at 50 wt% Vectra A950 concentration. Baird *et al*. [143] developed partially miscible TLCP/PEI blends. By comparing the mechanical properties obtained from the experimental measurements with the values predicted by the rule of mixtures, positive deviations were found in terms of the tensile and flexural modulus. The synergistic behavior was thought to be caused by the combined effects of miscibility, the TLCP properties and the final blend morphology. The degree of anisotropy also showed an increasing trend as the TLCP concentration increased.

Several studies have attempted to reduce the anisotropy in mechanical properties. Handlos and Baird [146] tried to develop bottles from in situ composites using extrusion blow molding. Vectra A950 and HX-6000 were generated into microfibrils in the PP matrix, using the co-extrusion system described in Figure 2.17. The resulting strands were then blow molded into bottles with a blow-up ratio of 2, in the hope that the transverse properties would be improved by the hoop stretching. Because of the weldlines induced by the mandrel support, the TLCP concentration was limited to a maximum of 20 wt%. The machine and hoop direction properties were not balanced well in the composite bottles. The degree of anisotropy was found to be still in the range of 1.5 to 1.8, which was attributed to the relative low blow-up ratio. In another paper

published from the same group, PP strands containing pregenerated TLCP microfibrils were extruded into sheets through an coat-hanger die [147]. The extruded sheets did show good properties with isotropy in the machine and transverse directions. The tensile modulus was improved with the increasing strand modulus and TLCP concentration. However, the modulus of the sheets exhibited negative deviations from the predictions of the composite theory, which might be due to the nonuniform distribution of the TLCP fibrils.

Compression molding of the in situ composite strands, fibers and films is another technique frequently adopted to overcome the anisotropy of in situ composites. By laying each layer of the in situ composite to a certain direction, the compression molded lamellar structure is less anisotropic than it's components. Sabol *et al*. [148] performed compression molding on randomly arranged pregenerated TLCP/PP strands to obtain planar isotropic mechanical properties. The compression molding temperature was only high enough to melt PP, so that the TLCP fibrillar morphology was maintained in the final plaque. The SEM images illustrated the random orientation of the TLCP fibrils on a global scale. The mechanical properties of the compression molded materials were the same or higher than the pregenerated strands from which they were derived. Property improvements were observed as the strand draw ratio increased. Additionally, the highest properties were close to the limit values predicted by composite theory. Ultrax KR-4002 (a copolymer of HBA, HQ and terephthaloyl)/PP Sheets extruded through a coat hanger die were also pressed to form the laminate composites [149], the best mechanical properties were found in the cross-stacked laminate ($-45^{o}/+45^{o}$) containing 50 wt% TLCP, whose modulus and strength reached 13 GPa and 60 MPa, respectively. The properties of the compression molded composites were dependent on the sheet draw ratio and the reduction ratio in compression molding.

References

[1] G. Friedel, "The mesomorphic states of matter", *Annalen der Physik*, vol.18, pp 273-474, 1922.

[2] W. R. Burghardt, "Molecular orientation and rheology in sheared lyotropic liquid crystalline polymers", *Macromolecular Chemistry and Physics*, vol.199, pp 471-488, 1998.

[3] A. Donald, A. Windle and S. Hanna, *Liquid Crystalline Polymers*, Cambridge University, 2006.

[4] A. A. Collyer, *Liquid crystal polymers From structures to applications*, Elsevier Applied Science, 1992.

[5] Q. F. Zhou and R. W. Lenz, "Substituent effects on the liquid-crystalline properties of thermotropic polyesters", *Polymer Preprint*, vol.24, pp 255-256, 1983.

[6] S. Antoun, R. W. Lenz and J. I. Jin, "Liquid crystal polymers. IV. Thermotropic polyesters with flexible spacers in the main chain", *Journal of Polymer Science Polymer Chemistry Edition*, vol.19, pp 1901-1920, 1981.

[7] Q. Zhun, R. Lenz and J. Jin, *Polymeric liquid crystals*, Blumstein Plenum Press, New York, 1984.

[8] S.G. Cottis, A.J. Economy and B. E. Nowak, "Fabricable infusible para-oxybenzoyl polyester production", U.S. Patent, 3829406,1971.

[9] J. Blackwell and A. Biswas, in *Development in Oriented Polymers, Vol. 2* (Ed.: I. M. Ward), Elservier Applied Science, London, 1987.

[10] J. I. Jin, S. Antoun, C. Ober and R. W. Lenz, "Thermotropic liquid crystalline polyesters with rigid or flexible spacer groups", *British Polymer Journal*, vol.12, pp 132-146, 1980.

[11] R. N. Demartino, "Improved processing of thermotropic liquid crystalline polyesters", *Journal of Applied Polymer Science*, vol.28, pp 1805-1810, 1983.

[12] B. P. Griffin and M. K. Cox, "Thermotropic polyesters with nonlinear links", *British Polymer Journal*, vol.12, pp 147-153, 1980.

[13] D. J. Blundell, "The nature of crystallites in solidified, rigid-chain, liquid crystal polymers", *Polymer*, vol.23, pp 359-364, 1982.

[14] B. Wunderlich, *Macromolecular Physics, Vol. 2, Crystal Nucleation, Growth, Annealing*, Academic Press, New York, 1976.

[15] G. D. Butzbach, J. H. Wendorff and H. J. Zimmermann, "Structure formation in a rigid chain polymer", *Makromol. Chem., Rapid Commun*, vol.6, pp 821-827, 1985.

[16] G. D. Butzbach, J. H. Wendorff and H. J. Zimmermann, "Structure and structure formation of a main chain thermotropic polymer", *Polymer*, vol.27, pp 1337-1344, 1986.

[17] S. Hanna, T. J. Lemmon, R. J. Spontak and A. H. Windle, "Dimensions of crystallites in a thermotropic random copolyester", *Polymer*, vol.33, pp 3-10, 1992.

[18] R. J. Spontak and A. H. Windle, "Electron microscopy of non-periodic layer crystallites in thermotropic random copolymers", *Journal of Material Science*, vol.25, pp 2727-2736, 1990.

[19] D. J. Wilson, C. G. Vonk and A. H. Windle, "Diffraction measurements of crystalline morphology in a thermotropic random copolymer", *Polymer*, vol.34, pp 227-237, 1993.

[20] S. Hanna and A. H. Windle, "Influence of temperature on the crystal structure of poly(hydroxybenzoic acid)", *Polymer Communication*, vol.29, pp 236-239, 1988.

[21] S. Z. D. Cheng, "Kinetics of mesophase transitions in thermotropic copolyesters. 1. Calorimetric study", *Macromolecules*, vol.21, pp 2475-2484, 1988.

[22] B. Wunderlich, *Macromolecular Physics, Crystal Melting*, vol. 3, Academic, New York, 1980.

[23] T. Ozawa, "Kinetics of nonisothermal crystallization", *Polymer*, vol.12, pp 150-158, 1971.

[24] P. Cebe and S. D. Hong, "Crystallization behavior of poly(ether ether ketone)", *Polymer*, vol.27, pp 1183-1192, 1986.

[25] S. Fai Lau, H. Suzuki and B. Wunderlich, "The thermodynamic properties of polytetrafluoroethylene", *Journal of Polymer Science: Polymer Physics Edition*, vol.22, pp 379-405, 1984.

[26] A. Kaito, M. Kyotani and K. Nakayama, "Effects of annealing on the structure formation in a thermotropic liquid crystalline copolyester", *Macromolecules*, vol.23, pp 1035-1040, 1990.

[27] T.-S. Chung, M. Cheng, S. H. Goh, M. Jaffe and G. W. Calundann, "Revisit the crystallization mechanism of Vectra, a liquid crystal polymer", *Journal of Applied Polymer Science*, vol.72, pp 1139-1150, 1999.

[28] D. Done and D. G. Baird, "Solidification behavior and recovery kinetics of liquid crystlline polymers", *Polymer Engineering and Science*, vol.30, pp 989, 1990.

[29] M. A. McLeod and D. G. Baird, "The crystallization behavior of blends of thermotropic liquid crystalline polymers", *Polymer*, vol.40, pp 3743-3752, 1999.

[30] Y. G. Lin and H. H. Winter, "Structural relaxation behaviour of a thermotropic liquid crystal aromatic copolyester in the super-cooled liquid state", *Liquid Crystals*, vol.3, pp 593-604, 1988.

[31] S. M. Guskey and H. H. Winter, "Transient shear behavior of a thermotropic liquid-crystalline polymer in the nematic state", *Journal of Rheology*, vol.35, pp 1191-1207, 1991.

[32] A. Romo-Uribe, T. J. Lemmon and A. H. Windle, "Structure and linear viscoelastic behavior of main-chain thermotropic liquid crystalline polymers", *Journal of Rheology*, vol.41, pp 1117-1145, 1997.

[33] E. Somma and M. R. Nobile, "The linear viscoelastic behavior of a series of molecular weights of the thermotropic main-chain liquid crystal polymers HBA/HNA 73/27", *Journal of Rheology*, vol.48, pp 1407-1423, 2004.

[34] Y. G. Lin and H. H. Winter, "Formation of high melting crystal in a thermotropic aromatic copolyester", *Macromolecules*, vol.21, pp 2439-2443, 1988.

[35] F. Cocchini, M. R. Nobile and D. Acierno, "Transient and steady rheological behavior of the thermotropic liquid crystal copolymer 73/27 HBA/HNA", *Journal of Rheology*, vol.35, pp 1171-1189, 1991.

[36] S. Onogi and T. Asada, "Rheology and rheo-optics of polymer liquid crystals", *Proceedings of the Eighth International Congress on Rheology*, edited by G. Astarita, G. Marrucci, L. Nicolais (Plenum, New York, 1980), vol. 1, 127-147.

[37] D. W. Giles and M. M. Denn, "The effect of suppression of offgassing on the rheometry of thermotropic liquid crystalline polymers", *Journal of Rheology*, vol.38, pp 617-637, 1994.

[38] T. De’ Nève, P. Navard and M. Kléman, "Shear rheology and shear‐induced textures of a thermotropic copolyesteramide", *Journal of Rheology*, vol.37, pp 515-529, 1993.

[39] F. Beekmans, A. D. Gotsis and B. Norder, "Transient and steady-state rheological behavior of the thermotropic liquid crystalline polymer Vectra B950", *Journal of Rheology*, vol.40, pp 947-966, 1996.

[40] G. G. Viola and D. G. Baird, "Studies on the transient shear flow behavior of liquid crystalline polymers", *Journal of Rheology*, vol.30, pp 601-628, 1986.

[41] D. G. deGennes, *The Physics of Liquid Crystals*, Clarendon Press, Oxford, 1974.

[42] D. Done and D. G. Baird, "Transient flow of thermotropic liquid crystal polymers in step strain experiments", *Journal of Rheology*, vol.34, pp 749, 1990.

[43] M. H. Wagner, "Analysis of time-dependent non-linear stress-growth data for shear and elongational flow of a low-density branched polyethylene melt", *Rheologica Acta*, vol.15, pp 136-142, 1976.

[44] G. Marrucci and P. L. Maffettone, "A description of the liquid-crystalline phase of rodlike polymers at high shear rates", *Macromolecules*, vol.22, pp 4076-4082, 1989.

[45] F. Cocchini, M. R. Nobile and D. Acierno, "Letter: About negative first normal stress differences in a thermotropic liquid crystalline polymer", *Journal of Rheology*, vol.36, pp 1307-1311, 1992.

[46] C. Dae Han and S. Chang, "Note: On the first normal stress difference of the thermotropic copolyester 73/27 HBA/HNA", *Journal of Rheology*, vol.38, pp 241-244, 1994.

[47] S. S. Kim and C. D. Han, "Transient rheological behavior of a thermotropic liquid - crystalline polymer. I. The startup of shear flow", *Journal of Rheology*, vol.37, pp 847-866, 1993.

[48] H. C. Langelaan and A. D. Gotsis, "The relaxation of shear and normal stresses of nematic liquid crystalline polymers in squeezing and shear flows", *Journal of Rheology*, vol.40, pp 107-129, 1996.

[49] C. D. Han and S. S. Kim, "Transient rheological behavior of a thermotropic liquid-crystalline polymer. II. Intermittent shear flow and evolution of dynamic moduli after cessation of shear flow", *Journal of Rheology*, vol.38, pp 13-30, 1994.

[50] C. D. Han and S. S. Kim, "Transient rheological behavior of a thermotropic liquid-crystalline polymer. III. Step strain experiment and shear stress relaxation modulus", *Journal of Rheology*, vol.38, pp 31-40, 1994.

[51] M. Mortier, P. Moldenaers and J. Mewis, "Transient rheological behavior of poly(p-phenyleneterephthalamide) (PpPTA) in sulfuric acid", *Rheologica Acta*, vol.35, pp 57-68, 1996.

[52] P. Moldenaers, M. Mortier and J. Mewis, "Transient normal stresses in lyotropic liquid-crystalline polymers", *Chemical Engineering Science*, vol.49, pp 699-707, 1994.

[53] T. Guo, G. M. Harrison and A. A. Ogale, "Transient shear rheology and rheo-optical microstructural characterization of a thermotropic liquid crystalline polymer", *Polymer Engineering and Science*, vol.45, pp 187-197, 2005.

[54] H.C. Linstid III, D.L. Cangiano, R.N. Demartino, J.E. Kuder, V. J. Provino and R. Jester, "Melt processability; stretching; multilayer laminates", U.S. Patent, 6294640,2001.

[55] F. M. Leslie, "Theory of flow phenomena in liquid crystals", *Advances in Liquid Crystals*, vol.4, pp 1-81, 1979.

[56] M. Srinivasarao and G. C. Berry, "Rheooptical studies on aligned nematic solutions of a rodlike polymer", *Journal of Rheology*, vol.35, pp 379-397, 1991.

[57] W. R. Burghardt and G. G. Fuller, "Role of director tumbling in the rheology of polymer liquid crystal solutions", *Macromolecules*, vol.24, pp 2546-2555, 1991.

[58] N. Grizzuti, S. Cavella and P. Cicarelli, "Transient and steady‐state rheology of a liquid crystalline hydroxypropylcellulose solution", *Journal of Rheology*, vol.34, pp 1293-1310, 1990.

[59] P. Moldenaers and J. Mewis, "Transient Behavior of Liquid Crystalline Solutions of Poly(benzylglutamate)", *Journal of Rheology*, vol.30, pp 567-584, 1986.

[60] K. Hongladarom and W. R. Burghardt, "Molecular alignment of polymer liquid crystals in shear flows. 2. Transient flow behavior in poly(benzyl glutamate) solutions", *Macromolecules*, vol.26, pp 785-794, 1993.

[61] K. Hongladarom, V. Secakusuma and W. R. Burghardt, "Relation between molecular orientation and rheology in lyotropic hydroxypropyl cellulose solutions", *Journal of Rheology*, vol.38, pp 1505-1523, 1994.

[62] S. G. Baek, J. J. Magda and R. G. Larson, "Rheological differences among liquid-crystalline polymers. I. The first and second normal stress differences of PBG solutions", *Journal of Rheology*, vol.37, pp 1201-1224, 1993.

[63] G. Kiss and R. S. Porter, "Rheology of concentrated solutions of helical polypeptides", *Journal of Polymer Science, Polymer Physics Edition*, vol.18, pp 361-388, 1980.

[64] S. Rendon, W. Burghardt and R. Bubeck, "Orientation dynamics in commercial thermotropic liquid crystalline polymers in transient shear flows", *Rheologica Acta*, vol.46, pp 945-956, 2007.

[65] T. S. Wilson and D. G. Baird, "Transient elongational flow behavior of thermotropic liquid crystalline polymers", *Journal of Non-Newtonian Fluid Mechanics*, vol.44, pp 85-112, 1992.

[66] J. J. Linster and J. Meissner, "Melt elongation and structure of linear polyethylene (HDPE)", *Polymer Bulletin*, vol.16, pp 187-194, 1986.

[67] H. Münstedt, "Dependence of the Elongational Behavior of Polystyrene Melts on Molecular Weight and Molecular Weight Distribution", *Journal of Rheology*, vol.24, pp 847-867, 1980.

[68] A. D. Gotsis and M. A. Odriozola, "Extensional viscosity of a thermotropic liquid crystalline polymer", *Journal of Rheology*, vol.44, pp 1205-1223, 2000.

[69] W. A. Kernick, III and N. J. Wagner, "Transient Viscosity and Molecular Order of a Thermotropic Polyester LCP in Uniaxial Elongational Flow", *Macromolecules*, vol.32, pp 1159-1166, 1999.

[70] D. Acierno and A. A. Collyer, *Rheology and Processing of Liquid Crystal Polymers*, vol. 2, Chapman & Hall, London, 1996.

[71] Z. Ophir and Y. Ide, "Injection molding of thermotropic liquid crystal polymers", *Polymer Engineering and Science*, vol.23, pp 792-796, 1983.

[72] Y. Ide and Z. Ophir, "Orientation development in thermotropic liquid crystal polymers", *Polymer Engineering and Science*, vol.23, pp 261-265, 1983.

[73] H. Thapar and M. Bevis, "The micromorphology of an injection molded thermotropic liquid crystal polymer", *Journal of Material Science Letter*, vol.2, pp 733-736, 1983.

[74] T. Weng, A. Hiltner and E. Baer, "Hierarchical structure in a thermotropic liquid-crystalline copolyester", *Journal of Material Science*, vol.21, pp 744-750, 1986.

[75] E. Joseph, G. L. Wilkes and D. G. Baird, "Effect of thermal history on the morphology of thermotropic liquid crystalline copolyesters based on PET and PHB", *Polymer*, vol.26, pp 689-703, 1985.

[76] S. D. Hudson, A. J. Lovinger, S. K. Venkataraman, C. Liu and L. T. Manzione, "Processing/morphology correlations in poly(benzoate-co-naphthoate) liquid crystalline polymers", *Polymer Engineering and Science*, vol.34, pp 1327-1335, 1994.

[77] A. Pirnia and C. S. P. Sung, "Molecular orientation profiles in an injection-molded liquid-crystalline copolyester characterized by Fourier transform infrared attenuated total reflection dichroism", *Macromolecules*, vol.21, pp 2699-2706, 1988.

[78] M. J. Folkes and D. A. M. Russell, "Orientation effects during the flow of short fiber-reinforced thermoplastics", *Polymer*, vol.21, pp 1252-1258, 1980.

[79] M. W. Darlington and P. L. McGinley, "Fiber orientation distribution in short fiber reinforced plastics", *Journal of Material Science*, vol.10, pp 906-910, 1975.

[80] Y. L. Wang, C. Y. Yue, K. C. Tam and X. Hu, "Relationship between processing, microstructure, and mechanical properties of injection molded thermotropic LCP", *Journal of Applied Polymer Science*, vol.88, pp 1713-1718, 2003.

[81] S. Rendon, W. R. Burghardt, R. A. Bubeck, L. S. Thomas and B. Hart, "Mechanical and morphological anisotropy in injection molding of thermotropic liquid crystalline copolyesters", *Polymer*, vol.46, pp 10202-10213, 2005.

[82] C. J. G. Plummer, Y. Wu, M. M. Gola and H. H. Kausch, "Impact tests on filled and unfilled thermotropic liquid crystalline polymer injection mouldings", *Polymer Bulletin*, vol.30, pp 587-594, 1993.

[83] D. Boles, M. Cakmak and B. Yalcin, "A novel microstream injection molding method for thermotropic liquid crystalline polymers to promote mechanical isotropy: A matrixing microbeam X-ray study", *Polymer*, vol.49, pp 3541-3553, 2008.

[84] W. W. Graessley, "Some phenomenological consequences of the Doi–Edwards theory of viscoelasticity", *Journal of Polymer Science: Polymer Physics Edition*, vol.18, pp 27-34, 1980.

[85] R. Selden, "Effect of processing on weld line strength in five thermoplastics", *Polymer Engineering and Science*, vol.37, pp 205-218, 1997.

[86] T.-s. Chung, *Thermotropic liquid crystal polymers : thin-film polymerization, characterization, blends, and applications*, Technomic Pub. Co., Lancaster, 2001.

[87] K. Engberg, A. Knutsson, P. E. Werner and U. W. Gedde, "Knit line fractures in injection molded liquid crystalline polymers", *Polymer Engineering and Science*, vol.30, pp 1620-1627, 1990.

[88] D. Acierno, F. P. La Mantia, G. Polizzotti, A. Ciferri and B. Valenti, "Ultra-high modulus liquid crystalline polyesters. p-Hydroxybenzoic acid copolyesters", *Macromolecules*, vol.15, pp 1455-1460, 1982.

[89] H. Muramatsu and W. R. Krigbaum, "Fiber spinning from the nematic melt. IV. Effect of P oxybenzoate crystallinity on the spinning and fiber properties of the copolyester of polyethylene terephthalate and p-oxybenzoate", *Journal of Polymer Science Part B: Polymer Physics*, vol.25, pp 2303-2314, 1987.

[90] J. Sarlin and P. Törmälä, "Isothermal heat treatment of a thermotropic LCP fiber", *Journal of Polymer Science Part B: Polymer Physics*, vol.29, pp 395-405, 1991.

[91] S. B. Warner and J. Lee, "Towards understanding the increase in strength of thermotropic polyesters with heat treatment", *Journal of Polymer Science Part B: Polymer Physics*, vol.32, pp 1759-1769, 1994.

[92] H. N. Yoon, L. F. Charbonneau and G. W. Calundann, "Synthesis, processing sand properties of thermotropic liquid-crystal polymers", *Advanced Materials*, vol.4, pp 206-214, 1992.

[93] J. Sarlin and P. Tormala, "Fiber formation and characterization of a thermotropic LCP [liquid crystal polymer]", *Journal of Applied Polymer Science*, vol.40, pp 453-469, 1990.

[94] L. C. Sawyer and M. Jaffe, "The structure of thermotropic copolyesters", *Journal of Materal Science*, vol.21, pp 1897-1913, 1986.

[95] L. C. Sawyer, R. T. Chen, M. G. Jamieson, I. H. Musselman and P. E. Russell, "Microfibrillar structures in liquid-crystalline polymers", *Journal of Material Science Letter*, vol.11, pp 69-72, 1992.

[96] L. C. Sawyer, R. T. Chen, M. G. Jamieson, I. H. Musselman and P. E. Russell, "The fibrillar hierarchy in liquid crystalline polymers", *Journal of materials science*, vol.28, pp 225-238, 1993.

[97] A. Garcia-Jejon, *Advances in Blow Moulding Process Optimization*, Rapra Technology Limited, Shawbury, UK, 1995.

[98] N. C. Lee, *Plastic Blow Molding Handbook*, Van Nostrand Reinhold, New York, 1990.

[99] F. M. Schmidt, J. F. Agassant, M. Bellet and L. Desoutter, "Viscoelastic simulation of PET stretch/blow molding process", *Journal of Non-Newtonian Fluid Mechanics*, vol.64, pp 19-42, 1996.

[100] M. H. Wagner, T. Ixner and K. Geiger, "A note on the melt strength of liquid crystalline polymer", *Journal of Rheology*, vol.41, pp 1087-1093, 1997.

[101] K. G. Blizard and D. G. Baird, "Blow molding of thermotropic liquid crystalline polyemrs", *International Polymer Processing*, vol.3, pp 172, 1989.

[102] C.F. Corallo, R.B. Sandor and R. S. Black, "Extrusion blow molding of thermotropic liquid crystalline polymers", U.S. Patent, 5336446,1992.

[103] C.F. Corallo, R.B. Sandor, R.S. Black and D. B. McKie, "Extrusion blow molding of filled liquid crystalline polymers", U.S. Patent, 5306461,1994.

[104] K. G. Blizard, T. S. Wilson and D. G. Baird, "Film blowing of thermotropic liquid-crystalline polymers", *International Polymer Processing*, vol.5, pp 53-61, 1990.

[105] A.C. Harvey, R.W. Lusignea, J.L. Racich, M. Baars, D.D. Bretches and R. B. Davis, "Biaxially oriented ordered polymer films", U.S. Patent, 4963428,1990.

[106] A.C. Harvey, R.W. Lusignea and J. L. Racich, "Multiaxially oriented thermotropic aromatic polyester films and method of preparation", U.S. Patent, 4966807,1990.

[107] R. W. Lusignea, "Orientation of LCP blown film with rotating dies", *Polymer Engineering and Science*, vol.39, pp 2326-2334, 1999.

[108] A. C. Harvey and R. W. Lusignea, "Coextrusion of liquid crystal polymers and thermoplastic polymers to form a container", U.S. Patent, 5843539 A,1998.

[109] W. Chinsirikul, T. C. Hsu and I. R. Harrison, "Liquid crystalline polymer (LCP) reinforced polyethylene blend blown film: Effects of counter-rotating die on fiber orientation and film properties", *Polymer Engineering and Science*, vol.36, pp 2708-2717, 1996.

[110] A. Datta and D. G. Baird, "Compatibilization of thermoplastic composites based on blends of polypropylene with two liquid crystalline polymers", *Polymer*, vol.36, pp 505-514, 1995.

[111] H. J. O'Donnell and D. G. Baird, "In situ reinforcement of polypropylene with liquid-crystalline polymers: effect of maleic anhydride-grafted polypropylene", *Polymer*, vol.36, pp 3113-3126, 1995.

[112] S. Saengsuwan, S. Bualek-Limcharoen, G. R. Mitchell and R. H. Olley, "Thermotropic liquid crystalline polymer (Rodrun LC5000)/polypropylene in situ composite films: rheology, morphology, molecular orientation and tensile properties", *Polymer*, vol.44, pp 3407-3415, 2003.

[113] A. M. Sukhadia, A. Datta and D. G. Baird, "Mixing history on the morphology and properties of thermoplastic/LCP blends", *International Polymer Processing*, vol.7, pp 218-228, 1992.

[114] Y. Z. Meng and S. C. Tjong, "Preparation and properties of injection-molded blends of poly(vinyl chloride) and liquid crystal copolyester", *Polymer*, vol.40, pp 2711-2718, 1999.

[115] G. Crevecoeur and G. Groeninckx, "Morphology and mechanical properties of thermoplastic composites containing a thermotropic liquid crystalline polymer", *Polymer Engineering and Science*, vol.30, pp 532-542, 1990.

[116] P. Zhuang, T. Kyu and J. L. White, "Characteristics of hydroxybenzoic acid-ethylene terephthalate copolymers and their blends with polystyrene, polycarbonate, and polyethylene terephthalate", *Polymer Engineering and Science*, vol.28, pp 1095-1106, 1988.

[117] J. Seppala, M. Heino and C. Kapanen, "Injection-molded blends of a thermotropic liquid-crystalline polymer with poly(ethylene terephthalate), polypropylene, and poly(phenylene sulfide)", *Journal of Applied Polymer Science*, vol.44, pp 1051-1060, 1992.

[118] G. Kiss, "In situ composites: Blends of isotropic polymers and thermotropic liquid crystalline polymers", *Polymer Engineering and Science*, vol.27, pp 410-423, 1987.

[119] D. Dutta, R. A. Weiss and J. He, "Compatibilization of blends containing thermotropic liquid crystalline polymers with sulfonate ionomers", *Polymer*, vol.37, pp 429-435, 1996.

[120] R. K. Krishnaswamy, S. E. B. Wadud and D. G. Baird, "Influence of a reactive terpolymer on the properties of in situ composites based on polyamides and thermotropic liquid crystalline polyesters", *Polymer*, vol.40, pp 701-716, 1998.

[121] S. H. Jang and B. S. Kim, "Morphology and mechanical properties of liquid crystalline copolyester and poly(ethylene 2,6-naphthalate) blends", *Polymer Engineering and Science*, vol.35, pp 538-545, 1995.

[122] A. I. Isayev and P. R. Subramanian, "Blends of a liquid-crystalline polymer with poly(ether ether ketone)", *Polymer Engineering and Science*, vol.32, pp 85-93, 1992.

[123] T. G. Gopakumar, S. Ponrathnam, A. Lele, C. R. Rajan and A. Fradet, "In situ compatibilization of poly(phenylene sulfide)/wholly aromatic thermotropic liquid crystalline polymer blends by reactive extrusion: morphology, thermal and mechanical properties", *Polymer*, vol.40, pp 357-364, 1998.

[124] S. S. Bafna, T. Sun, J. P. de Souza and D. G. Baird, "The effect of miscibility on the morphology and properties of blends of poly(ether imide) with liquid crystalline polymers", *Polymer*, vol.36, pp 259-266, 1995.

[125] B. J. Bentley and L. G. Leal, "An experimental investigation of drop deformation and breakup in steady, two-dimensional linear flows", *Journal of Fluid Mechanics*, vol.167, pp 241-283, 1986.

[126] L. A. Utracki and Z. H. Shi, "Development of polymer blend morphology during compounding in a twin-screw extruder. Part I: Droplet dispersion and coalescence - a review", *Polymer Enginnering and Science*, vol.32, pp 1824-1833, 1992.

[127] S. Torza, R. G. Cox and S. G. Mason, "Particle motions in sheared suspensions. XXVII. Transient and steady deformation and burst of liquid drops", *Journal of Colloid and Interface Science*, vol.38, pp 395-411, 1972.

[128] H. P. Grace, "Dispersion phenomena in high viscosity immiscible fluid systems and application of static mixers as dispersion devices in such systems", *Chemical Engineering Communications*, vol.14, pp 225-277, 1982.

[129] H. J. Karam and J. C. Bellinger, "Deformation and breakup of liquid droplets in a simple shear field", *Industrial and Engineering Chemistry Fundamentals*, vol.7, pp 576-581, 1968.

[130] R. W. Flumerfelt, "Drop breakup in simple shear fields of viscoelastic fluids", *Industrial and Engineering Chemistry Fundamentals*, vol.11, pp 312-318, 1972.

[131] M. V. Tsebrenko, G. P. Danilova and A. Y. Malkin, "Fracture of ultrafine fibers in the flow of mixtures of non-Newtonian polymer melts", *Journal of Non-Newtonian Fluid Mechanics*, vol.31, pp 1-26, 1989.

[132] M. V. Tsebrenko, A. V. Yudin, T. I. Ablazova and G. V. Vinogradov, "Mechanism of fibrillation in the flow of molten polymer mixtures", *Polymer*, vol.17, pp 831-834, 1976.

[133] K. G. Blizard and D. G. Baird, "The morphology and rheology of polymer blends containing a liquid crystalline copolyester", *Polymer Engineering and Science*, vol.27, pp 653-662, 1987.

[134] C. D. Han, *Multiphase Flow in Polymer Processing* Academic Press, New York, 1981.

[135] Z. S. Petrovic and R. Farris, "Structure-property relationship in fibers spun from poly(ethylene terephthalate) and liquid crystalline polymer blends. I. The effect of composition and processing on fiber morphology and properties", *Journal of Applied Polymer Science*, vol.58, pp 1077-1085, 1995.

[136] A. I. Isayev and M. Modic, "Self-reinforced melt-processible polymer composites: extrusion, compression, and injection molding", *Polymer Composite*, vol.8, pp 158-175, 1987.

[137] A. Kohli, N. Chung and R. A. Weiss, "The effect of deformation history on the morphology and properties of blends of polycarbonate and a thermotropic liquid-crystalline polymer", *Polymer Engineering and Science*, vol.29, pp 573-580, 1989.

[138] A. Siegmann, A. Dagan and S. Kenig, "Polyblends containing a liquid-crystalline polymer", *Polymer*, vol.26, pp 1325-1330, 1985.

[139] M. S. Silverstein, A. Hiltner and E. Baer, "Hierarchical structure in liquid crystal polymer (LCP)/PET blends", *Journal of Applied Polymer Science*, vol.43, pp 157-173, 1991.

[140] D.G. Baird and A. Sukhadia, "Mixing process for generating in-situ reinforced thermoplastics", U.S. Patent, 5225488,1991.

[141] A. A. Handlos and D. G. Baird, "Processing and associated properties of in situ composites based on thermotropic liquid crystalline polymers and thermoplastics", *J Macromol Sci Polymer Rev*, vol.C35, pp 183-238, 1995.

[142] A. Mehta and A. I. Isayev, "Rheology, morphology, and mechanical characteristics of poly(ether ether ketone)-liquid crystal polymer blends", *Polymer Engineering and Science*, vol.31, pp 971-980, 1991.

[143] D. G. Baird, S. S. Bafna, J. P. De Souza and T. Sun, "Mechanical properties of in situ composites based on partially miscible blends of poly(ether imide) and liquid-crystalline polymers", *Polymer Composite*, vol.14, pp 214-223, 1993.

[144] S. S. Bafna, J. P. De Souza, T. Sun and D. G. Baird, "Mechanical properties of in-situ composites based on partially miscible blends of glass-filled polyetherimide and liquid-crystalline polymers", *Polymer Engineering and Science*, vol.33, pp 808-818, 1993.

[145] A. Datta, H. H. Chen and D. G. Baird, "The effect of compatibilization on blends of polypropylene with a liquid-crystalline polymer", *Polymer*, vol.34, pp 759-766, 1993.

[146] A. A. Handlos and D. G. Baird, "Extrusion blow molding of microcomposites based on thermotropic liquid crystalline polymers and polypropylene", *Polymer Engineering and Science*, vol.36, pp 378-386, 1996.

[147] A. A. Handlos and D. G. Baird, "Sheet extrusion of microcomposites based on thermotropic liquid crystalline polymers and polypropylene", *Polymer Composites*, vol.17, pp 73-85, 1996.

[148] E. A. Sabol, A. A. Handlos and D. G. Baird, "Composites based on drawn strands of thermotropic liquid crystalline polymer reinforced polypropylene", *Polymer Composites*, vol.16, pp 330-345, 1995.

[149] A. Isayev, "Self reinforced thermoplastic composite laminate", U.S. Patent, 5268225,1993.

3 The Transient Shear Rheology of a Thermotropic Liquid Crystalline Polymer in the Super-cooled State

The Transient Shear Rheology of a Thermotropic Liquid Crystalline Polymer in the Super-cooled State

Chen Qian[a], Donald G. Baird[a*]

[a]Department of Chemical Engineering, Virginia Polytechnic Institute and State University,

Blacksburg, VA 24061

3.1 Abstract

To determine the processing temperature of a representative thermotropic liquid crystalline polymer (TLCP) in the super-cooled state, small amplitude oscillatory shear (SAOS), the startup of shear flow and differential scanning calorimetry (DSC) measurements were performed. Good agreement on the onset crystallization temperature was obtained from the SAOS and the startup of shear flow. Compared with DSC, the rheological measurements were more sensitive for detecting crystallization in the super-cooled state. The rheological study suggested that crystallization did not occur unless the TLCP was cooled 30^{o}C below its melting point, and its viscosity was significantly increased as the material was super cooled. Additionally, super cooling the TLCP did not significantly affect the relaxation of shear stress after preshearing. However, the recovery of transient shear stress in the interrupted shear measurements was suppressed to a great extent in the super-cooled state.

3.2 Introduction

Thermotropic liquid crystalline polymers (TLCPs) are high performance engineering thermoplastics, which offer a balance of properties unmatched by most other resins. TLCPs are well known for their outstanding mechanical properties. For example, the specific tensile modulus of a commercial TLCP fiber, Vectran®, is 5.6 times higher than steel, and its specific strength is 1.8 times higher [1]. In addition to their mechanical properties, the highly compact structure of liquid crystalline polymers significantly decreases the solubility of gas molecules, making TLCPs one of the least permeable thermoplastics [2-3]. Weinkauf and Paul [4-6] systematically investigated the transport phenomena of various gases in the a TLCP prepared from 73 mol% hydroxybenzoic acid (HBA) and 27 mol% hydroxynaphthoic acid (HNA) (commercial name Vectra A950), and they showed the permeability of O_2 in the 73/27 HBA/HNA was more than two orders of magnitude lower relative to the commonly used barrier resin poly(ethylene terephthalate) (PET). The exceptional barrier properties make TLCPs promising candidates for some packaging applications [7-8] and for hydrogen and oxygen storage.

Commercial TLCPs exhibit inherently low viscosity relative to many other conventional thermoplastics. The low melt viscosity gives rise to enhanced processability of TLCPs using techniques such as injection molding. However, it is detrimental to processes requiring high melt strength, such as extrusion blow molding, film blowing, thermoforming and multilayer coextrusion [8].

Several methods have been developed to modify the rheological characteristics of TLCPs, such that their viscosity can be enhanced. Carbon fillers, including carbon black, graphite and carbon fiber, have been added to TLCP matrices to effectively increase the viscosity [9-11]. Nevertheless, it is uncertain whether the addition of fillers will influence the great barrier

properties of TLCPs, as voids may exist between the fillers and matrix due to the lack of adhesion between the two phases.

Efforts were also made on tuning the rheological properties of TLCPs by chemical modification. Li *et al.* [12] conducted melt-state reaction using a HBA/HNA TLCP and triphenyl phosphite. In this case one triphenyl phosphite molecule could react with up to three TLCP chain-end functionalities. It was found the shear viscosity can be enhanced by a factor of 20 over the neat resin. In a later publication, the authors reported the reaction between TLCP and diepoxy reagent in the molten state. The product was used to prepare high quality multilayer films [8]. Corallo *et al.* [13-14] patented the extrusion blow molding from both neat and glass fiber filled 73/27 HBA/HNA. In this case the viscosity enhancement resulted from the heat treatment of the raw materials. When TLCP molecules were exposed to air, polymerization occurred at elevated temperatures in the solid state, giving rise to molecules with higher molecular weight and viscosity. However, these two patents did not specify whether solid state polymerization led to linear or cross linked polymers.

Done and Baird [15-16] developed a unique method to increase the viscosity of TLCPs by first raising the temperature above the melting point (T_m) to exclude all solid crystalline structure and then lowering the temperature below T_m to super cool the materials [17]. The processing temperature window in the super-cooled state was determined by small amplitude oscillatory shear measurements in the temperature ramp mode. When being processed in the super-cooled state, the viscosity and melt strength of TLCPs were effectively improved. This resulted in the successful extrusion blow molding and film blowing of TLCPs.

The shear rheology of commercial TLCPs has been well documented under conventional processing conditions above T_m [18-29]. Other than the 73/27 HBA/HNA, two other commercial

TLCPs have been widely studied. One is a copolyester synthesized from 40 mol% PET and 60 mol% HBA. The other is a polyesteramide containing 60 mol% HNA, 20 mol% terephthalic acid (TA) and 20 mol% 4-aminophenol (commercial name Vectra B950). TLCPs have demonstrated some unusual flow behavior, such as the three region flow curve [19, 21, 23, 26], the debatable negative primary normal stress difference [24-26, 28, 30], the scaling of shear stress growth curves with strain at different shear rates [18-19, 23], and the strong dependence of transient rheological behaviors on flow history [18, 27].

The complicated rheology of TLCP melts originates from their structured fluid nature. TLCP molecules form the nematic phase with a polydomain structure in the molten state [20-21, 31]. Within each domain, the orientations of the rigid, rod-like molecules are relatively uniform. However, the domain orientations are distributed heterogeneously in space. Upon shearing, the structure evolution of TLCP melts involve both the reorientation of molecules and the rearrangement of the domain structure [18, 20-21, 27, 29]. Viola and Baird [27] compared the simulation data with the experimental results for 40/60 PET/HBA. They concluded that instead of the shear induced orientation of the molecules, the domain structure change was responsible for the stress growth response in the starup of shear flow. On the other hand, Beekmans *et al.* [18] studied the influence of mechanical history on the stress growth of 60/20/20 HNA/TA/ aminophenol. The startup and relaxation stress transients were at least partially attributed to the rotation and orientation of the molecules. Therefore, the origin for the complex transient rheological behavior could be very complicated and highly material dependent.

McLeod and Baird [32] melted the TLCP containing HBA/TA/HQ/HQ-derivatives (HX8000) first, and cooled the material down at various cooling rates to track the crystallization temperatures, using both small amplitude oscillatory shear measurements and DSC analysis.

However, the crystallization temperature alone is not enough to guide processing in the super-cooled state, it is of equal importance to know how fast the TLCPs crystallize at temperatures below the melting points. Done and Baird [17] studied the crystallization behaviors of three different TLCPs (40/60 PET/HBA, 20/80 PET/HBA and 73/27 HBA/HNA). Moreover, the onset crystallization temperatures of these TLCPs were investigated in the super-cooled state, which were obtained from both dynamic mechanical measurements and DSC. Nevertheless, the flow behavior of the TLCPs under steady shear was not reported. The first objective of our study is to determine the onset crystallization temperatures in the super-cooled, using the copolyester of HBA/TA/HQ/HQ-derivatives (HX8000) as a representative material. The practical significance of this part of the work is to provide guidance for processing. To achieve this objective, we used not only small amplitude oscillatory shear and DSC measurements, but transient experiments at the startup of shear flow. As far as we know, this is the first time the transient stress growth of a TLCP is measured in the super-cooled state. We also aim to quantify the viscosity increment as a TLCP is cooled to the super-cooled state. The viscosity at low shear rates indicates melt strength, which is critical to melt processing.

Additionally, the transient rheology of TLCPs above T_m has been well documented, which indicates the structure evolution of TLCPs. However, the transient rheology of TLCPs in the super-cooled state has yet to be investigated. Our second objective is to determine how cooling the TLCP to the super-cooled state will affect the transient rheological behavior.

3.3 Experimental

3.3.1 Materials

Zenite HX8000 was provided by DuPont and was used as received. The Zenite series of TLCPs is believed to be synthesized from different ratios of terephthalic acid (TA), 4-hydroxybenzoic acid (HBA), hydroquinone (HQ) and hydroquinone derivatives (HQ-derivatives) [32]. Nevertheless, the specific monomer ratio for HX8000 is unknown. The HX8000 has the clearing temperature above its melting point, and the polymer degrades before the nametic-isotropic transition occurs.

3.3.2 Differential Scanning Calorimetry

DSC measurement in the temperature ramp mode was carried out using a TA instrument's Discovery DSC. The temperature ramp test was used to obtain the melting point, as well as the crystallization temperatures of the TLCP. Ca. 10 mg of sample was equilibrated at 350^{o}C for 1 min, the material was cooled to 40^{o}C (first cooling scan), and then heated back up to 350^{o}C (second heating scan). A constant rate of 20^{o}C/min was applied in both heating and cooling scans, and the measurement was performed under a dry nitrogen environment. It was found the melting and crystallization temperatures were independent of the equilibration time at 350^{o}C. To avoid the chemical change of the material at high temperature, such as degradation and transesterification, the equilibration time was set as 1 min [32-34]. The melting point as well as the melting enthalpy were calibrated using indium.

DSC tests were also performed in the isothermal time sweep mode. Ca. 10 mg of HX8000 was first equilibrated at 310^{o}C for 10 mins and then cooled to 270, 260 and 250^{o}C at 20^{o}C/min. Heat flow was traced as the TLCP was held at a given temperature.

3.3.3 Rheological Measurements

Small amplitude oscillatory shear measurements were performed in the temperature ramp mode, using a TA instrument's ARES-G2 rheometer with 25 mm diameter parallel disks fixtures. HX8000 pellets were dried in a vacuum oven at 100 ^{o}C for at least 24 hr prior to testing. In the sample loading process, pellets were directly loaded between the parallel disks and melted for 3 min, then the gap was closed to 0.2 mm at a rate of 2 μm/s. With 0.2 mm gap, each sample was brought to the starting temperature of 310^{o}C and equilibrated for 10 min. After equilibration the temperature was lowered at a rate of 20^{o}C/min. Oscillatory shear with 2.5 % strain and 10 rad/s angular frequency were applied, and the storage modulus G' and loss modulus G" were monitored as a function of temperature. All measurements were performed within a dry nitrogen environment.

Small amplitude oscillatory shear tests were also conducted in the time sweep mode. The same sample loading procedures adopted were the same as those described in the temperature ramp mode. TLCP pellets were first melted at 310^{o}C, and then the temperature was lowered to 270, 260 and 250^{o}C at 20 ^{o}C/min. The samples were then sheared at a frequency of 10 rad/s with 2.5 % strain. The growths of G' and G" were observed as a function of time.

For the transient rheological measurements, parallel disk fixtures with a 0.2 mm gap were used. The sample loading procedures were essentially the same as those used in the small amplitude oscillatory shear tests described above. Besides 310^{o}C, which was above T_m, measurements were also carried out at temperatures in the super-cooled state, namely 270, 260 and 250^{o}C. For experiments in the super-cooled state, samples were first equilibrated at 310^{o}C, and then they were cooled below the melting point of 280^{o}C at 20^{o}C/min.

Four different types of transient experimental protocols were applied. The first type of transient measurements conducted was the startup of shear flow. A shear rate, $\dot{\gamma}$, of either 0.1 or 0.5 s^{-1} was applied until the TLCP reached a steady state. The second type of test was the relaxation after flow cessation. The material was first presheared at 0.5 s^{-1} for 1600 s to a steady state, then shearing was stopped and the shear stress was allowed to relax for 1000 s. In the third set of measurements, after preshearing at 0.5 s^{-1} for 1600 s, oscillatory shear of 2.5 % strain and 10 rad/s frequency was immediately applied. The last type of experiment was that of the interrupted shear. After preshearing at 0.5 s^{-1} for 1600 s, TLCP relaxed for various periods of 50, 200 and 500 s, then shearing was resumed at 0.5 s^{-1}.

3.4 Results and Discussion

3.4.1 DSC measurements

The results of DSC heating and cooling scans are shown in Fig 3.1. The heating scan indicates the high temperature end of the melting endotherm is 276^{o}C, which is defined as the melting point of the TLCP. Therefore, equilibrating the material at 310^{o}C ensures all the crystalline structure is excluded. Upon cooling, the TLCP starts to crystallize at 232^{o}C, and the peak crystallization temperature is 228^{o}C.

Isothermal DSC is a commonly used technique to monitor the crystallization of TLCPs below their melting points [17]. After completely melted at 310^{o}C, the TLCP was cooled to one of the predetermined temperatures of 270, 260 and 250^{o}C. The change in heat flow was recorded as a function of time, as shown in Fig 3.2. At all three given temperatures, DSC tests sense no heat released from the samples, which suggests isothermal crystallization does not occur at these temperatures.

3.4.2 Small amplitude oscillatory shear measurements

To complement the crystallization temperature of the TLCP obtained from DSC, dynamic mechanical measurements in the temperature ramp mode were performed, as shown in Fig 3.3. Once melted, G" is greater than G' as the TLCP is cooled below its 280^{o}C melting point, suggesting the material is still in the fluid state. Both G' and G" gradually increase as temperature decreases. At 235^{o}C, G' surpasses G" and the crossover of G' and G" is observed. Fig 3.3 shows the degree of supercooling is roughly 45^{o}C (280 to 235^{o}C). The crossover of G' and G" may result from either the crystallization of the TLCP, or the crosslinking of the material [35]. To investigate the origin of the crossover of G' and G", the TLCP is first equilibrated at 310^{o}C and cooled at 20^{o}C till G' and G" crossovers (first run). Then the same sample is heated up again to 310^{o}C and cooled at the same rate (second run). In case of crystallization, the changes in G' and G" as a function of temperature are expected to be repeatable in the two successive measurements, which is because of the reversibility of the crystalline-nematic phase transition. On the other hand, if crosslinking reaction occurs, in the second run the amplitude of G' should be greater than G" at 310^{o}C, which is due to the increment in the elasticity of the material. The experiments described above were carried out, and the results show the crossover of G' and G" is due to crystallization rather than crosslinking. Although it is hard to determine the exact time when the first crystal appears from SAOS results, the crossover of G' and G" is taken as a signature to indicate the early stage of crystallization. The crystallization temperature obtained from SAOS (235^{o}C) is in good agreement with that in the DSC test (onset crystallization temperature of 232^{o}C).

Meanwhile it is equally important to determine how long the TLCP could maintain fluidity at a given temperature in the super-cooled state. Therefore, dynamic rheological measurement was performed in the isothermal time sweep mode, and the result is shown in Figs 3.4. From the

rheological test, it can be observed when the TLCP is cooled to 270 and 260^{o}C, G' and G" are mostly parallel with one another and no crossover can be identified within the extended test period (1.5 hour). At these two temperatures the TLCP is relatively stable. On the other hand, crystallization occurs at 250^{o}C as G' and G" display a crossover 2550s after the measurement starts. The slow crystallization rate of the TLCP at this temperature indicates this temperature in the super-cooled state can also be used for rheological tests.

Both SAOS and DSC suggest crystallization does not occur when the TLCP melt is cooled to 270 and 260^{o}C. However, the discrepancy between DSC and rheological results is observed at 250^{o}C. SAOS indicates crystallization occurs at this temperature, but DSC does not. The discrepancy is due to the two possible reasons. First, shear-induced crystallization may only occur in the SAOS measurements. The strain applied in the measurement could align the molecules and accelerate crystallization. Second, DSC may not possess sufficient sensitivity for detecting the onset of crystallization. That is, the initial stage of TLCP crystallization may only release a traceable amount of heat, which is not detectable by DSC. Lin and Winter [36] showed DSC results were not sensitive enough to pick up the melting transition of residual 73/27 HBA/HNA crystals in the heating scan. In contrast, the detection for the onset of crystallization in SAOS relies on the influence of TLCP crystals on the flow behavior of the polymer melt, which is independent of the heat change during the phase transition. We shall show later that the transient rheology in the super-cooled state suggests shear-induced crystallization is less likely to occur, and we suggest the rheological measurement is a more effective method in sensing the onset of TLCP crystallization in the super-cooled state.

3.4.3 Startup of shear flow

To complement the results obtained from small amplitude oscillatory shear measurements, transient shear in the startup of shear flow was carried out. Liquid crystalline polymers are known to be unusually susceptible to the edge fracutre instability in steady shear flow when being tested by rotational rheometers with the cone-and-plate fixtures [37-38]. Only relatively low shear rates are applied to avoid the occurance of edge fracutre. In our work as the TLCP was cooled to the super-cooled state, it became higly elastic, as indicated by the increase in G' in Fig 3.3. The high elasticity of the material made measuring the transient rheology a challenging task. No reliable results can be obtained using the conventional cone-and-plate fixtures because of inevitable edge fracture. Baek *et al.* [37-38] suggested using fixtures with narrow gaps at the rim to delay edge fracture at higher shear rates. This approach was adopted in our work and parallel disks fixtures with 0.2 mm gap were used. Even so the maximum shear rate achieved was only 0.5 s^{-1}. The cone-and-plate fixtures are usually preferrable for transient rheological measurments because of the uniform shear rate across the radius. Therefore, a comparison between the results obtained from these two fixtures is necessary to ascertain whether at least qualitative agreement can be achieved. The comparison of stress growth curves in flow inception at 310 ^{o}C and 0.5 s^{-1} is shown in Fig 3.5. Although quantitatively the two curves do not match completely, parallel disks capture the same features of transient shear stress behavior as those obtained from the cone-and-plate. Both curves exhibit an initial overshoot, followed by an undershoot and a second overshoot. Additionally, when the material is sheared to a steady state, the values of both shear stresses are quite close. Thus, transient measurements using parallel disks allow at least a qualitative investigation into the effect of temperature on the shear induced structure evolution of the TLCP.

Although a negative first normal stress difference, N_1, was frequently observed for lyotropic liquid crystalline polymers, and the mechanism was well understood [39], the sign of N_1 was still under debate for TLCPs. Guskey and Winter [28] reported negative N_1 values at low shear rates for the 73/27 HBA/HNA. In contrast Cocchini *et al.* [25] reported all positive N_1 values over the shear rate range from 0.02 to 10 s^{-1}. Cocchini *et al.* explained the discrepancy by demonstrating the long decay of the normal stress after sample loading/squeezing procedures and the significant residual normal stress at the startup of shear flow. If the residual stress experienced by the transducer at the beginning of flow inception was taken as the "zero level stress", during the transient experiments, the continuous decay of the normal stress led to erroneous interpretations of the negative N_1 values. In this study, the sample loading procedure of closing the gap to 0.2 mm led to a significant amount of residual normal stress before the tests started. The N_1 values given by the instrument were caused by not only the material response, but the decay of residual stress. Consequently N_1 was inaccurate and is not be reported in the discussions below.

Figs 3.6 and 3.7 show the respective growth of the transient shear stress or viscosity as a function of time in the flow inception experiments at shear rates of 0.1 and 0.5 s^{-1}. First of all, the steady state viscosity of the TLCP is significantly enhanced when it is cooled to the super-cooled state. For example, when the temperature is lowered from 310 to 250 ^oC, the viscosity at 0.1 and 0.5 s^{-1} is increased from 1180 Pa•s^{-1} to 11,000 Pas•s^{-1} and from 1030 Pa•s^{-1} to 6500 Pa•s^{-1}, respectively.

Additionally, when the TLCP is super cooled below its melting point, it is interesting that the shapes of the stress growth curves in the super-cooled state are qualitatively similar to that at 310^oC. Previous work shows two physical phenomena are potentially responsible for the complicated stress behavior. One is the reorientation of the rod-like molecules [18] and the other

is the rearrangement of the domain structure [27]. The similarity in the shapes of the curves suggests the transient rheological behavior is caused by the same type of structure change, both at 310^{o}C and in the super-cooled state. It could be the orientation of molecules, or the rearrangement of the domain structure, or the combination of both. Nevertheless, the information provided by the flow inception alone is not enough to interpret which one was the cause.

It should also be noticed as the temperature is lowered, the location of the stress overshoots and undershoots is shifted to the right along the time axis, and the detailed location of the peaks is shown in Table 3.1. The shift of the peak location indicates the structure evolution that causes the stress growth is slowed down when the TLCP is cooled down to the super-cooled state.

At 250 ^{o}C, it takes about the same amount of time (2400 s) before both stress growth curves at 0.1 and 0.5 s^{-1} exhibit a continuous increase. In the dynamic mechanical measurements in Fig 3.4, the crossover of G' and G" also occurs at 2550 s. Therefore, the continuous increase in transient shear stress at 250 ^{o}C after 2400 s is attributed to the crystallization of HX8000. When crystallization occurs, the total amount of strain ($\dot{\gamma}$t) applied to the TLCP in the startup of shear flow at 0.1 and 0.5 s^{-1} is 240 and 1200 strain units, respectively. Because the crystallization rates at 250 ^{o}C at these two shear rates are comparable and independent of strain, we believe shear-induced crystallization does not occur at this temperature. Otherwise the stress at 0.5 s^{-1} should grow faster than that at 0.1 s^{-1}.

3.4.4 Relaxation after flow cessation

Fig 3.8 shows the relaxation of shear stress after 1600 s preshearing at 0.5 s^{-1}. At 310 ^{o}C, the relaxation of shear stress consists a fast initial drop and a much slower decay. Interestingly enough, after being sheared in the super-cooled state, all the shear stress relaxation curves contain

both the fast and slow decay regions as well, similar to that at 310^{o}C. Even in the super-cooled state, most of the residual shear stress eventually dies out.

The relaxing shear stress at different temperatures is also normalized with respect to the steady states value obtained in preshearing, and the normalized shear stress is plotted as a function of time in Fig 3.9. The initial fast decay part of the curves overlaps really well for different temperatures. This part of each curve is expected to be associated with the rearrangement of the molecules, for example the relaxation of molecular orientation [40]. Thus it seems cooling the material to the super-cooled state does not significantly altered the relaxation of molecular orientation.

3.4.5 Small amplitude oscillatory shear after flow cessation

Applying small amplitude oscillatory shear immediately after flow cessation has been a convenient approach to probe the structure evolution during relaxation. In this method a decrease in loss modulus, G", suggests an increase in the degree of molecular orientation and vice versa. Here we also adopted this indirect method to track the evolution of molecular orientation after shearing at 310, 270 and 260 ^{o}C. After the TLCP was sheared at 0.5 s^{-1} for 1600s, small amplitude oscillatory shear with 2.5% strain and 10 rad/s frequency was imposed for 600s. The change in G" as a function of time is recorded in Fig 3.10. At 310 ^{o}C, G" keeps increasing, indicating the relaxation of shear-induced orientation.

Before we analyze the change of G" in the super-cooled state and relate that to the molecular orientation evolution, it is important to ascertain whether the change of G" is caused by the relaxation of molecular orientation instead of the crystallization of the TLCP. Based on the crystallization kinetics study in Fig 3.4, the change of G" is negligible at 270 and 260 ^{o}C.

Consequently, the apparent increase in G" in Fig 3.10 at these two temperatures could only be attributed to the relaxation of molecular orientation. In contrast, at 250 ^{o}C, the change in G" after preshearing will not be only due to the molecular orientation evolution, it will also be greatly influenced by crystallization, as suggested by Fig 3.2. Thus the result at 250 ^{o}C will not be shown.

When the TLCP is cooled to 270 and 260^{o}C, G" gradually increases as time elapses. One critical finding from Fig 3.10 is the curves at all three temperatures are almost parallel with one another. This serves as further evidence that super cooling the TLCP below its melting point probably does not influence the orientation dynamics of the molecules significantly.

3.4.6 Interrupted shear

The structure recovery after flow cessation was investigated by interrupted shear experiments at temperatures both above the melting point and in the super-cooled state. In this set of tests after the TLCP was sheared to steady state, the material was allowed to relax for 50, 200 and 500s and flow was resumed. The stress growth after flow restarted at 310^{o}C is presented in Fig 3.11. To better elucidate the recovery of transient stress as a function of relaxation time, the shear stress is normalized by dividing by the steady state value. The shear stress growth obtained in the startup of shear flow is also presented as a reference. With the use of a longer relaxation time, the magnitude of both undershoot and second overshoot is increased. The key observation in Fig 3.11 is the longer the TLCP is allowed to relax, the more similar the transient stress behavior upon flow resumption is relative to the initial curve in the flow inception. This is because of the structure recovery of the material. When flow is turned off, the average degree of orientation decrease, as suggested by Fig 3.10. Meanwhile it is highly possible that the domain structure disturbed in the startup of shear flow can recover its original status, before shearing is applied. For example, Guo *et al.* [21] directly observed the deformation of domains and reduction in domain

size upon shearing using a rheo-optical technique. Although it may take a relative long time, the domain structure did recover to a certain degree after flow stopped.

Now we turn our attention to the transient stress growth after relaxation in the super-cooled state. Figs 3.12 to 3.14 show the transient stress behavior at the temperatures of 310, 270 and 260^{o}C, after relaxing for 50, 200 and 500s. Although the absolute value of stress increases as temperature is lowered, each curve is divided by the steady state stress, such that the influence of temperature on the transient stress behavior could be better visualized. As discussed earlier, the longer the relaxation time, the higher the degree of recovery in the transient shear stress is observed at 310^{o}C. However, this is not the case for the temperatures of 270 and 260 ^{o}C. Even after 500s relaxation, stress recovery at 270 and 260 ^{o}C can be barely observed.

The unusual low degree of transient stress recovery in the super-cooled state indicates the structure evolution is slowed down significantly after flow inception. Figs 3.9 and 3.10 suggest lowering the temperature to the super-cooled state surprisingly does not greatly alter the relaxation of the average molecular orientation when flow is stopped. Consequently, the reorientation of the TLCP molecules should not be the reason for the complicated transient stress behavior. Otherwise gradual recovery in shear stress should be observed at 270 and 260^{o}C. As we exclude the orientation evolution to be the cause for the transient stress behavior, it seems the rearrangement in the domain structure is solely responsible for the transient shear stress growth. The evolution in domain structure is believed to be slowed down as the TLCP is cooled to the super-cooled state. Although we did not assess the change in domain structure and size directly by using rheo-optical methods, our interpretation is in good agreement with that from the study on 40/60 PET/HBA [27].

3.5 Conclusions

The onset of crystallization of the liquid crystalline copolyester of HBA/TA/HQ/HQ-derivatives (HX8000) does not occur unless the polymer melt is cooled to at least 250^{o}C, which is 30^{o}C below its melting point. This temperature serves as the lower temperature limit for the processing of the TLCP in the super-cooled state. The onset of crystallization is suggested by both small amplitude oscillatory shear tests and transient experiments at the startup of shear flow. Rheological measurements are more sensitive to detecting the onset of TLCP crystallization in the super-cooled state relative to DSC, and these measurements can be used on other TLCPs to guide processing in the super-cooled state. As the TLCP is cooled 30^{o}C below its melting point, one order magnitude increase in viscosity is obtained at a shear rate of 0.1 s^{-1}.

The transient rheology of HX8000 in the super-cooled state has been determined for the first time. Super cooling the liquid crystalline copolyester composed of HBA/TA/HQ/HQ-derivatives (HX8000) does not remarkably affect the relaxation of shear stress after preshearing. Nevertheless, in the interrupted shear measurements, the recovery of transient shear stress after preshearing is significantly suppressed in the super-cooled state.

3.6 Acknowledgements

Materials provided by Dupont are gratefully acknowledged. The authors acknowledge Prof. Dr. Garth L. Wilkes of Virginia Tech for the tremendous inputs and productive discussions. The authors would also like to thank the Department of Energy through the Savanah River National Laboratories for the financial support.

References

[1] H. G. Chae and S. Kumar, "Rigid-rod polymeric fibers", *Journal of Applied Polymer Science*, vol.100, pp 791-802, 2006.

[2] J. S. Chiou and D. R. Paul, "Gas transport in a thermotropic liquid-crystalline polyester", *Journal of Polymer Science Part B: Polymer Physics*, vol.25, pp 1699-1707, 1987.

[3] N. R. Miranda, J. T. Willits, B. D. Freeman and H. B. Hopfenberg, "Organic vapor sorption and transport in a thermotropic liquid crystalline polyester", *Journal of Membrane Science*, vol.94, pp 67-83, 1994.

[4] D. H. Weinkauf and D. R. Paul, "Gas transport properties of thermotropic liquid-crystalline copolyesters. II. The effects of copolymer composition", *Journal of Polymer Science Part B: Polymer Physics*, vol.30, pp 837-849, 1992.

[5] D. H. Weinkauf and D. R. Paul, "Gas transport properties of liquid crystalline poly (ethylene terephthalate-co-p-oxybenzoate)", *Journal of Polymer Science Part B: Polymer Physics*, vol.29, pp 329-340, 1991.

[6] D. H. Weinkauf and D. R. Paul, "Gas transport properties of thermotropic liquid-crystalline copolyesters. I. The effects of orientation and annealing", *Journal of Polymer Science Part B: Polymer Physics*, vol.30, pp 817-835, 1992.

[7] J. Lange and Y. Wyser, "Recent innovations in barrier technologies for plastic packaging - a review", *Packaging Technology and Science*, vol.16, pp 149-158, 2003.

[8] Z. Li, Z. Zhou, S. R. Armstrong, E. Baer, D. R. Paul and C. J. Ellison, "Multilayer coextrusion of rheologically modified main chain liquid crystalline polymers and resulting orientational order", *Polymer*, vol.55, pp 4966-4975, 2014.

[9] K. Araki, T. Kitano, A. Lengalova and P. Saha, "Transient shear flow properties of carbon fiber–filled liquid crystalline polymer", *Polymer Composites*, vol.26, pp 470-476, 2005.

[10] T. K. Katsuhiko Araki, Berenika Hausnerova, "Rheological properties of carbon fiber and carbon black filled liquid crystalline polymer melts", *Applied Rheology*, vol.11, pp 188, 2001.

[11] J. A. King, T. M. Tambling, F. A. Morrison, J. M. Keith, A. J. Cole and R. M. Pagel, "Effects of carbon fillers on the rheology of highly filled liquid-crystal polymer based resins", *Journal of Applied Polymer Science*, vol.108, pp 1646-1656, 2008.

[12] Z. Li, P. A. Gonzalez Garza, E. Baer and C. J. Ellison, "Modification of rheological properties of a thermotropic liquid crystalline polymer by melt-state reactive processing", *Polymer*, vol.53, pp 3245-3252, 2012.

[13] C.F. Corallo, R.B. Sandor and R. S. Black, "Extrusion blow molding of thermotropic liquid crystalline polymers", U.S. Patent, 5336446,1992.

[14] C.F. Corallo, R.B. Sandor, R.S. Black and D. B. McKie, "Extrusion blow molding of filled liquid crystalline polymers", U.S. Patent, 5306461,1994.

[15] K. G. Blizard and D. G. Baird, "Blow molding of thermotropic liquid crystalline polyemrs", *International Polymer Processing*, vol.3, pp 172, 1989.

[16] K. G. Blizard, T. S. Wilson and D. G. Baird, "Film blowing of thermotropic liquid-crystalline polymers", *International Polymer Processing*, vol.5, pp 53-61, 1990.

[17] D. Done and D. G. Baird, "Solidification behavior and recovery kinetics of liquid crystlline polymers", *Polymer Engineering and Science*, vol.30, pp 989, 1990.

[18] F. Beekmans, A. D. Gotsis and B. Norder, "Influence of the flow history on stress growth and structure changes in the thermotropic liquid crystalline polymer Vectra B950", *Rheologica Acta*, vol.36, pp 82-95, 1997.

[19] F. Beekmans, A. D. Gotsis and B. Norder, "Transient and steady-state rheological behavior of the thermotropic liquid crystalline polymer Vectra B950", *Journal of Rheology*, vol.40, pp 947-966, 1996.

[20] T. De’ Nève, P. Navard and M. Kléman, "Shear rheology and shear‐induced textures of a thermotropic copolyesteramide", *Journal of Rheology*, vol.37, pp 515-529, 1993.

[21] T. Guo, G. M. Harrison and A. A. Ogale, "Transient shear rheology and rheo-optical microstructural characterization of a thermotropic liquid crystalline polymer", *Polymer Engineering and Science*, vol.45, pp 187-197, 2005.

[22] D. Done and D. G. Baird, "Transient flow of thermotropic liquid crystal polymers in step strain experiments", *Journal of Rheology*, vol.34, pp 749, 1990.

[23] H. C. Langelaan and A. D. Gotsis, "The relaxation of shear and normal stresses of nematic liquid crystalline polymers in squeezing and shear flows", *Journal of Rheology*, vol.40, pp 107-129, 1996.

[24] C. Dae Han and S. Chang, "Note: On the first normal stress difference of the thermotropic copolyester 73/27 HBA/HNA", *Journal of Rheology*, vol.38, pp 241-244, 1994.

[25] F. Cocchini, M. R. Nobile and D. Acierno, "Letter: About negative first normal stress differences in a thermotropic liquid crystalline polymer", *Journal of Rheology*, vol.36, pp 1307-1311, 1992.

[26] F. Cocchini, M. R. Nobile and D. Acierno, "Transient and steady rheological behavior of the thermotropic liquid crystal copolymer 73/27 HBA/HNA", *Journal of Rheology*, vol.35, pp 1171-1189, 1991.

[27] G. G. Viola and D. G. Baird, "Studies on the transient shear flow behavior of liquid crystalline polymers", *Journal of Rheology*, vol.30, pp 601-628, 1986.

[28] S. M. Guskey and H. H. Winter, "Transient shear behavior of a thermotropic liquid-crystalline polymer in the nematic state", *Journal of Rheology*, vol.35, pp 1191-1207, 1991.

[29] S. Rendon, W. Burghardt and R. Bubeck, "Orientation dynamics in commercial thermotropic liquid crystalline polymers in transient shear flows", *Rheologica Acta*, vol.46, pp 945-956, 2007.

[30] A. D. Gotsis and D. G. Baird, "Primary normal-stress difference for two liquid-crystalline copolyesters", *Rheologica Acta*, vol.25, pp 275-286, 1986.

[31] A. Donald, A. Windle and S. Hanna, *Liquid Crystalline Polymers*, Cambridge University, 2006.

[32] M. A. McLeod and D. G. Baird, "The crystallization behavior of blends of thermotropic liquid crystalline polymers", *Polymer*, vol.40, pp 3743-3752, 1999.

[33] C. M. McCullagh, J. Blackwell and A. M. Jamieson, "X-ray Analysis of the Kinetics of Transesterification in Blends of Wholly Aromatic Thermotropic Copolyesters", *Macromolecules*, vol.30, pp 4837-4844, 1997.

[34] C. M. McCullagh, J. Blackwell and A. M. Jamieson, "Transesterification in Blends of Wholly Aromatic Thermotropic Copolyesters", *Macromolecules*, vol.27, pp 2996-3001, 1994.

[35] H. H. Winter and F. Chambon, "Analysis of linear viscoelasticity of a crosslinking polymer at the gel point", *Journal of Rheology (1978-present)*, vol.30, pp 367-382, 1986.

[36] Y. G. Lin and H. H. Winter, "High-temperature recrystallization and rheology of a thermotropic liquid crystalline polymer", *Macromolecules*, vol.24, pp 2877-2882, 1991.

[37] S. G. Baek, J. J. Magda, R. G. Larson and S. D. Hudson, "Rheological differences among liquid‐crystalline polymers. II. Disappearance of negative N1 in densely packed lyotropes and thermotropes", *Journal of Rheology*, vol.38, pp 1473-1503, 1994.

[38] S. G. Baek, J. J. Magda and R. G. Larson, "Rheological differences among liquid-crystalline polymers. I. The first and second normal stress differences of PBG solutions", *Journal of Rheology*, vol.37, pp 1201-1224, 1993.

[39] G. Marrucci and P. L. Maffettone, "A description of the liquid-crystalline phase of rodlike polymers at high shear rates", *Macromolecules*, vol.22, pp 4076-4082, 1989.

[40] W. R. Burghardt and G. G. Fuller, "Role of director tumbling in the rheology of polymer liquid crystal solutions", *Macromolecules*, vol.24, pp 2546-2555, 1991.

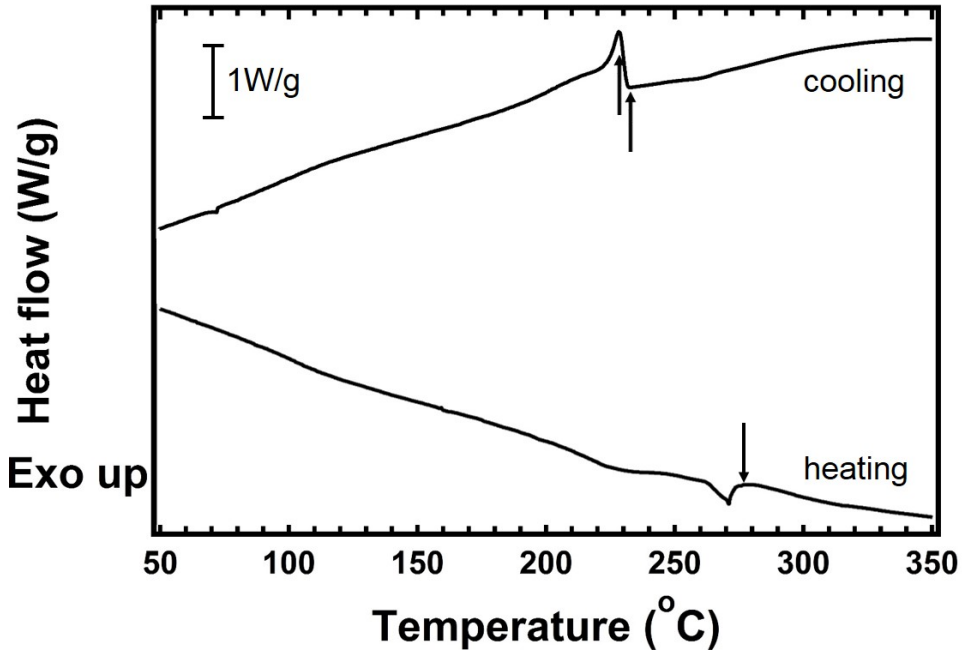

Figure 3.1: DSC heating and cooling scans of HX8000 at the rate of 20ºC/min. The arrow pointing down indicates the melting point of the TLCP, and the arrows pointing up suggest the onset and peak crystallization temperatures, respectively. The vertical bar suggests the scale in heat flow.

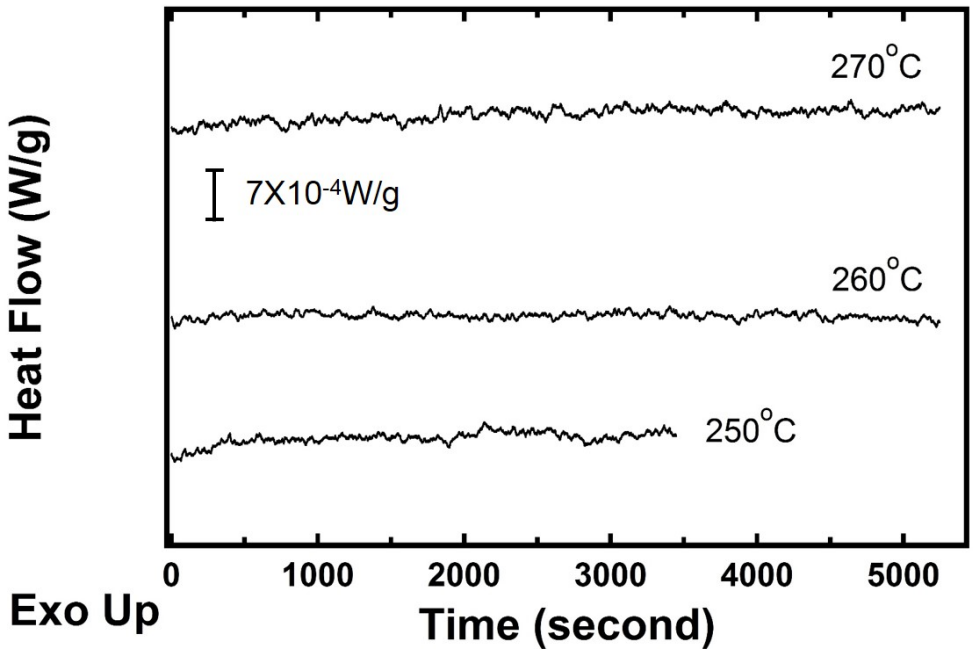

Figure 3.2: Isothermal DSC scans for HX8000 at 270, 260 and 250°C, HX8000 was cooled from 310°C. The vertical bar suggests the scale in heat flow.

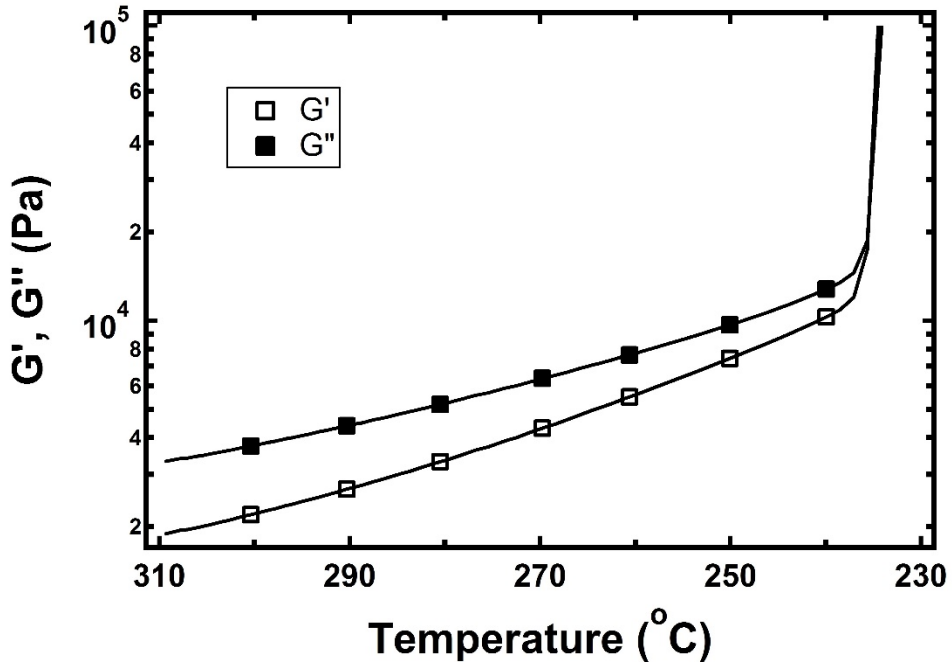

Figure 3.3: The storage modulus G’ and loss modulus G” versus temperature as HX8000 was cooled at a rate of 20°C/min.

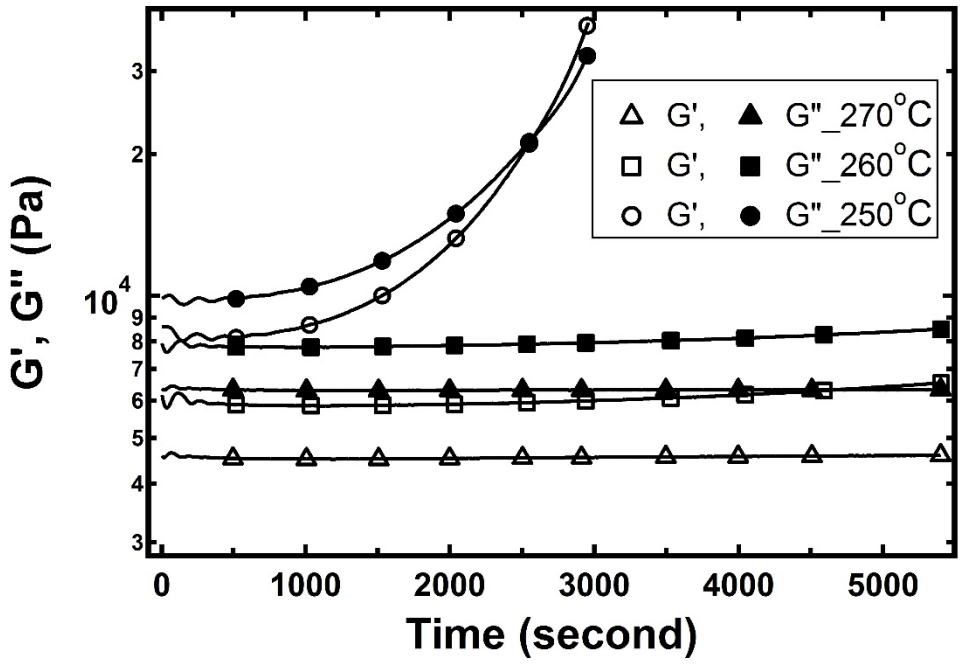

Figure 3.4: The storage modulus G’ and loss modulus G” versus time as HX8000 was cooled to different temperatures below T_m.

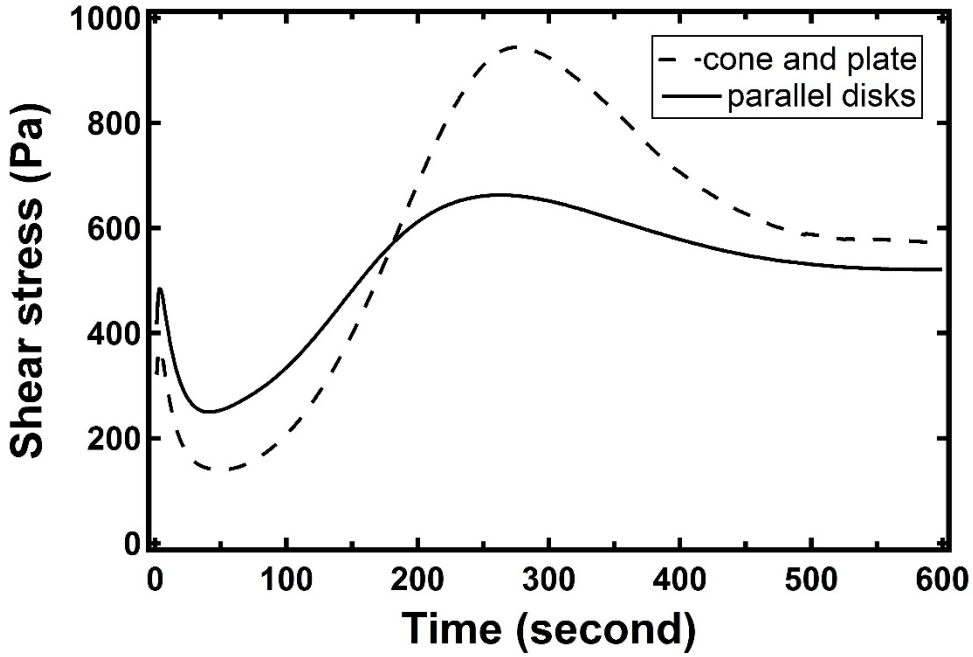

Figure 3.5: Transient stress growth of HX8000 in flow incpetion at 310^{o}C and 0.5 s^{-1}, using cone-and-plate (0.1 rad, 25 mm diameter) and parallel disks fixtures (25 mm diameter), respectively.

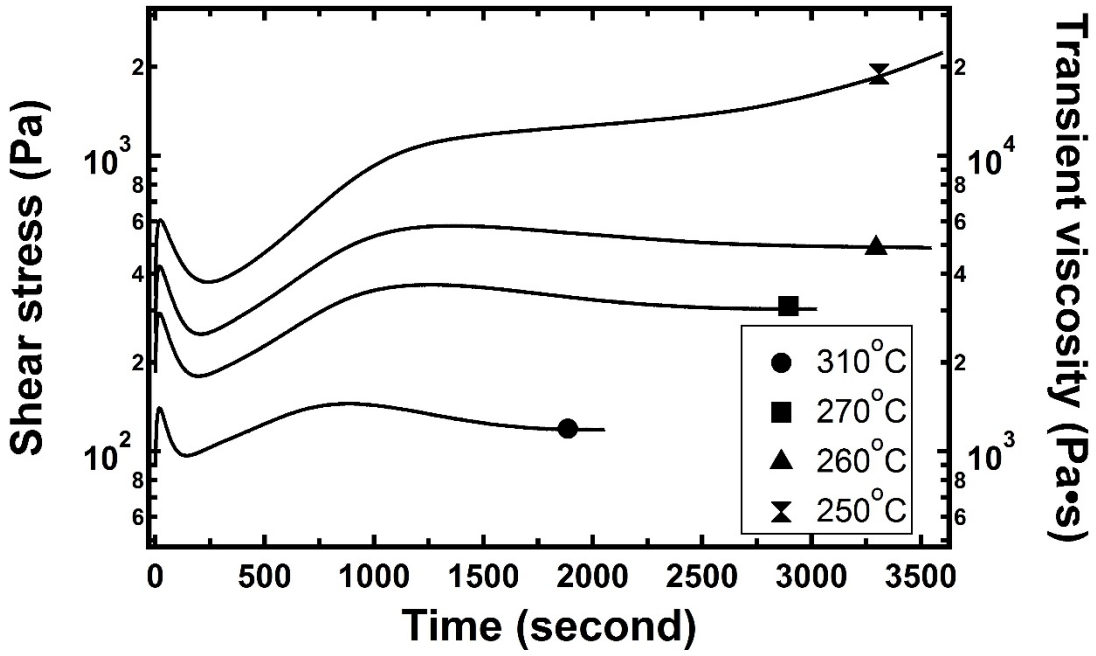

Figure 3.6: Growth curves of transient shear stress and viscosity above the melting point (310°C) and in the super-cooled state (270, 260 and 250°C) for HX8000. Shear rate equals 0.1 s^{-1}.

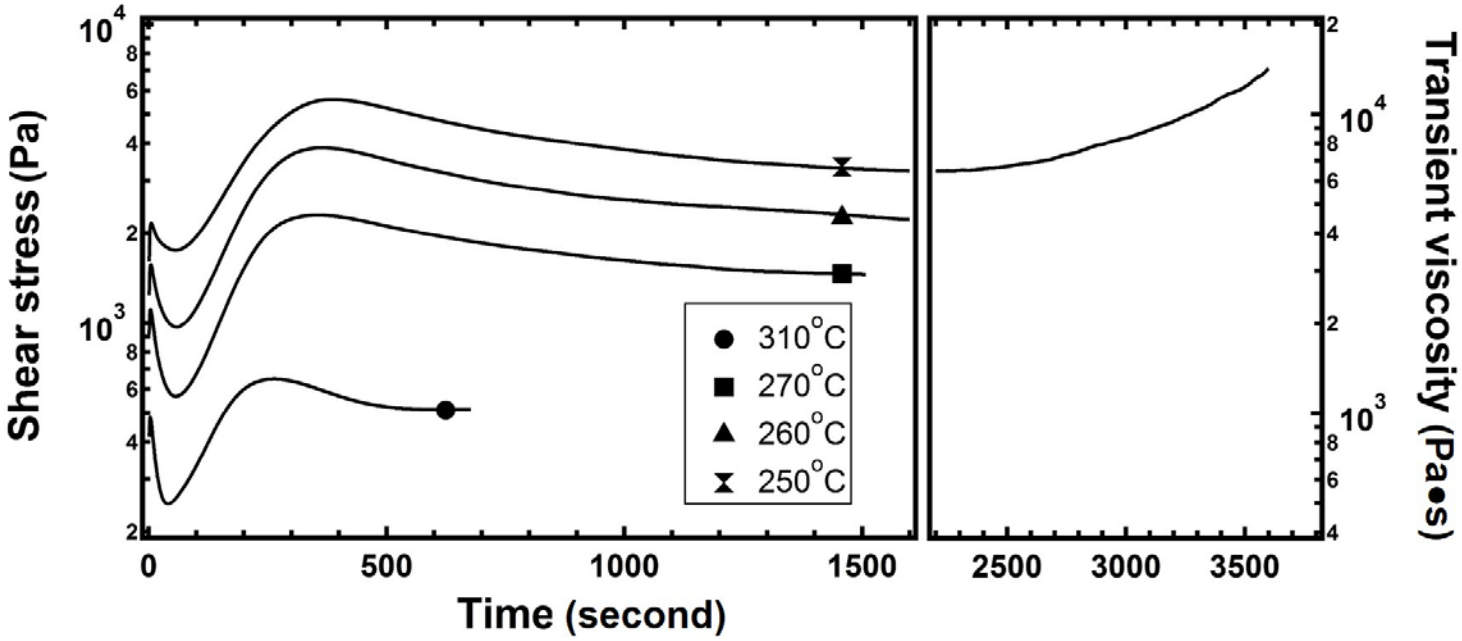

Figure 3.7: Growth curves of transient shear stress and viscosity above the melting point (310°C) and in the super-cooled state (270, 260 and 250°C) for HX8000. Shear rate equals 0.5 s^{-1}.

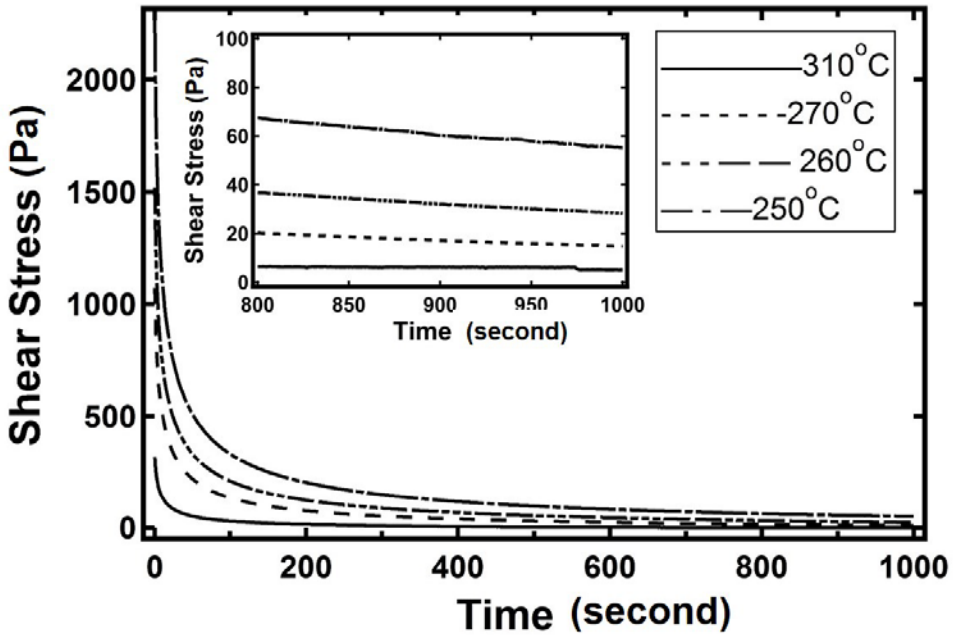

Figure 3.8: Relaxation of shear stress after flow cessation. Experiments were performed at the temperature of 310^{o}C and in the super-cooled state (270, 260 and 250^{o}C) for HX8000. The small figure embeded magnified the amount of residual stress after 800s of relaxation.

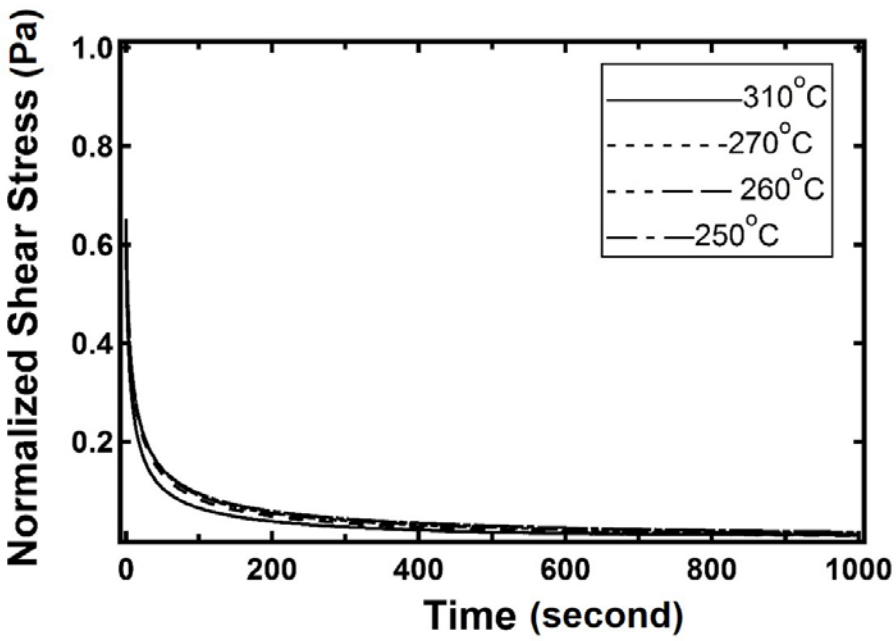

Figure 3.9: Relaxation of shear stress after flow cessation. Experiments were performed at the temperature of 310°C and in the super-cooled state (270, 260 and 250°C) for HX8000. The shear stress was normalized with respect to the steady state value obtained in preshearing.

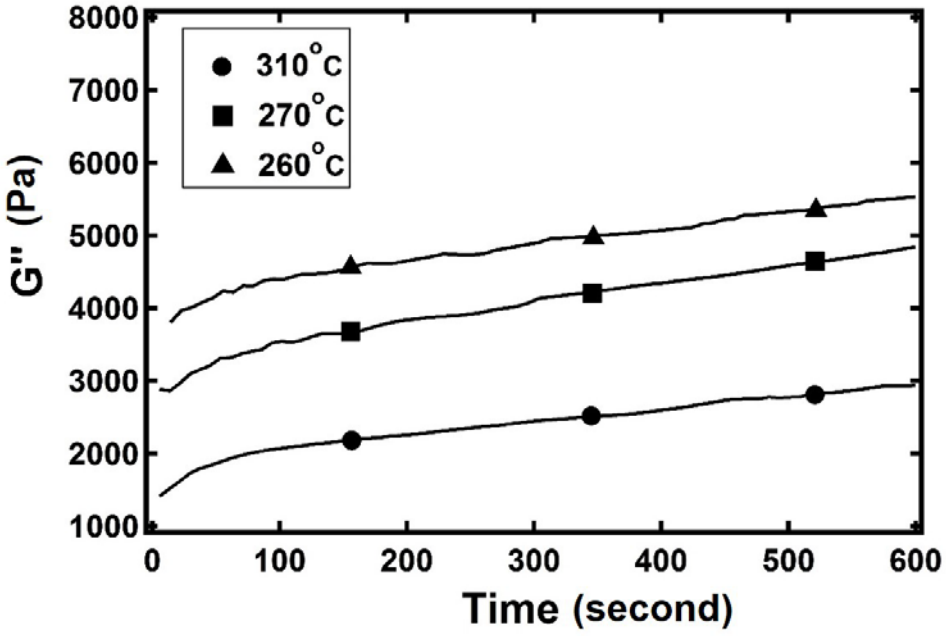

Figure 3.10: Evolution of G" after flow at 0.5 s^{-1} for 1600s for HX8000. Experiments were performed at the temperature of 310°C and in the super-cooled state (270, 260°C). The strain and frequency used were 1.0% and 10 rad/s, respectively.

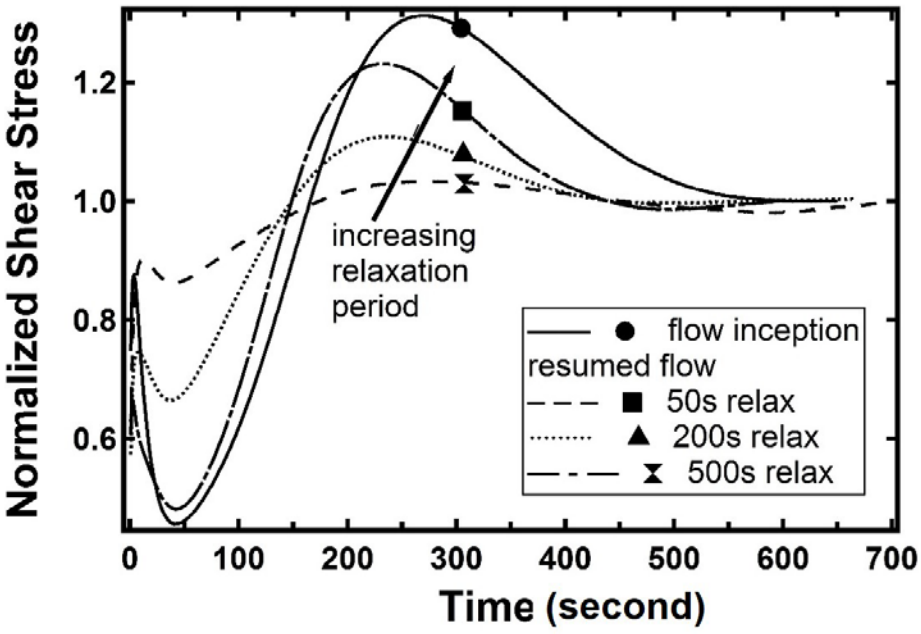

Figure 3.11: Trace of normalized transient shear stress after relaxaing for 50, 200 and 500s at 310^{o}C. The stress growth in the startup of shear flow is also shown as a reference.

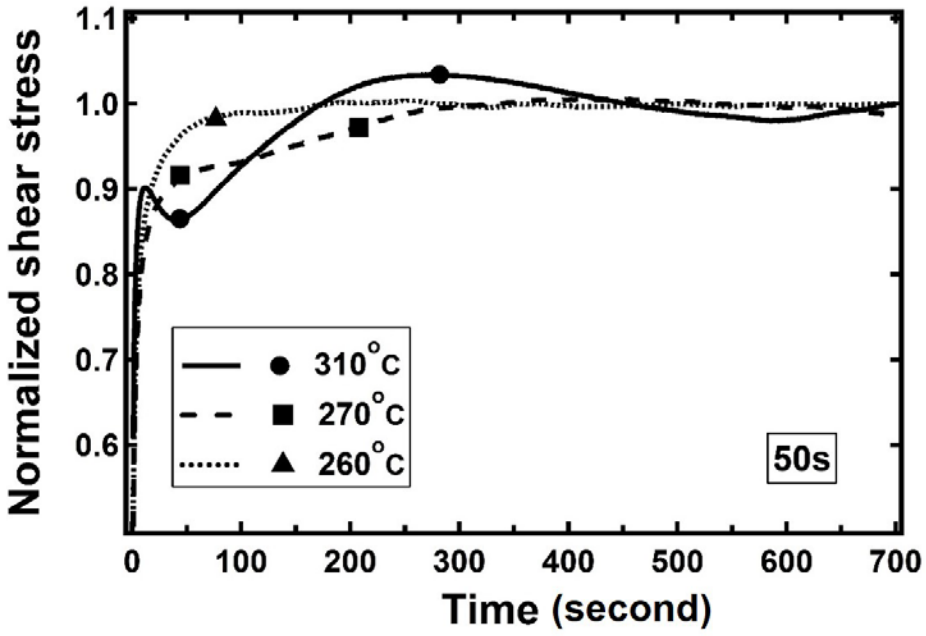

Figure 3.12: Trace of normalized transient shear stress after 50s relaxation. Measurements were performed at 310, 270 and 260ºC.

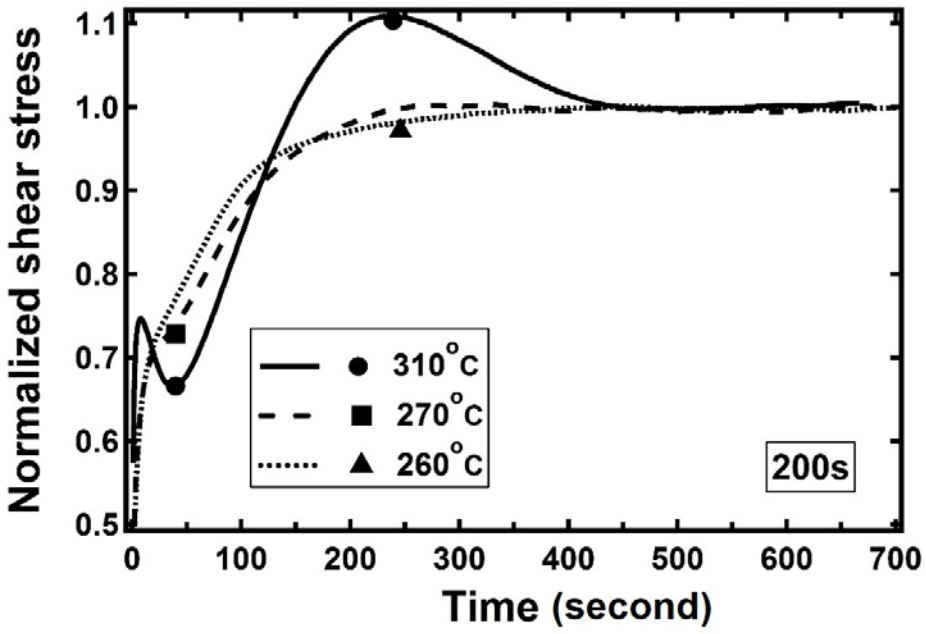

Figure 3.13: Trace of normalized transient shear stress after 200s relaxation. Measurements were performed at 310, 270 and 260ºC.

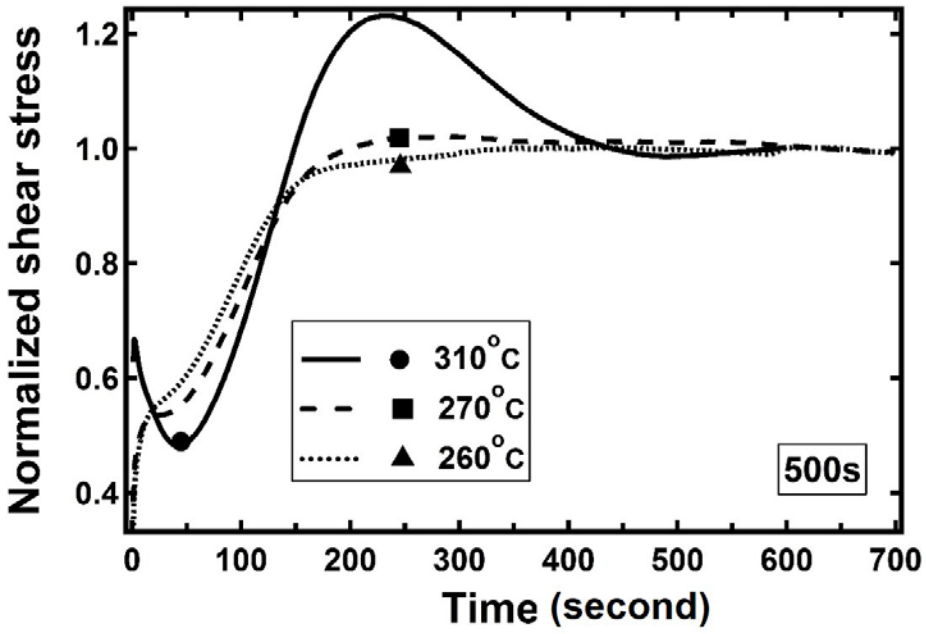

Figure 3.14: Trace of normalized transient shear stress after 500s relaxation. Measurements were performed at 310, 270 and 260ºC.

Table 3.1 Locations the overshoots and undershoot of shear stress in time units at 310 ^{o}C (above the melting point) and in the super-cooled state (270, 260 and 250^{o}C).

Shear rate /s^{-1}	Temperature /^{o}C	Peak position on time axis /s		
		Initial overshoot	undershoot	Second overshoot
0.1	310	18	146	861
	270	19	197	1277
	260	21	210	1373
	250	23	240	NA
0.5	310	3	40	263
	270	4	58	333
	260	5	62	357
	250	5	60	394

4 Extrusion Blow Molding of Polymeric Blends Based on Thermotropic Liquid Crystalline Polymer and High Density Polyethylene

Extrusion Blow Molding of Polymeric Blends Based on Thermotropic Liquid Crystalline Polymer and High Density Polyethylene

Chen Qian[a], Craig D. Mansfield[a], Donald G. Baird[a*]

[a]Department of Chemical Engineering, Virginia Polytechnic Institute and State University,

Blacksburg, VA 24061

4.1 Abstract

This work is concerned with the extrusion blow molding of polymeric blends containing thermotropic liquid crystalline polymer (TLCP) and high density polyethylene (HDPE), using a single screw extruder. The TLCP is synthesized from terephthalic acid, 4-hydroxybenzoic acid, hydroquinone and hydroquinone derivatives, the melting point of which is 280 ^{o}C. Because the TLCP is usually processed at much higher temperatures than HDPE, the thermal stability of HDPE at elevated temperature is evaluated. It is shown HDPE is stable in the processing temperature range of the TLCP used in this work (260 to 300 ^{o}C). Bottles are successfully produced from the blends containing 10, 20 and 50 wt% TLCP. The TLCP/HDPE blend bottles exhibit enhanced modulus relative to pure HDPE. However, the improvement in tensile strength is marginal. At 10 and 20 wt% TLCP contents, the TLCP phase exists as platelets aligning along the machine direction, while a co-continuous morphology is observed for the blend containing 50 wt% TLCP. To further enhance the mechanical properties of the blends, the preliminary effectiveness of maleic anhydride grafted HDPE (MA-g-HDPE) as a compatibilizer is studied. The injection molded ternary blends of TLCP/HDPE/MA-g-HDPE have demonstrated superior mechanical properties over the binary TLCP/HDPE blends, which suggests MA-g-HDPE as a potential compatibilizer for developing high performance TLCP/HDPE containers with enhanced mechanical properties.

4.2 Introduction

To exploit the outstanding mechanical properties of thermotropic liquid crystalline polymers (TLCPs), TLCPs have been blended with various thermoplastics, including poly(vinyl chloride) [1], polystyrene [2-3], polyethylene terephthalate (PET) [3-4], polybutylene terephthalate [5], polyamide 66 [6], polyamide 6 [7], polycarbonate [5], polyethylene naphthalate [8] and polyether ether ketone [5, 9]. For most polymeric blends reported so far, TLCPs are the minor components and form a microfibrillar phase to provide mechanical reinforcement. The blends with superior mechanical properties relative to the pure matrices are usually referred to as in situ composites.

Among all thermoplastics, the processing and associated properties of the in situ composites based on TLCPs and polyolefins have also been well documented [10-28]. One predominant processing technique applied is injection molding. Datta and Baird [23] injection molded the binary blends of polypropylene (PP) and TLCP into rectangular plaques. The two TLCPs used in this study were a copolyester synthesized from 73 mol% hydroxybenzoic acid (HBA) and 23 mol% hydroxynaphthoic acid (HNA), and a copolyester from 60 mol% HBA and 40 mol% PET, respectively. As the content of TLCP was increased to 50 wt%, the machine direction tensile modulus of the in situ composite was increased by roughly 3.6 times. However, the enhancement in the tensile strength was negligible, which was due to lack of interfacial adhesion between the TLCP and the matrix. In contrast to the significant improvement in modulus in the machine direction, the mechanical properties in the transverse direction remained almost unchanged.

Besides injection molding, other techniques used for processing TLCP/polyolefin blends include film extrusion and film blowing. Saengsuwan *et al.* [14] first melt compounded PP with

the TLCP of 80/20 HBA/PET using a twin screw extruder, the blends were then extruded into films. The tensile modulus of the 15/85 TLCP/PP blend was 130% higher than that of the neat PP in the machine direction. Nevertheless, the strength in the machine direction was gradually decreased as the TLCP content increased. Again, marginal improvement in the mechanical properties were obtained in the transverse direction. To overcome the property anisotropy, Chinsirikul *et al.* [27] produced in situ composite films based on TLCP/polyethylene (PE) using film blowing with a counter-rotating die. The counter rotating of both the concentric surfaces of the annular die imparted an orientation gradient of the TLCP fibrils through the film thickness. With this setup, comparable moduli in both the machine and transverse directions were achieved for the 10 wt% TLCP composite, which were about 4 times higher than that of neat PE. Interestingly, the strength was also doubled in both the machine and transverse directions.

Sukhadia and co-workers [29] developed a unique method of generating in situ composites, which was referred to as the dual-extruder mixing method. In this process PP and TLCP were plasticized separately using two individual single screw extruders. The melt streams were then brought together and blended by a static mixer. This method had two main advantages over the conventional processing techniques for developing in situ composites. First, in most studies, TLCPs and matrix polymers were processed with one extruder or injection molding unit, in which the two polymer components shared the same thermal history. This required the nominal processing temperatures of the two components to overlap, such that both components were melted, but the low melting components were not degraded. This made the manufacturing of in situ composites based on TLCPs and polyolefins a challenging task, because the melting points of polyolefins were usually lower than those of TLCPs. In the dual-extruder mixing method, the TLCP reinforcing phase and the matrix polymers were plasticized separately in two extruders, thus

the processing temperatures of the two phases did not have to overlap. Second, in the conversional processes the formation of TLCP fibrils with small diameter and large length to diameter (L/D) ratio was controlled by several factors, including the viscosity ratio of the dispersed phase (TLCPs) to the continuous phase (thermoplastics), interfacial tension, blend compositions, and the combination of elongation/shear flow fields. Nevertheless, using the dual-extruder mixing method, the formation of TLCP fibrils was realized by the redistribution of the TLCP melt streams in the matrix melt, which was independent of the viscosity ratio of the TLCP phase to the matrix materials. The TLCP fibrils generated were long and continuous, which was preferable for mechanical reinforcement. Using this method, the tensile modulus of the extruded PP strand was enhanced by 25 times relative to that when it was directly blended with 26 wt% polyesteramide TLCP (synthesized from 60 mol% HNA, 20 mol% terephthalic acid (TA) and 20 mol% 4-aminophenol).

Although the addition of TLCPs significantly enhances the mechanical properties of polyolefins, the binary TLCP/polyolefin blends are known to have poor interactions between the two phases, which prevents realizing the full potential of TLCPs as reinforcing components. A third component known as the compatibilizer is usually added to enhance the interfacial adhesion between TLCPs and polyolefins, such that the properties of the blends can be further improved. Compatibilizers can be grouped into two categories: physical compatibilizers and reactive compatibilizers [24]. Physical compatibilizers are usually chemical modified polyolefins, which promote the interfacial adhesion through intermolecular interactions, such as hydrogen bonding [10, 12-13, 16, 22-23, 28]. On the other hand, reactive compatibilizers are capable of reacting with TLCPs chemically and result in graft copolymers [18, 24-26], which reside along the interface of TLCPs and polyolefins to enhance the compatibility.

One class of widely used physical compatibilizer is the maleic anhydride grafted polyolefins. For instance, maleic anhydride graft PP (MA-g-PP) was compounded with the TLCP/PP blends [22]. The compatibilized ternary blends exhibited higher adhesion between the TLCP phase and the PP matrix. Additionally, MA-g-PP decreased the surface tension, which led to a finer dispersion of the TLCP phase in the matrix and facilitated the formation of a more fibrillary structure. Comparing with the uncompatibilized blend, significant improvements in both modulus and strength were observed for the ternary TLCP/PP/MA-g-PP blend.

Efforts were also made on the reactive compatibilization of TLCP and polyolefins. Zhang *et al.* [24] reported the melt reaction between the sodium salt of poly(ethylene-*co*-acrylic acid) and the TLCP of 73/27 HBA/HNA. The product was expected to contain the backbone of polyethylene and the branches of TLCP. Such a graft copolymer was suitable for compatibilizing TLCP and polyethylenes.

The polymer blends based on TLCPs and polyolefins have been processed by means of injection molding, film extrusion, filament extrusion and film blown. Nevertheless, it remains unknown whether bottles based on TLCP and HDPE can be produced by extrusion blow molding. Our objective to this work is threefold. First, determine the processing conditions for the extrusion blow molding of TLCP/HDPE. The second objective is to determine the mechanical properties as well as the morphology of the blow molded bottles. Additionally, previous work only reported using poly(ethylene-*co*-methacrylic acid) as a physical compatibilizer for TLCP and polyethylene [10, 27]. The compatibilization effect of maleic anhydride graft HDPE (MA-g-HDPE) for TLCP and HDPE is yet to be investigated. Therefore, the final objective is to at least qualitatively determine whether MA-g-HDPE is capable of compatibilizing TLCP and HDPE. Although the extrusion blow molding of the ternary blends based on TLCP/HDPE/MA-g-HDPE is not reported

in this paper, comparing the mechanical properties of the injection molded ternary blends with the binary TLCP/HDPE blends provides information on the preliminary effectiveness of MA-g-HDPE as a compatibilizer.

4.3 Experimental

4.3.1 Materials

Zenite HX8000 was provided by DuPont and was used as received. The Zenite series of TLCPs is believed to be synthesized from different ratios of terephthalic acid (TA), 4-hydroxybenzoic acid (HBA), hydroquinone (HQ) and hydroquinone derivatives (HQ derivatives) [30]. Nevertheless, the specific monomer ratio for HX8000 is unknown. Differential scanning calorimetry (DSC) shows HX8000 is a semi-crystalline polymer with a glass transition temperature around 110^{o}C. Temperatures higher than 280 ^{o}C are needed to guarantee the melting of all the crystalline structure [30].

The HDPE with a commercial name of Marlex HHM 5502 was obtained from Chevron Phillips. Marlex HHM 5502 is a high viscosity grade HDPE. The weight average molecular weight of Marlex HHM 5502 is $1.35X10^{5}$ g/mol, and the polydispersity index is 6.6. Marlex HHM 5502 is a chrome resin. The melt flow index and the density of the HDPE are 0.25 g/10 min and 0.96 g/cm^{3}, respectively.

Amplify 205 is a maleic anhydride graft HDPE (MA-g-HDPE) provided by the Dow Chemical Company. The melting point of Amplify 205 is 127 ^{o}C, and the melt flow index is 2.0 g/10 min. The density of Amplify 205 is 0.96 g g/cm^{3}.

4.3.2 Thermal stability measurements of HDPE

The thermal stability of HDPE at 260, 270, 290 and 300 ^{o}C was investigated using a TA instrument's ARES-G2 rheometer. HDPE was dried in a vacuum oven at 100 ^{o}C for at least 24 hr before use. Small amplitude oscillatory measurements were carried out in the time sweep mode. HDPE pellets were directly loaded between the parallel disk fixtures at the designated temperatures under both air and nitrogen environments. A 1 mm gap was used. Additional experimental settings included 5% strain and 10 rad/s angular frequency. The evolution of complex viscosity, η^*, as a function of time was recorded.

4.3.3 Melt compounding of the TLCP/HDPE blends

The viscosity scheme of the TLCP/HDPE blends helps determining the processing conditions for blow molding. To obtain the samples for rheological measurements, the two materials were mixed by tumbling in a container for 5 min, with the TLCP contents of 10, 20 and 50 wt%. The mixed pellets were dried in a vacuum oven at 100 ^{o}C for at least 24 hr, which were then extruded into strands. When extruding, polymer pellets were feed in a nitrogen purged hopper. A Killion KL-100 single screw extruder was used for plasticizing the TLCP/HDPE blends. A Maddock screw with 25.4 mm diameter and 30:1 *L:D* was used with a capillary die of 1.59 mm diameter. The temperatures of the solid convey zone and the extruder barrel were set as 220 ^{o}C and 290 ^{o}C, respectively, which ensured the melting of both components. The screw speed applied was 25 rpm. After existing the die, the strands were quenched in a water bath and then pelletized into pellets.

4.3.4 Viscosity measurements

Frequency sweeps were performed at the temperatures of 260, 270, 290 and 300 ^{o}C. The blend pellets were directly loaded between the parallel disk fixtures and a 1 mm gap was used. 5% strain was applied and the angular frequency was in the ranged of 0.1 to 100 rad/s. For the testing temperatures of 260 and 270 ^{o}C, the pellets were first equilibrated at 290 ^{o}C for 3 mins to ensure all the solid crystalline structure of TLCP was excluded. The temperature was then lowered to 260 and 270 ^{o}C at a rate of 20 ^{o}C/min. After the materials were cooled to the predetermined temperatures, they were equilibrated for 2 mins before oscillatory shear started. 1mm gap was applied in the frequency sweep measurements.

4.3.5 Extrusion blow molding of the TLCP/HDPE blends

The Killion KL-100 extruder was used for extrusion blow molding. The annular die used for producing tubular shape parisons contained an inner mandrel supported by four spider legs. The inner diameter of the die was 27.9 mm, and the slit width was 3.68 mm. During the extrusion blow molding process, the extruder temperature was 290 ^{o}C, and the die temperature was set as 260 ^{o}C. The screw speed was 25 rpm. The residence time of the resin in the extruder was less than 600s, and the time consumed to form a parison was roughly 50 s. After the mold closed around the parison, 25 psi compressed air inflated the parison into the shape of a hollow bottle. The blow up ratio was about 2. The mold temperature was kept at 25 ^{o}C.

4.3.6 Injection molding of the ternary TLCP/MA-g-HDPE/HDPE blends

The pellets of TLCP, MA-g-HDPE and HDPE were manually blended. The content of TLCP in the blends was kept constant as 20 wt%. The ratios of MA-g-HDPE to HDPE were varied from 10:90, 25:75 and 50:50. The drying protocol of the materials was exactly the same as that

used in the extrusion blow molding. Injection molding was performed with a BOY 35E machine. The barrel temperatures of the injection molder were 265 ^{o}C for the first zone and 290 ^{o}C for zones two to four. The temperature of the nozzle was lowered to 260 ^{o}C, and the mold temperature was 40 ^{o}C. The ternary blends were injection molded into rectangular plaques with the dimensions of 80 mm X 76mm X 1.56mm.

4.3.7 Tensile properties

For the blow molded TLCP/HDPE blends, specimens for tensile measurements were cut along the machine direction from the midsection of the bottles. For the injection molded ternary blends, 7 mm wide strips were cut along both the flow and transverse directions. All samples were tested by an Instron Model 4204 machine. A 5 kN load cell was used. The crosshead speed was 1 mm/min, and an extensometer was applied to measure of the tensile modulus accurately.

4.3.8 Morphological characterization

The morphology of the blow molded TLCP/HDPE bottles was analyzed by scanning electron microscope (SEM). Test specimen was fractured along both the machine and hoop directions. To facilitate the cryofracture of the specimen, samples were embedded in epoxy. After breaking the specimen under the liquid nitrogen environment, the fracture surface was sputter coated with gold, and the morphology of the fracture surfaces was visualized by means of a LEO 1550 environmental SEM with an accelerating voltage of 5 kV. For the 50 wt% TLCP blend, the samples were recycled after the initial scan. The samples were treated with trichlorobenzene to dissolve the HDPE phase, and then recharacterized by SEM.

4.4 Results and Discussion

4.4.1 Thermal stability of HDPE

The thermal stability of HDPE in the temperature range from 260 to 300 ^{o}C is first investigated to determine the processing temperatures for extrusion blow molding. Because TLCP and HDPE were plasticized and mixed using one single screw extruder, the two materials shared the same thermal history. The TLCP melts at a much higher temperature than HDPE, and the extruder temperature needs to be above the melting point of the TLCP to melt both components. Therefore, it is important to know how thermally stable HDPE is in the temperature range that TLCP can be processed.

The thermal stability is studied by means of small amplitude oscillatory shear measurements in the time sweep mode. Among the four temperatures used, 290 and 300 ^{o}C are above the melting point of the TLCP. Our previous studies have shown once the TLCP is melted, it is still processable when it is super cooled to the temperatures of 270 and 260 ^{o}C [31-32]. Thus 260 and 270 ^{o}C could potentially be applied for the processing of the TLCP/HDPE blends, providing the temperature of the blends is first raised above 280 ^{o}C. The measurements were performed under both nitrogen and air environments. Because a nitrogen purge hopper is used, the results obtained under nitrogen environment reflects the stability of HDPE in the extruder. On the other hand, when the parisons exit the die, they are exposed to air, and their stability can be interpreted from the results obtained under air environment. In these measurements the complex viscosity, η^{*}, is monitored as a function of time, as shown in Figs 4.1 and 4.2. To better visualize the evolution of η^{*}, the curves are normalized with respect to their initial values.

In both Figs 4.1 and 4.2, η^* gradually increases as time elapses. The increase in η^* is due to the thermal degradation of HDPE, most likely crosslinking [33-35]. As it is expected, HDPE degrades faster at higher temperatures and under an air environment. However, the degree of degradation under nitrogen is limited. At the highest temperature of 300 ^oC, η^* increases by 20% in 1200 s. We have recorded the time from when the materials are feed to the extruder till the time parisons exist the die, and the total time consumed is less than 600 s. Within this time period, the increment of η^* is limited under nitrogen. Additionally, the exposure time of the parisons in air is less than 60 s. As indicated by Fig 4.2, the degradation of the parisons exposed to air should also be almost negligible within such short time period. We believe the HDPE is stable if the increment in the normalized complex viscosity is less than 20%. Within the residence time in the extruder, the thermal degradation of the HDPE is negligible. Lower temperatures, such as 260 and 270 ^oC, are preferential to minimize the degradation of HDPE.

4.4.2 Melt viscosity of the TLCP/HDPE blends

The viscosity of the TLCP/HDPE blends is obtained using the small amplitude oscillatory shear in the frequency sweep mode. The measurements were performed at 300, 290, 270 and 260 ^oC. For tests at 270 and 260 ^oC, the blends were first equilibrated at 290 ^oC to ensure the TLCP was melted, then the temperature was lowered to super cool the TLCP. The results are presented in Figs 4.3 to 4.6. Because of the very broad molecular weight distribution, the Newtonian region is not observed within the shear rate of 0.1 to 100 rad/s in Fig3 4.3 to 4.6 for the neat HDPE. At each temperature, the viscosity of HDPE is more than one order of magnitude higher than that of TLCP. This is not surprising, as TLCPs are well known for their low viscosity [36-39]. A three region steady shear viscosity scheme have been reported for other commercial TLCPs, in which the steady shear viscosity exhibits a shear thinning region at low shear rates, followed by a

Newtonian region and another shear thinning region as the shear rate increases. However, only two viscosity regions are observed in Figs 4.3 to 4.6, the initial shear thinning region is not obtained. This is most likely due to the fact that the shear rate used is not low enough.

As the TLCP content increases in the blends, the viscosity is reduced. The viscosity of all blends is also increased as the temperature drops, as expected. Nevertheless, even at the highest TLCP content of 50 wt%, the viscosity of the blends is still above 10^4 Pas•s^{-1} at 0.1 s^{-1} for all four temperatures. The relative high viscosity at low shear rate is a good indication of good melt strength [40].

Combining the results in Figs 4.1to 4.6, the barrel temperature of the extruder for extrusion blow molding is set as 290 ^oC, such that both the TLCP and HDPE are melted. The temperature of the annular die is lowered to 260 ^oC, at which the TLCP is in its super-cooled state. Two main benefits are obtained from lowering the temperature of the die. First, the degradation of HDPE can be minimized. Second, the viscosity as well as the melt strength of the parisons can be further enhanced, which is of critical importance to the success of extrusion blow molding.

4.4.3 Mechanical properties of the TLCP/HDPE bottles

The tensile properties of the extrusion blow molded TLCP/HDPE bottles in the machine direction are shown in Figs 4.7 to 4.8. The tensile modulus increases monotonically as the TLCP content is increased. It can also be observed that the tensile modulus is a linear function of TLCP content. With 50 wt% TLCP content, the modulus of the bottle developed from the blend is 3.2 times higher than that of the pure HDPE bottle. On the other hand, the increment in tensile strength is marginal. The strength of the bottles from the 10 and 20 wt% blends is comparable with that of the blow molded HDPE. Comparing with pure HDPE, the addition of 50 wt% TLCP enhances the

strength from 15.4 MPa to 17.3 MPa. The standard deviations for these two values are 0.4 and 0.7 MPa, which corresponds to 2.5% and 4% of the average strength, respectively. Limited improvement in tensile strength is probably due to the poor interfacial interaction between HDPE and TLCP.

4.4.4 Morphology of blow molded TLCP/HDPE bottles

A schematic representation of the midsection of blow molded TLCP/HDPE bottles with cylindrical coordinates is shown in Fig 4.9. The fracture surface in the r-θ plane is obtained by fracturing the sample along the machine direction, while fracturing the sample along the hoop direction give the surface in the r-z plane. The SEM images representing the morphology in both fracture planes are shown in Figs 4.10 to 4.12, for the TLCP contents of 10, 20 and 50 wt%, respectively.

For the 10 wt% TLCP blend, an immiscible two-phase morphology is observed. In the r-θ plane, it can be observed that the TLCP phase is elongated along the θ direction, the authors believe this is due to the planar extension in the parison inflation process. The surface voids are due to the pull out of the TLCP phase from the HDPE matrix when the sample is fractured. They also indicate lack of adhesion between the TLCP and HDPE phases. The fracture surface in the r-z plane shows the TLCP phase is highly stretched along the machine direction. Therefore, the TLCP phase exists as platelets with small θ/z aspect ratios. The small dimension in the θ direction is most likely due to the relatively low blow up ratio. The morphology of the 20 wt% TLCP blend is qualitatively similar to that of the 10wt% blend, except the size of the TLCP domains seems to be larger in the r-θ plane. At the 50 wt% TLCP content it is hard to distinguish one phase from another from either the r-θ or r-z plane. At this TLCP content we speculate a co-continuous morphology is formed. To

verify our speculation, the same samples used to obtain Fig 4.12 were treated with trichlorobenzene, such that the HDPE phase was dissolved, leaving only the TLCP "skeleton". The continuous phase of TLCP can be clearly observed from Fig 4.13, which demonstrates the co-continuous structure is formed for the 50 wt% TLCP blend.

4.4.5 Mechanical properties of the ternary TLCP/HDPE/MA-g-HDPE blends

To further improve the mechanical properties of the polymeric blends based on TLCP and HDPE, the compatibilizing effect of MA-g-HDPE is investigated by analyzing the mechanical properties of the ternary TLCP/HDPE/MA-g-HDPE blends. For all three ternary blends the content of TLCP is a constant value of 20 wt%, but the ratios of MA-g-HDPE to HDPE are 10/90, 25/75 and 50/50, respectively. The ternary blends were injection molded into square plaques, and the tensile modulus and strength were measured along both the machine and transverse directions, as shown in Figs 4.14 to 4.17.

In the machine direction, there is no obvious change in modulus as the ratio of MA-g-HDPE to HDPE increases. However, the strength is significantly improved when a higher amount of MA-g-HDPE is blended. The tensile strength is 17.7±1.2, 18.3±1.6 and 20.4±1.5 MPa for the MA-g-HDPE/HDPE ratios of 10/90, 25/75 and 50/50, respectively. In comparison, the strength of the binary blend without MA-g-HDPE is 15.6 MPa. Therefore, a 31% increment in strength is achieved from the 50/50 MA-g-HDPE to HDPE ratio.

In the transverse direction, due to the overlap of error bars, there is no statistical difference in terms of modulus for various MA-g-HDPE/HDPE ratios. Again, an obvious enhancement in strength is observed when the MA-g-HDPE content is increased. A 34% enhancement in strength is obtained for the 25/75 MA-g-HDPE/HDPE ratio relative to the binary blend. Then the strength

levels off as the MA-g-HDPE/HDPE ratio is further increased from 25/75 to 50/50. The better mechanical properties of the ternary blends are probably the result of the interactions between the maleic anhydride groups of the MA-g-HDPE and the carboxylic end groups of the TLCP.

4.5 Conclusions

Despite the processing temperature for HDPE usually being lower than that of TLCP, HDPE has been shown to be thermally stable enough at elevated temperatures at which both components can be melted and plasticized. Blow molding the blends at the super-cooled temperatures of the TLCP minimizes the degradation of HDPE and improves the melt strength of the parisons, which leads to high quality products.

Blending TLCP with HDPE significantly improved the modulus of the bottles in the machine direction. However, the enhancement in strength is limited. At the TLCP contents of 10 and 20 wt%, a platelet TLCP morphology is observed. Because of the relatively small blow-up ratio, the dimension of the TLCP platelets in the hoop direction is much lower than that in the machine direction. With 50 wt% TLCP content, a co-continuous structure of the TLCP and HDPE is obtained.

The ternary TLCP/HDPE/MA-g-HDPE blends exhibit greatly improved mechanical properties compared with the binary TLCP/HDPE blends, especially the tensile strength. Consequently, it is promising to apply the ternary blends of TLCP/HDPE/MA-g-HDPE in the blow molding process for improved mechanical properties.

4.6 Acknowledgements

The authors would like to thank the Department of Energy through the Savanah River National Laboratories for the financial support. Moreover, materials provided by Dupont, Chevron

Phillips and Dow Chemical are gratefully acknowledged. Prof. Dr. Garth Wilkes at Virginia Polytechnic Institute and State University provided tremendous inputs for this report, which is greatly appreciated by the authors. The authors would also like to thank Steve McCartney and the Nanoscale Characterization and Fabrication Laboratory at Virginia Tech for assisting SEM measurements and analysis.

References

[1] Y. Z. Meng and S. C. Tjong, "Preparation and properties of injection-molded blends of poly(vinyl chloride) and liquid crystal copolyester", *Polymer*, vol.40, pp 2711-2718, 1999.

[2] G. Crevecoeur and G. Groeninckx, "Morphology and mechanical properties of thermoplastic composites containing a thermotropic liquid crystalline polymer", *Polymer Engineering and Science*, vol.30, pp 532-542, 1990.

[3] P. Zhuang, T. Kyu and J. L. White, "Characteristics of hydroxybenzoic acid-ethylene terephthalate copolymers and their blends with polystyrene, polycarbonate, and polyethylene terephthalate", *Polymer Engineering and Science*, vol.28, pp 1095-1106, 1988.

[4] J. Seppälä, M. Heino and C. Kapanen, "Injection-moulded blends of a thermotropic liquid crystalline polymer with polyethylene terephthalate, polypropylene, and polyphenylene sulfide", *Journal of Applied Polymer Science*, vol.44, pp 1051-1060, 1992.

[5] G. Kiss, "In situ composites: Blends of isotropic polymers and thermotropic liquid crystalline polymers", *Polymer Engineering and Science*, vol.27, pp 410-423, 1987.

[6] D. Dutta, H. Fruitwala, A. Kohli and R. A. Weiss, "Polymer blends containing liquid crystals: A Review", *Polymer Engineering and Science*, vol.30, pp 1005-1018, 1990.

[7] R. K. Krishnaswamy, S. E. B. Wadud and D. G. Baird, "Influence of a reactive terpolymer on the properties of in situ composites based on polyamides and thermotropic liquid crystalline polyesters", *Polymer*, vol.40, pp 701-716, 1998.

[8] S. H. Jang and B. S. Kim, "Morphology and mechanical properties of liquid crystalline copolyester and poly(ethylene 2,6-naphthalate) blends", *Polymer Engineering and Science*, vol.35, pp 538-545, 1995.

[9] A. I. Isayev and P. R. Subramanian, "Blends of a liquid-crystalline polymer with poly(ether ether ketone)", *Polymer Engineering and Science*, vol.32, pp 85-93, 1992.

[10] T. C. Hsu, A. M. Lichkus and I. R. Harrison, "Liquid crystal polymer/polyethylene blends for thin film applications", *Polymer Engineering and Science*, vol.33, pp 860-863, 1993.

[11] W. Chinsirikul, T. C. Hsu and I. R. Harrison, "Liquid crystalline polymer (LCP) reinforced polyethylene blend blown film: Effects of counter-rotating die on fiber orientation and film properties", *Polymer Engineering & Science*, vol.36, pp 2708-2717, 1996.

[12] E. A. Sabol, A. A. Handlos and D. G. Baird, "Composites based on drawn strands of thermotropic liquid crystalline polymer reinforced polypropylene", *Polymer Composites*, vol.16, pp 330-345, 1995.

[13] S. Bualek-Limcharoen, J. Samran, T. Amornsakchai and W. Meesiri, "Effect of compatibilizers on mechanical properties and morphology of in-situ composite film of thermotropic liquid crystalline polymer/polypropylene", *Polymer Engineering and Science*, vol.39, pp 312-320, 1999.

[14] S. Saengsuwan, S. Bualek-Limcharoen, G. R. Mitchell and R. H. Olley, "Thermotropic liquid crystalline polymer (Rodrun LC5000)/polypropylene in situ composite films: rheology, morphology, molecular orientation and tensile properties", *Polymer*, vol.44, pp 3407-3415, 2003.

[15] A. G. C. Machiels, K. F. J. Denys, J. Van Dam and A. P. De Boer, "Effect of processing history on the morphology and properties of polypropylene/thermotropic liquid crystalline polymer blends", *Polymer Engineering and Science*, vol.37, pp 59-72, 1997.

[16] M. T. Heino and J. V. Seppälä, "Studies on compatibilization of blends of polypropylene and a thermotropic liquid crystalline polymer", *Journal of Applied Polymer Science*, vol.48, pp 1677-1687, 1993.

[17] M. T. Heino and J. V. Seppälä, "Extruded blends of a thermotropic liquid crystalline polymer with polyethylene terephthalate, polypropylene, and polyphenylene sulfide", *Journal of Applied Polymer Science*, vol.44, pp 2185-2195, 1992.

[18] Y.-P. Chiou, K.-C. Chiou and F.-C. Chang, "In situ compatibilized polypropylene/liquid crystalline polymer blends", *Polymer*, vol.37, pp 4099-4106, 1996.

[19] A. R. Postema and P. J. Fennis, "Preparation and properties of self-reinforced polypropylene/liquid crystalline polymer blends", *Polymer*, vol.38, pp 5557-5564, 1997.

[20] M. T. Heino, P. T. Hietaoja, T. P. Vainio and J. V. Seppälä, "Effect of viscosity ratio and processing conditions on the morphology of blends of liquid crystalline polymer and polypropylene", *Journal of Applied Polymer Science*, vol.51, pp 259-270, 1994.

[21] A. A. Handlos and D. G. Baird, "Processing and Associated Properties of In Situ Composites Based on Thermotropic Liquid Crystalline Polymers and Thermoplastics", *Journal of Macromolecular Science, Part C*, vol.35, pp 183-238, 1995.

[22] H. J. O'Donnell and D. G. Baird, "In situ reinforcement of polypropylene with liquid-crystalline polymers: effect of maleic anhydride-grafted polypropylene", *Polymer*, vol.36, pp 3113-3126, 1995.

[23] A. Datta and D. G. Baird, "Compatibilization of thermoplastic composites based on blends of polypropylene with two liquid crystalline polymers", *Polymer*, vol.36, pp 505-514, 1995.

[24] H. Zhang, R. A. Weiss, J. E. Kuder and D. Cangiano, "Reactive compatibilization of blends containing liquid crystalline polymers", *Polymer*, vol.41, pp 3069-3082, 2000.

[25] Y. Son and R. A. Weiss, "Compatibilizers for thermotropic liquid crystalline polymer/polyolefin blends prepared by reactive mixing: the effect of processing conditions", *Polymer Engineering and Science*, vol.41, pp 329-340, 2001.

[26] Y. Son and R. A. Weiss, "Compatibilizers for thermotropic liquid crystalline polymer/polyethylene blends prepared by reactive mixing", *Polymer Engineering and Science*, vol.42, pp 1322-1332, 2002.

[27] W. Chinsirikul, T. C. Hsu and I. R. Harrison, "Liquid crystalline polymer (LCP) reinforced polyethylene blend blown film: Effects of counter-rotating die on fiber orientation and film properties", *Polymer Engineering and Science*, vol.36, pp 2708-2717, 1996.

[28] A. Datta, H. H. Chen and D. G. Baird, "The effect of compatibilization on blends of polypropylene with a liquid-crystalline polymer", *Polymer*, vol.34, pp 759-766, 1993.

[29] A. M. Sukhadia, A. Datta and D. G. Baird, "Mixing history on the morphology and properties of thermoplastic/LCP blends", *International Polymer Processing*, vol.7, pp 218-228, 1992.

[30] M. A. McLeod and D. G. Baird, "The crystallization behavior of blends of thermotropic liquid crystalline polymers", *Polymer*, vol.40, pp 3743-3752, 1999.

[31] C. Qian, "PhD dissertation", PhD dissertation, Virginia Tech, 2016.

[32] C. Qian and D. G. Baird, *Submitted*, 2016.

[33] A. Harlin and T. Vainio, "Effect of polydispersity on the thermomechanical degradation of high-density polyethylene polymerized using a chromium catalyst", *Polymer Degradation and Stability*, vol.39, pp 29-34, 1993.

[34] D. Yan, W. J. Wang and S. Zhu, "Effect of long chain branching on rheological properties of metallocene polyethylene", *Polymer*, vol.40, pp 1737-1744, 1998.

[35] E. Epacher, J. Tolveth, K. Stoll and B. Pukanszky, "Two-step degradation of high-density polyethylene during multiple extrusion", *Journal of Applied Polymer Science*, vol.74, pp 1596-1605, 1999.

[36] F. Beekmans, A. D. Gotsis and B. Norder, "Transient and steady-state rheological behavior of the thermotropic liquid crystalline polymer Vectra B950", *Journal of Rheology*, vol.40, pp 947-966, 1996.

[37] T. Guo, G. M. Harrison and A. A. Ogale, "Transient shear rheology and rheo-optical microstructural characterization of a thermotropic liquid crystalline polymer", *Polymer Engineering and Science*, vol.45, pp 187-197, 2005.

[38] A. D. Gotsis and D. G. Baird, "Rheological Properties of Liquid Crystalline Copolyester Melts. II. Comparison of Capillary and Rotary Rheometer Results", *Journal of Rheology*, vol.29, pp 539-556, 1985.

[39] H. C. Langelaan and A. D. Gotsis, "The relaxation of shear and normal stresses of nematic liquid crystalline polymers in squeezing and shear flows", *Journal of Rheology*, vol.40, pp 107-129, 1996.

[40] C. D. McGrady, "PhD dissertation", PhD dissertation, Virginia Tech, 2009.

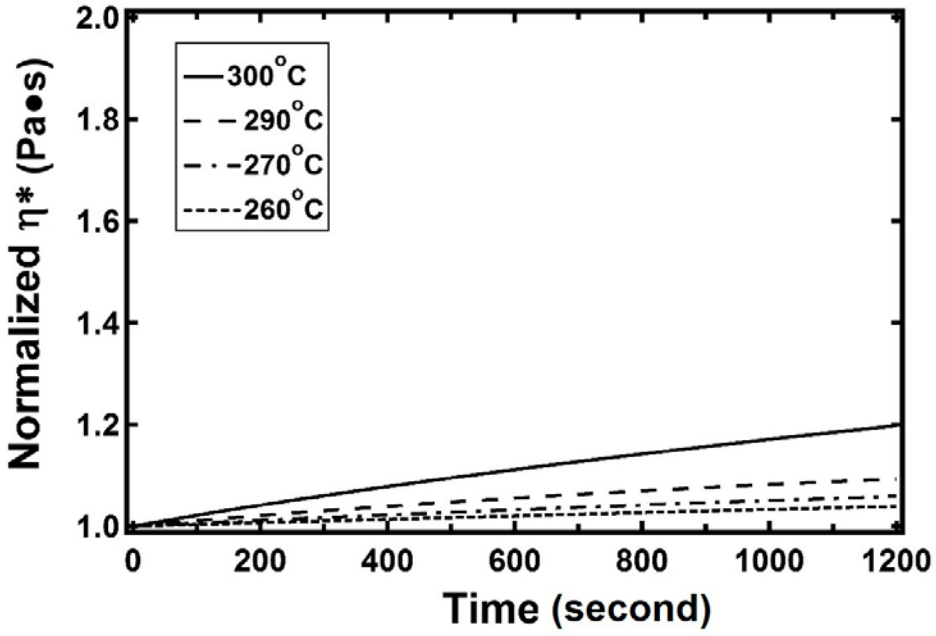

Figure 4.1: The normalized complex viscosity η* versus time of HDPE at the temperatures of 260, 270, 290 and 300°C, under nitrogen environment.

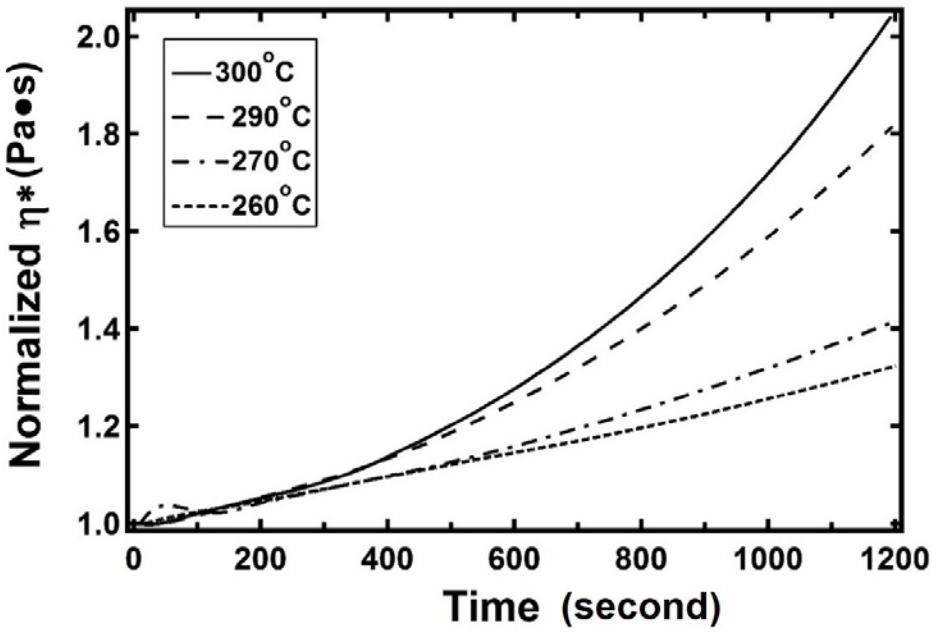

Figure 4.2: The normalized complex viscosity η* versus time of HDPE at the temperatures of 260, 270, 290 and 300°C, under an air environment.

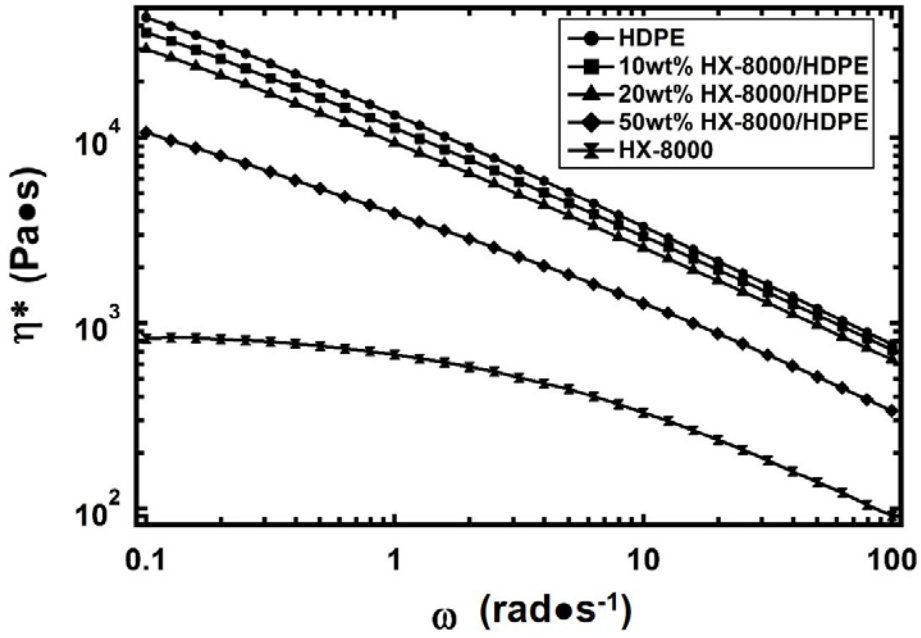

Figure 4.3: Frequency sweep of the TLCP/HDPE blends at 300^{o}C.

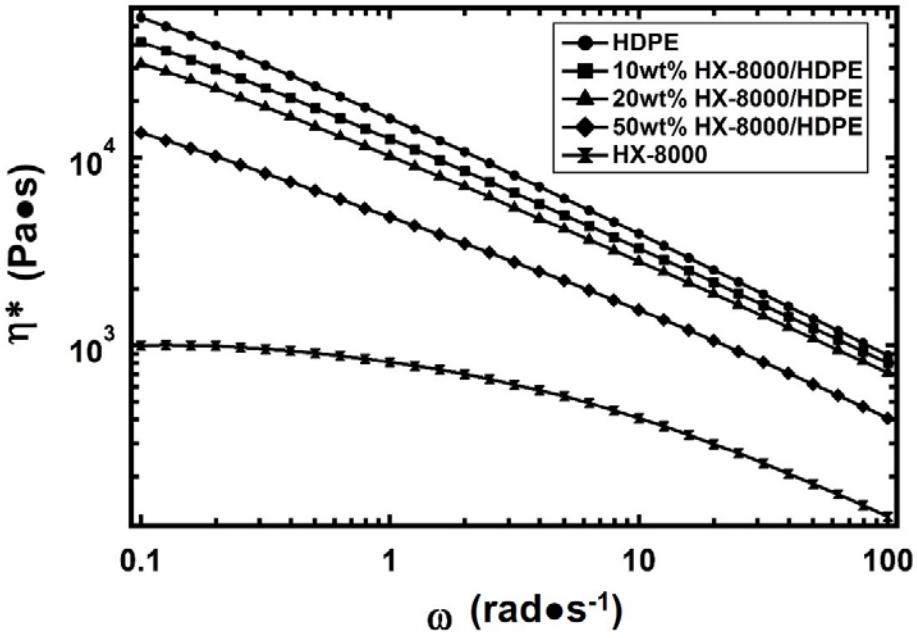

Figure 4.4: Frequency sweep of the TLCP/HDPE blends at 290^{o}C.

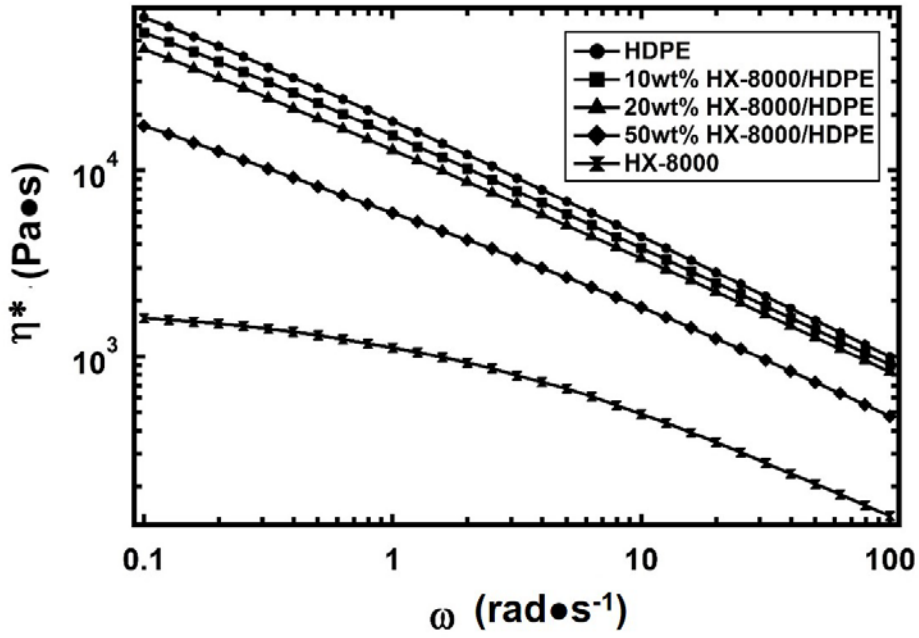

Figure 4.5: Frequency sweep of the TLCP/HDPE blends at 270°C. The materials were first equilibrated at 290°C, and then cooled to 270°C.

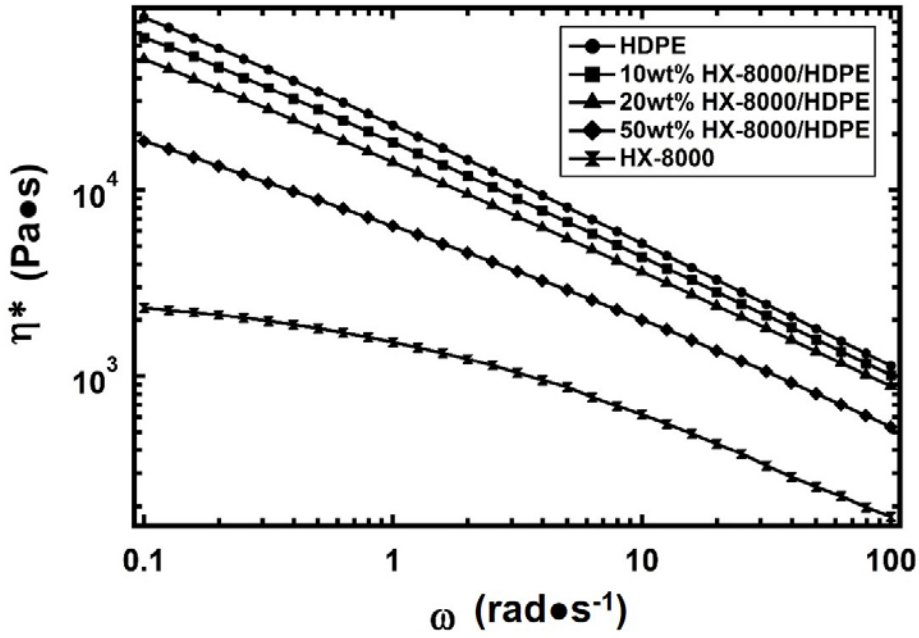

Figure 4.6: Frequency sweep of the TLCP/HDPE blends at 260°C. The materials were first equilibrated at 290°C, and then equilibrated to 260°C.

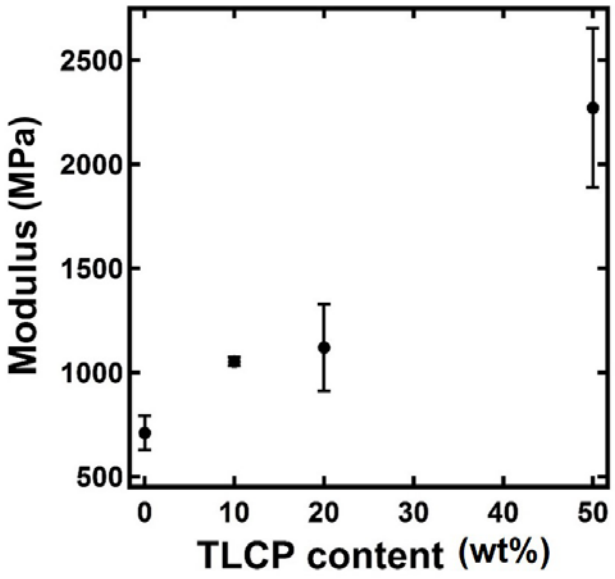

Figure 4.7: Tensile modulus of the blow molded TLCP/HDPE bottles in the machine direction.

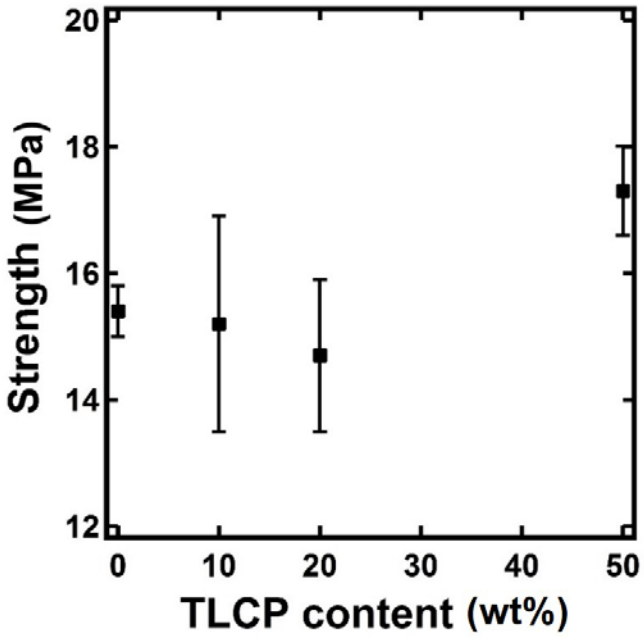

Figure 4.8: Tensile strength of the blow molded TLCP/HDPE bottles in the machine direction.

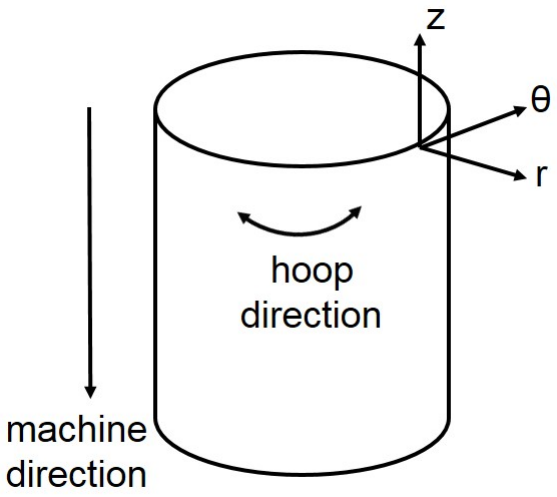

Figure 4.9: A schematic representation of the midsection of the blow molded TLCP/HDPE bottle with cylindrical coordinates, from which samples were cut and fractured for SEM analysis.

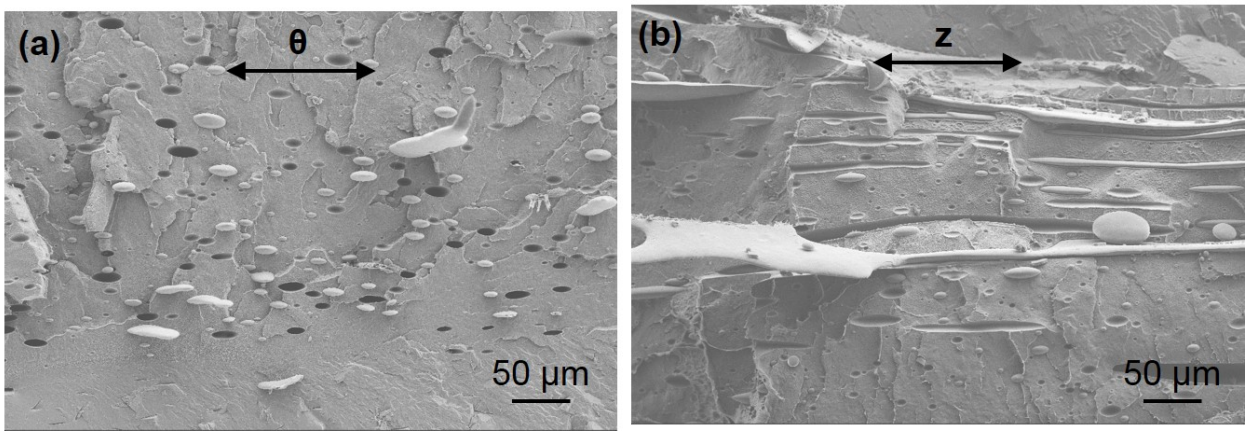

Figure 4.10: SEM images of 10 wt% TLCP/HDPE bottle. (a) and (b) are the fracutre surfaces in the r-θ and r-z planes, respectively. The horizontal direction represents θ direction in (a) and z direction in (b).

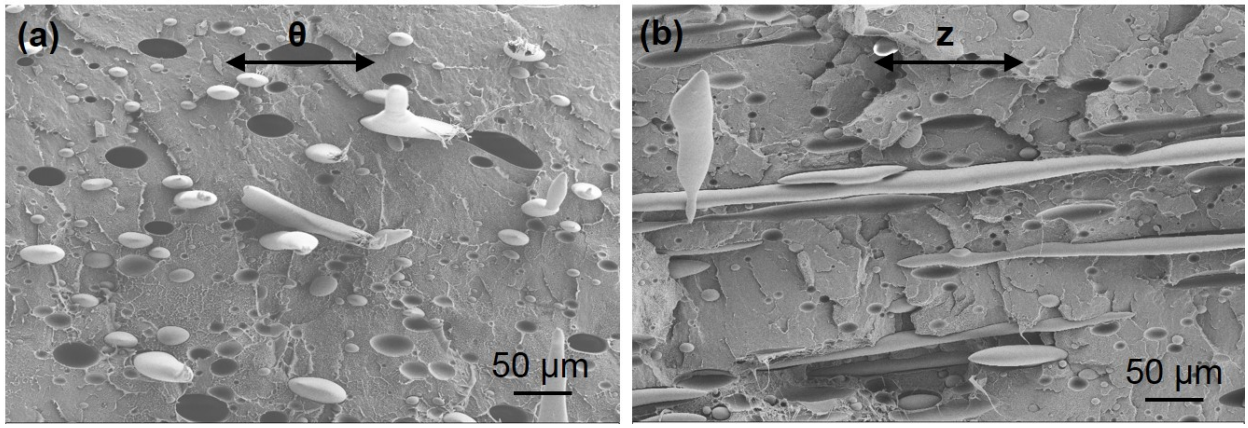

Figure 4.11: SEM images of 20 wt% TLCP/HDPE bottle. (a) and (b) are the fracutre surfaces in the r-θ and r-z planes, respectively. The horizontal direction represents θ direction in (a) and z direction in (b).

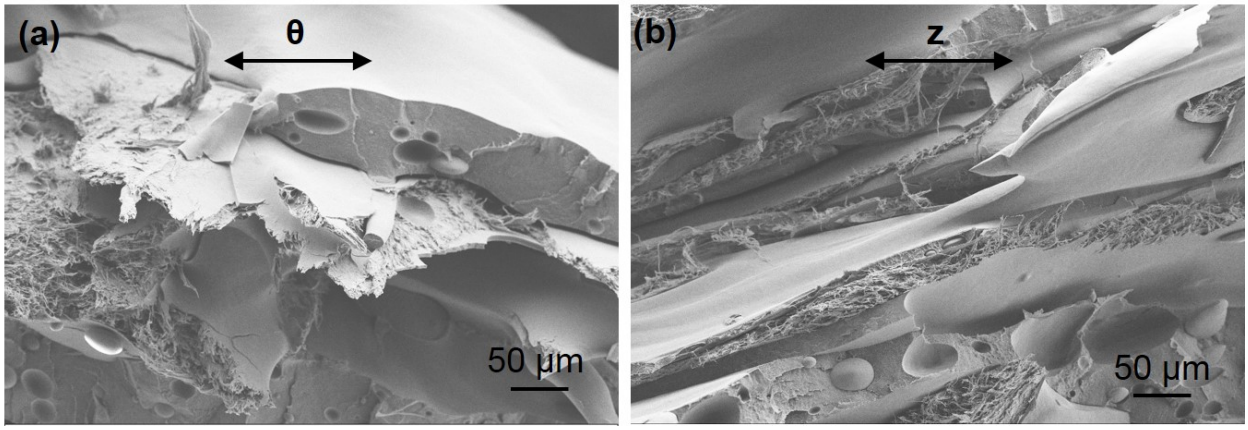

Figure 4.12: SEM images of 50 wt% TLCP/HDPE bottle. (a) and (b) are the fracutre surfaces in the r-θ and r-z planes, respectively. The horizontal direction represents θ direction in (a) and z direction in (b).

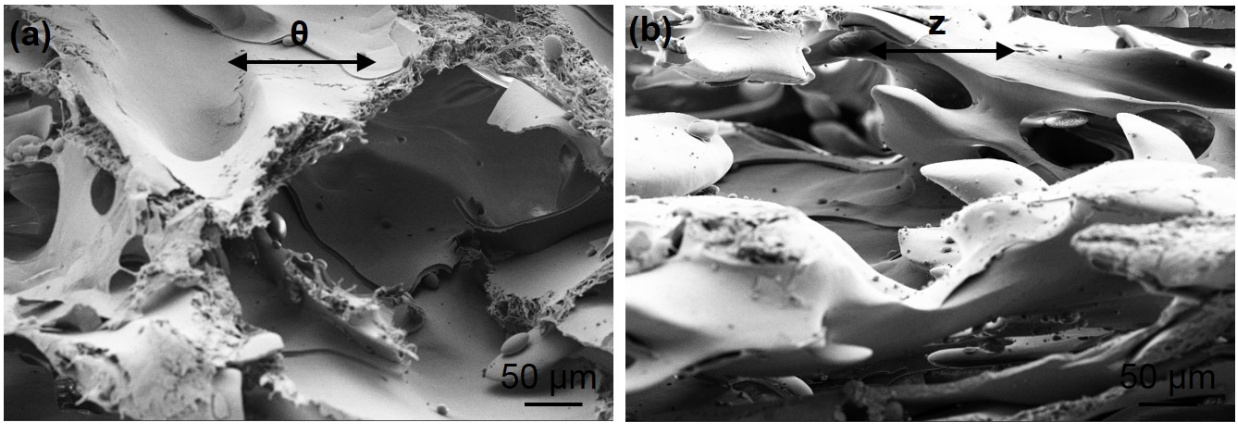

Figure 4.13: SEM images of 50 wt% TLCP/HDPE bottle after dissolving HDPE. (a) and (b) are the fracutre surfaces in the r-θ and r-z planes, respectively. The horizontal direction represents θ direction in (a) and z direction in (b).

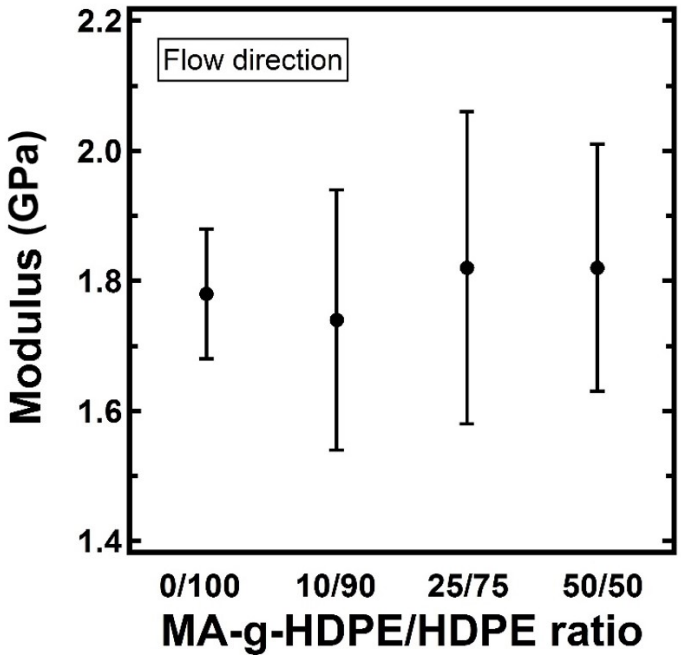

Figure 4.14: Tensile modulus as a function of the MA-g-HDPE to HDPE ratios for the injection molded ternary blends (TLCP/HDPE/MA-g-HDPE) along the flow direction.

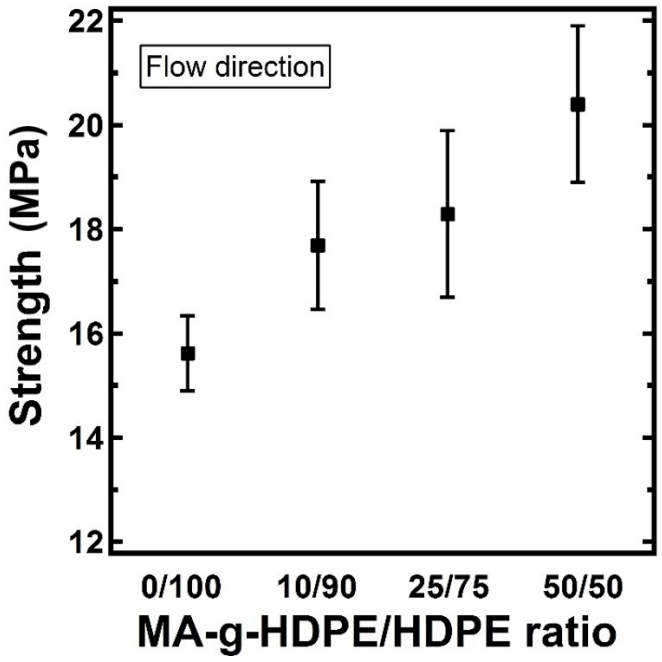

Figure 4.15: Tensile strength as a function of the MA-g-HDPE to HDPE ratios for the injection molded ternary blends (TLCP/HDPE/MA-g-HDPE) along the flow direction.

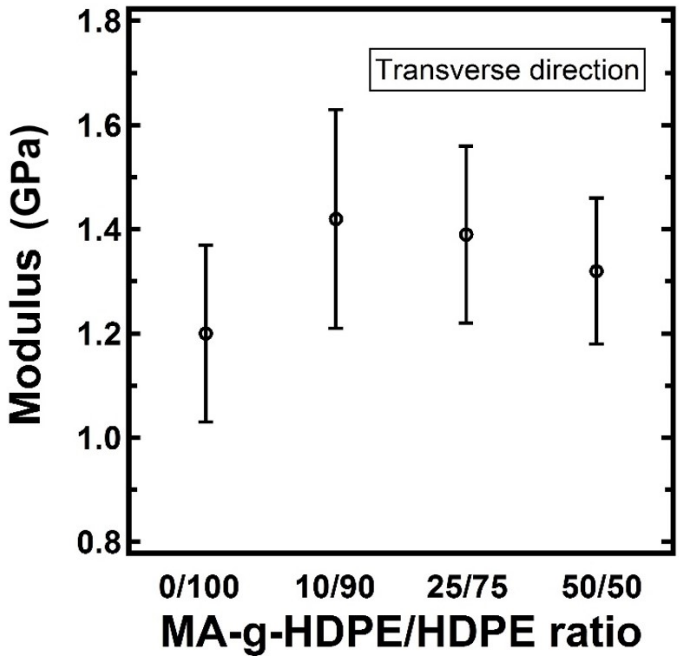

Figure 4.16: Tensile modulus as a function of the MA-g-HDPE to HDPE ratios for the injection molded ternary blends (TLCP/HDPE/MA-g-HDPE) along the transverse direction.

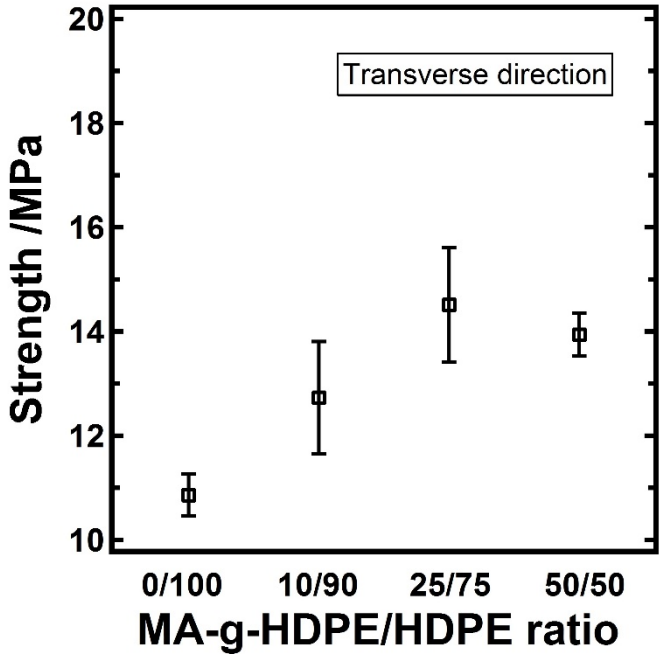

Figure 4.17: Tensile strength as a function of the MA-g-HDPE to HDPE ratios for the injection molded ternary blends (TLCP/HDPE/MA-g-HDPE) along the transverse direction.

5 Isothermal Crystallization of Blends Containing Two Thermotropic Liquid Crystalline Polymers

Isothermal Crystallization of Blends Containing Two Thermotropic Liquid Crystalline Polymers

Chen Qian[a], Guigui Wan[b], Charles E. Frazier[b], Donald G. Baird[a*],

[a]Department of Chemical Engineering, Virginia Polytechnic Institute and State University,

Blacksburg, VA 24061

[b]Department of Sustainable Biomaterials, Virginia Polytechnic Institute and State University,

Blacksburg, VA 24061

5.1 Abstract

The intention of this work is to determine how the isothermal crystallization behavior of a thermotropic liquid crystalline polymer (TLCP) can be adjusted by blending it with a pure TLCP of lower melting point. One TLCP (T_m~350^{o}C) used is a copolyester synthesized from terephthalic acid, 4-hydroxybenzoic acid, hydroquinone and hydroquinone derivatives. The other TLCP (T_m~280 ^{o}C) is a copolyesteramide of 60 mol% hydroxynaphthoic acid, 20 mol% terephthalic acid and 20 mol% 4-aminophenol. As the content of the low melting TLCP increases in the blends, the temperature at which isothermal crystallization occurs decreases. Comparing with pure TLCPs, the blend of 75% low melting TLCP crystallizes at a lower temperature than the pure matrix, and the blend remains as a stable super-cooled fluid in the temperature range from 220 to 280^{o}C for 1200s. Because of the low energy released during the phase transition, small amplitude oscillatory shear (SAOS) is more sensitive to detecting the onset of isothermal crystallization than differential scanning calorimetry (DSC).

5.2 Introduction

Thermotropic liquid crystalline polymers (TLCPs) have attracted great research interests because of the combination of their promising properties, which includes high stiffness and strength, low permeability to gas molecules, low linear thermal expansion coefficient, reduced dielectric constants and outstanding chemical resistance [1-5]. Because of these properties, TLCPs have been used in various applications, such as the reinforcing components in TLCP/thermoplastic blends, barrier material for packaging, as well as electrical parts [4, 6-9]. TLCPs also show promise in the emerging fields, including high pressure gas storage and fused filament fabrication [10-12].

Because of the limited types of commercial TLCPs available, researchers have blended two TLCPs to expand the potential applications of TLCPs. The TLCP/TLCP blends have demonstrated distinctive properties relative to the neat components. One important character possessed by the blends is the improved mechanical properties [13-17]. For example, Vallejo *et al.* [13] injection molded the blends containing two TLCPs, which were the 20/80 poly(ethylene terephthalate) (PET)/hydroxybenzoic acid (HBA) and 73/27 HBA/2,6-hydroxynaphthoic acid (HNA). The modulus and strength for the 20/80 PET/HBA material were 9.8 GPa and 175 MPa, respectively. For the 73/27 HBA/HNA copolyester, the modulus and strength were 9.5 GPa and 210 MPa, respectively. For the blend with 80% TLCP of HBA/HNA, the modulus was 1.18 GPa, and the strength was 300 MPa. Both values were greater than those of either pure TLCP components.

Depending on the miscibility and the chemical composition of the materials, the TLCP/TLCP blends also exhibit lower viscosity relative to each of the two neat resins, which could be beneficial for processing [14, 18-19]. Kenig *et al.* [14] blended two TLCPs using a single screw extruder. The two TLCPs used were the 73/27 HBA/HNA and a copolymer composed of 60 mol%

HNA, 20 mol% terephthalic acid (TA), and 20 mol% acetoxy-acid aniline, respectively. The viscosity of the blends was measured in the shear rate range of 10 to 10^4 Pa•s^{-1} with a capillary rheometer. Within this a shear rate range, the viscosity curves of the blends containing 25, 50, and 75% HBA/HNA copolymer nearly overlapped. The viscosity of these blends was lowered than that of either of the neat components, especially in the shear rate range of 10 to 10^2 Pa•s^{-1}. Lin and Winter [18] measured the viscosity of the blends containing the copolymers of 73/27 HBA/HNA and 40/60 PET/HBA at the shear rates from 0.05 to 0.4 s^{-1}. The viscosity of the blends was lower than that of the neat materials. It was interesting to observe that with the addition of 10 wt% 40/60 PET/HBA, the viscosity of the blend was reduced by a factor of 4 relative to the neat 73/27 HBA/HNA. Heish *et al.* [19] speculated the lower viscosity of the blends was due to the enhanced orientation, as well as the lubrication between the two different TLCP molecules.

The thermal properties of the blends containing two TLCPs with the same chemical moiety also vary from those of the pure materials. McLeod and Baird [20] reported the melting and crystallization temperatures of a TLCP can be tailored by blending it with a second TLCP of lower melting point. Both TLCPs used in this work were synthesized from HBA, terephthalic acid (TA), hydroquinone and hydroquinone derivatives, but the monomer ratios were different for the two TLCPs. The TLCP containing a greater amount of HBA exhibited a higher melting point of around 330^{o}C, while the other TLCP melted at about 272^{o}C. One intriguing observation was that the crystallization temperature of the blends was a linear function of the ratio of the two TLCPs. The lower melting and crystallization temperatures of the TLCP/TLCP blends allowed them to be combined with thermoplastics possessing lower processing temperatures.

McLeod and Baird's work focused on the effect of the cooling rate on the crystallization temperatures of the TLCP/TLCP melts. However, to process TLCP/TLCP blends in the super-

cooled state, knowing the melting and crystallization temperatures from the temperature ramp experiments is not enough. The isothermal crystallization behavior at different temperatures below the melting point needs to be investigated to guide processing. The main objective of this work is to determine how the isothermal crystallization behavior of a TLCP can be adjusted by blending it with another TLCP of lower melting temperature. In this work the TLCP/TLCP blends and neat resins are fully melted first, and then cooled down to a constant temperatures below the melting point. The isothermal crystallization is monitored using both dynamic mechanical and DSC measurements. In addition to this focus, the sensitivities of the two approaches on detecting isothermal crystallization are compared. The practical significance of this work is to tailor the super-cooling behavior of a high melting TLCP, such that it can be blended with thermoplastic of lower processing temperatures.

5.3 Experimental

5.3.1 Materials

Two commercial TLCPs were used in this study. The first TLCP was provided by Dupont with a commercial name of Zenite HX6000. It is a liquid crystalline copolyester synthesized from hydroxybenzoic acid (HBA), terephthalic acid (TA), hydroquinone (HQ) and hydroquinone derivatives (HQ-derivatives). However, the monomer ratio for this material is unknown. It has a density of 1.38 g/cm^3, and it is usually processed at temperatures of 360^{o}C and above. In this report this TLCP will be designated as TLCP-A.

The second TLCP was supplied by Ticona-Celanese, and its commercial name is Vectra B950. Vectra B950 is a copolyesteramide of 60 mol% 2,6-hydroxynaphthoic acid (HNA), 20 mol% (TA), and 20 mol% p-amino-phenol (PA). Compared with Zenite HX6000, Vectra B950 has a lower melting point of around 280^{o}C. Vectra B950 will be referred to as TLCP-B in later discussion. Both TLCPs were used as received.

5.3.2 Melt compounding of the TLCP/TLCP blends

The pellets of the two TLCP resins were mixed by tumbling in a container for 5 min, with the weight ratios of 25/75, 50/50 and 75/25, respectively. The mixed pellets as well as the neat resins were dried in a vacuum oven at 100 ^{o}C for at least 24 hr before use. A Killion KL-100 single screw extruder with a 1.59 mm diameter capillary die was used for melt compounding. A Maddock screw with 25.4 mm diameter and 30:1 L:D was employed. The temperatures from zone 1 to zone 4 were set at 300, 340, 350 and 360^{o}C, respectively. The screw speed was 30 rpm. After being plasticated in the extruder, the polymer melt was quenched in a cold water bath. The obtained

polymer strands were then chopped into pellets, using a Killion Model 2” pelletizer. The pellets were used for rheological and thermal analysis.

5.3.3 Differential Scanning Calorimetry

DSC measurements in the temperature ramp mode were first perfomed using a TA instrument’s Discovery DSC. The temperature ramp tests were used to obtain the melting points, as well as the crystallization temperatures of the TLCP/TLCP blends and the neat materials. Ca. 10 mg of each samples was first equilibrated at 40 ^{o}C, then the temperature was increased to 360^{o}C. After equilibration at 360^{o}C for 1 min, the materials were cooled to 40^{o}C (first cooling scan), and then heated back up to 360^{o}C (second heating scan). A constant 10^{o}C/min temperature cycle was applied in all the heat/cool/heat cycles, and all measurements were performed under a dry nitrogen environment. The results were found to be independent of the equilibration time at 360^{o}C. Therefore, 1 min equilibration time guaranteed the complete melting of the materials. The melting point as well as the melting enthalpy were calibrated using indium.

To investigate the isothermal crystallization of the materials, DSC tests were also carried out in the isothermal time sweep mode. In this case the materials were first equilibrated at 360^{o}C for 1 min, then the temperature was lowered to the predetermined values below the melting points at a rate of 10^{o}C/min. The heat flow was tracked as a function of time for 40 mins.

5.3.4 Small amplitude oscillatory shear measurements

Small amplitude oscillatory shear (SAOS) measurements were performed in the temperature ramp mode to obtain the crystallization temperatures, using a TA instrument’s ARES-G2 rheometer. The pellets of the melt compounded TLCP/TLCP blends and the neat resins were compression molded into disks at 360^{o}C. All samples were dried at 100^{o}C under vacuum for at

least 24 hr prior to testing. 25 mm parallel disks fixtures with 1 mm gap were used. Each sample was first equilibrated at 360^{o}C for 3 min, then the temperature was decreased at a rate of 10^{o}C/min. Meanwhile dynamic shear with 5% strain and 10 rad/s angular frequency was applied. The storage modulus G' and loss modulus G" were recorded as a function of time. All experiments were conducted under a dry nitrogen environment.

SAOS was also used to investigate the isothermal crystallization of the TLCP/TLCP blends as well as the neat resins in the super-cooled state. All materials were first equilibrated at 360^{o}C for 3 mins, such that the exclusion of crystalline structure was ensured. Then the materials were cooled to different designated supercooling temperatures below the melting points at 10^{o}C/min. G' and G" were monitored as a function of time while the samples were sheared at 10 rad/s frequency and 5% strain.

To investigate the effect of strain on the isothermal crystallization rate in SAOS measurements, after being equilibrated at 360 ^{o}C, each sample was cooled to a temperature below the melting point. SAOS was applied with a constant angular frequency, ω, of 10 rad/s, and the strain used was 1, 2 and 5%, respectively. The crossover time of G' and G" was recorded, and the values obtained from different strain amplitudes were compared.

5.4 Results and Discussion

5.4.1 DSC heat/cool/heat scans

Figs 5.1 and 5.2 show the results of DSC second heating and first cooling scans, respectively. In the heating scan the melting point of the material is defined as the temperature at which all crystalline structures are excluded. Therefore, the melting point refers to the high-temperature end of the melting endotherm, as indicated by the arrows in Fig 5.1. In the cooing

scan, the onset and peak crystallization temperatures are extracted, as represented in Fig 5.2. The melting and crystallization enthalpies obtained from the two figures are summarized in Table 5.1.

It can be observed that both the melting and crystallization temperatures of the TLCP-A are lowered when it is blended with the TLCP-B. It should be noticed that the TLCP-B exhibits repeatable double melting peaks in Fig 5.1. Therefore, the uppermost temperature of the higher melting peak is designated as the melting point for TLCP-B, as indicated by the arrow in Fig 5.1. The melting point is decreased from 349 ^{o}C for the neat TLCP-A to 341 and 308^{o}C for the blends containing 25 and 50% of TLCP B, respectively. For the 75% TLCP B blend, no melting point was observed from the heating scan. Additionally, the TLCP/TLCP blends also exhibit lower onset and peak crystallization temperatures relative to the neat TLCP-A. For example, the onset crystallization temperature of the pure TLCP-A is decreased from 301^{o}C to 278 and 247^{o}C for the blends of 25 and 50% of TLCP-B, respectively. The most striking case occurs in the blend containing 75% TLCP-B. Its onset crystallization temperature is 194^{o}C, which is lower than the onset crystallization temperature of either of the neat TLCPs.

Table 5.1 shows the addition of the TLCP-B to the TLCP-A decreases both the melting and crystallization enthalpies. It should be noted that the melting and crystallization enthalpies of the blends are even lower than those of the neat resins. For the blend with the 75% TLCP-B, the enthalpy of crystallization is only 0.8 $J \bullet g^{-1}$. We suggest the lack of a melting endotherm for this blend in Fig 5.1 is due to the small amount of energy consumed for melting, which is not detected by DSC.

There are two possible reasons for the unusually low crystallization temperature for the 75% TLCP-B blend. First, a transesterification reaction can occur in the extruder, when the two TLCPs

are blended [21]. The product of the reaction might well be a new material with lower crystallization temperature. Second, the melting and crystallization peaks of the blends are single peaks, which are also shifted relative to those of the neat materials. This suggests, but does not verify that the two TLCPs are compatible or possibly miscible. At the particular content of 75% TLCP-B, the two TLCPs may co-crystallize at a lower temperature.

5.4.2 SAOS cooling ramp

To complement the crystallization temperatures obtained from DSC, SAOS measurements were carried out, the results are presented in Fig 5.3. The crossover temperatures of G' and G" are recorded as the crystallization temperatures. A comparison of the crystallization temperatures obtained from DSC and SAOS is shown in Fig 5.4. For the neat TLCP-A, and the blends containing 25 and 50% TLCP-B, the crossover temperatures of G' and G" are within the ranges of the onset and peak crystallization temperatures obtained from DSC. For the 75% TLCP-B blend as well as the neat TLCP-B, the crossover temperatures of G' and G" are closer to the peak crystallization temperatures. Overall, the crystallization temperatures obtained from SAOS are in good agreement with those measured from DSC.

5.4.3 Isothermal crystallization

Figs 5.5 and 5.6 show the isothermal crystallization of the TLCP-A at the temperatures of 330, 320, 315 and 310^{o}C, using the methods of SAOS and DSC. The SAOS results indicate crystallization does not occur at 330 and 320^{o}C within 1200s. The crossovers of G' and G" are observed at 847 and 415s at the temperature of 315 and 310^{o}C, respectively. This indicates the crystallization the TLCP is accelerated at lower temperature, as expected. Isothermal DSC also shows no sign of crystallization at 330 and 320^{o}C. However, the DSC trace is flat at 315^{o}C. Even

though the DSC test is carried out for an extended time of 2400s, still no exothermal peak is observed. At 310^{o}C, the DSC trace exhibits an exothermic peak, which suggests crystallization. Therefore, the results from SAOS and DSC are at least in qualitative agreement at the temperatures of 330, 320 and 310^{o}C. Nevertheless, DSC does not detect any sign of crystallization at 315^{o}C, but SAOS does.

The discrepancy between the results obtained from the two methods at 315^{o}C can be due to two reasons. One possibility is that the TLCP only releases a small amount of energy during crystallization, and it is not detected by DSC. During the crystallization process, the rigid molecules can only slide pass each other along the chain direction, or rotate along their axes [22]. As a consequence, the crystallization of TLCPs is proposed to be induced by the matching of counits among adjacent molecules, resulting in weak cohesion of chains in the crystal lattice. This process is associated with a low enthalpy change. Strain induced crystallization is another potential reason that introduces the distinctive results obtained from the two techniques. The effect of strain on the crystallization rate in the SAOS measurements will be discussed in detail in §5.4.4.

Although SAOS suggests the occurrence of crystallization at 310^{o}C, it is challenging to extract detailed information regarding the crystallization kinetics from SAOS. Employing SAOS to track the isothermal crystallization of TLCPs is performed to a much lesser extent relative to DSC. Few have related the dynamic rheological behavior to the physical phenomena associated with the crystallization of TLCPs, neither has any model been proposed to fit the evolution of moduli for TLCPs and TLCP/TLCP blends. As a result, SAOS is more suitable to qualitatively determining the occurrence of a phase transition under isothermal conditions. The practical significance of the rheological measurements is to elucidate how long the TLCPs and their blends

can stay fluid in the super-cooled state, and whether processing operation can be carried out at given temperatures.

The isothermal phase transition of the neat TLCP-B is shown in Figs 5.7 and 5.8, respectively. SAOS results in Fig 5.7 suggest the TLCP maintain its fluidity within 1200s at 270 and 260^{o}C, while crystallization is observed at 250, 245 and 240^{o}C. In Fig 5.8 DSC also demonstrates the occurrence of crystallization in the temperature range from 240 to 250^{o}C, but no crystallization exotherm is observed at 270 and 260^{o}C. Comparing with the neat TLCP-A, better agreement is achieved from the SAOS and DSC results for the TLCP-B.

Now we turn our attention to the isothermal crystallization of TLCP/TLCP blends. SAOS experiments (Fig 5.9) suggest once melted, the blend containing 25% TLCP-B remains as a relatively stable fluid at 320 and 310^{o}C in 1200s. Crystallization is observed when the temperature is decreased below 305^{o}C. Because the neat TLCP-A exists as a super-cooled fluid at 320^{o}C and above, the addition of 25% TLCP-B allows the material to be processed 10^{o}C lower in the super-cooled state. Moreover, when the content of the TLCP B is increased to 50%, the lowest temperature at which the blend remains as stable a super-cooled fluid is 260^{o}C (Fig 5.11). Using the SAOS method, isothermal crystallization is observed at 300 and 305^{o}C for the 25% TLCP-B blend, and at 250 and 255^{o}C for the 50% TLCP-B blend, respectively. Nevertheless, at all these temperatures DSC traces are flat, with no crystallization exotherm shown, as presented in Figs 5.10 and 5.12.

The most interesting blend is the one that contains 75% TLCP-B. In the DSC cooling scans it exhibits a lower crystallization temperature relative to both the neat TLCPs. A DSC heating scan fails to identify the melting point of this blend, and an alternative method is adopted, which is the

SAOS experiment in the isothermal time sweep mode. In this method the time sweep experiments were performed at 270, 280, 290 and 300^{o}C. The evolutions of G' and G" as a function of time were monitored while oscillatory shear with 10 rad/s frequency and 5% strain was applied. It is found that G' and G" gradually increase at 270 and 280^{o}C. In contrast, they are each constant as time elapses at temperatures higher than 290^{o}C (results not represent here). Thus the melting point of the blend is between 280 and 290^{o}C. As shown in Figs 5.13 a) and b), the rheological approach indicates the blend is in a stable super-cooled state in the temperature range from 220 to 270^{o}C. This temperature range overlaps well with the processing temperatures of some commodity thermoplastics, such as polyolefins. Figs 5.14 a) and b) show the DSC traces for isothermal crystallization. Crystallization can be observed at 200 and 205^{o}C. Although SAOS also suggests the occurrence of crystallization at 210^{o}C, the DSC is unable to detect a crystallization exotherm at this temperature.

5.4.4 Effect of strain on the isothermal crystallization rate in SAOS measurements

Shear-induced crystallization is one possible reason that causes the discrepency between the isothermal crystallization results obtained from SAOS and DSC. Shear-induced crystallization is common among flexible chain polymers like polyethylene and polypropylene [23-26]. The strain applied in the SAOS tests may result in the alignment of TLCP molecules and accelerated crystallization [27-28], such that crystallization will be observed in the dynamic rheological experiments, but not in DSC tests. To investigate whether the strain amplitude applied in SAOS has an impact on the isothermal crystallization rate, the TLCP/TLCP blends and neat resins were tested at the predetermined temperatures with 1, 2.5 and 5% strain, respectively. For each sample, the temperature used was the one at which disagreement in SAOS and DSC results were found.

The results are shown in Fig 5.15. If strain does play an important role on crystallization, we would expect it takes less time for G' and G" to crossover at a higher strain level.

Fig 5.15 shows the crossover time of G' and G" is generally comparable for different strain amplitude. Higher strain does not necessarily lead to shorter crossover time and faster crystallization. Therefore, the disagreement in the SAOS and DSC reults is believed due the lack of sensitivity of DSC on detecting isothermal crystallization, rather than the strain induced crystallization in SAOS experiments.

5.5 Conclusions

As the content of the low melting TLCP (TLCP -B) increases in the blends, the temperature at which isothermal crystallization occurs decreases. This suggests relative to the high melting TLCP (TLCP A), the blends can be potentially processed at lower temperatures in the super-cooled state. The blend containing 75% TLCP B is of most interest. In the cooling experiments, it exhibits a lower crystallization temperature relative to both pure TLCPs. Once melted, the isothermal crystallization does not occur unless the material is cooled to 210 ^{o}C or below. The low crystallization temperature allows this blend to be combined with low melting temperature thermoplastics, such as polyolefins.

DSC frequently fails in detecting the isothermal crystallization for both TLCP/TLCP blends and neat TLCPs, which is well captured by SAOS. We believe this is due to the low crystallization enthalpy of the TLCP materials and the TLCP/TLCP blends under isothermal conditions. Therefore, SAOS is more sensitive on characterizing the onset of isothermal crystallization. Although in practical polymer processing, high shear rate and high strain are usually applied, SAOS measurements at least provide the lower temperature limit for the processing of neat TLCP resins and TLCP/TLCP blends in the super-cooled state.

5.6 Acknowledgements

The author would like to thank the Department of Energy through the Savanah River National Laboratories for the financial support. The authors acknowledge Prof. Dr. Garth L. Wilkes of Virginia Tech for the tremendous inputs and productive discussions. The authors would also like to thank Ms. Ann Norris in the Department of Sustainable Materials at Virginia Tech for providing assistance on DSC measurements.

References

[1] H. G. Chae and S. Kumar, "Rigid-rod polymeric fibers", *Journal of Applied Polymer Science*, vol.100, pp 791-802, 2006.

[2] J. S. Chiou and D. R. Paul, "Gas transport in a thermotropic liquid-crystalline polyester", *Journal of Polymer Science Part B: Polymer Physics*, vol.25, pp 1699-1707, 1987.

[3] N. R. Miranda, J. T. Willits, B. D. Freeman and H. B. Hopfenberg, "Organic vapor sorption and transport in a thermotropic liquid crystalline polyester", *Journal of Membrane Science*, vol.94, pp 67-83, 1994.

[4] T.-s. Chung, *Thermotropic liquid crystal polymers : thin-film polymerization, characterization, blends, and applications*, Technomic Pub. Co., Lancaster, 2001.

[5] A. Donald, A. Windle and S. Hanna, *Liquid Crystalline Polymers*, Cambridge University, 2006.

[6] X. Zhao, K. Nair, P. Yung, G. Barber, S. Gray, Y. S. Kim and A. Maliqi, U.S. Patent, US9206300 B2,2015.

[7] A. A. Handlos and D. G. Baird, "Processing and Associated Properties of In Situ Composites Based on Thermotropic Liquid Crystalline Polymers and Thermoplastics", *Journal of Macromolecular Science, Part C*, vol.35, pp 183-238, 1995.

[8] J. Lange and Y. Wyser, "Recent innovations in barrier technologies for plastic packaging - a review", *Packaging Technology and Science*, vol.16, pp 149-158, 2003.

[9] R. Lusignea, "High-barrier packaging with liquid crystal polymers", *Tappi Journal*, vol.80, pp 205-212, 1997.

[10] C. Qian, C. Mansfield and D. G. Baird, "Thermotropic liquid crystalline polymers and their fiber reinforced composites for hydrogen storage applications", *Annual Technical Conference*, edited by (Society of Plastics Engineers, 2014), vol.

[11] R. W. Gray, D. G. Baird and J. H. Bøhn, "Effects of Processing Conditions on Short TLCP Fiber Reinforced FDM Parts", *Rapid Prototyping Journal*, vol.4, pp 14-25, 1998.

[12] D. G. Baird, M. Ansari, C. D. Mansfield and C. Qian, "Generation of thermotropic liquid crystalline polymer thermoplastic composite filaments and their processing in fused filament fabrication", *251st ACS National Meeting*, edited by (American Chemical Society, 2016), vol.

[13] F. J. Vallejo, I. Iribarren, J. I. Eguiazabal and J. Nazabal, "Structure and mechanical properties of blends of two thermotropic copolyesters", *Polymer Engineering and Science*, vol.42, pp 1686-1693, 2002.

[14] S. Kenig, M. T. DeMeuse and M. Jaffe, "Properties of blends containing two liquid crystalline polymers", *Polymers for Advanced Technologies*, vol.2, pp 25-30, 1991.

[15] F. J. Vallejo, J. I. Eguiazábal and J. Nazábal, "Blends of a thermotropic copolyester and a thermotropic copoly(ester–amide): structure and mechanical properties", *Polymer*, vol.42, pp 9593-9599, 2001.

[16] F. J. Vallejo, J. I. Eguiazabal and J. Nazabal, "Blends of two thermotropic liquid crystalline polymers: the influence of reactions during injection molding on the phase structure and the mechanical behavior", *Polymer Engineering and Science*, vol.41, pp 1115-1123, 2001.

[17] M. Garcia, J. I. Eguiazabal and J. Nazabal, "Miscibility level and mechanical characterization of blends of two liquid-crystalline polymers based on p-hydroxybenzoic acid", *Journal of Polymer Science Part B: Polymer Physics*, vol.41, pp 1022-1032, 2003.

[18] Y. G. Lin and H. H. Winter, "Rheology of phase-separated blends of two thermotropic liquid-crystalline copolyesters", *Polymer Engineering and Science*, vol.32, pp 773-776, 1992.

[19] T.-T. Hsieh, C. Tiu, G. P. Simon and R. Yu Wu, "Rheology and miscibility of thermotropic liquid crystalline polymer blends", *Journal of Non-Newtonian Fluid Mechanics*, vol.86, pp 15-35, 1999.

[20] M. A. McLeod and D. G. Baird, "The crystallization behavior of blends of thermotropic liquid crystalline polymers", *Polymer*, vol.40, pp 3743-3752, 1999.

[21] C. M. McCullagh, J. Blackwell and A. M. Jamieson, "Transesterification in Blends of Wholly Aromatic Thermotropic Copolyesters", *Macromolecules*, vol.27, pp 2996-3001, 1994.

[22] D. J. Blundell, "The nature of crystallites in solidified, rigid-chain, liquid crystal polymers", *Polymer*, vol.23, pp 359-364, 1982.

[23] L. Yang, R. H. Somani, I. Sics, B. S. Hsiao, R. Kolb, H. Fruitwala and C. Ong, "Shear-Induced Crystallization Precursor Studies in Model Polyethylene Blends by in-Situ Rheo-SAXS and Rheo-WAXD", *Macromolecules*, vol.37, pp 4845-4859, 2004.

[24] R. R. Lagasse and B. Maxwell, "An experimental study of the kinetics of polymer crystallization during shear flow", *Polymer Engineering and Science*, vol.16, pp 189-199, 1976.

[25] S. Vleeshouwers and H. E. H. Meijer, "A rheological study of shear induced crystallization", *Rheologica Acta*, vol.35, pp 391-399,

[26] A. Nogales, B. S. Hsiao, R. H. Somani, S. Srinivas, A. H. Tsou, F. J. Balta-Calleja and T. A. Ezquerra, "Shear-induced crystallization of isotactic polypropylene with different molecular weight distributions: in situ small- and wide-angle X-ray scattering studies", *Polymer*, vol.42, pp 5247-5256, 2001.

[27] Y. G. Lin and H. H. Winter, "Formation of high melting crystal in a thermotropic aromatic copolyester", *Macromolecules*, vol.21, pp 2439-2443, 1988.

[28] Y. G. Lin, H. H. Winter and G. Lieser, "Equibiaxial extension of a thermotropic liquid-crystalline polymer Flow induced orientation, relaxation of orientation, and strain recovery", *Liquid Crystals*, vol.3, pp 519-529, 1988.

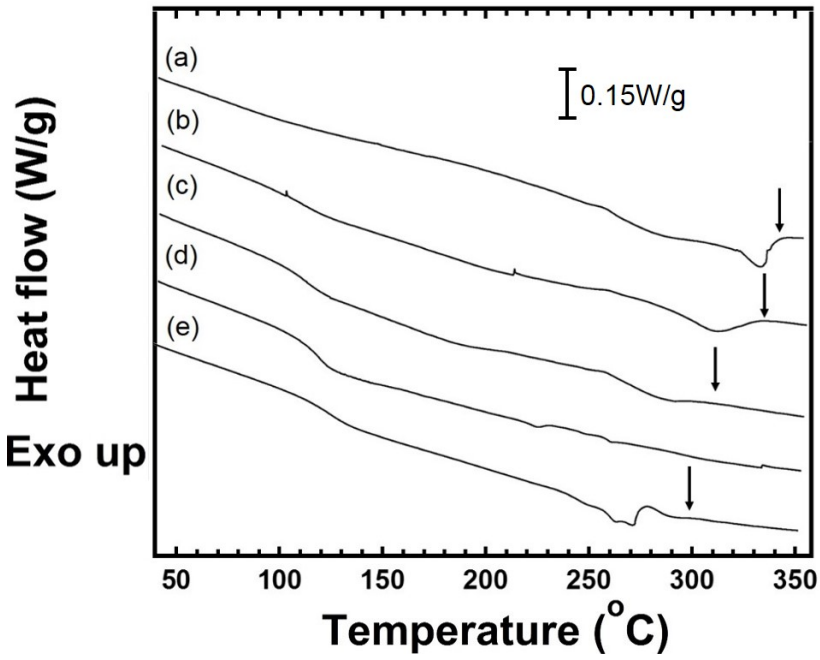

Fig 5.1 DSC second heating scan of the TLCP/TLCP blends, along with the neat components. The weight contents of the low melting TLCP-B from top to bottom are (a) 0%, (b) 25%, (c) 50%, (d) 75% and (e) 100%. Arrows indicate the melting points for each material. The vertical bar suggests the scale in heat flow.

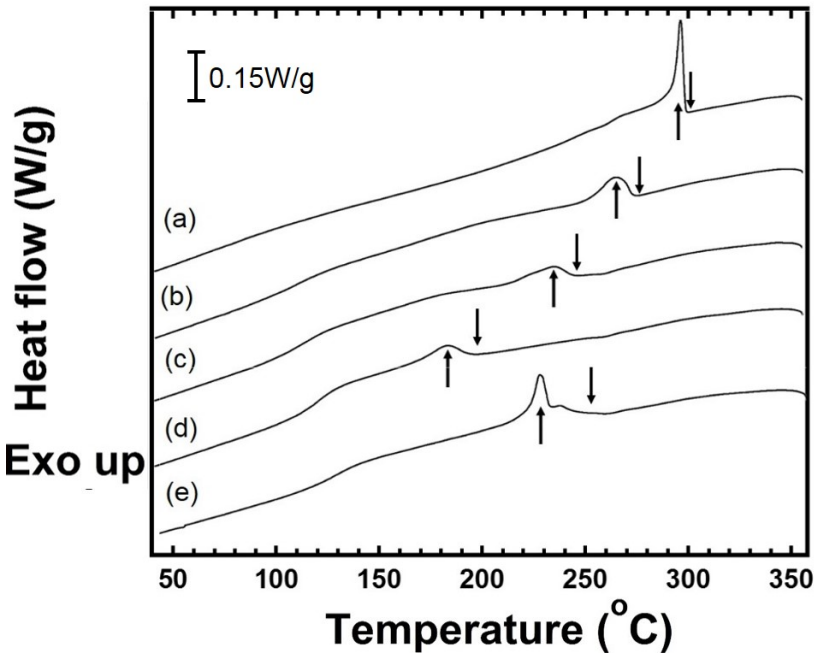

Fig 5.2 DSC first cooling scan of TLCP/TLCP blends, along with neat components. The weight contents of the low melting TLCP-B from top to bottom are (a) 0%, (b) 25%, (c) 50%, (d) 75% and (e) 100%. Arrows pointing down indicate the onset crystallization temperatures, while arrows pointing up represent the peak crystallization temperatures.

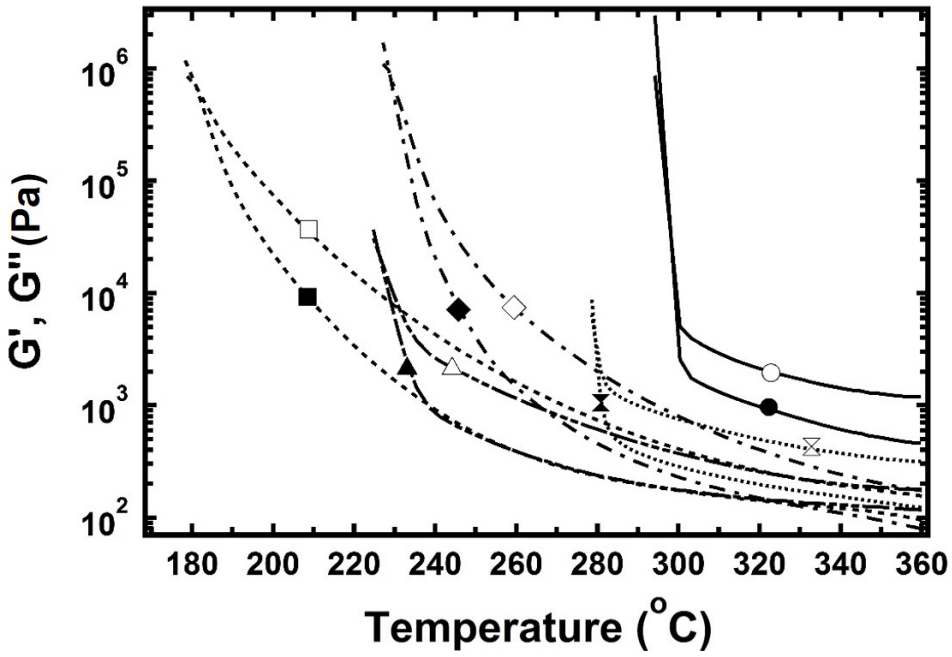

Fig 5.3 G’ and G” as a function of temperature obtained from the SAOS temperature ramp measurements. The symbols represent the content of the TLCP-B as follows: 0% ● G' ○ G" , 25% ⧗ G' ⧖ G" , 50% ▲ G' △ G" , 75% ■ G' □ G" and 100% ◆ G' ◇ G".

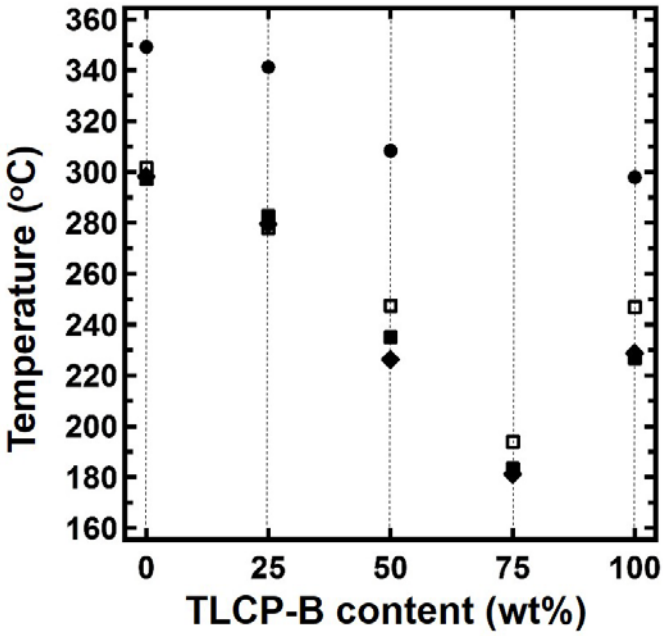

Fig 5.4 Comparison of the crystallization temperatures obtained from DSC and SAOS. ● is the melting point obtained from DSC, □ represents the onset crystallization temperature from DSC, ■ is the peak crystallization temperature from DSC, and ◆ indicates the crystallization temperature from SAOS.

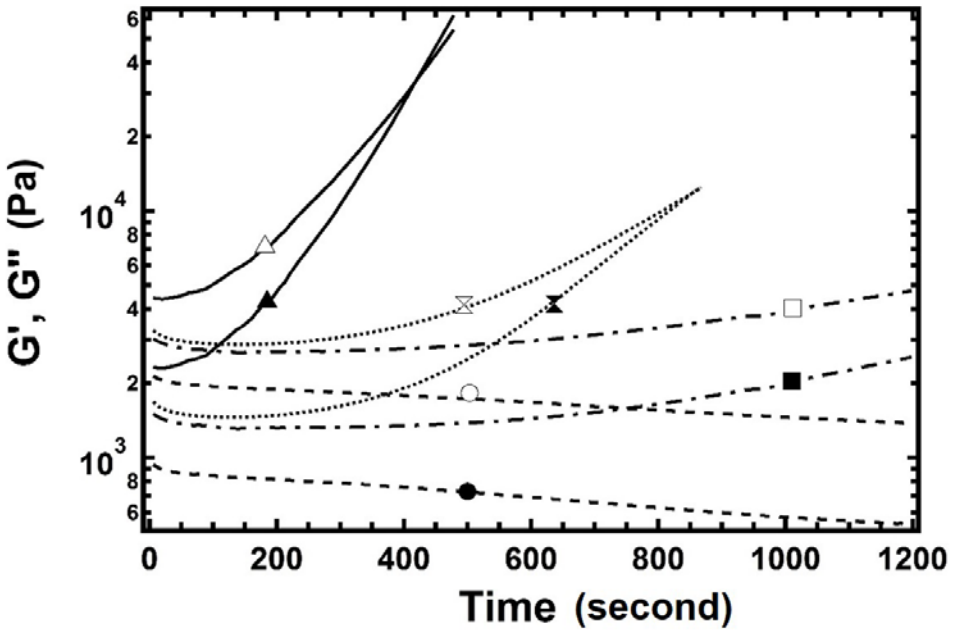

Fig 5.5 SAOS measurements in the isothermal time sweep mode for neat TLCP-A. The material is first melted at 360°C, then cooled to the temperatures indicated by the symbols: 330°C - - - ● G' ○ G" , 320°C — · - ■ G' □ G" , 315°C ····· ⧗ G' ⧖ G" and 310°C —— ▲ G' △ G" .

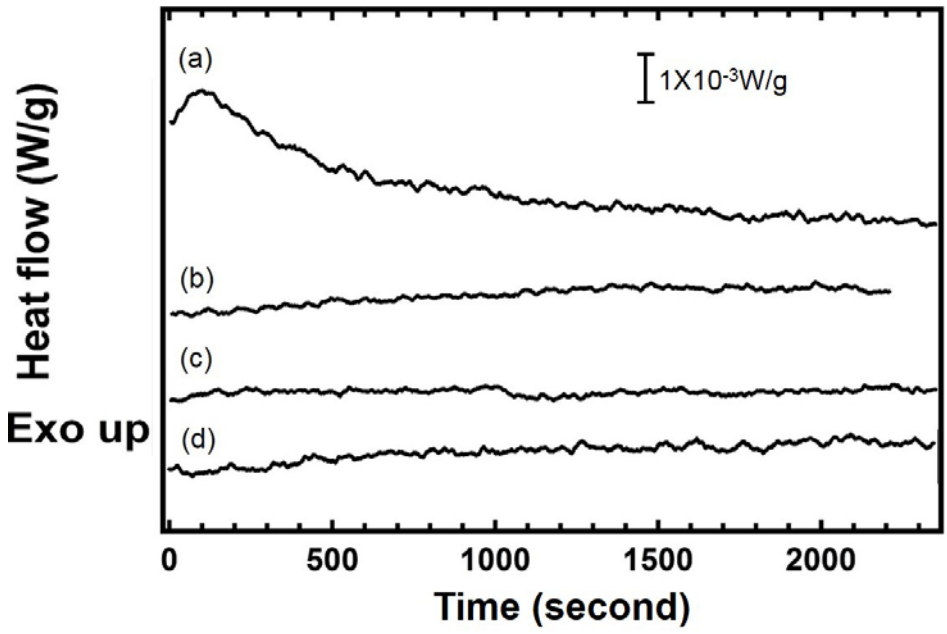

Fig 5.6 DSC measurements in the isothermal time sweep mode for neat TLCP-A. The material is first melted at 360^{o}C, then cooled to the predetermined temperatures. From top to bottom are the results obtained at (a) 310^{o}C, (b) 315^{o}C, (c) 320^{o}C and (d) 330^{o}C.

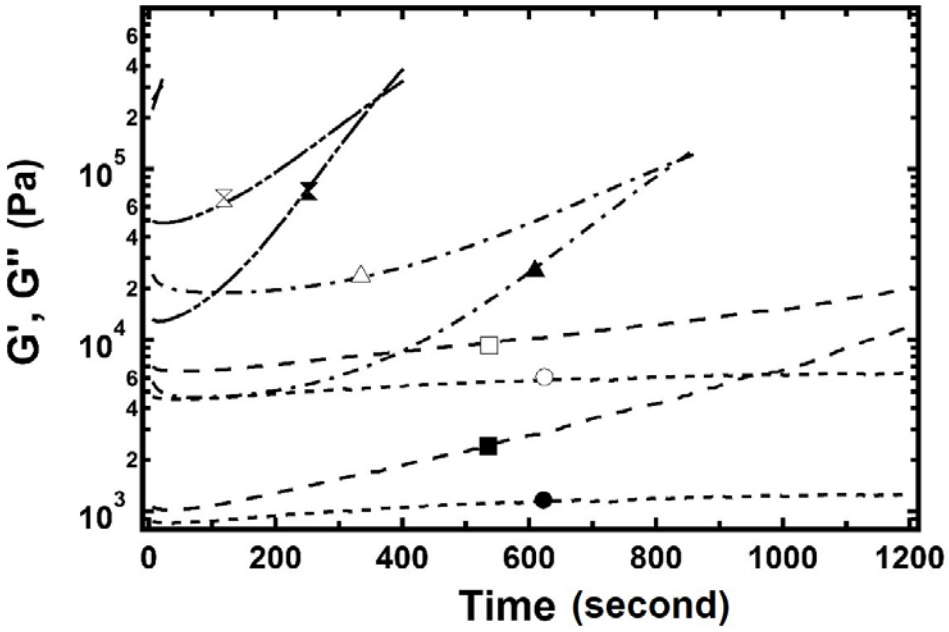

Fig 5.7 SAOS measurements in the isothermal time sweep mode for the neat TLCP-B. The material is first melted at 360°C, then cooled to the temperatures indicated by the symbols: 270°C ● G' ○ G'' , 260°C ■ G' □ G'' , 250°C ▲ G' △ G'' , 245°C ⧗ G' ⧖ G'', and 240°C —.

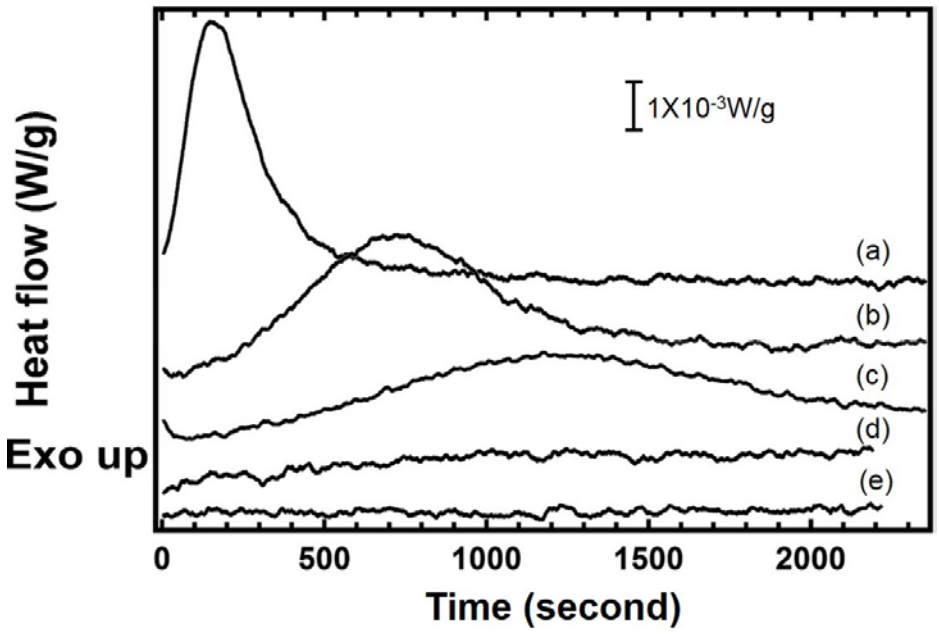

Fig 5.8 DSC measurements in the isothermal time sweep mode for the neat TLCP-B. The material is first melted at 360^{o}C, then cooled the predetermined temperatures. From top to bottom are the results obtained at (a) 240^{o}C, (b) 245^{o}C, (c) 250^{o}C, (d) 260^{o}C and (e) 270^{o}C.

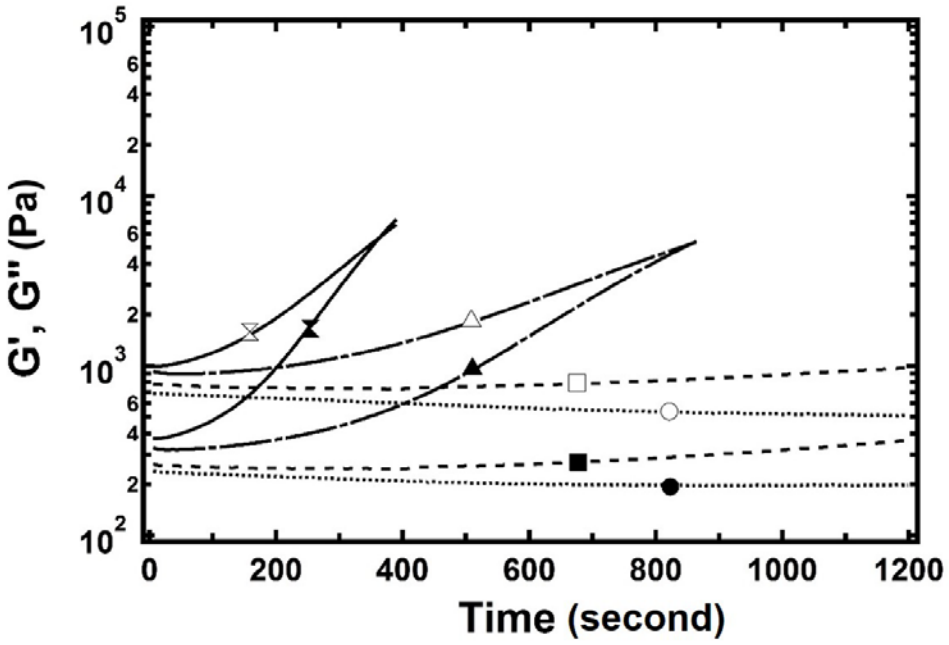

Fig 5.9 SAOS measurements in the isothermal time sweep mode for the blend containing 25% TLCP-B. The material is first melted at 360°C, then cooled to the temperatures indicated by the symbols: 320°C ····· ● G' ○ G", 310°C - - - ■ G' □ G", 305°C —— ▲ G' △ G", and 300°C —— ⧗ G' ⧖ G".

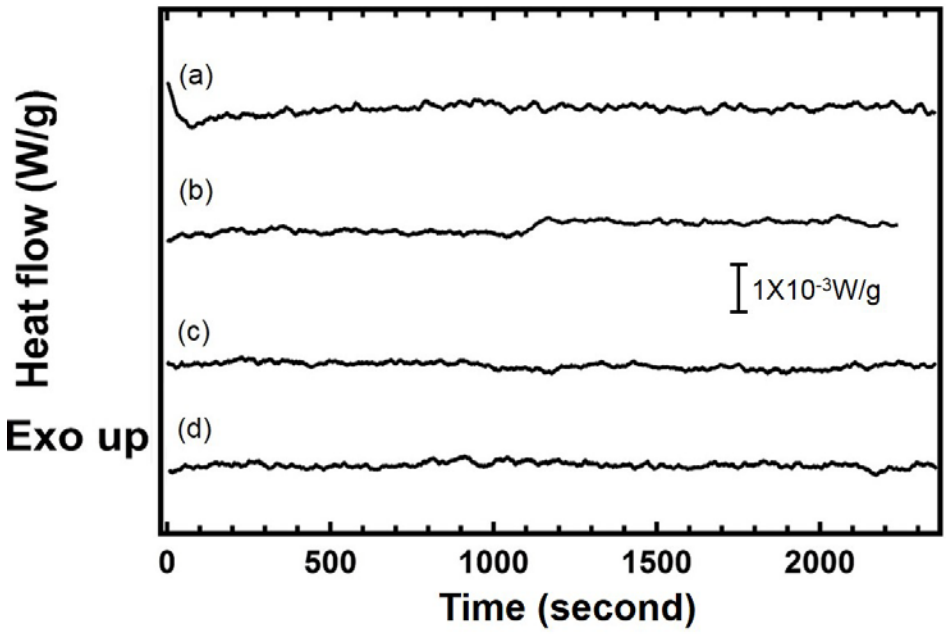

Fig 5.10 DSC measurements in the isothermal time sweep mode for the blend containing 25% TLCP-B. The material is first melted at 360^{o}C, then cooled to the predetermined temperatures. From top to bottom are the results obtained at (a) 300 ^{o}C, (b) 305^{o}C, (c) 310^{o}C and (d) 320^{o}C.

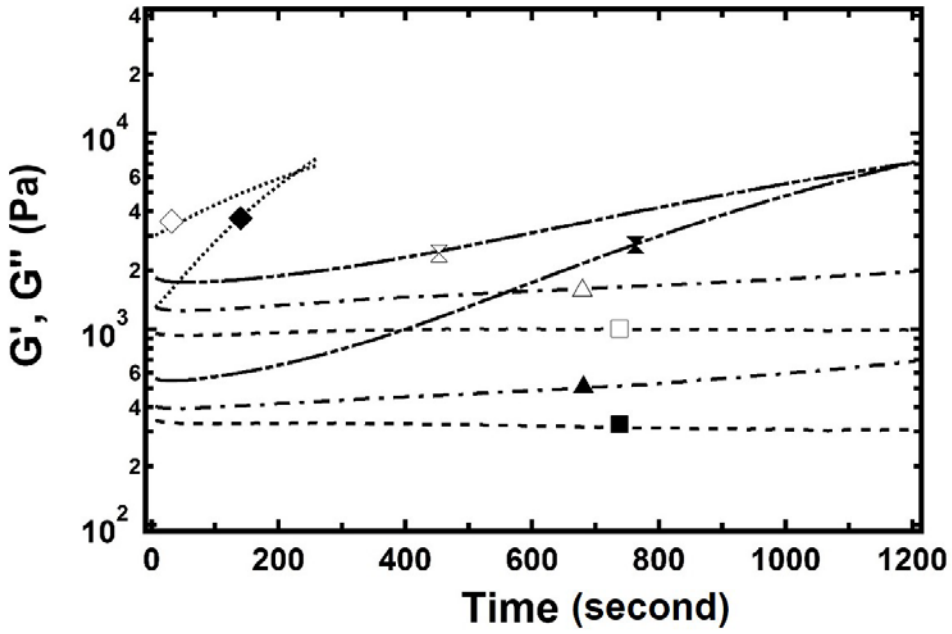

Fig 5.11 SAOS measurements in the isothermal time sweep mode for the blend containing 50% TLCP-B. The material is first melted at 360 °C, then cooled to the temperatures indicated by the symbols: 270°C - - - ■ G' □ G'' , 260°C ─ · · ▲ G' △ G'' , 255°C ── ⧗ G' ⧖ G'' , and 250°C ····· ◆ G' ◇ G''.

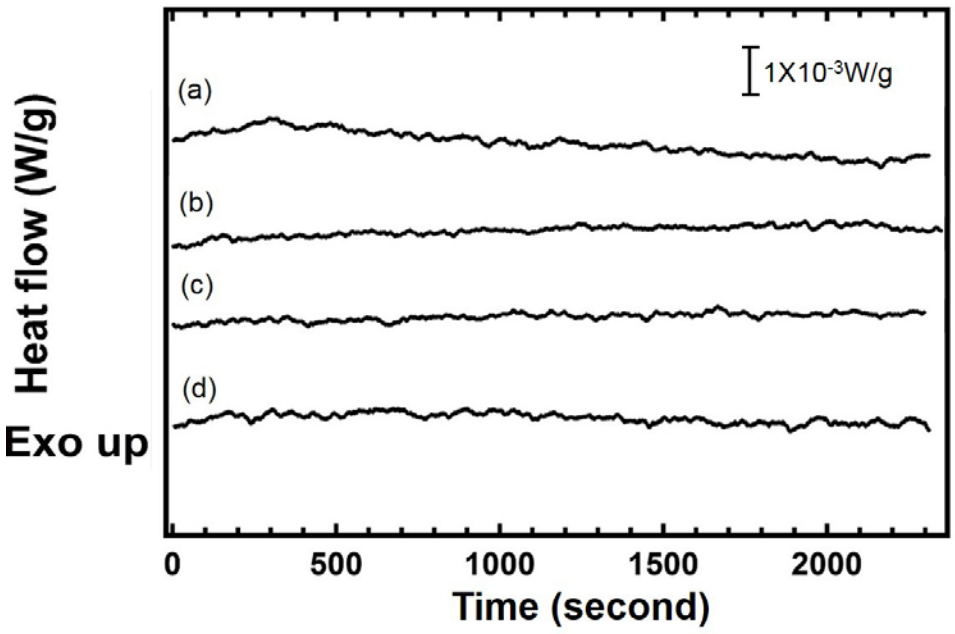

Fig 5.12 DSC measurements in the isothermal time sweep mode for the blend containing 50% TLCP-B. The material is first melted at 360^{o}C, then cooled to the predetermined temperatures. From top to bottom are the results obtained at (a) 250^{o}C, (b) 255^{o}C, (c) 260^{o}C and (d) 270^{o}C.

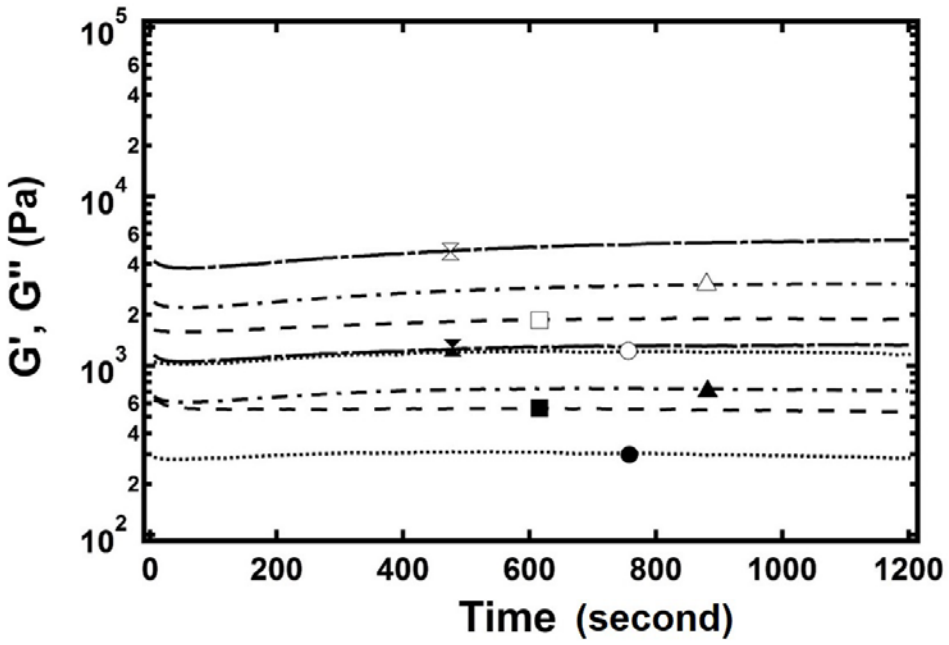

Fig 5.13 a) SAOS measurements in the isothermal time sweep mode for the blend containing 75% TLCP-B. The material is first melted at 360°C, then cooled to the temperatures indicated by the symbols: 270°C ····· ● G' ○ G", 260°C – – ■ G' □ G", 250°C – · · ▲ G' △ G", and 240°C —— ⧗ G' ⧖ G".

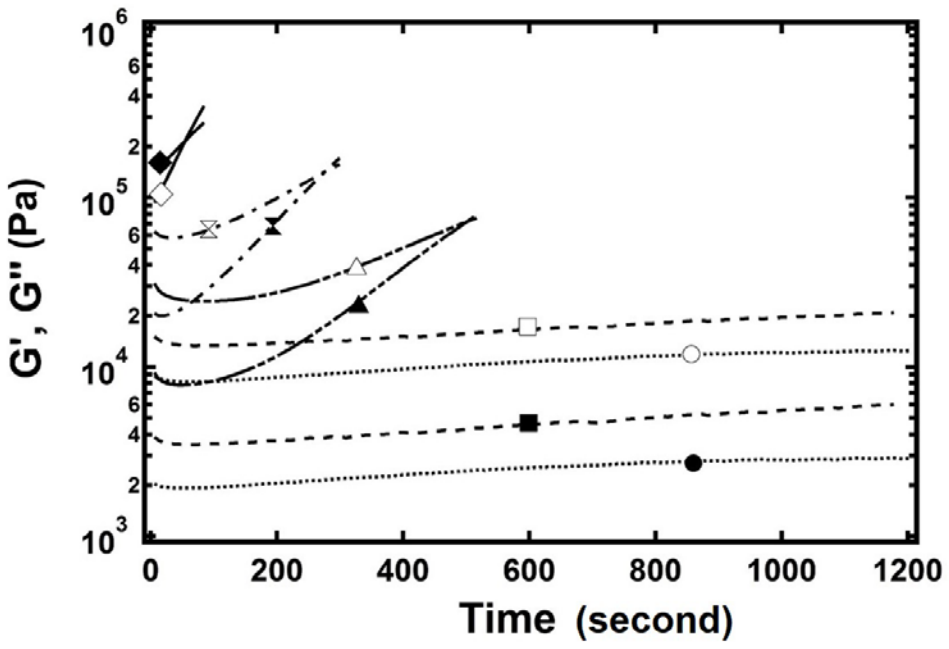

Fig 5.13 b) SAOS measurements in the isothermal time sweep mode for the blend containing 75% TLCP-B. The material is first melted at 360°C, then cooled to the temperatures indicated by the symbols: 230°C····· ● G' ○ G", 220°C- - - ■ G' □ G", 210°C—— ▲ G' △ G", 205°C—·· ⧗ G' ⧖ G", and 200°C—— ◆ G' ◇ G".

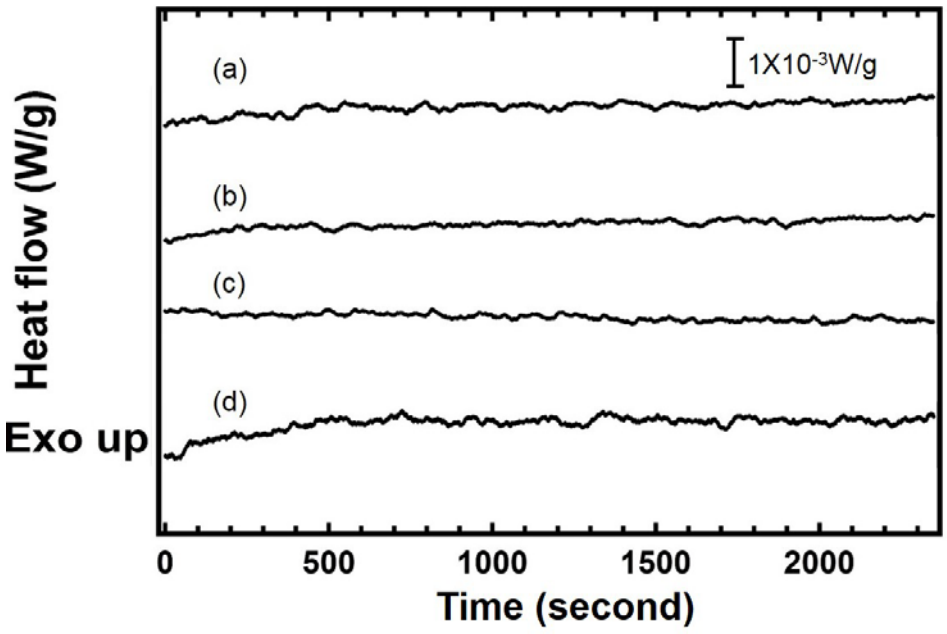

Fig 5.14 a) DSC measurements in the isothermal time sweep mode for the blend containing 75% TLCP-B. The material is first melted at 360^{o}C, then cooled to the predetermined temperatures. From top to bottom are the results obtained at (a) 240^{o}C, (b) 250^{o}C, (c) 260^{o}C and (d) 270^{o}C.

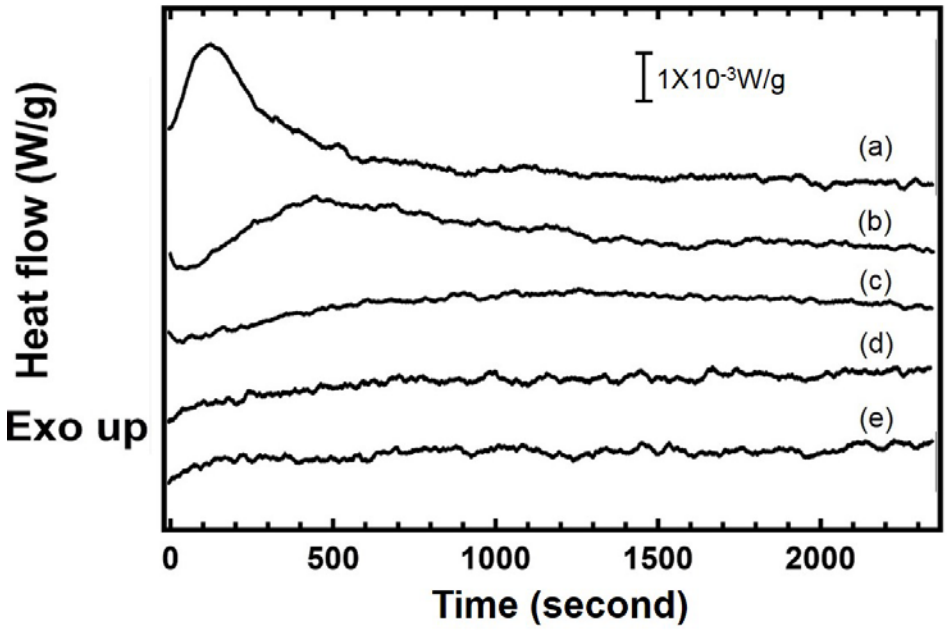

Fig 5.14 b) DSC measurements in the isothermal time sweep mode for the blend containing 75% TLCP-B. The material is first melted at 360^{o}C, then cooled to the predetermined temperatures. From top to bottom are the results obtained at (a) 200^{o}C, (b) 205^{o}C, (c) 210^{o}C, (d) 220^{o}C and (e) 230^{o}C.

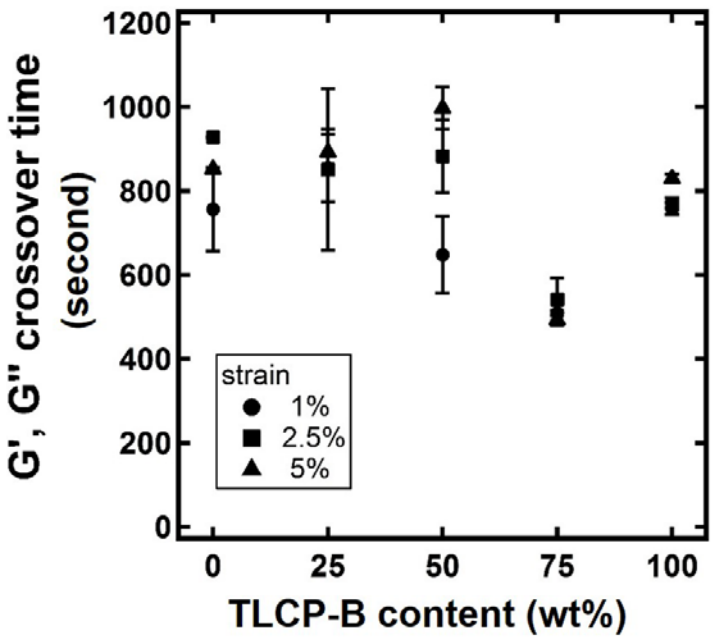

Fig 5.15 Effect of strain on the crossover time of G’ and G” for the TLCP/TLCP blends and the neat TLCPs. All materials are melted in the first place, and then cooled to the predetermined temperatures. For different TLCP-B contents, the measurements are performed at the following temperatures: 0% 315^{o}C, 25% 305^{o}C, 50% 255^{o}C, 75% 210^{o}C and 100% 250^{o}C.

Table 5.1 Enthalpies of melting and crystallization obtained from Figs 5.1 and 5.2

Low melting TLCP-B content /wt%	Melting enthalpy /J•g^{-1}	Crystallization enthalpy /J•g^{-1}
0	6.5	5.2
25	2.9	1.7
50	1.0	1.2
75	N/A	0.8
100	2.2	2.8

6 Conclusions and Recommendations

6.1 Overall Conclusions

1. The processing temperature in the super-cooled state for the liquid crystalline copolyester composed of HBA/TA/HQ/HQ-derivatives (T_m~280^{o}C) can be as low as 250 ^{o}C, as suggested by both SAOS and transient experiments at the startup of shear flow. As the TLCP was cooled 30 ^{o}C below its melting point, a one order magnitude increase in viscosity was obtained at a shear rate of 0.1 s^{-1}. Super cooling the TLCP did not remarkably affect the relaxation of the shear stress after preshearing. Nevertheless, in the interrupted shear measurements, the recovery of the transient shear stress after preshearing was significantly suppressed in the super-cooled state.

2. The bottles of TLCP/HDPE blends were successfully produced by extrusion blow molding. The addition of TLCP significantly improved the modulus of the bottles in the machine direction. However, the enhancement in strength is limited. At the TLCP contents of 10 and 20 wt%, a platelet TLCP morphology was observed. Because of the relatively small blow-up ratio, the dimension of the TLCP platelets in the hoop direction was much lower than that in the machine direction. With 50 wt% TLCP content, a co-continuous structure of the TLCP and HDPE was obtained.

3. The isothermal crystallization behavior of a TLCP was adjusted by blending it with another TLCP with lower melting point. As the content of the low melting TLCP increased in the blends, the temperature at which isothermal crystallization occurred decreased. For the blends containing 75% low melting TLCP, once melted, the isothermal crystallization did not occur unless the material was cooled to 210 ^{o}C or below. The low crystallization temperature allows this blend to be combined with low melting thermoplastics, such as polyolefins. Comparing with DSC, SAOS is more sensitive on characterizing isothermal crystallization, and it should be used on determining the processing temperatures in the super-cooled state for neat TLCP resins and TLCP/TLCP blends.

6.2 Recommendations for Future Work

1. When the TLCP is super cooled, it becomes highly elastic, and edge fracture occurs at very low shear rates in the rotational rheometer. In this work, to delay edge fracture from occurring, the transient rheology of TLCP was measured using parallel disks fixtures with a small gap of 0.2 mm. This method has two major limitations. First, even using a 0.2 mm gap, shear rate is still limited to low values because of edge fracture. The maximum shear rate achieved was 0.5 s^{-1}. Second, squeezing the TLCP to 0.2 mm induced a large amount of residual normal stress at the beginning of the transient measurements. The residual normal stress relaxed during the experiment, which made the first normal stress different (N_1) results inaccurate. TA instrument's cone and partitioned plate fixtures are recommended for further exploring the transient rheology of TLCP in the super cooled state. This set of fixtures is designed for measuring the transient rheology of highly elastic materials, such that the rheological characters may be obtained at higher shear rates. Additionally, because the cone and partitioned plate fixtures do not squeeze the sample to a great extent during sample loading, they may provide more accurate N_1 data. Additionally, using the rheo-optical device to observe the domain structure evolution in the super-cooled state is highly desirable. This results will support the interpretation of the structure evolution from the rheological results, which is discussed in Chapter 3.

2. In this work the preliminary effectiveness of maleic anhydride grafted HDPE (MA-g-HDPE) as a compatibilizer for the TLCP/HDPE blends was studied. The ternary blends of TLCP/HDPE/MA-g-HDPE have not been processed by extrusion blow molding because of the limited time available. The extrusion blow molding of the ternary blends with MA-g-HDPE is recommended to further improve the mechanical properties of the bottles.

3. The TLCP/TLCP blends studied in this dissertation were prepared by direct blending, and they exhibited one melting and one crystallization temperatures in the DSC heating and cooling scans, respectively. An ongoing effort in our laboratory is to develop in situ composite containing two TLCPs with different melting points, using the dual-extruder mixing method. The in situ composite is expected to maintain the two individual melting points of the neat components, such that when the low melting TLCP is melted, the high melting TLCP could still maintains its solid behavior and properties. The author recommends the thermal properties and morphology of the in situ TLCP/TLCP composites to be analyzed, and the results to be compared with those of the direct blended TLCP/TLCP studied in this dissertation. Such comparison will help elucidate the processing-structure-properties relationship of TLCP/TLCP blends, and it is of critical importance on evaluating whether the in situ TLCP/TLCP composites could be applied on extrusion blow molding.

4. Although the glass fiber and carbon fiber reinforced TLCPs are available in the laboratory, the super cooling behavior of these materials is not extensively explored. The main reason for that is the lack of the matrix resin (Vectra A950) for comparison. If Vectra A950 can be obtained, it is recommended to investigate the super cooling behavior of the fiber reinforced TLCPs, and apply the knowledge to the extrusion blow molding of the fiber reinforced TLCP composites.

Appendix A: Small Amplitude Oscillatory Shear Data

Table A.1 SAOS in the temperature sweep mode for the TLCP of HBA/TA/HQ/HQ-derivatives (Zenite HX-8000). The cooling rate is 20 ^{o}C/min.

Temperature /^{o}C	G' /Pa	G" /Pa	η^* /Pa●s^{-1}
307.84	1938.76	3395.28	390.982
306.969	1953.13	3416.78	393.562
307.84	1938.76	3395.28	390.982
306.151	1976.98	3457.03	398.24
305.348	2004.16	3489.11	402.375
304.584	2030.02	3528.93	407.116
303.827	2061.91	3568.13	412.105
303.093	2087.22	3604.66	416.534
302.347	2114.3	3642.18	421.138
301.099	2171.18	3716.38	430.412
300.392	2193.81	3751.13	434.555
299.694	2219.14	3784.22	438.69
298.504	2275.58	3859.97	448.081
297.835	2295.6	3892.76	451.922
296.707	2354.36	3965.37	461.164
296.042	2379.51	4001.6	465.563
294.927	2434.61	4074.8	474.671
294.234	2465.29	4111.77	479.419
293.111	2523.4	4197.47	489.758
292.438	2555.68	4234	494.554
291.35	2616.73	4313.94	504.553
290.314	2678.28	4389.14	514.176
289.267	2731.17	4460.7	523.041
288.594	2765.6	4501.2	528.293
287.605	2829.09	4591.81	539.337
286.626	2887.94	4661.6	548.367
285.686	2948.13	4732.73	557.586
284.689	3014.42	4819.57	568.463
283.694	3076.96	4905.05	579.027
282.774	3148.01	4982.94	589.403
281.816	3218.58	5064.33	600.056
280.504	3317.02	5195.49	616.407
279.819	3364.35	5249.58	623.514
278.478	3477.03	5381.88	640.736
276.902	3623.56	5558.29	663.512
276.164	3675.33	5616.59	671.224
275.467	3724.87	5674.28	678.765
273.91	3881.12	5865.96	703.368
273.201	3948.8	5936.35	712.975

272.507	4002.32	6001.53	721.366
271.102	4161.37	6182.19	745.229
269.775	4310.6	6358.68	768.207
269.065	4382.7	6435.82	778.639
268.38	4450.42	6513.61	788.881
267.055	4620.3	6691.93	813.198
265.823	4781.01	6872.48	837.192
264.543	4953.22	7056.68	862.155
263.844	5039.85	7147.05	874.531
262.509	5219.2	7346.42	901.165
261.284	5408.38	7543.52	928.199
260.591	5504.22	7641.59	941.755
259.311	5698.93	7853.71	970.353
258.184	5883.56	8049.86	997.079
257.005	6085.64	8258.3	1025.84
255.807	6294.32	8477.9	1055.9
254.638	6512.94	8698.46	1086.65
253.477	6727.48	8928.24	1117.91
252.295	6959.57	9175.09	1151.6
251.193	7187.09	9411.47	1184.19
250.087	7430.67	9658.29	1218.59
248.975	7680.58	9917.29	1254.37
247.92	7927.56	10183.3	1290.53
246.903	8177.32	10441.8	1326.27
245.855	8445.88	10732.8	1365.75
244.85	8713.05	11025.1	1405.24
243.892	8983.44	11322.8	1445.37
242.958	9263.06	11630.9	1486.88
241.376	9774.97	12201.7	1563.43
239.951	10279.8	12771.9	1639.5
238.545	10845.8	13422.5	1725.67
237.059	11978.2	14502.3	1880.95
235.657	17293.2	18588	2538.84
232.75	1.41135e+06	452450	148210
231.943	2.96792e+06	701059	304960
231.245	4.17749e+06	861029	426530
230.596	5.11801e+06	991520	521317
229.891	5.9305e+06	1.09999e+06	603165
229.004	6.79348e+06	1.21947e+06	690206
228.105	7.54926e+06	1.33494e+06	766638
227.43	8.07537e+06	1.41452e+06	819832

Table A.2 SAOS in the time mode for the TLCP of HBA/TA/HQ/HQ-derivatives (Zenite HX-8000) at the temperatures of 270, 260 and 250 ^{o}C (the TLCP is first melted at 310 ^{o}C, then cooled to the predetermined temperatures at 20 ^{o}C/min).

270 ^{o}C			260 ^{o}C			250 ^{o}C		
Time /s	G' /Pa	G" /Pa	Time /s	G' /Pa	G" /Pa	Time /s	G' /Pa	G" /Pa
5.68949	4581	6357.96	5.68967	6160.78	7932.31	5.68966	8605.82	9876.13
15.1537	4541.62	6316.93	15.8998	5953.86	7739.52	18.3197	8597.81	9921.78
25.3135	4541.38	6314.64	27.7317	5821.38	7623.6	30.9873	8609.86	9982.33
33.8677	4566.15	6336.28	40.5753	5778.27	7588.82	43.369	8601.27	10012.6
42.2217	4591.29	6363.77	54.201	5831.4	7632.3	54.289	8590.08	10027.7
50.5757	4619.23	6391.84	66.8027	5944.95	7714.88	64.505	8557.18	10014.7
59.8017	4636.99	6418.37	77.3045	6048.62	7788.33	73.675	8521.56	9991.16
68.1555	4646.94	6437.77	85.9805	6114.08	7839.41	82.029	8463.01	9943.47
79.1662	4641.71	6436.93	94.3347	6167.45	7895.54	90.3832	8392.79	9887.77
87.3757	4635.08	6438.54	103.759	6204.22	7948.67	99.521	8307.9	9818.69
95.7297	4623.29	6426.24	113.171	6218.32	7989.46	108.185	8229.03	9755.46
104.084	4603.26	6409.05	123.309	6218.75	8019.62	117.553	8152.04	9697.2
112.438	4587.06	6391.55	133.392	6205.35	8030.02	127.361	8090.8	9642.34
120.792	4567.72	6370.03	143.42	6183.75	8029.7	138.061	8050.14	9610.43
129.146	4557.24	6358.24	152.744	6147.75	8002.18	148.771	8034.84	9596.47
137.5	4548.38	6346.92	161.254	6105.85	7963.81	158.635	8029.08	9580.32
145.854	4547.14	6344.45	169.608	6059.42	7919.3	168.587	8058.29	9597.4
154.208	4549.67	6345.9	177.962	6017.79	7883.19	177.879	8100.57	9624.54
162.562	4556.23	6351.81	186.316	5969.58	7843.4	186.233	8136.47	9646.24
170.916	4562.04	6357.94	194.861	5935.18	7813.98	194.587	8172.8	9682.34
179.27	4568.71	6366.25	203.228	5910.18	7790.75	202.965	8205.81	9715.58
187.624	4571.23	6371.72	211.981	5908.04	7790.54	211.319	8241.91	9761.21
195.978	4570.81	6372.54	220.403	5916.8	7791.46	219.829	8264.01	9802.04
206.801	4566	6366.77	228.757	5925.9	7801.12	228.901	8287.18	9840.85
215.207	4561.19	6365.37	237.111	5955.61	7826.15	238.181	8295.23	9868.8
227.124	4555.05	6355.9	245.465	5972.25	7845.8	247.429	8304.14	9892.91
235.054	4548.53	6350.57	253.887	5987.03	7862.65	256.533	8299.68	9903.03
246.156	4550.5	6349.53	262.241	5988.61	7871.15	265.319	8287.52	9901.03
254.512	4544.15	6346.72	270.595	5996.31	7887.88	273.851	8269.12	9890.18
262.866	4543.86	6341.71	278.949	5986.46	7882.2	282.205	8249.42	9874.73
271.22	4540.83	6336.63	287.303	5974.72	7873.81	290.559	8224.75	9854.81
279.574	4540.95	6338.45	295.657	5958.04	7862.79	299.345	8194.7	9829.83
287.928	4541.59	6342.07	304.011	5946.46	7853.27	307.699	8161.42	9805.44
296.283	4545.07	6341.19	312.365	5927.76	7833.39	316.053	8135.57	9781.3
304.637	4544.21	6343.55	320.719	5911.86	7819.81	324.407	8110.42	9761.98
314.391	4543.6	6343.6	329.073	5904.33	7810.16	332.761	8087.52	9741.3

322.747	4541.02	6344.6	337.427	5896.08	7804.42	341.416	8078.54	9732.26
331.101	4541.27	6342.4	345.781	5894.46	7799.89	349.828	8072.83	9723.58
339.455	4540.43	6342.01	354.135	5897.35	7800.02	358.182	8077.37	9726.31
347.809	4537.92	6338.83	362.49	5899.24	7801.35	366.536	8090.18	9729.63
356.163	4535.81	6335.25	370.844	5902.58	7808.95	374.89	8112.51	9751.7
364.517	4533.91	6331.55	379.198	5908.38	7812.42	383.244	8136.63	9772.92
372.871	4535.19	6333.09	388.248	5915.04	7817.9	393.371	8163.36	9801.72
381.225	4532.58	6332.38	396.602	5915.64	7822.09	401.726	8179.67	9820.76
389.579	4528.94	6329.25	404.956	5915.67	7820.79	410.08	8192.41	9839
397.933	4527.58	6329.24	413.31	5912.63	7823.8	418.434	8203.79	9858.79
406.287	4530.51	6326.46	421.664	5910.18	7820.41	426.788	8219.25	9879.35
414.641	4527.46	6327.42	433.903	5899.73	7811.83	435.142	8226.91	9893.26
422.995	4526.82	6327.68	442.144	5893.36	7807.18	443.496	8224.07	9898.04
431.35	4525.76	6325.14	450.498	5888.93	7800.03	451.85	8220.2	9897.41
439.704	4525.45	6324.23	460.428	5885.33	7798.14	460.204	8217.88	9898.48
448.058	4524.52	6324.54	468.782	5881.01	7797.13	468.558	8212.66	9897.99
456.412	4525.67	6323.47	477.136	5881.19	7795.98	476.912	8200.95	9890.7
464.766	4522.57	6320.96	485.49	5880.63	7794.61	485.266	8192.56	9883.44
473.12	4523.21	6321.47	493.844	5878.23	7793.22	493.7	8182.47	9877.01
481.474	4522.71	6319.24	502.198	5879.73	7796.34	502.054	8170.89	9867.81
489.828	4521.68	6319.13	510.552	5873.64	7788.23	510.408	8156.41	9855.42
498.182	4520.89	6320.58	518.906	5877.68	7791.86	518.762	8154.3	9852.18
506.536	4522.86	6317.1	527.26	5877.73	7794.63	527.117	8151.3	9852.04
514.89	4519.77	6319.48	535.614	5875.74	7791.23	535.471	8152.61	9852.46
523.244	4518.87	6317.25	543.968	5877.67	7793.1	543.825	8158	9855.94
531.598	4516.29	6318.92	554.03	5880.67	7795.86	552.179	8163.62	9862.38
539.953	4518.02	6314.17	562.384	5875.18	7792.84	560.533	8175.81	9871.4
548.307	4518.57	6316.27	570.738	5877	7795.73	568.887	8186.76	9882.83
556.661	4514.89	6314.48	580.103	5875.8	7794.07	577.241	8198.86	9895.32
565.975	4518.22	6315.41	588.078	5872.91	7793.86	586.785	8218.8	9916.41
574.329	4515.11	6315.88	596.438	5873.25	7792.22	595.139	8229.41	9931.42
582.683	4514.83	6309.56	604.792	5871.82	7791.07	603.493	8241.16	9948.42
591.037	4514.49	6311.37	613.146	5866.45	7787.59	611.847	8251.16	9959.96
599.391	4511.11	6311.02	621.5	5867.58	7785.82	620.201	8257.65	9969.4
607.745	4513.79	6310.6	629.854	5865.6	7785.22	628.555	8266.04	9981.16
616.099	4511.34	6309.19	639.838	5864	7786.54	636.909	8269.06	9986.57
624.453	4512.07	6308.61	648.194	5864.01	7782.58	645.263	8273.01	9994.24
632.807	4513.59	6306.92	656.549	5862.8	7784.14	653.617	8275.83	9999.39
641.161	4511.29	6310.06	664.902	5860.99	7781.35	661.971	8275.35	10003.6
649.515	4511.29	6309.26	673.257	5856.57	7780.85	670.325	8275.2	10000.9
657.87	4512.99	6310.21	681.611	5858.17	7780.4	678.679	8278.17	10006.1
666.224	4512.23	6311.91	689.965	5857.31	7778.67	688.653	8278.72	10007.1
677.055	4515.33	6312.69	698.319	5857.05	7781.19	697.007	8277.48	10008.8
685.41	4513.04	6312.13	706.673	5857.2	7781.78	705.879	8274.54	10008.2
693.764	4512.87	6312.3	715.027	5857.1	7782.67	714.343	8281.1	10014.8

702.118	4515.19	6314.85	723.381	5857.57	7782.82	722.698	8285.02	10020.1
710.472	4511.33	6310.22	731.735	5857.72	7782.79	731.051	8292.34	10028.9
718.826	4511.83	6308.39	741.697	5857.99	7785.17	739.405	8299.4	10037.3
727.18	4508.63	6304.56	750.051	5858.73	7784.18	747.76	8307.44	10042.8
735.534	4509.07	6306.7	758.405	5859.84	7784.67	756.114	8319.29	10055.7
743.888	4508.58	6305.73	766.759	5856.38	7783.03	764.468	8331.46	10069.5
752.242	4509.64	6307.41	775.113	5854.81	7783.25	772.822	8344.02	10082.2
760.596	4507.93	6307.73	783.467	5855.63	7782.37	781.176	8354.83	10098
768.95	4507.34	6304.54	791.821	5856.24	7785.48	790.226	8373.11	10116.4
777.304	4505.29	6306.39	800.175	5855.8	7785.04	798.58	8381.56	10127.6
785.658	4510.05	6306.39	808.529	5852.86	7784.26	806.934	8392.78	10138.3
794.012	4507.47	6304.68	821.092	5850.57	7780.57	815.288	8402.45	10151.6
803.898	4507.51	6304.77	829.63	5852.29	7782.96	823.642	8410.13	10162.1
812.716	4506.86	6304.43	839.68	5852.47	7781.6	831.996	8419.82	10173.1
821.07	4507.44	6301.06	847.607	5852.92	7782.96	840.35	8427.58	10182.1
829.424	4504.65	6302.54	855.967	5854.62	7786.04	848.704	8433.48	10190.1
837.778	4507.09	6304.63	867.819	5849.75	7778.26	857.058	8444.08	10201.5
846.132	4506.99	6303.33	875.815	5849.5	7779.18	865.412	8448.88	10208.7
854.486	4507.18	6303.55	884.175	5845.52	7777.98	873.766	8454.68	10217.8
862.84	4507.48	6304.47	892.529	5846.5	7781.11	882.121	8465.33	10228.2
871.194	4507.2	6304.97	901.706	5841.8	7772.35	891.721	8476.13	10243.7
879.549	4506.84	6305.56	909.869	5842.8	7776.7	900.076	8483.03	10249.2
887.902	4507.56	6304.41	918.229	5846.59	7778.6	908.43	8491.78	10258.4
896.257	4506.69	6302.08	926.583	5846.34	7778.88	916.787	8499.13	10267.5
904.611	4507.88	6304.5	934.937	5849.57	7781.48	925.141	8506.68	10276.2
912.965	4509.56	6304.52	945.229	5846.09	7777.31	933.495	8516.37	10287
921.319	4508.6	6306.1	953.583	5847.88	7780.44	941.851	8528.29	10298.3
929.673	4509.4	6305.67	961.937	5842.7	7774.46	950.205	8541.11	10312.8
938.027	4506	6303.04	970.291	5843.11	7774.94	958.559	8551.84	10325.4
946.381	4505.01	6301.06	978.645	5844.92	7777.16	966.913	8566.82	10339.5
954.735	4506.12	6300.17	986.999	5844.17	7777.7	975.267	8582.74	10358
963.089	4503.91	6302.05	995.354	5843.81	7779.63	983.621	8598.8	10375
971.443	4504.96	6301.85	1003.71	5845.21	7781.59	991.975	8612.47	10389.9
979.797	4508.31	6303.48	1012.06	5847.44	7784.8	1000.33	8627.29	10406
989.957	4508.43	6303.6	1020.42	5848.02	7782.85	1011.09	8650.57	10429.3
998.311	4506.22	6304.68	1028.77	5847.76	7786.35	1019.44	8664.73	10450.8
1006.67	4506.35	6300.37	1037.12	5848.77	7785.18	1027.79	8680.65	10466.6
1015.02	4508.5	6303.7	1046.34	5849.48	7788.19	1036.15	8697.21	10484.2
1023.37	4508.84	6304.22	1056.74	5848.14	7783.89	1044.5	8709.07	10500
1031.73	4506.06	6302.19	1064.94	5843.92	7782.76	1052.86	8725.44	10516.4
1040.08	4505.86	6302.75	1073.3	5844.19	7780.62	1063.18	8740.57	10532.8
1048.44	4505.46	6301.63	1081.65	5844.02	7786.07	1071.45	8754.68	10548.6
1056.79	4505.54	6301.92	1090	5844.14	7782.66	1079.8	8767.12	10561.6
1065.14	4506.99	6300.47	1098.36	5841.88	7781.13	1088.16	8779.52	10575.8
1073.5	4506.62	6299.96	1106.71	5839.85	7781.37	1096.51	8792.2	10589.2

1081.85	4506.02	6302.57	1115.6	5847.7	7786.54	1107.42	8808.34	10606.6
1090.21	4506.36	6300.59	1123.95	5838.95	7780.16	1117.51	8833.75	10633.8
1098.56	4505.87	6303.69	1132.3	5840.96	7780.54	1125.87	8847.51	10650.3
1106.91	4509.8	6301.88	1140.66	5841.6	7780.45	1134.22	8859.61	10661.9
1115.27	4508.12	6302.12	1149.01	5838.27	7779.44	1142.57	8872.96	10679.4
1125.01	4504.92	6298.35	1157.37	5840.89	7779.99	1150.93	8891.54	10698.8
1133.23	4503.82	6299.11	1165.72	5839.97	7780.56	1159.28	8906.57	10715.8
1141.58	4504.71	6302.27	1174.07	5843.58	7783.43	1167.64	8922.91	10733.1
1149.94	4505.59	6301.04	1182.43	5843.12	7780.96	1175.99	8942.29	10751.4
1158.29	4507.11	6300.15	1190.78	5842.77	7782.54	1186.09	8964.34	10775.1
1166.65	4506.03	6299.32	1199.14	5842.93	7784.18	1194.59	8980.31	10793.7
1175	4504.88	6298.74	1207.49	5844.34	7781	1202.94	9000.32	10811
1185.04	4501.49	6293.2	1215.84	5846.15	7785.28	1211.3	9019.92	10836.6
1192.97	4501.09	6294.59	1224.2	5844.13	7785.46	1219.65	9040.99	10854.4
1202.95	4503.28	6295.23	1237.66	5849.59	7791.08	1228.01	9066.22	10882.2
1211.3	4504.67	6293.84	1245.83	5850.39	7792.59	1236.36	9086.01	10903.2
1219.66	4505.45	6296.25	1254.19	5848.86	7792.25	1244.71	9105.93	10927.9
1228.01	4506.34	6298.76	1262.55	5851.74	7796.56	1253.76	9124.65	10946.7
1236.36	4505.35	6296.71	1270.9	5852.54	7794.91	1262.05	9147.33	10969.9
1244.72	4504.18	6300.39	1283.08	5847.71	7792.52	1270.4	9171.84	10990.9
1255.26	4508.4	6302.07	1291.38	5853.01	7797.82	1278.76	9195.49	11020.7
1263.63	4510.52	6303.18	1300.98	5849.25	7796.08	1287.11	9217.22	11040.5
1271.98	4510.95	6302.41	1309.36	5848.57	7796.97	1295.46	9239.02	11066.8
1280.34	4509.83	6303.63	1317.71	5850.4	7795.87	1306.49	9279.58	11106.2
1288.69	4509.91	6300.49	1326.07	5849.48	7797.21	1314.85	9303.53	11131.7
1297.05	4507.18	6298.23	1334.42	5848.26	7794.94	1323.2	9324.63	11156
1305.4	4508.97	6299.52	1343.29	5848.88	7796.05	1331.56	9346.13	11178.1
1313.76	4508.45	6299.97	1351.65	5849.01	7797.07	1339.91	9371.78	11204.1
1322.11	4508.4	6297.46	1360	5849.55	7796.38	1350.63	9398.19	11232.2
1330.47	4507.55	6298.89	1368.36	5851.54	7799.43	1359.14	9424.63	11262.2
1338.82	4506.07	6295.83	1376.71	5849.77	7800.3	1367.49	9451.36	11288.2
1349.5	4508	6299.94	1385.07	5849.49	7797.52	1375.84	9480.02	11315.4
1357.85	4505.07	6297.78	1393.42	5852.86	7799.2	1387.8	9508.23	11347
1366.21	4506.82	6297.86	1401.77	5849.89	7800.57	1396.91	9533.79	11373.6
1374.56	4507.18	6296.87	1410.13	5853.27	7803.49	1405.32	9563.24	11405.1
1382.92	4510.42	6302.84	1418.48	5851.28	7802.92	1413.67	9590.15	11432
1391.27	4508.6	6300.01	1426.84	5852.45	7802.11	1422.03	9618.99	11460.1
1403.21	4505.94	6296.01	1435.19	5851.77	7801.75	1430.38	9645.89	11489.4
1411.68	4505.76	6297.42	1443.54	5852.67	7802.9	1438.74	9677.04	11521.2
1420.11	4508.92	6297.34	1451.9	5853.69	7800.67	1447.09	9705.07	11549.1
1428.46	4509.01	6297.83	1460.25	5853.26	7803.88	1455.44	9733.31	11580.6
1436.81	4508.12	6298.23	1468.61	5852.43	7803.46	1463.8	9764.26	11611.5
1445.17	4509.21	6298.95	1476.96	5852.27	7805.27	1472.15	9795.74	11641.4
1453.52	4506.84	6299.98	1485.31	5854.79	7804.84	1481.14	9826.79	11675.3
1461.88	4508.42	6296.7	1493.67	5854.85	7804.81	1489.6	9861.42	11708.7

1470.23	4506.79	6298.18	1502.02	5855.32	7806.45	1497.96	9892.75	11742.4
1478.58	4508.46	6298.19	1510.38	5854.74	7804.98	1506.31	9926.59	11775.9
1489.26	4507.7	6296.45	1518.73	5856.36	7810.19	1514.66	9956.44	11807.9
1497.18	4506.73	6295.15	1527.08	5856.89	7808.13	1523.02	9988.73	11838.7
1505.54	4506.64	6294.82	1535.44	5857.87	7809.97	1531.37	10021.8	11872.1
1513.89	4506.18	6298.72	1543.79	5860.68	7812.8	1539.73	10053.2	11905.9
1522.25	4509.48	6297.42	1552.15	5859.7	7812.7	1548.08	10087.1	11940.6
1530.6	4506.13	6296.13	1560.5	5858.65	7811.53	1556.44	10120.4	11972.4
1538.96	4508.2	6296.52	1568.85	5861.26	7812.56	1564.79	10155.9	12009.3
1547.31	4506.82	6295.42	1577.21	5860.29	7811.03	1573.14	10192.4	12044.8
1555.66	4509.6	6297.72	1585.56	5858.12	7811.04	1581.5	10226.2	12081.8
1564.02	4510.72	6299.81	1593.92	5859.04	7811.69	1589.85	10260.9	12116.2
1572.37	4508.86	6300.77	1602.27	5859.46	7812.45	1598.21	10300.9	12153.7
1580.73	4509.96	6298.49	1610.63	5863.45	7817.55	1606.56	10336.5	12188.2
1589.08	4510.02	6298.37	1620.87	5867.68	7819.33	1614.91	10371.2	12223.4
1597.43	4512.59	6297.11	1629.23	5868.59	7822.22	1623.27	10407.8	12260.8
1605.79	4511.26	6299.65	1637.59	5865.79	7822.48	1631.62	10451.6	12304.1
1614.14	4509.46	6298.56	1645.95	5867.46	7823.02	1639.98	10491.3	12342.5
1622.5	4510.63	6299.61	1654.99	5867.97	7821.92	1649.35	10531.9	12385.2
1630.85	4509.3	6298.28	1663.29	5867.01	7820.35	1657.32	10574.5	12428.4
1639.21	4511.19	6299.35	1671.65	5866.35	7823.25	1665.68	10619.3	12472.1
1647.56	4511.15	6300.69	1680	5866.97	7821.22	1674.03	10659.5	12510.8
1655.91	4511.5	6300.79	1688.36	5867.21	7822.51	1682.39	10704.4	12555.7
1664.27	4510.76	6299.39	1696.71	5869.2	7822.65	1690.74	10746.8	12601.5
1672.62	4512.12	6299.4	1705.99	5865.65	7820.97	1699.1	10796.6	12646.5
1680.98	4513.23	6302.44	1714.05	5867.35	7823.91	1708.22	10845.1	12696.5
1689.33	4514.88	6303	1722.41	5868.58	7821.01	1716.58	10893.2	12739.4
1697.68	4512.9	6302.48	1730.77	5871.81	7823.57	1724.93	10938.1	12786.8
1706.04	4514.99	6301.07	1739.12	5867.02	7822.24	1733.95	10991.7	12838.1
1714.39	4515.81	6306.29	1747.47	5868.71	7823.29	1742.3	11039.7	12882.4
1722.75	4516.29	6303.84	1755.83	5870.73	7824.38	1750.65	11088	12934
1731.1	4516.16	6302.44	1764.18	5870.56	7824.11	1759.01	11137.7	12982.7
1739.45	4517.37	6303.92	1772.54	5871.84	7828.69	1767.36	11184.6	13029.2
1747.81	4516.49	6303.59	1780.89	5874.06	7828.98	1783.48	11265.6	13101.7
1756.16	4515.05	6301.86	1789.24	5874.72	7832.78	1791.61	11317.6	13155.4
1764.52	4517.06	6303.73	1797.6	5874.93	7831.16	1799.97	11374.1	13207.8
1772.87	4515.37	6304.26	1805.95	5873.99	7828.71	1808.33	11430.2	13260.4
1781.22	4517.1	6303.95	1814.31	5874.68	7829.81	1816.68	11485.1	13316.5
1789.58	4515.89	6305.68	1822.66	5878.33	7833.09	1825.04	11541.3	13370.3
1797.93	4516.48	6303.52	1831.01	5876.03	7833.19	1833.39	11597.1	13421.4
1806.29	4514.35	6299.27	1839.37	5877.97	7834.36	1841.74	11653.1	13478
1814.64	4513	6301.66	1847.72	5880.43	7837.32	1851.87	11719	13538.8
1822.99	4514.29	6301.63	1856.08	5879.96	7838.3	1860.34	11775	13594.8
1831.35	4513.95	6298.98	1864.43	5882.63	7838.34	1868.7	11833.8	13646.2
1839.7	4513.87	6297.22	1872.78	5879.06	7835.46	1877.05	11894.6	13706.8

1848.06	4513.98	6300.61	1881.14	5875.87	7835.86	1885.41	11951.3	13759.3
1856.41	4516.33	6303.45	1889.49	5880.17	7838.78	1893.76	12013.9	13817.6
1864.76	4517.89	6303.1	1897.85	5883.81	7838.51	1902.11	12073.9	13872.5
1873.12	4515.37	6303.28	1906.2	5882.83	7842.34	1910.47	12135.9	13932.5
1881.47	4512.82	6299.4	1914.56	5884.29	7839.85	1918.82	12201.8	13993.9
1889.83	4516.44	6301.15	1922.91	5884.61	7840.01	1927.18	12264.1	14051.5
1898.18	4517.35	6303.13	1931.26	5880.61	7837.92	1935.53	12327.4	14113
1906.54	4519.03	6304.05	1939.98	5882.63	7842.66	1943.88	12400.7	14179.5
1914.89	4518.03	6304.2	1948.34	5887.24	7844.69	1952.24	12463.6	14237.1
1923.24	4517.48	6305.58	1956.69	5885.87	7845.28	1962.27	12538.5	14304.9
1931.6	4518.03	6304.9	1965.05	5891.11	7846.63	1970.24	12607.2	14370.6
1939.95	4517.55	6304.27	1973.4	5890.13	7847.93	1978.56	12677.1	14436.3
1948.31	4519.23	6304.76	1981.75	5889.83	7848.24	1986.91	12751.8	14500.4
1956.66	4519.94	6305.29	1990.11	5889.55	7847.96	1995.27	12824	14567.7
1965.01	4521.23	6306.27	1998.46	5890.22	7850.45	2003.62	12896.9	14636.7
1973.37	4519.98	6306.51	2006.82	5891.77	7851.8	2011.97	12969.8	14699.5
1981.72	4521.73	6307.65	2015.17	5890.88	7849.78	2020.33	13046.8	14768
1990.08	4518.45	6305.04	2023.52	5889.07	7847.34	2031.4	13136.2	14847
1998.43	4521.51	6305.45	2031.88	5893.06	7849.41	2041.36	13251.2	14955.8
2006.78	4522.38	6305.57	2040.23	5892.2	7847.43	2049.73	13323.7	15021
2015.14	4519.37	6306.95	2048.59	5891.24	7849.61	2058.08	13403.7	15092.8
2023.49	4522.72	6308.07	2056.94	5892.93	7850.4	2066.44	13480.9	15159.4
2031.85	4522.86	6310.07	2065.29	5892.91	7853.28	2074.79	13560.9	15233
2040.2	4522.82	6308.67	2073.65	5894.81	7853.78	2086.45	13664	15322.1
2048.55	4522.95	6308.68	2082	5894.43	7852.37	2094.64	13759.1	15407.8
2056.91	4522.65	6308.08	2090.36	5894.7	7854.18	2103	13847.9	15485
2065.26	4522.61	6308.79	2098.71	5895.88	7852.14	2111.36	13933.3	15562.7
2073.62	4525.06	6310.74	2107.06	5894.77	7853.25	2119.71	14025.1	15641.9
2081.97	4522.64	6307.24	2115.42	5899.94	7858.19	2129.14	14120	15723
2090.32	4522.47	6306.42	2123.77	5899.78	7858.71	2138.08	14218.1	15811.8
2098.68	4522.63	6308.16	2132.13	5900.25	7858.64	2146.04	14316.2	15892.6
2107.03	4520.15	6305.02	2140.48	5900.22	7859.76	2154.4	14414.3	15982.8
2115.39	4523.54	6307.85	2148.83	5900.81	7858.15	2162.75	14510.8	16066.1
2123.74	4521.16	6306.27	2157.19	5901.45	7859.98	2171.11	14609.2	16151.7
2132.09	4523.49	6308.07	2165.54	5902.03	7861.68	2179.46	14705.1	16231.8
2140.45	4520.95	6306.12	2173.9	5902.22	7860.58	2187.82	14805.9	16318.8
2148.8	4524.66	6307.04	2182.25	5902.26	7860.84	2196.17	14904.9	16402.9
2157.16	4521.32	6304.8	2190.6	5904.9	7861.8	2204.52	15014.4	16496.8
2165.51	4523.46	6303.85	2198.96	5905.04	7864	2212.88	15120	16586.4
2173.87	4520.97	6302.07	2207.31	5903.48	7861.85	2221.23	15226.5	16676.8
2182.22	4524.1	6303.56	2215.67	5905.2	7863.83	2229.59	15334.1	16767.5
2190.57	4521.23	6305.17	2224.02	5905.78	7864.53	2240.3	15506.1	16915.1
2198.93	4523.24	6306.29	2232.38	5910.75	7871.06	2248.65	15607.4	17000.4
2207.28	4526.52	6307.7	2240.73	5907.53	7866.53	2257	15721.1	17094.6
2215.64	4523.97	6307.44	2249.08	5909.31	7869.68	2265.36	15835.2	17189

2223.99	4525.61	6310.04	2257.44	5908.51	7868.88	2273.71	15950.1	17284.9
2232.34	4526.58	6307.39	2265.79	5913.21	7874.55	2282.07	16072.3	17382.9
2240.7	4525.3	6308.52	2274.15	5908.06	7869.71	2290.42	16193.7	17484.5
2249.05	4526.98	6310.44	2282.5	5912.54	7870.91	2298.77	16320.3	17586.7
2257.41	4528.2	6308.12	2290.85	5912.94	7872.43	2309.71	16468.9	17706
2265.76	4526.09	6307.09	2299.21	5915.11	7873.69	2318	16611.3	17822.4
2274.11	4527.33	6307.43	2307.56	5912.65	7870.97	2326.35	16752	17940
2282.47	4526	6310.02	2315.92	5914.92	7872.96	2334.71	16889.7	18051.6
2290.82	4527.67	6309.67	2324.27	5912.6	7872.2	2343.06	17034	18168.6
2299.18	4525.59	6307.45	2332.62	5914.42	7871.44	2351.42	17178.3	18284.7
2307.53	4529.72	6309.5	2340.98	5916.56	7872.9	2360.12	17329.3	18403.7
2315.88	4529.12	6307.96	2349.33	5916.93	7874.67	2368.13	17466.5	18512
2324.24	4529.49	6307.94	2357.69	5916.72	7876.88	2376.49	17610.2	18630.1
2332.59	4529.58	6308.37	2366.04	5919.73	7877.07	2384.84	17765.5	18750
2340.95	4530.75	6311.01	2376.18	5918.06	7877.37	2397.2	17934.5	18873
2349.3	4529.11	6310.8	2384.64	5918.2	7876.6	2406.78	18153.7	19052.1
2357.65	4531.28	6311.29	2393	5917.85	7875.99	2415.14	18289.4	19163.5
2367.98	4533.85	6315.19	2401.35	5917.71	7875.79	2423.49	18439	19277.8
2380	4532.47	6313.96	2409.7	5919.42	7880.04	2431.84	18594.7	19397.1
2388.46	4533.87	6315.66	2418.06	5923.69	7882.77	2440.2	18754.7	19518.2
2396.81	4533.49	6316.04	2426.41	5927.64	7886.95	2448.55	18918.5	19646.7
2405.17	4532.47	6313.31	2436.3	5930.35	7892.35	2456.91	19080.4	19771.9
2413.52	4531.95	6312.54	2444.65	5929.6	7887.54	2465.26	19246	19896.3
2421.88	4532.34	6313.75	2455.96	5926.69	7886.11	2473.61	19418.1	20029.4
2430.23	4530.13	6312.66	2463.87	5929.37	7888.08	2481.97	19587.7	20157.1
2438.59	4529.93	6309.8	2472.23	5929.02	7891.89	2490.32	19759.2	20284.1
2448.9	4529.44	6313.45	2480.59	5928.64	7888.15	2498.68	19929.3	20412.8
2457.25	4531	6311.05	2488.94	5930.59	7893.65	2507.03	20115.5	20549.3
2465.61	4529.85	6308.94	2497.29	5934.45	7894.52	2515.38	20294.3	20688.5
2473.96	4530.13	6310.14	2505.65	5939.14	7899.07	2523.74	20471.9	20816.5
2482.32	4529.79	6309.76	2514	5934.9	7896.02	2532.09	20661.5	20958.6
2490.67	4532.34	6311.32	2524.94	5932.26	7890.94	2540.45	20842.7	21091.2
2501.72	4532.77	6311.27	2533.23	5933.79	7893.04	2548.8	21035.1	21225.8
2511.72	4534.34	6311.61	2541.58	5938.1	7897.12	2557.16	21220.5	21363.6
2520.08	4532.53	6313.91	2549.94	5936.24	7897.05	2565.51	21415.3	21501.5
2528.43	4534.03	6313.98	2558.29	5938.63	7898.04	2573.86	21618.5	21650.4
2536.79	4533.5	6312.36	2566.65	5941.1	7899.99	2582.22	21815	21787.2
2545.14	4537.95	6312.87	2575	5939.9	7901.78	2590.57	22013	21923.3
2553.5	4536.25	6313.33	2583.35	5941.74	7901.64	2598.93	22222.7	22074.5
2561.85	4535.42	6315.78	2592.58	5939.71	7900.71	2607.28	22436.9	22225
2570.2	4536.33	6314	2600.7	5945.32	7905.02	2615.64	22651.7	22378.7
2578.56	4534.92	6314.94	2609.06	5944.71	7905.8	2625.04	22878.2	22533.3
2586.91	4537.26	6312.84	2617.41	5944.94	7908.68	2632.98	23117.1	22705.9
2595.27	4537.02	6310.39	2625.77	5947.13	7910.96	2641.34	23349.4	22863.2
2603.62	4534.97	6315.05	2634.12	5951.57	7910.38	2649.69	23575.5	23025.3

2611.98	4538.05	6312.99	2642.47	5949.01	7911.09	2658.05	23805.8	23182.3
2620.33	4535.21	6314.37	2652.08	5951.49	7912.15	2666.4	24050.5	23353
2628.68	4534.32	6314.1	2660.45	5952.02	7915.5	2675.49	24344	23551.6
2637.04	4535.59	6314.19	2668.8	5954.6	7919.04	2683.85	24576.9	23709.3
2645.39	4534.58	6312.65	2677.15	5950.8	7913.41	2692.2	24833.8	23880.3
2653.75	4534.39	6312.92	2687.86	5954.19	7917.22	2700.56	25086	24055.7
2662.1	4537.59	6314.15	2695.76	5958.1	7919.68	2708.91	25353	24231.1
2670.45	4535.21	6312.11	2704.12	5961	7924.06	2717.26	25643.1	24430.6
2678.81	4535.69	6311.5	2712.47	5957.44	7921.15	2725.62	25916.6	24608.1
2687.16	4537.55	6311.93	2720.83	5959.18	7922.21	2733.97	26193.8	24797.1
2695.52	4537.13	6312.5	2729.18	5960.5	7925.25	2742.33	26497.3	25001.6
2703.87	4537.71	6315.33	2737.53	5960.83	7924.32	2750.68	26804.4	25202.2
2712.22	4537.46	6315.6	2745.89	5963.06	7926.05	2759.03	27117.3	25408.4
2720.58	4537.75	6314.09	2754.24	5964.87	7927.99	2767.39	27427.7	25610.6
2728.93	4538.74	6315	2762.6	5962.98	7926.36	2775.74	27755.2	25829.3
2737.29	4537.85	6312.99	2770.95	5961.88	7926.96	2784.1	28110	26065.3
2745.64	4535.17	6312.15	2779.3	5964.37	7928.07	2792.45	28452	26292.3
2753.99	4536.65	6313.94	2787.66	5965.47	7929.94	2800.8	28815	26526.2
2764.62	4539.69	6313.58	2796.01	5966.69	7930.59	2809.16	29180.6	26769.2
2772.97	4536.86	6311.87	2804.37	5965.97	7931.55	2817.51	29562.5	27014.8
2781.32	4537.42	6312.01	2814.61	5971.31	7936.79	2825.87	29953.4	27271.9
2789.68	4537.46	6310.66	2822.97	5971.32	7937.09	2834.22	30362.3	27540.9
2798.03	4540.15	6312.03	2831.32	5974.03	7938.87	2842.57	30774.7	27815.9
2806.39	4538.36	6313.31	2839.68	5973.37	7937.38	2850.93	31212.1	28098.7
2814.74	4539.53	6313.49	2848.03	5974.9	7939.78	2859.28	31668.4	28401.9
2823.1	4542.84	6312.18	2857.86	5976.9	7939.68	2867.64	32138.5	28716.3
2833.64	4540.37	6309.53	2866	5975.28	7940.24	2875.99	32603.1	29032.1
2841.69	4542.05	6317.47	2874.36	5981.04	7945.21	2884.35	33093.8	29352.9
2851.6	4546.76	6319.55	2882.71	5980.67	7943.47	2892.7	33588.1	29681.8
2859.95	4543.52	6317.63	2891.07	5978.83	7944.61	2901.05	34096.5	30028.8
2868.31	4545.1	6318.92	2899.42	5980.7	7945.86	2909.41	34618.8	30376.1
2876.66	4544.76	6318.51	2907.77	5979.86	7943.35	2917.76	35152.7	30739
2886.56	4541.61	6316.71	2916.13	5980.75	7945.5	2926.12	35717.9	31128.8
2894.63	4544.3	6316.14	2924.48	5982.12	7950.08	2934.47	36298.2	31520.2
2902.99	4540.68	6318.01	2932.84	5984.65	7947.79	2942.82	36860.1	31917.2
2911.35	4540.41	6313.24	2941.19	5986.26	7953.07	2951.18	37436.9	32320.8
2919.7	4543.07	6313.06	2949.55	5988.32	7951.22	2959.53	38032.4	32733.3
2928.06	4539.9	6310.75	2957.9	5988.44	7953.36			
2938.47	4543.83	6315.98	2968.12	5987.4	7949.19			
2946.82	4542.13	6316.13	2976.49	5986.64	7952.59			
2955.18	4543.45	6316.75	2984.85	5990.31	7955.34			
2963.53	4546.2	6315.27	2993.2	5989.19	7955.26			
2971.89	4541.47	6313.1	3001.55	5992.73	7957.26			
2980.24	4537.98	6311.78	3009.91	5994.64	7960.58			
2988.59	4536.87	6307.61	3018.26	6000.39	7965.05			

2996.95	4542.14	6311.97	3026.62	5999.27	7962.96			
3005.3	4543.57	6312.26	3034.97	5999.07	7963.9			
3013.66	4544.79	6313.77	3043.32	5999.8	7963.96			
3022.01	4543.04	6314.77	3051.68	5998.81	7965.17			
3030.36	4545.66	6313.86	3060.03	6002.74	7967.74			
3038.72	4546.88	6315.07	3068.39	6003.64	7965.98			
3047.07	4545.25	6315.89	3076.74	6001.97	7967.84			
3055.43	4547.57	6314.54	3085.09	6004.95	7969.03			
3063.78	4546.8	6316.8	3093.45	6005.3	7971.32			
3072.13	4546.73	6314.56	3101.8	6007.58	7971.65			
3082.48	4550.29	6317.74	3110.16	6008.13	7972			
3090.84	4548.1	6320.81	3118.51	6010.53	7975.77			
3099.19	4549.05	6320.55	3127.14	6012.79	7975.03			
3107.54	4553.03	6320.38	3139.07	6009.73	7973.75			
3115.9	4549.51	6323.83	3147.35	6014.01	7976.86			
3124.25	4548.73	6320.64	3155.7	6013.05	7979.38			
3132.61	4548.35	6316.79	3164.05	6013.75	7976.93			
3140.96	4549.2	6317.69	3172.41	6015.41	7980.52			
3149.31	4550.78	6317.82	3180.76	6017.72	7982.34			
3157.67	4549.1	6319.5	3189.12	6016.87	7981.89			
3168.54	4545.6	6313.97	3197.47	6021.18	7987.71			
3176.89	4545.24	6313.78	3205.82	6020.67	7987.05			
3185.25	4545.83	6312.64	3214.18	6021.75	7987.96			
3194.9	4547.52	6314.79	3222.53	6026.17	7988.74			
3203.26	4547.67	6316.11	3230.89	6026.82	7989.77			
3211.61	4549.37	6315.71	3239.24	6026.76	7991.61			
3219.96	4547.69	6314.84	3247.59	6028.43	7990.03			
3228.32	4547.12	6315.77	3255.95	6027.17	7991.71			
3236.67	4548.34	6316.41	3264.3	6031.83	7994.9			
3245.03	4548.94	6315.76	3272.66	6032.64	7996.47			
3253.38	4550.78	6315.98	3281.01	6034.55	7999.61			
3261.73	4550.7	6317.47	3289.36	6035.77	7998.24			
3270.09	4550.46	6318.52	3297.72	6033.18	7997.92			
3278.44	4549.6	6317.34	3306.07	6036.06	8000.17			
3286.8	4551.78	6318.38	3314.43	6041.83	8007.42			
3295.15	4551.91	6318.89	3324.21	6042.85	8006.84			
3303.51	4549.85	6317.71	3332.57	6043.33	8008.14			
3311.86	4552.05	6317.14	3340.92	6044.97	8009.51			
3320.21	4552.25	6315	3349.28	6046.27	8010.41			
3328.57	4550.7	6313.16	3357.63	6049.59	8014.64			
3336.92	4549.77	6318.12	3365.98	6048.83	8015.3			
3345.28	4551.02	6318.06	3374.34	6051.01	8016.4			
3353.63	4551.39	6318.39	3382.69	6051.91	8018.77			
3361.98	4553.76	6317.66	3391.05	6051.35	8015.12			
3370.34	4553.69	6315.92	3399.4	6056.6	8019.78			

3378.69	4553.29	6314.77	3407.75	6054.27	8022.93			
3387.05	4553.64	6316.75	3420.01	6054.6	8019.5			
3395.4	4555.16	6317.99	3428.23	6055.91	8022.25			
3403.75	4555.88	6317.4	3436.59	6057.94	8023.19			
3412.11	4555.87	6318.74	3444.94	6059.73	8025.3			
3420.46	4553.78	6317.34	3453.3	6057.19	8024.87			
3428.82	4553.55	6318.22	3461.65	6058.07	8023.24			
3437.17	4554.31	6316.5	3470	6062.81	8026.72			
3445.52	4554.85	6319.45	3478.36	6062.76	8026.2			
3453.88	4554.09	6318.19	3488.94	6062.64	8024.59			
3462.23	4554.2	6319.98	3496.96	6066.31	8032.49			
3470.59	4554.94	6317.3	3505.32	6070.42	8034.77			
3478.94	4554.39	6318.59	3513.67	6070.94	8038.74			
3487.29	4555.27	6316.19	3522.02	6070.65	8039.67			
3495.65	4555.21	6315.61	3530.38	6071.21	8037.71			
3504	4551.31	6314.04	3539.15	6075.09	8039.93			
3512.36	4554.6	6315.5	3547.09	6079.12	8044.47			
3520.71	4554.06	6311.93	3555.45	6082.11	8047.46			
3529.06	4552.87	6314.99	3563.8	6082.62	8049.63			
3537.42	4553.92	6312.11	3574.39	6080.7	8045.2			
3545.77	4553.22	6312.73	3582.4	6081.71	8049.24			
3554.13	4554.4	6313.97	3593.54	6082.28	8046.41			
3562.48	4555.2	6313.79	3601.63	6086.51	8053.3			
3570.83	4552.15	6310.73	3609.99	6088.12	8053.4			
3579.19	4553.52	6313.54	3618.35	6087.35	8051.69			
3587.54	4553.32	6314.06	3626.7	6090.82	8053.91			
3595.9	4554.23	6312.72	3635.05	6093.95	8058.49			
3604.25	4554.54	6312.37	3644.23	6093.72	8059.8			
3612.61	4552.6	6312.48	3652.4	6096.72	8063.33			
3620.96	4554.91	6310.91	3660.76	6096.55	8063.57			
3629.32	4555.39	6312.1	3673.15	6095.86	8058.72			
3637.67	4554.73	6312.07	3681.24	6101.09	8064.72			
3646.02	4556.85	6315.34	3689.61	6098.55	8064.76			
3654.38	4557.59	6315.65	3701.51	6097.62	8062.78			
3662.73	4557.52	6313.92	3709.46	6101.46	8067.95			
3671.09	4557.85	6315.52	3717.82	6102.39	8067.91			
3679.44	4559.7	6314.41	3728.45	6101.63	8067.96			
3687.79	4555.53	6314.73	3736.41	6105.07	8070.01			
3696.15	4559.7	6314.4	3744.77	6110.53	8075.43			
3704.5	4558.12	6315.05	3753.13	6111.28	8077.07			
3712.86	4555.9	6312.83	3761.48	6113.48	8079.27			
3721.21	4555.79	6313.45	3769.83	6114.96	8077.85			
3729.56	4558.91	6316.29	3778.19	6114.76	8080.46			
3737.92	4560.67	6319.05	3786.54	6114.38	8079.95			
3746.27	4560.35	6319.57	3794.9	6119.36	8082.74			

3754.63	4560.22	6315.51	3803.25	6118.62	8083.14			
3762.98	4558.84	6316.85	3811.6	6121.64	8086.71			
3771.33	4557.66	6314.53	3819.96	6125.74	8088.86			
3779.69	4559.54	6316.93	3828.31	6124.46	8090.55			
3788.04	4561.65	6317.16	3836.67	6127.61	8092.27			
3796.4	4559.9	6316.23	3845.02	6127.38	8092.1			
3804.75	4561.56	6315.5	3853.38	6130.9	8094.42			
3813.1	4559.71	6314.74	3861.73	6128.42	8095.97			
3821.46	4557.63	6315.31	3870.08	6133.79	8097.82			
3829.81	4560.36	6316.96	3878.44	6136.12	8100.41			
3838.17	4558.58	6314.73	3886.79	6137.8	8104.35			
3846.52	4561.49	6315.55	3895.15	6138.07	8101.84			
3854.88	4559.33	6313.79	3903.5	6139.53	8103.83			
3863.23	4559.96	6313.65	3911.85	6139.66	8105.94			
3871.58	4560.54	6313.67	3920.21	6142.81	8109.4			
3879.94	4560.97	6315.14	3928.56	6143.74	8110.73			
3888.29	4560.52	6315.57	3936.92	6146.23	8109.9			
3896.65	4562.98	6318.49	3945.27	6147.88	8111.47			
3905	4559.84	6314.74	3953.62	6149.45	8116.33			
3913.35	4560.6	6313.88	3961.98	6155.35	8119.9			
3921.71	4561.68	6315.91	3970.33	6156.5	8120.84			
3930.06	4562.28	6315.1	3978.69	6155.9	8121.06			
3938.42	4562.41	6314.45	3987.04	6156.8	8120.62			
3946.77	4563.91	6316.66	3995.39	6157.58	8125.72			
3955.13	4562.19	6317.5	4003.75	6158.53	8121.67			
3963.48	4561.59	6315.64	4012.1	6163.1	8125.2			
3971.83	4562.11	6314.52	4020.46	6163.15	8128.2			
3980.19	4560.72	6316.34	4028.81	6164.88	8129.97			
3988.54	4560.55	6315.52	4037.16	6165.93	8130.02			
3996.9	4560.89	6312.61	4045.52	6168.2	8134.57			
4005.25	4563.86	6314.88	4053.87	6173.17	8136.33			
4013.6	4562.43	6311.77	4062.23	6176.42	8143.99			
4021.96	4563.89	6314.78	4070.58	6176.63	8145.51			
4030.31	4562.9	6313.65	4078.93	6176.39	8140.52			
4038.67	4560.67	6312.97	4087.29	6180.62	8143.94			
4047.02	4562.92	6312.73	4095.64	6178.58	8146.13			
4055.37	4562.36	6312.5	4104	6182.79	8148.78			
4063.73	4565.09	6312.43	4116.04	6182.32	8149.81			
4072.08	4562.08	6311.53	4124.48	6186	8152.41			
4080.44	4562.63	6312	4132.83	6189.67	8154.67			
4088.79	4563.21	6315.11	4141.19	6190.36	8155.86			
4097.15	4564	6316.07	4149.54	6194.95	8161.73			
4105.5	4564.94	6316.02	4157.9	6197.15	8164.71			
4113.85	4565.48	6315.76	4166.25	6196.5	8164.9			
4122.21	4566.64	6316.49	4174.6	6199.92	8166.2			

4130.56	4565.63	6313.82	4182.96	6202.19	8168.86			
4138.92	4563.08	6315.35	4191.31	6203.94	8171.27			
4147.27	4565.47	6313.21	4199.67	6202.17	8169.63			
4155.62	4565.47	6312.48	4210.96	6205.2	8172.51			
4163.98	4565.35	6313.95	4218.89	6208.28	8175.07			
4172.33	4568.76	6317.22	4227.25	6214.34	8180.22			
4180.69	4567.34	6315.64	4235.6	6214.45	8179.68			
4189.04	4568.64	6315.47	4243.96	6215.4	8182.63			
4197.39	4566.28	6315.23	4252.31	6217.82	8185.6			
4205.75	4566.54	6314.96	4260.66	6220.49	8188.51			
4214.1	4567.52	6315.28	4269.02	6220.59	8187.48			
4222.46	4566.97	6315.94	4277.37	6221.28	8187.87			
4230.81	4569.2	6314.76	4292.67	6220.02	8189.55			
4239.16	4570.69	6318.43	4301.23	6228.27	8193.42			
4247.52	4568.48	6315.11	4309.34	6224.81	8193.22			
4255.87	4568.36	6317.52	4317.7	6230.38	8197.74			
4264.23	4568.28	6315.34	4326.06	6232.29	8201.38			
4272.58	4567.34	6314.44	4334.41	6235.84	8204			
4280.93	4568.2	6312.7	4345.56	6236.61	8203.44			
4289.29	4566.95	6315.79	4353.63	6235.67	8202.41			
4297.64	4567.75	6316.11	4363.97	6235.81	8204.69			
4306	4569.98	6317.67	4376.27	6236.58	8203.33			
4314.35	4568.69	6316.75	4384.37	6241.7	8207			
4322.7	4570.28	6315.14	4396.75	6240.98	8206.76			
4331.06	4570.4	6317.21	4404.86	6244.24	8210.7			
4339.41	4567.99	6315.71	4414.02	6248.12	8215.65			
4347.77	4569.53	6315.56	4423.58	6246.49	8211.94			
4356.12	4569.31	6316.05	4431.99	6248.97	8214.64			
4364.48	4569.37	6317.03	4440.34	6249.62	8216.25			
4372.83	4570.08	6316.01	4451.15	6254.46	8221.32			
4381.18	4569.82	6315.66	4459.57	6259.23	8224.04			
4389.54	4569.44	6314.99	4467.93	6261.62	8225.7			
4397.89	4569.71	6315.5	4476.28	6263.78	8229.67			
4406.25	4568.77	6313.65	4484.63	6267.76	8233.85			
4414.6	4568.62	6316.19	4492.99	6267.87	8234.32			
4422.95	4569.11	6314.24	4505.01	6266.39	8230.57			
4431.31	4570.99	6312.09	4513.47	6272.38	8236.09			
4439.66	4568.79	6315.72	4521.82	6275.23	8241.17			
4448.02	4568.83	6312.65	4530.18	6279.54	8243.04			
4456.37	4571.16	6315.73	4538.53	6281.65	8248.86			
4464.72	4570.76	6314.94	4548.02	6289.42	8253.31			
4473.08	4574.29	6316.82	4556.37	6290.95	8258.27			
4481.43	4572.94	6316.22	4564.73	6293.11	8260.07			
4489.79	4571.74	6317.48	4573.08	6295.85	8263.82			
4498.14	4574.35	6319.17	4581.44	6297.34	8268.79			

4506.49	4572.25	6316.01	4589.79	6301.85	8272.14			
4514.85	4571.09	6313.43	4598.14	6302.46	8270.86			
4523.2	4573.17	6316.23	4606.5	6303.37	8270.89			
4531.56	4573.7	6315.64	4614.85	6302.87	8274.73			
4539.91	4574.49	6316.32	4623.21	6307.6	8274.82			
4548.26	4573.77	6318.09	4631.56	6309.14	8279.81			
4556.62	4574.38	6318.66	4639.91	6311.27	8281.67			
4564.97	4575.36	6317.86	4649.28	6313.9	8284.37			
4574.6	4577.71	6325.56	4657.64	6316.8	8287.39			
4582.96	4578.15	6322.16	4665.99	6319.02	8289.27			
4591.31	4579.39	6320.19	4674.34	6321	8289.64			
4599.67	4577.58	6321.83	4682.7	6322.51	8292.68			
4608.02	4577.41	6321.41	4691.05	6326.59	8296.74			
4618.83	4574.12	6318.76	4699.41	6329.27	8299.31			
4627.25	4577.45	6318.37	4707.76	6332.8	8298.74			
4635.6	4576.21	6317.89	4716.11	6333.2	8302.42			
4643.95	4576.51	6320.88	4724.47	6331.74	8302			
4652.31	4576.99	6317.12	4732.82	6336.75	8306.27			
4660.66	4574.88	6317.07	4741.18	6339.88	8307.94			
4669.02	4576.49	6315.57	4749.53	6341.61	8306.57			
4677.37	4576.17	6317.42	4757.88	6341.84	8312.26			
4685.73	4575.54	6317.93	4766.24	6342.96	8311.16			
4694.08	4575.8	6317.3	4774.59	6345.12	8312.8			
4702.43	4575.53	6317.41	4782.95	6345.71	8315.88			
4710.79	4575.29	6318.68	4791.3	6347.29	8313.35			
4719.14	4577.42	6317.37	4799.65	6351.88	8320.34			
4727.5	4577.25	6316.9	4808.01	6356.96	8325.5			
4735.85	4577.07	6316.81	4818.21	6354.46	8318.57			
4744.21	4577.89	6317.42	4826.6	6358.43	8322.8			
4752.56	4575.61	6317.76	4834.96	6363	8330.56			
4760.91	4579.95	6323.94	4843.31	6365.35	8332.5			
4769.27	4580.49	6320.34	4851.66	6367.35	8333.14			
4777.62	4581.12	6319.43	4860.02	6369.9	8336.09			
4785.98	4579.71	6321.33	4868.37	6371.04	8338.9			
4794.33	4578.53	6320.54	4876.73	6375.96	8340.22			
4802.68	4578.07	6321.09	4885.08	6377.42	8344.88			
4811.04	4579.14	6320.44	4893.43	6379.71	8346.99			
4819.39	4578.68	6319.78	4901.79	6381.93	8347.43			
4827.75	4579.43	6320.07	4910.14	6385.08	8353.1			
4836.1	4578.04	6318.86	4918.5	6387.91	8355.16			
4844.45	4577.76	6318.94	4926.85	6388.65	8355.77			
4852.81	4577.78	6318.23	4939.4	6388.34	8355.32			
4861.16	4579.92	6318.73	4947.34	6396.29	8363.19			
4869.52	4579.61	6318.87	4960.08	6396.77	8362.04			
4877.87	4577.4	6317.08	4970.28	6401.69	8366.92			

4886.22	4581.99	6319.2	4979.04	6406.14	8371.79			
4894.58	4579.13	6320.42	4987.43	6408.41	8374.15			
4902.93	4580.15	6319.31	4995.48	6410.34	8378.46			
4911.29	4579.88	6317.62	5003.84	6413.84	8382.73			
4919.64	4581.97	6320.3	5012.19	6418.18	8384.98			
4927.99	4577.95	6317.89	5020.54	6421.19	8389.34			
4936.35	4582.2	6318.71	5028.9	6424.69	8392.32			
4944.7	4581.56	6318.23	5040.38	6422.84	8391.01			
4953.06	4580.14	6318.99	5051.73	6421.82	8390.95			
4961.41	4580.42	6316.86	5060.28	6428.25	8395.05			
4969.76	4579.07	6315.35	5068.61	6431.27	8400.66			
4978.12	4582.58	6317.9	5076.97	6432.22	8403.03			
4986.47	4579.99	6319.42	5085.32	6434.11	8404.46			
4994.83	4581.05	6319.17	5093.68	6436.44	8406.49			
5003.18	4582.73	6319.88	5102.03	6439.75	8409.07			
5011.54	4582.63	6319.54	5110.38	6442.43	8411.2			
5019.89	4580.14	6316.22	5120.76	6441.08	8411.81			
5028.24	4582.16	6318.19	5128.97	6443.75	8410.59			
5036.6	4580.21	6319.52	5139.15	6452.83	8420.81			
5044.95	4583.27	6317.87	5147.5	6456.46	8423			
5053.31	4581.26	6319.09	5155.85	6454.35	8424.21			
5061.66	4581.5	6318.65	5164.21	6459.54	8428.68			
5070.01	4583.27	6321.26	5172.56	6459.42	8426.41			
5078.37	4585.29	6321.45	5180.92	6463.13	8428.85			
5086.72	4584.97	6321.95	5189.27	6464.61	8431			
5095.08	4585.51	6320.47	5197.62	6467.22	8433.19			
5103.43	4581.53	6316.1	5205.98	6470.69	8434.17			
5111.78	4582.37	6318.86	5214.33	6473.75	8439.29			
5120.14	4585.86	6318.83	5222.9	6477.2	8441.91			
5128.49	4585.49	6322.8	5231.63	6479.16	8443.45			
5136.85	4582.96	6319.12	5240.03	6483.93	8447.76			
5145.2	4584.56	6319.04	5248.39	6486.09	8451.58			
5153.55	4583.38	6323.78	5256.74	6487.06	8452.42			
5161.91	4583.88	6322.03	5265.09	6489.59	8455.13			
5170.26	4586.38	6319.33	5273.45	6495.62	8460.55			
5178.62	4586.61	6320.11	5281.8	6498.88	8462.87			
5186.97	4585.66	6320.1	5290.16	6499.71	8463.72			
5195.32	4583.03	6320.62	5298.51	6504.36	8467.41			
5203.68	4586.82	6318.29	5306.87	6502.92	8469.67			
5212.03	4584.95	6317.37	5316.69	6511.04	8477.49			
5220.39	4583.29	6318.46	5325.05	6513.8	8480.58			
5228.74	4586.89	6320.32	5333.4	6517.54	8480.63			
5237.09	4586.2	6318.39	5341.76	6519.38	8484.22			
5245.45	4584.51	6319.87	5350.11	6519.46	8487.14			
5253.8	4585.43	6317.75	5358.47	6523.79	8490.79			

5262.16	4587.14	6318.78	5369.36	6528.06	8490.96			
5270.51	4587.22	6319.04	5380.73	6527.01	8492.33			
5278.87	4586.16	6318.9	5389.19	6531.72	8495.63			

Table A.3 SAOS in the frequency sweep mode for the TLCP/HDPE blends at 300 ºC, under nitrogen environment.

Frequency /rad●s^{-1}	TLCP η* /Pa●s^{-1}	10 wt% TLCP η* /Pa●s^{-1}	20 wt% TLCP η* /Pa●s^{-1}	50 wt% TLCP η* /Pa●s^{-1}	HDPE η* /Pa●s^{-1}
0.1	823.136	36903	29915.8	10640.5	44251.2
0.125893	835.612	33165.2	26979.7	9654.5	39743.7
0.158489	831.365	29687.5	24207	8786.55	35674.6
0.199526	817.052	26486	21665	7974.86	31805
0.251189	808.627	23567.2	19331.4	7214.3	28254.3
0.316228	793.393	20916.2	17195.8	6515.93	25006.3
0.398107	776.245	18536.8	15273.9	5885.2	22105.9
0.501187	754.339	16382	13542.2	5307.83	19510.8
0.630957	730.12	14460	11982.9	4785.28	17176.1
0.794328	703.88	12757.6	10579.8	4314.24	15095.1
1	674.605	11228.7	9355.59	3887.3	13237.5
1.25893	644.421	9876.64	8254.97	3495.75	11599.9
1.58489	612.754	8677.18	7278.4	3152.09	10133.1
1.99526	579.901	7614.76	6410.8	2836.22	8850.01
2.51189	546.949	6646.38	5638.46	2548.56	7742.15
3.16228	508.592	5798.55	4919.65	2270.81	6698.11
3.98107	473.537	5071.6	4321.58	2034.39	5831.47
5.01187	440.989	4426.52	3789.84	1824.29	5063.49
6.30957	402.446	3861.59	3318.82	1623.36	4397.04
7.94328	364.583	3367.84	2904.63	1441.75	3815.48
10	328.875	2932.97	2538.57	1277.69	3314.53
12.5893	297.186	2559.26	2220.68	1133.84	2873.22
15.8489	264.334	2229.92	1937.45	998.289	2487.03
19.9526	234.047	1939.12	1693.68	877.644	2151.1
25.1189	207.971	1685.55	1476.53	772.433	1859.5
31.6228	181.936	1463.92	1284.57	674.068	1606.52
39.8107	158.688	1270.79	1116.99	587.524	1387.35
50.1187	139.041	1102.66	971.256	512.915	1197.55
63.0957	121.883	956.398	844.268	447.517	1033.19
79.4328	105.458	828.922	732.401	387.433	891.223
100	91.4299	718.236	635.462	336.925	768.255

Table A.4 SAOS in the frequency sweep mode for the TLCP/HDPE blends at 290 ºC, under nitrogen environment.

Frequency /rad●s^{-1}	TLCP η* /Pa●s^{-1}	10 wt% TLCP η* /Pa●s^{-1}	20 wt% TLCP η* /Pa●s^{-1}	50 wt% TLCP η* /Pa●s^{-1}	HDPE η* /Pa●s^{-1}
0.1	993.819	41240.1	31621	13566	55659.2
0.125893	999.217	37110.8	28774.8	12327	49867.4
0.158489	994.383	33295.7	25932.1	11194.4	44621.1
0.199526	990.605	29730.2	23268.3	10139.8	39730.7
0.251189	970.439	26475.7	20802.3	9151.33	35230.5
0.316228	953.546	23471.7	18540.2	8238.19	31095.7
0.398107	932.389	20790.5	16498.5	7413.11	27420.8
0.501187	906.442	18369.3	14641.4	6658.75	24093.1
0.630957	878.176	16197	12967.6	5980.35	21127.2
0.794328	845.315	14269.5	11484.2	5361.47	18513.3
1	811.035	12547.6	10159	4816.36	16162.1
1.25893	775.964	11029.2	8976.03	4322.1	14121
1.58489	737.873	9683.34	7924.98	3868.36	12328.8
1.99526	699.343	8468.38	6990.77	3465.28	10736.9
2.51189	659.112	7431.94	6157.51	3110.88	9332.85
3.16228	614.568	6464.48	5381.91	2762.76	8046.86
3.98107	573.479	5653.2	4734.44	2468.63	6981.34
5.01187	535.258	4934.35	4157.81	2206.07	6041.02
6.30957	491.39	4304.97	3644.31	1958.86	5235.06
7.94328	448.274	3754.55	3195.53	1737.18	4534.62
10	407.277	3275.11	2797.62	1537.43	3916.53
12.5893	370.192	2858.52	2451.12	1362.94	3384.18
15.8489	332.197	2487.36	2148.12	1199.69	2920.34
19.9526	296.686	2162.99	1875.92	1054.53	2518.26
25.1189	265.388	1880.56	1638	927.767	2170.47
31.6228	234.364	1633.28	1427.43	810.35	1869.84
39.8107	206.195	1417.96	1243.36	707.171	1610.39
50.1187	181.84	1230.76	1082.93	618.388	1386.35
63.0957	160.277	1067.98	941.933	540.884	1192.9
79.4328	139.709	925.768	818.866	469.096	1026.18
100	121.85	802.342	711.785	407.45	882.6

Table A.5 SAOS in the frequency sweep mode for the TLCP/HDPE blends at 270 ºC, under nitrogen environment.

Frequency /rad●s^{-1}	TLCP η* /Pa●s^{-1}	10 wt% TLCP η* /Pa●s^{-1}	20 wt% TLCP η* /Pa●s^{-1}	50 wt% TLCP η* /Pa●s^{-1}	HDPE η* /Pa●s^{-1}
0.1	1605.29	55285.6	44817.2	17321	66372
0.125893	1574.01	49103.5	39942.4	15670.5	59299.9
0.158489	1537.64	43517.2	35473.9	14099.7	52572
0.199526	1497.69	38450.3	31429	12670.2	46451.4
0.251189	1455.74	33920.5	27774	11375.8	40954.7
0.316228	1404.68	29842.4	24497.4	10199.7	35986.4
0.398107	1355.01	26236.9	21590.6	9162.76	31593.7
0.501187	1299.74	23015.9	19008	8192.21	27662.2
0.630957	1236.52	20161	16711.6	7352.33	24182.3
0.794328	1174.39	17654.9	14689	6590.95	21134.2
1	1115.5	15429.7	12891.6	5903.44	18368.5
1.25893	1051.73	13451.6	11316.3	5289.63	16070.6
1.58489	988.277	11774.1	9927.26	4735.93	13989.1
1.99526	925.009	10270	8679.93	4228.19	12164.8
2.51189	861.165	8944	7620.89	3787.84	10559.4
3.16228	791.129	7731.14	6623.19	3354.56	9099.87
3.98107	728.973	6726.64	5794.02	2989.32	7893.62
5.01187	672.579	5840.45	5061.48	2665.12	6825.51
6.30957	608.553	5071.27	4417.67	2358.04	5907.1
7.94328	547.021	4414.11	3854.65	2084.59	5107.24
10	490.06	3827.49	3368.58	1838.7	4409.88
12.5893	440.264	3321.23	2938.19	1624.17	3810.09
15.8489	390.077	2877.76	2557.6	1424.79	3287.86
19.9526	344.602	2492.19	2224.85	1248.56	2835.54
25.1189	305.59	2157.87	1935.45	1095.63	2444.87
31.6228	267.714	1866.79	1675.48	954.622	2106.96
39.8107	234.277	1614.54	1456.29	833.61	1813.54
50.1187	206.016	1396.33	1264.49	727.094	1561.82
63.0957	181.452	1207.05	1097.54	634.024	1344.71
79.4328	158.502	1042.48	950.903	549.693	1157.38
100	138.961	900.209	823.936	477.529	996.01

Table A.6 SAOS in the frequency sweep mode for the TLCP/HDPE blends at 260 ºC, under nitrogen environment.

Frequency /rad●s^{-1}	TLCP η* /Pa●s^{-1}	10 wt% TLCP η* /Pa●s^{-1}	20 wt% TLCP η* /Pa●s^{-1}	50 wt% TLCP η* /Pa●s^{-1}	HDPE η* /Pa●s^{-1}
0.1	2334.88	66300.7	50522.1	18273.9	18273.9
0.125893	2261.88	59034.1	44903.9	16591.3	16591.3
0.158489	2202.14	52199.2	39717.1	14969.7	14969.7
0.199526	2133.83	45932.5	35067.8	13494.1	13494.1
0.251189	2060.81	40378.9	30912.9	12156.2	12156.2
0.316228	1976.22	35420.6	27200.1	10934	10934
0.398107	1889.98	31045.4	23925.6	9838.09	9838.09
0.501187	1802.76	27154.4	21001.4	8840.56	8840.56
0.630957	1710.56	23725.5	18424.6	7942.13	7942.13
0.794328	1616.93	20678.1	16156.5	7133.13	7133.13
1	1519.2	18067.7	14149.2	6401.09	6401.09
1.25893	1422.98	15748.4	12392.3	5741.68	5741.68
1.58489	1327.02	13717	10823.9	5132.25	5132.25
1.99526	1233.89	11938.5	9493.82	4604.69	4604.69
2.51189	1141.44	10373.9	8297.06	4123.56	4123.56
3.16228	1040.76	8946.83	7195.41	3653.44	3653.44
3.98107	951.999	7767.26	6285.31	3257.87	3257.87
5.01187	873.737	6748.4	5480.2	2905.76	2905.76
6.30957	770.594	5846.98	4775.74	2570.03	2570.03
7.94328	692.556	5064.4	4172.53	2272.79	2272.79
10	619.19	4382.11	3631.59	2007.78	2007.78
12.5893	554.379	3795	3163.81	1775.06	1775.06
15.8489	490.02	3281.41	2751.05	1558.93	1558.93
19.9526	432.357	2835.93	2390.43	1368.26	1368.26
25.1189	382.424	2451.15	2079.16	1201.95	1201.95
31.6228	329.775	2116.6	1803.06	1056.24	1056.24
39.8107	287.516	1827.31	1563.78	920.102	920.102
50.1187	253.995	1577.19	1356.52	803.976	803.976
63.0957	226.403	1361.04	1176.02	702.567	702.567
79.4328	196.833	1173.69	1018.15	611.06	611.06
100	175.605	1012.12	881.739	532.695	532.695

Table A.7 SAOS in the temperature sweep mode for Vectra B950 under nitrogen environment. The cooling rate is 10 °C/min.

Temperature /°C	tanσ	G' /Pa●s^{-1}	G" / Pa●s^{-1}	η* /Pa●s^{-1}
360.022	2.19816	78.8376	173.298	19.0388
358.887	2.17028	80.9546	175.694	19.3448
357.514	2.15169	82.9914	178.572	19.6915
355.902	2.13276	85.6808	182.737	20.1826
354.25	2.12612	88.1734	187.467	20.7168
352.625	2.13012	90.1948	192.126	21.2244
351.02	2.12999	92.7165	197.485	21.8167
349.483	2.14008	94.8556	202.999	22.4067
347.998	2.14242	97.1191	208.07	22.962
346.556	2.13179	100.211	213.629	23.5965
345.125	2.14719	101.92	218.84	24.141
343.734	2.1763	103.679	225.637	24.8317
342.323	2.16823	106.831	231.633	25.5082
339.922	2.21827	109.747	243.448	26.7042
338.581	2.23141	112.084	250.106	27.4073
336.527	2.266	115.358	261.402	28.5724
334.536	2.29959	119.089	273.856	29.8629
332.66	2.33828	122.458	286.342	31.1429
330.878	2.4076	124.058	298.683	32.3422
329.304	2.43971	127.606	311.323	33.646
327.763	2.48051	130.24	323.063	34.8328
326.382	2.51564	133.599	336.088	36.1668
324.995	2.53037	137.527	347.993	37.4183
323.595	2.58514	139.928	361.732	38.7853
322.206	2.63363	143.113	376.908	40.3164
320.832	2.68537	146.333	392.957	41.9319
318.189	2.73775	154.27	422.353	44.9646
315.803	2.81132	161.195	453.171	48.0987
313.648	2.90281	167.718	486.853	51.4932
311.572	2.98508	174.419	520.656	54.9094
309.685	3.0499	182.154	555.551	58.4651
308.01	3.12286	188.709	589.313	61.879
306.449	3.18831	195.419	623.057	65.2985
305.02	3.25059	202.22	657.333	68.7735
303.704	3.31728	208.262	690.863	72.1571
302.314	3.36868	216.404	728.997	76.0439
300.918	3.43406	224.21	769.949	80.1929
299.537	3.49853	232.298	812.702	84.525
298.144	3.5672	241.372	861.021	89.4213

296.75	3.63512	250.882	911.985	94.5863
294.663	3.69551	268.616	992.673	102.838
292.647	3.81087	284.072	1082.56	111.922
290.773	3.89431	302.221	1176.94	121.513
289.079	3.97874	319.351	1270.62	131.013
287.477	4.05928	338.688	1374.83	141.593
285.303	4.15262	367.036	1524.16	156.773
283.327	4.24027	396.941	1683.14	172.931
281.195	4.33261	433.363	1877.59	192.696
279.534	4.41436	464.872	2052.11	210.411
278.06	4.48171	496.846	2226.72	228.148
276.721	4.54024	530.623	2409.15	246.69
275.315	4.59363	567.676	2607.69	266.877
273.936	4.64313	610.091	2832.73	289.769
272.53	4.67922	658.605	3081.76	315.135
271.148	4.72337	709.96	3353.41	342.774
268.64	4.77349	819.302	3910.93	399.583
266.728	4.83393	914.501	4420.63	451.423
265.024	4.8678	1019.5	4962.73	506.636
262.793	4.88597	1190.56	5817.04	593.763
260.763	4.90678	1372.49	6734.49	687.292
258.745	4.90212	1603.7	7861.51	802.342
257.136	4.87699	1840.2	8974.63	916.135
255.541	4.84635	2122.02	10284	1050.07
254.135	4.77976	2447.31	11697.6	1195.08
252.82	4.69535	2828.94	13282.9	1358.08
250.725	4.4639	3676.71	16412.5	1681.92
248.19	4.15434	5209.63	21642.6	2226.08
245.831	3.83215	7409.82	28395.5	2934.64
243.855	3.55053	10341.6	36718.1	3814.67
242.198	3.34431	13822.7	46227.5	4824.99
240.813	3.19226	17874.6	57060.3	5979.44
238.589	2.99639	27612.1	82736.7	8722.26
235.415	2.61648	64219.9	168030	17988.4
232.654	1.89902	184360	350104	39567.9
230.096	1.27947	502721	643218	81636.8
228.514	0.949077	1.01302e+06	961437	139663

Table A.8 SAOS in the temperature sweep mode for HX6000 under nitrogen environment. The cooling rate is 10 °C/min.

Temperature /°C	tanσ	G' /Pa●s^{-1}	G" / Pa●s^{-1}	η^* /Pa●s^{-1}
359.773	2.59675	461.159	1197.52	128.324
358.604	2.57061	460.467	1183.68	127.009
357.217	2.54643	466.263	1187.31	127.558
355.647	2.52954	473.316	1197.27	128.744
354.018	2.50516	484.065	1212.66	130.57
352.392	2.48097	495.771	1229.99	132.615
350.828	2.45826	508.229	1249.36	134.878
349.32	2.44367	520.289	1271.41	137.375
346.567	2.40113	538.437	1292.86	140.05
345.198	2.3932	557.74	1334.78	144.662
342.98	2.36116	575.159	1358.04	147.482
340.936	2.33974	598.186	1399.6	152.207
339.01	2.31821	621.755	1441.36	156.974
337.201	2.30441	644.663	1485.57	161.942
335.591	2.28686	667.935	1527.47	166.713
334.073	2.27054	692.433	1572.2	171.792
332.608	2.26114	715.039	1616.8	176.786
331.197	2.24611	741.011	1664.4	182.19
329.819	2.23881	764.514	1711.6	187.459
328.481	2.22724	789.626	1758.69	192.782
327.098	2.21686	816.545	1810.16	198.581
325.717	2.21017	843.718	1864.76	204.675
324.318	2.20028	874.673	1924.53	211.397
322.929	2.19427	906.908	1990	218.691
320.945	2.18248	948.963	2071.09	227.815
319.163	2.17985	995.051	2169.07	238.641
316.716	2.17595	1062.54	2312.04	254.451
314.49	2.18184	1134.11	2474.45	272.196
312.559	2.1893	1206.47	2641.31	290.381
310.775	2.19907	1281.97	2819.14	309.693
309.064	2.21275	1361.75	3013.22	330.664
307.456	2.22676	1446.22	3220.37	353.02
305.974	2.24236	1535.32	3442.73	376.956
304.564	2.25807	1630.94	3682.78	402.776
303.172	2.27122	1739.89	3951.69	431.776
300.425	1.98403	2536.32	5032.13	563.518
294.219	0.291357	2.96807e+06	864766	309148

Table A.9 SAOS in the temperature sweep mode for Vectra B950/HX6000 blend containing 25% Vectra B950 under nitrogen environment. The cooling rate is 10 °C/min.

Temperature /°C	tanσ	G' /Pa●s^{-1}	G" / Pa●s^{-1}	η^* /Pa●s^{-1}
359.904	2.58786	122.75	317.661	34.0553
358.814	2.557	124.067	317.24	34.0638
357.5	2.53027	125.563	317.707	34.1619
355.983	2.4967	128.024	319.638	34.4324
354.405	2.48907	129.927	323.397	34.852
352.818	2.45721	133.289	327.518	35.3602
350.59	2.45465	135.547	332.721	35.9272
349.095	2.44795	137.868	337.495	36.4569
347.654	2.44254	140.502	343.182	37.083
346.101	2.42974	143.448	348.543	37.6908
344.033	2.41832	146.686	354.735	38.3867
342.628	2.43445	148.505	361.529	39.0841
341.208	2.41727	152.139	367.762	39.7989
339.813	2.41532	154.584	373.37	40.4105
338.422	2.43184	156.516	380.621	41.1545
335.809	2.42137	161.448	390.926	42.2952
333.225	2.44312	165.712	404.853	43.7454
331.043	2.44999	169.934	416.338	44.9683
329.022	2.45226	174.754	428.543	46.2804
327.405	2.4761	177.775	440.189	47.4732
325.802	2.47749	182.003	450.91	48.6256
324.18	2.49942	185.147	462.76	49.8424
322.69	2.51116	188.797	474.099	51.0308
321.344	2.5157	193.058	485.676	52.264
319.954	2.52529	197.243	498.095	53.5727
318.58	2.53428	201.474	510.593	54.8905
317.193	2.5582	205.093	524.669	56.333
315.802	2.55246	210.791	538.035	57.7853
314.422	2.56153	215.391	551.729	59.2282
313.016	2.56687	220.994	567.263	60.879
311.625	2.58126	226.45	584.528	62.6859
310.249	2.59334	231.955	601.537	64.4709
308.858	2.60494	237.743	619.309	66.3374
307.468	2.60917	244.261	637.32	68.2525
306.079	2.62269	251.073	658.487	70.4729
304.06	2.6277	261.092	686.07	73.4072
302.026	2.64451	272.033	719.393	76.9109
300.034	2.64001	285.098	752.662	80.4848
298.283	2.6537	296.399	786.553	84.0546

295.772	2.66043	315.269	838.752	89.6047
293.578	2.64801	336.212	890.291	95.1659
291.601	2.64348	357.766	945.746	101.115
289.707	2.63352	381.37	1004.35	107.432
287.956	2.61131	409.572	1069.52	114.526
286.384	2.57589	443.198	1141.63	122.464
284.952	2.53337	482.621	1222.66	131.446
283.639	2.46372	538.332	1326.3	143.139
282.224	2.25568	673.574	1519.37	166.198
280.839	1.75736	1161.63	2041.4	234.877
278.638	0.715373	8926.15	6385.53	1097.5

Table A.10 SAOS in the temperature sweep mode for Vectra B950/HX6000 blend containing 50% Vectra B950 under nitrogen environment. The cooling rate is 10 °C/min.

Temperature /°C	tanσ	G' /Pa●s^{-1}	G" / Pa●s^{-1}	η^* /Pa●s^{-1}
360.03	1.53632	116.837	179.499	21.4175
358.298	1.5173	117.542	178.347	21.3598
356.452	1.50725	118.851	179.138	21.4979
354.67	1.50162	119.747	179.815	21.6039
351.486	1.50459	122.012	183.579	22.0427
348.815	1.48917	124.843	185.912	22.394
346.573	1.51413	124.96	189.205	22.6746
344.543	1.49339	127.261	190.05	22.8724
342.759	1.51999	127.7	194.102	23.2343
341.17	1.51266	129.695	196.185	23.5179
339.72	1.54073	129.068	198.859	23.7072
338.337	1.53065	131.547	201.353	24.0516
336.94	1.5544	131.541	204.466	24.3124
335.563	1.56741	132.51	207.697	24.6368
334.174	1.57987	133.363	210.696	24.9356
332.785	1.5937	134.5	214.352	25.3056
331.422	1.62148	134.154	217.529	25.557
329.286	1.62812	136.861	222.825	26.15
327.228	1.65558	139.523	230.991	26.9858
325.323	1.67447	140.842	235.836	27.4691
323.51	1.71639	141.39	242.681	28.0865
321.816	1.72933	143.773	248.63	28.7206
320.267	1.76827	144.026	254.677	29.2581
318.763	1.78212	146.477	261.04	29.9328
316.667	1.80763	149.569	270.365	30.8979
314.579	1.84517	152.022	280.506	31.9052
312.707	1.87571	155.185	291.082	32.9865
310.938	1.91118	156.782	299.639	33.8178
309.363	1.9319	159.871	308.854	34.7778
307.716	1.95771	162.039	317.225	35.6214
306.232	1.98523	165.129	327.82	36.706
304.79	2.02666	166.598	337.638	37.6503
303.449	2.03872	169.986	346.554	38.5999
301.806	2.06153	173.551	357.78	39.7651
300.469	2.11695	174.132	368.628	40.7686
299.074	2.13371	177.601	378.95	41.8504
297.674	2.16036	181.452	392.003	43.1963
296.299	2.1941	183.82	403.321	44.3236
294.902	2.21276	188.114	416.25	45.6783

293.505	2.25118	191.191	430.406	47.096
292.121	2.28316	194.982	445.174	48.6002
290.721	2.30963	199.407	460.556	50.1872
289.343	2.34032	203.027	475.147	51.6705
287.955	2.37473	207.572	492.929	53.485
285.837	2.41061	216.257	521.313	56.4388
284.436	2.45289	220.449	540.738	58.3948
282.363	2.49849	228.847	571.772	61.5868
280.288	2.55695	236.889	605.713	65.0388
278.361	2.60481	245.394	639.205	68.469
276.448	2.63013	256.678	675.097	72.2246
274.683	2.67496	265.815	711.045	75.9106
272.984	2.71845	275.223	748.179	79.7194
271.39	2.74705	286.627	787.377	83.7924
269.09	2.78983	303.897	847.82	90.064
266.867	2.84247	320.607	911.315	96.6066
264.626	2.88848	339.412	980.383	103.747
262.651	2.9232	358.499	1047.96	110.759
260.726	2.9633	378.417	1121.36	118.349
258.918	2.99891	399.224	1197.23	126.204
257.138	3.01637	423.148	1276.37	134.468
255.479	3.03972	447.547	1360.42	143.214
253.859	3.06452	472.074	1446.68	152.175
252.365	3.08736	497.457	1535.83	161.438
250.867	3.09987	525.873	1630.14	171.286
249.427	3.12015	554.339	1729.62	181.628
248.072	3.13795	583.618	1831.36	192.211
246.676	3.14384	617.856	1942.44	203.834
245.307	3.15861	653.48	2064.09	216.506
243.277	3.14743	713.905	2246.97	235.765
241.303	3.13529	786.352	2465.44	258.781
238.641	3.02207	946.07	2859.09	301.155
235.471	2.62589	1426.74	3746.46	400.894
233.18	2.15931	2344.59	5062.69	557.924
231.042	1.71631	4327.05	7426.55	859.518
229.243	1.39757	7798.8	10899.4	1340.21
227.669	1.17591	13335.7	15681.5	2058.52
224.767	0.840074	36552.6	30706.9	4773.89

Table A.11 SAOS in the temperature sweep mode for Vectra B950/HX6000 blend containing 75% Vectra B950 under nitrogen environment. The cooling rate is 10 °C/min.

Temperature /°C	tanσ	G' /Pa●s^{-1}	G" / Pa●s^{-1}	η* /Pa●s^{-1}
360.793	1.65618	92.877	153.821	17.9686
359.833	1.65098	94.3075	155.7	18.2034
358.402	1.60443	98.4774	158.001	18.6177
356.658	1.60945	100.587	161.891	19.0595
354.816	1.57408	104.298	164.174	19.4503
352.975	1.57743	105.805	166.9	19.7611
351.174	1.57572	108.483	170.939	20.2457
349.489	1.57632	110.516	174.209	20.6307
347.91	1.56913	112.752	176.923	20.9797
346.457	1.56069	114.842	179.234	21.287
345.018	1.5638	116.105	181.565	21.5514
343.641	1.57859	117.289	185.151	21.9174
342.234	1.5724	119.166	187.376	22.206
340.868	1.58549	120.224	190.614	22.5361
339.5	1.59066	121.805	193.75	22.8857
338.123	1.60696	122.419	196.722	23.1703
336.754	1.6172	124.231	200.908	23.6214
335.367	1.62775	125.361	204.057	23.9488
334.01	1.6254	127.664	207.504	24.3631
332.627	1.6446	128.921	212.024	24.8143
331.242	1.6695	129.349	215.948	25.1724
329.858	1.67656	131.454	220.39	25.6617
327.297	1.71556	133.766	229.483	26.5624
325.025	1.74826	136.346	238.369	27.4609
322.917	1.79915	137.297	247.017	28.2609
321.18	1.81944	140.207	255.098	29.1089
319.504	1.85369	142.034	263.287	29.9155
318.145	1.87495	144.341	270.633	30.6719
316.767	1.90622	145.783	277.894	31.3811
315.43	1.93943	147.101	285.294	32.0985
314.022	1.96708	149.934	294.933	33.0856
312.629	1.99195	151.853	302.483	33.846
310.843	2.03101	154.878	314.559	35.062
309.525	2.07092	156.77	324.659	36.0528
308.118	2.11999	158.306	335.606	37.1069
306.747	2.1544	160.119	344.962	38.0311
305.353	2.18898	163.234	357.317	39.2837
303.966	2.22176	166.257	369.384	40.5075
302.556	2.27076	168.157	381.844	41.723

301.171	2.31629	170.651	395.277	43.0541
299.736	2.35347	174.257	410.109	44.5596
298.393	2.39715	177.362	425.163	46.0675
296.993	2.44912	180.35	441.699	47.71
295.022	2.51868	184.263	464.099	49.934
293.104	2.58429	189.386	489.428	52.4792
291.341	2.66386	193.104	514.403	54.9454
289.751	2.72914	197.803	539.832	57.4931
288.265	2.7797	203.11	564.586	60.001
286.865	2.84234	207.831	590.724	62.6218
284.8	2.9299	214.564	628.651	66.4259
283.452	2.99745	219.357	657.511	69.3136
281.664	3.08276	225.903	696.404	73.2127
279.987	3.1378	234.206	734.891	77.1309
278.532	3.22848	240.143	775.298	81.1638
277.146	3.29904	246.857	814.391	85.0982
275.751	3.36855	254.404	856.975	89.3939
274.357	3.43787	261.916	900.432	93.7751
272.958	3.50716	270.681	949.322	98.7158
271.569	3.58003	279.347	1000.07	103.835
270.181	3.66059	288.29	1055.31	109.398
268.775	3.71767	299.685	1114.13	115.373
267.389	3.79014	310.688	1177.55	121.785
266.018	3.85094	323.384	1245.33	128.664
264.623	3.92527	336.134	1319.41	136.156
263.211	3.9863	350.641	1397.76	144.107
261.831	4.05003	366.206	1483.15	152.769
260.434	4.10996	383.105	1574.55	162.048
259.047	4.17659	400.796	1673.96	172.127
257.004	4.23381	430.231	1821.51	187.163
255.348	4.30351	456.978	1966.61	201.901
253.697	4.36862	485.382	2120.45	217.529
252.322	4.41514	514.534	2271.74	232.928
250.93	4.45994	545.318	2432.09	249.247
249.531	4.50285	578.35	2604.22	266.767
247.544	4.5415	629.654	2859.58	292.808
245.848	4.58006	680.989	3118.97	319.244
244.359	4.60679	733.255	3377.95	345.662
243.013	4.62943	786.182	3639.57	372.352
241.348	4.6447	854.828	3970.42	406.14
239.997	4.66399	918.257	4282.74	438.008
238.62	4.67102	991.985	4633.58	473.858
237.221	4.67332	1074.54	5021.69	513.537
235.824	4.67276	1165.3	5445.17	556.847
234.42	4.66671	1265.94	5907.79	604.191

232.346	4.64274	1437.02	6671.7	682.471
230.423	4.62053	1618.24	7477.13	765.024
228.704	4.59922	1810.73	8327.96	852.254
227.146	4.56334	2018	9208.83	942.735
225.128	4.51598	2328.44	10515.2	1076.99
223.318	4.47732	2647.61	11854.2	1214.63
221.628	4.43341	3003.58	13316.1	1365.06
220.115	4.39532	3376.27	14839.8	1521.9
218.679	4.34608	3790.7	16474.7	1690.51
217.331	4.30186	4226.6	18182.2	1866.7
215.947	4.24697	4759.98	20215.5	2076.83
213.855	4.14784	5701.74	23649.9	2432.75
211.984	4.06345	6714	27282	2809.6
209.479	3.93608	8457.73	33290.3	3434.79
207.363	3.83332	10295.8	39467.3	4078.81
205.562	3.7302	12286.2	45829.8	4744.81
204.029	3.63705	14387.2	52327	5426.89
202.643	3.54431	16670.5	59085.4	6139.21
201.249	3.44411	19435.5	66937.9	6970.23
199.855	3.33581	22769.7	75955.1	7929.47
197.949	3.16945	28397.4	90004.2	9437.78
196.625	3.05092	33531.3	102301	10765.6
195.238	2.91051	40011.5	116454	12313.6
193.525	2.71292	50476.1	136938	14594.4
191.633	2.47107	66968	165482	17851.9
190.214	2.28597	84579.5	193346	21103.6
188.822	2.08251	109391	227808	25271.1
186.309	1.6943	185569	314410	36508.8
184.889	1.48757	258910	385145	46408.1
182.359	1.14539	492817	564470	74932.9
180.975	0.986001	709455	699523	99632.2
178.249	0.744056	1.20206e+06	894401	149830